Economic & sustainable operation of renewable energy integrated electric distribution system

Thesis

Submitted by

Anirban Chowdhury

PhD Registration No:1021814004 of 2018

Index No: 18/18/E

Doctor of Philosophy (Engineering)

Department of Power Engineering

Faculty Council of Engineering and Technology

Jadavpur University

Kolkata, India

2025

JADAVPUR UNIVERSITY

KOLKATA 700032, INDIA

INDEX NO: 18/18/E

1. **Title of the Thesis**
   Economic & sustainable operation of renewable energy integrated electric distribution system

2. **Name, Designation, & Institution of the Supervisors**

   - **Dr. Kamal Krishna Mandal** – Professor, Department of Power Engineering, Jadavpur University, Salt Lake Campus, Kolkata – 700106, India

   - **Dr. Ranjit Roy** – Professor & Dean, Faculty of Engineering & Technology, SRM University, Delhi-NCR, Sonepat, Haryana-131029, India

3. **List of publications (Referred Journals):**

[1] **Chowdhury, A.**, Roy, R. and Mandal, K.K., 2024. Sustainability and Capacity Estimation of Photovoltaic Based Distribution Network Integrated with Demand Response Using Arithmetic Optimizer Algorithm. Iranian Journal of Science and Technology, Transactions of Electrical Engineering, pp.1-30., Springer Publication (SCI-E, Impact Factor: 1.7) **DOI:** https://doi.org/10.1007/s40998-024-00762-6

[2] **Chowdhury, A.**, Roy, R. and Mandal, K.K., 2024. Enhancement of technical, economic & environmental benefits in multi-point PV & wind-based DG integrated radial distribution network using Aquila optimizer. Expert Systems with Applications, p.124307., Elsevier Publication (SCI-E, Impact Factor: 7.5) **DOI:** https://doi.org/10.1016/j.eswa.2024.124307

[3] **Chowdhury, A.**, Roy, R. and Mandal, K.K., 2024. Enhancement of Technical, Economic and Environmental Benefits of RDN Using Jaya Algorithm Considering Renewables Uncertainties. Electric Power Components and Systems, pp.1-15., Taylor & Francis Publication (SCI-E, Impact Factor: 1.9) **DOI:** http://dx.doi.org/10.1080/15325008.2024.2303066

[4] **Chowdhury, A.**, Roy, R. and Mandal, K.K., 2024. Benefit analyses of radial networks by optimal allocation of charging station, vehicle charging-discharging distribution & pricing

using Jaya Algorithm, Electric Power Components and Systems, Taylor & Francis Publication (SCI-E, Impact Factor: 1.9), Accepted on 13.03.2024. (In Press)

[5] **Chowdhury, A.**, Roy, R. and Mandal, K.K., 2019. Optimal Single Point Injection of PV based DG Maximizing Technical, Social and Environmental Benefits in Radial Distribution Systems using JAYA Algorithm. Power Research-A Journal of CPRI, pp.39-45. **DOI:** https://doi.org/10.33686/pwj.v15i1.144728

4. List of Patents

NIL

5. List of Presentations in National / International / Conferences / Workshops

[1] **Chowdhury, A.**, Roy, R. and Mandal, K. K., "Demand Response Based Techno-Socio-Economic Improvements with Time-Varying Incentives at DN using Cuckoo Search Algorithm," 2024 *IEEE International Conference on Intelligent Systems, Smart and Green Technologies (ICISSGT)*, Visakhapatnam, India, 2024, pp. 102-107, IEEE **DOI:** https://doi.org/10.1109/ICISSGT58904.2024.00030

[2] **Chowdhury, A.**, Roy, R. and Mandal, K.K., 2022, December. Techno-socio-economic improvements due to optimal location of EV charging station at IEEE 22 bus using Cuckoo Search Algorithm. *In 2022 22nd National Power Systems Conference (NPSC)* (pp. 77-81). IEEE. **DOI:** https://doi.org/10.1109/NPSC57038.2022.10069267

[3] **Chowdhury, A.**, Roy, R. and Mandal, K.K., 2021, February. Techno-Socio-Economic Improvements by PV based DG & BESS Integration in Radial Distribution Networks using CSA. *In 2021 International Conference on Advances in Electrical, Computing, Communication and Sustainable Technologies (ICAECT)* (pp. 1-5). IEEE. **DOI:** https://doi.org/10.1109/ICAECT49130.2021.9392520

[4] **Chowdhury, A.**, Roy, R. and Mandal, K.K., 2020, February. Optimal allocation of wind based DG for enhancement of technical, economic and social benefits using Jaya algorithm for radial distribution networks. *In 2020 International Conference on Convergence to Digital World-Quo Vadis (ICCDW)* (pp. 1-6). IEEE. **DOI:** https://doi.org/10.1109/ICCDW45521.2020.9318659

[5] Roy, R., **Chowdhury, A.** and Mandal, K.K., 2020, October. Techno-Socio-Economic Benefits using CS Algorithm in Radial Distribution. *In 2020 IEEE India Council International Subsections Conference (INDISCON)* (pp. 175-179). IEEE. **DOI:** https://doi.org/10.1109/INDISCON50162.2020.00045

[6] **Chowdhury, A.**, Roy, R. and Mandal, K.K., 2020, December. Optimal allocation of Wind Turbine & SVC using Cuckoo Search Algorithm for enhancement of techno-socio-

environmental benefits in distribution network. *In 2020 21st National Power Systems Conference (NPSC)* (pp. 1-5). IEEE. **DOI:** https://doi.org/10.1109/NPSC49263.2020.9331856

[7] **Chowdhury, A.**, Roy, R. and Mandal, K.K., 2020, February. Optimal allocation of wind based DG for enhancement of technical, economic & social benefits using Cuckoo Search Algorithm for radial distribution networks. *In 2020 International Conference on Computer, Electrical & Communication Engineering (ICCECE)* (pp. 1-6). IEEE. **DOI:** https://doi.org/10.1109/ICCECE48148.2020.9223085

[8] **Chowdhury, A.**, Roy, R., Mandal, K.K., Bhattacharya, S., Biswas, P. and Nandy, S., 2020. Comparison of improvement in technical, commercial and environmental benefits by optimal single-point, twin-point and triple-point deterministic PV-based DG injection by Jaya algorithm. *In Computational Advancement in Communication Circuits and Systems: Proceedings of ICCACCS 2018* (pp. 25-36). Springer Singapore. **DOI:** https://doi.org/10.1007/978-981-13-8687-9_3

[9] **Chowdhury, A.**, Roy, R. and Mandal, K.K., 2017, December. Cost Modelling, Sizing and Multi-Point Allocation of Solar Powered DG Using Multi-Objective Cuckoo Search Via Lévy Flights Considering Economic, Technical and Environmental Impacts Along with Voltage Stability. *In 2017 International Conference on Computer, Electrical & Communication Engineering (ICCECE)* (pp. 1-7). IEEE. **DOI:** https://doi.org/10.1109/ICCECE.2017.8526231

[10] **Chowdhury, A.**, Roy, R. and Mandal, K.K., 2017, December. Comparative study of single and multiple point renewable energy based DG allocation considering improvement of voltage stability, economic and environmental factors using Jaya algorithm. *In 2017 International Conference on Computer, Electrical & Communication Engineering (ICCECE)* (pp. 1-7). IEEE. **DOI:** https://doi.org/10.1109/ICCECE.2017.8526187

[11] **Chowdhury, A.**, Roy, R., Mandal, K.K. and Mandal, S., 2019. A comprehensive review on distribution system. *In Modelling and Simulation in Science, Technology and Engineering Mathematics: Proceedings of the International Conference on Modelling and Simulation (MS-17)* (pp. 133-143). Springer International Publishing. **DOI:** https://doi.org/10.1007/978-3-319-74808-5_12

JADAVPUR UNIVERSITY

KOLKATA 700032, INDIA

"Statement of Originality"

I, **Anirban Chowdhury**, registered on **8th June, 2018** hereby declare that this thesis entitled **"ECONOMIC & SUSTAINABLE OPERATION OF RENEWABLE ENERGY INTEGRATED ELECTRIC DISTRIBUTION SYSTEM"** contains literature survey and original research work done by the undersigned candidate as part of Doctoral studies.

All information in this thesis have been obtained and presented in accordance with existing academic rules and ethical conduct. I declare that, as required by these rules and conduct, I have fully cited and referred all materials and results that are not original to this work.

I also declare that I have checked this thesis as per the "Policy on Anti Plagiarism, Jadavpur University, 2019", and the level of similarity as checked by iThenticate software is 05%.

Signature of Candidate: Anirban Chowdhury.

Date: 09.04.2025.

Certified by Supervisors: (Signature with date, seal)

1. 9/4/25

Professor
Dept. of Power Engineering
Jadavpur University
Salt Lake, 2nd Campus
Kolkata-700 098

2. 09-04-25

Dean (E & T)
SRM University Delhi-NCR
39, RGEC, Sonepat -131029, HR.

JADAVPUR UNIVERSITY

KOLKATA 700032, INDIA

CERTIFICATE FROM THE SUPERVISORS

This is to certify that the thesis entitled "**ECONOMIC & SUSTAINABLE OPERATION OF RENEWABLE ENERGY INTEGRATED ELECTRIC DISTRIBUTION SYSTEM**" submitted by **Shri Anirban Chowdhury**, who got his name registered on **8th June, 2018** for the award of Ph. D. (Engg.) degree of Jadavpur University is absolutely based upon his own work under the supervision of **Prof. (Dr.) Kamal Krishna Mandal** & **Prof. (Dr.) Ranjit Roy** and that neither his thesis nor any part of the thesis has been submitted for any degree/diploma or any other academic award anywhere before.

1. _____ 9/4/25

Professor
Dept. of Power Engineering
Jadavpur University
Salt Lake, 2nd Campus
Kolkata-700 098

Signature of the Supervisor and date with Office Seal

2. _____ 09.04.25

Dean (E & T)
SRM University Delhi-NCR
39, RGEC, Sonepat -131029, HR.

Signature of the Supervisor and date with Office Seal

Dedicated

To

The Almighty

My Parents

My Supervisors

My Wife

&

Rest of the Family Members……..

Acknowledgement

I take this opportunity to express my sincere gratitude for my supervisors, Prof. (Dr.) Kamal Krishna Mandal and Prof. (Dr.) Ranjit Roy for their guidance, patience, encouragement, and blessings during the whole period of my Ph.D. journey. During the course of the Ph.D. work, they continuously provided me with enthusiasm, vision and wisdom. The guidance received from them cannot be acknowledged with few words. Their unconditional love, moral support and lucid illustrations of the technical matters have made my Ph.D. journey memorable.

I am extremely thankful to all the members of the respected Doctoral Committee for the valuable internal reviews they provided regarding the work which was pivotal in giving a perfect blend to the thesis.

I am also grateful to the Head of the Power Engineering Department for providing the necessary departmental laboratory and library facilities during my course of work. I would like to extend my heartfelt gratitude to all faculty and non-teaching staffs of this department for their helpful attitude and constant encouragement.

The work of this dissertation has been supported and funded by the West Bengal State Departmental Fellowship Scheme, Department of Higher Education, Government of West Bengal, India and I acknowledge the support that was provided.

I want to thank all my seniors and juniors who have helped me through this journey. The best part of having such research-mates has been that they have always made me feel insecure with their outstanding research capabilities and thus I was compelled to push myself further so that I could achieve my goal.

Most importantly, I want to pay my deepest gratitude to my parents Mrs. Sheela Chowdhury and Mr. Abhijit Chowdhury and my parents-in-law Mrs. Jyotsna Das and Late Mr. Samaresh Chandra Das for their endless support, care and love with lots of blessings.

I owe gratefulness to a very special person, my wife, Mrs. Jayati Chowdhury for her continued and unfailing love, support and understanding during my pursuit of Ph.D. degree that made the completion of thesis possible. I consider myself the luckiest person in the world to have such a lovely and caring family, standing beside me with their love and unconditional support.

Anirban Chowdhury

Jadavpur University

Table of Contents

Abstract

This research work is proposed to study the effects of different electrical components in enhancing the sustainability of electric distribution networks (DNs) based on technical, economic, and environmental benefits. It explores the impact of optimal allocation of different combinations of photovoltaic (PV) and wind distributed generator (DGs) on the sustainability of different standard IEEE bus networks/ practical test networks. The potential effects of battery energy storage systems (BESS) and Static Var Compensators (SVCs) in maximizing the sustainability indices of the DNs are elaborately explained in this work. The role of different electric vehicles (EVs) in enhancing the sustainability indices of the network with different penetration levels are analyzed and illustrated. The uncertainty associated with PV and wind power generation due to intermittent nature of wind, solar irradiation and their effects on the system parameters are explored. This work also provides an estimation of the optimal number of PV modules required for DG installation considering seasonal variations. A detailed analysis of the impact of a demand response (DR) program on the load-curtailment/shifting patterns and network performance indices is performed. The process of determining the optimal locations, capacities, and number of multiple DGs/BESS/SVCs/EV charging stations in different DNs with different optimization techniques to minimize the active power losses and enhance the sustainability indices of the network are investigated and presented. Statistical analyses of the performance parameters of different evolutionary computational algorithms considered in this work are provided for different case-studies.

List of Tables

Table No. & Caption ***Page No.***

List of Figures

Figure No. & Caption ***Page No.***

CHAPTER 1: Literature review, Gap, Motivation, and Contribution

This chapter presents a brief literature review of the work done by researchers on the sustainability of DNs. The motivation, contribution and organization of the work done is clearly explained in this chapter.

1.1. Introduction to DN and its sustainability

The distribution of electric power is the last step in the delivery of electricity. Distribution substations use transformers to reduce the transmission voltage to medium voltage after connecting to the transmission line. This medium-voltage power is delivered to distribution transformers close to the consumer premises via primary distribution lines. Once more, distribution transformers reduce the voltage to the utilization voltage required by home appliances, industrial machinery, and lighting. Secondary distribution lines are frequently used to supply multiple consumers from a single transformer. Through service drops, residential and commercial clients are linked to the secondary distribution lines. Either the major distribution level or the sub-transmission level may be directly connected to customers who require a large amount of power. DNs are characterized by a high R/X ratio due to their radial nature in comparison with transmission networks. A key factor in the development of new electric power systems is the penetration of distributed renewable generation into a DN, which is facilitated by renewable energy initiatives and the public's profound assessment of the environmental effects associated with generating electricity from fossil fuels. The use of renewable energy resources to generate electricity has become more popular as a result of abrupt shifts in power demand and inadequate distribution infrastructure brought on by both technical and economical limitations. Power companies have been forced by these trends to decentralize their power systems, connecting smaller renewable DG units directly to the DN at or close to the load points.

The distribution system benefits economically, environmentally, and technically from the integration of renewable energy-based DGs into a power system. BESSs have long been used to control power quality in DNs. The increasing innovation in energy density of BESS is interesting because it suggests more analytical freedom in their placement within the power system supply network to optimize the advantages of their operational capabilities. One major way to improve the energy efficiency of a DN is to deploy BESS. This study aims to provide an overview of the optimal BESS installation and operation to enhance the overall performance

of the DNs. SVCs provide reactive power injection or absorption to help sustain voltage stability in DNs. In order to prevent voltage collapse, this guarantees that voltage levels stay within allowable bounds. EV adaptations are being made worldwide in an effort to reduce pollution and combat climate change. More public EV charging stations must be made available in order to maintain this process. There will be major technical, financial, and environmental challenges as a result of the unplanned increase in EVs and their charging stations. These consequences will affect the DNs, the environment, EV users, and charging stations. To avoid the problems, EV charging and discharging at stations must be scheduled and coordinated. When used with appropriate charge/discharge control management, EVs can be used as sources of distributed energy storage and utilized to increase DN's performance and efficiency. DR is a technique that encourages users to alter their patterns of electricity usage in order to balance the demand on power systems. This can help to maintain the DNs stable and increase their efficiencies, dependability, and cost savings. DNs can apply DR in a variety of ways, including time-based rates, financial incentives, and flexible load models. DR gives users the chance to actively participate in the functioning of the electrical grid by adjusting or lowering their peak-time electricity use in response to time-based pricing or other types of monetary incentives.

In this work, sustainability of an electric power DN is defined as considering the technical, economical, and environmental benefits simultaneously as shown in **Table 1.0.1**. Absence of any one of the above three factors will make the DNs non-sustainable in the long run.

1.2. Literature review of the works done on sustainability of DNs in the recent years

Table 1.0.2 presents a concise literature review of the major works done in the recent years on the sustainability of DNs. The components of the objective function proposed in each of the cited works is analyzed on the basis of consideration of voltage profile, economic, environmental, and active power loss/demand impact factors. Consideration of different electrical components of a DN viz., PV, wind, BESS/Hydrogen energy storage system (HESS)/Capacitor, FACTS devices, EVs, Cogeneration sources, DR techniques adopted, and uncertainties are also studied and presented.

Table 1.0.1. Defining sustainability in this work			
Technical benefits	**Economic benefits**	**Environmental benefits**	**Overall sustainability**
x	x	x	x
✓	x	x	x
x	✓	x	x
x	x	✓	x
✓	✓	x	x
x	✓	✓	x
✓	x	✓	x
✓	✓	✓	✓

Table 1.0.2. A concise literature review of the major works done on the sustainability of DNs

Reference	Khasanov et al, 2023 **[1]**	javad Aliabadi and Radmehr, 2021 **[2]**	Home-Ortiz et al.,2019 **[3]**	Fathi et al.,2021 **[4]**	Ali et al., 2021 **[5]**	Gangwar et al., 2022 **[6]**	Ramadan et al.,2021 **[7]**	Boroumandfar et al., 2023 **[8]**
PV	✓	✓	✓	x	✓	✓	✓	✓
WIND	✓	✓	✓	✓	✓	✓	✓	✓
BESS/HESS/Capacitor	x	✓	✓	x	x	x	x	✓
FACTs devices	x	x	x	x	x	x	x	x
EV	x	x	x	x	x	x	x	x
Cogeneration sources	✓	x	x	x	x	x	x	x
DR	x	x	x	x	x	x	x	x
Source/Load Uncertainty	✓	✓	✓	✓	✓	✓	✓	✓
Algorithm	Artificial ecosystem-based optimization- opposite based learning (AEO-OBL)	Intelligent Crow Search Algorithm (ICSA)	Mixed Integer Canonical Program (MICP)	Improved Squirrel Search Algorithm (ISSA)	Multi-Objective Cat Swarm Optimization (MO-CSO)	Two-stage approach using Mixed Integer Linear Program (MILP) and Miner's rule	Election Optimizer Algorithm (EOA)	Flow Direction Algorithm (FDA)
Voltage Profile Factor	x	✓	x	x	✓	x	x	x
Economic Factor	x	x	✓	x	x	✓	x	✓
Environmental Factor	x	x	x	x	x	x	x	x
Active Power Loss Factor	✓	✓	✓	✓	x	✓	✓	x
DN under study	IEEE 33 and 85 bus DNs	IEEE 33 and 69 bus DNs	IEEE 69 bus DN	IEEE 33 and 69 DNs	Unbalanced IEEE 34-bus DN	IEEE 33, 141 and 115-node practical Indian DNs	IEEE 85 bus DN	IEEE 33 and 69 DNs
Goals	Minimization of power and energy losses by optimal placement of DGs	Minimization of active power losses and voltage deviation by optimal placement of DGs	Minimization of operational cost by optimal placement and sizing of DGs	Minimization of cost of power losses and increasing reliability by reconfiguration and optimal allocation of DGs	Minimization of the voltage variations in the distribution system by optimally setting the voltage control devices	Minimization of the investment and operation cost and the amount of load curtailment by optimal planning of BESS	Minimization of active power losses by optimal placement of DGs	Minimization of cost of network power loss and purchased power by optimal allocation of DGs

Table 1.0.2. A concise literature review of the major works done on the sustainability of DNs (Contd.)

Reference	Abdel-Mawgoud, et al., 2021 **[9]**	Rawat and Vadhera, 2020 **[10]**	Elkadeem et al., 2019 **[11]**	Rathore and Patidar, 2021 **[12]**	Samala and Kotapuri, 2020 **[13]**	Ahmadi et al.,2023 **[14]**	Naderipour et al., 2021 **[15]**	Yamchi et al., 2019 **[16]**
PV	✓	✓	✓	✓	✓	✓	x	✓
WIND	x	✓	✓	✓	✓	✓	✓	✓
BESS/HESS/Capacitor	✓	x	x	✓	x	x	x	✓
FACTs devices	x	x	x	x	x	x	x	x
EV	x	x	x	x	x	✓	x	x
Cogeneration sources	x	x	x	x	x	x	x	x
DR	x	x	x	x	x	x	x	x
Source/Load Uncertainty	✓	✓	✓	✓	✓	✓	✓	✓
Algorithm	Modified Henry Gas Solubility Optimization (MHGSO)	VSI–continuous power flow (CPF) based algorithm	Hybrid-Harris Hawks Optimization (HHO) - Particle Swarm Optimization (PSO)	Chaotic Particle Swarm Optimization (CPSO)	Hybrid Fuzzy Logic Control (FLC)-Ant Lion Optimizer (ALO)-PSO	Firefly Algorithm (FA)	β-chaotic Spotted Hyena Optimizer (SHO)	Multi-Objective Particle Swarm Optimization (MOPSO)
Voltage Profile Factor	x	✓	✓	x	✓	x	✓	x
Economic Factor	x	x	✓	x	✓	✓	x	✓
Environmental Factor	x	x	x	x	x	✓	x	x
Active Power Loss Factor	✓	✓	✓	✓	x	x	✓	x
DN under study	IEEE 69 bus DN	IEEE 33 and 69 DNs	IEEE 33, 69 bus and practical 94 bus DNs	IEEE 33 bus DN	IEEE 33 bus DN	IEEE 69 bus DN	IEEE 33 and 69 bus DNs	IEEE 33 bus DN
Goals	Minimization of active power loss by optimal sizing and allocation of DGs	Minimization of active power loss and enhancement of voltage stability by optimal sizing and placement of DGs	Minimization of voltage drop, *VSI*, network losses and maximization of annual profit by optimal sizing and placement of DG	Minimization of energy losses by optimal sizing and allocation of DGs	Minimization of cost of operation and voltage deviation by optimal sizing and allocation of DGs	Minimization of cost of operating costs and CO_2 emissions by optimal sizing and allocation of DGs and EV charging/discharging	Minimization of active power losses and maximization of VSI by optimal placement of DGs	Minimization of total cost and enhancement of reliability index by optimal sizing and allocation of DGs

Table 1.0.2. A concise literature review of the major works done on the sustainability of DNs (Contd.)

Reference	Nematollahi et al., 2021 **[17]**	Abid et al., 2022 **[18]**	Xu et al., 2021 **[19]**	Ullah et al., 2020 **[20]**	Wang et al., 2023 **[21]**	Davoudkhani et al.,2023 **[22]**	Pakdel and Ramezani, 2020 **[23]**	Sharma et al.,2020 **[24]**
PV	✓	✓	✓	✓	✓	✓	✓	✓
WIND	✓	✓	✓	✓	✓	✓	✓	✓
BESS/HESS/Capacitor	✓	x	x	x	✓	x	x	✓
FACTs devices	x	x	x	x	x	x	x	x
EV	x	x	x	x	x	x	x	x
Cogeneration sources	x	x	x	x	✓	x	x	x
DR	x	x	x	x	x	x	x	x
Source/Load Uncertainty	✓	✓	✓	✓	✓	✓	✓	✓
Algorithm	Lightning Attachment Procedure Optimization Algorithm (LAPO)	Artificial Hummingbird Algorithm (AHA)	Non-dominated Sorting Genetic Algorithm- II (NSGA-II)	Hybrid-Principal Component Analysis based PSO (PCA-PSO)-Gravitational Search Algorithm (GSA)	PSO	Multi-objective Salp Swarm Algorithm (MSSA)	Genetic Algorithm (GA)	NSGA-II
Voltage Profile Factor	x	✓	x	✓	x	✓	✓	x
Economic Factor	✓	✓	x	✓	✓	✓	✓	✓
Environmental Factor	x	x	x	x	x	x	x	x
Active Power Loss Factor	x	✓	✓	✓	x	✓	✓	✓
DN under study	IEEE 33 and 69 bus DNs	IEEE 33 and 69 bus DNs	IEEE 33 and 141 bus DNs	IEEE 33, 69 bus and practical 94 bus DNs	IEEE 33 and 69 DNs	IEEE 33 bus DN	IEEE 30 bus DN	IEEE 33 bus and Indian 108 bus DNs
Goals	Minimization of total cost of the system by optimal sizing and allocation of DGs	Minimization of voltage deviation, network power loss and improvement of voltage stability margin (VSM) enhancement, yearly economic savings by optimal sizing and allocation of DGs	Maximization of renewables utilization and minimization of the network losses	Maximization of techno-economic benefits and minimization of network losses by optimal sizing and placement of DGs	Minimization of the annual operation cost by optimal allocation and sizing of RES and diesel generators	Minimization of active power losses, system cost and improvement of voltage profile by optimal sizing and allocation of DGs	Minimization of active power losses, cost of conductors, capacitor banks and improvement of voltage profile by optimal sizing and allocation of DGs	Minimization of active power losses and network demand cost by optimal sizing and allocation of DGs

Table 1.0.2. A concise literature review of the major works done on the sustainability of DNs (Contd.)

Reference	Maity et al.,2020 **[25]**	Pandraju and Janamala, 2023 **[26]**	Sreenivasulu Reddy and Janamala, 2023	Janamala et al.,2023 **[28]**	Giridhar et al.,2022 **[29]**	Janamala and Radha Rani, 2022 **[30]**	Janamala and Reddy, 2021 **[31]**	Janamala, Kamal Kumar, and Pandraju, 2021 **[32]**
PV	x	✓	✓	✓	✓	✓	✓	✓
WIND	✓	x	✓	x	x	x	x	✓
BESS/HESS/Capacitor	x	x	✓	x	✓	x	✓	x
FACTs devices	x	x	x	x	✓	x	x	x
EV	x	✓	x	✓	x	x	x	✓
Cogeneration sources	x	x	x	x	x	x	x	x
DR	x	x	x	x	x	x	x	x
Source/Load Uncertainty	✓	x	x	x	x	x	x	x
Algorithm	Analytic Hierarchy Process (AHP)-Technique for Order of Preference by Similarity to Ideal Solution (TOPSIS)	Enhanced Pathfinder Algorithm (EPA)	Pathfinder Algorithm (PA)	Artificial Rabbits Optimization (ARO)	Mayfly Optimization Algorithm (MOA)	Archimedes Optimization Algorithm (ArO)	Coyote optimization algorithm (CoOA)	Future Search Algorithm (FSA)
Voltage Profile Factor	x	x	✓	✓	x	✓	✓	✓
Economic Factor	✓	x	x	x	x	x	x	x
Environmental Factor	✓	✓	✓	x	x	✓	x	✓
Active Power Loss Factor	✓	✓	✓	✓	✓	✓	✓	✓
DN under study	IEEE 33 bus DN	Indian 85 bus DN	IEEE 33 bus DN	IEEE 33 bus DN	IEEE 33 bus DN	Indian 22 and 28 bus feeder, and IEEE 85 bus DN	IEEE 33 bus DN	Indian 106 and 36-bus feeder
Goals	Maximization of reliability, operation, economics and environment impact of DNs by optimal sizing and allocation of DGs	Reduction of active power losses and emissions by PV and EV penetrations	Reduction of active power losses, emission, and voltage deviation by PV and wind penetration	Reduction of active power losses and voltage deviation by PV and EV penetration	Reduction of active power losses by PV, BESS, and D-STATCOM penetration	Reduction of active power losses, emission, and voltage deviation by PV penetration	Reduction of active power losses and voltage deviation by PV and BESS penetration	Reduction of active power losses, emission, and voltage deviation by PV, wind, and EV penetration

Table 1.0.2. A concise literature review of the major works done on the sustainability of DNs (Contd.)

Reference	Janamala, 2021 **[33]**	Gao et al., 2024 **[34]**	Dey et al. 2023 **[35]**	Yousri et al., 2024 **[36]**	Dixit et al., 2024 **[37]**	Zhang et al., 2023 **[38]**	Liu et al., 2023 **[39]**	Alikhani et al., 2023 **[40]**
PV	✓	✓	✓	✓	✓	✓	✓	✓
WIND	x	✓	✓	✓	✓	✓	✓	✓
BESS/HESS/Capacitor	x	✓	x	✓	✓	✓	x	✓
FACTs devices	x	x	x	x	x	x	x	x
EV	x	x	x	x	x	x	x	x
Cogeneration sources	x	x	x	x	x	✓	x	x
DR	x	✓	✓	✓	✓	✓	✓	✓
Source/Load Uncertainty	x	✓	x	✓	x	✓	x	✓
Algorithm	Pathfinder Algorithm (PFA)	Kullback–Leibler divergence-based DRO (KLD-DRO)	Hybrid CSA-JAYA Algorithm	Artificial hummingbird optimizer (AHO)	Differential Evolution (DE)	Multi-objective random algorithm	Deep reinforcement learning (DRL) algorithm	Enhanced Weighted Fuzzy Average (WFA) K-means clustering algorithm
Voltage Profile Factor	✓	x	✓	x	x	x	x	x
Economic Factor	x	✓	✓	x	✓	✓	✓	x
Environmental Factor	x	x	x	✓	✓	✓	x	x
Active Power Loss Factor	x	✓	✓	✓	✓	✓	✓	✓
DN under study	IEEE 33 and 69 bus systems	Practical 152-bus urban distribution	LV microgrid	Hybrid microgrid	Microgrid	Microgrid	Microgrid	33-bus Microgrid
Goals	Reduction in voltage deviation by PV penetration	Minimization of the present value of investment and operation costs over the planning period	Enhancement of the techno-economic benefits	Enhancement of the environmental benefits	Reduction of operating costs and environmental emissions	Reduction of power generation costs and environmental emissions	Improvement of efficiency and economic operation by incentive-based DR	Reduction of load factor using TOPSIS based DR algorithm

Table 1.0.2. A concise literature review of the major works done on the sustainability of DNs (Contd.)

Reference	Li et al, 2022 **[41]**	Amin et al, 2022 **[42]**	Tan et al, 2022 **[43]**	Shen et al, 2022 **[44]**	Eghbali et al, 2022 **[45]**	Lu & Zhang, 2022 **[46]**	Prajapati & Mahajan, 2022 **[47]**	Kholerdi & Ghasemi-Marzbali, 2022 **[48]**
PV	✓	✓	✓	✓	✓	✓	✓	X
WIND	✓	X	X	✓	✓	✓	✓	X
BESS/HESS/Capacitor	X	X	X	✓	✓	✓	X	X
FACTs devices	X	X	X	X	X	X	X	X
EV	X	X	X	X	X	X	X	X
Cogeneration sources	X	X	✓	✓	✓	X	X	X
DR	✓	✓	✓	✓	✓	✓	✓	✓
Source/Load Uncertainty	✓	X	✓	X	✓	X	✓	X
Algorithm	Jaya algorithm and interior point method (Jaya- IPM)	Cloud-based AI framework	Two-stage robust optimization framework	Multi-objective optimization model based on adaptive dynamic weights	Mixed-integer linear programming (MILP)	NSGA-II algorithm	k-means clustering algorithm and Monte Carlo simulation	Lagrange multiplier method
Voltage Profile Factor	X	X	X	X	X	X	✓	X
Economic Factor	✓	✓	✓	✓	✓	✓	✓	✓
Environmental Factor	X	X	X	✓	X	X	X	X
Active Power Loss Factor	✓	✓	✓	✓	✓	✓	✓	✓
DN under study	Microgrid	Real-time UK based DN	Integrated electricity and heat DNs	Multi-energy microgrid	Multi-energy microgrid	Residential DNs	Residential DNs	Cement plant connected Iranian DN
Goals	Optimal scheduling and economic operation of RTP-DR-driven microgrids	An intelligent Cloud-based DR for minimizing peak demand and costs	Maximize the DN profit by price-based integrated DR	Smoothening of fluctuations caused due to the intermittent nature of RES in DR driven multi-microgrid with a target to improve environmental and economic benefits.	DR framework for optimal day-ahead economic operation of microgrids	Dynamic electricity pricing mechanism and maximization of economic benefits using Nash-Stackelberg model-based DR	The impact of various DR programs on the technical and economic characteristics of the load profile is investigated.	The impact of three types of DR, viz., ToU, DB, and A/S, on annual load consumption and profit maximization of cement plants

Table 1.0.2. A concise literature review of the major works done on the sustainability of DNs (Contd.)

Reference	Harsh & Das, 2021 **[49]**	Chen et al, 2023 **[50]**	Gupta, Maulik, Das, & Singh, 2022 **[51]**	Astriani, Shafiullah & Shahnia, 2021 **[52]**	Wang et al, 2021 **[53]**	Nourollahi, Salyani, Zare, & Mohammadi-Ivatloo, 2021 **[54]**	Nayak, Maulik, & Das, 2021 **[55]**	Mimica, Dominkovi, Capuder, & Krajai, 2021 **[56]**
PV	✓	✓	✓	✓	✓	✓	✓	✓
WIND	✓	X	✓	✓	✓	✓	✓	✓
BESS/HESS/Capacitor	✓	✓	✓	X	✓	✓	X	X
FACTs devices	X	X	X	X	X	X	X	X
EV	X	✓	✓	X	X	X	X	X
Cogeneration sources	X	X	X	X	✓	✓	X	X
DR	✓	✓	✓	✓	✓	✓	✓	✓
Source/Load Uncertainty	✓	✓	X	X	✓	✓	✓	X
Algorithm	Hong's (2m+1) point estimation method (PEM)	Gap theory-based population-based multi-objective state transition	Hong's 2 m point estimate method	Genetic Algorithm (GA) solver	ε-constrained technique using fuzzy approach	Hybrid stochastic-robust optimization (HSRO)	Fuzzy dynamic programming (DP) - Particle swarm optimization (PSO)	Simulation model
Voltage Profile Factor	✓	X	X	X	X	X	X	✓
Economic Factor	✓	✓	✓	✓	✓	✓	✓	✓
Environmental Factor	X	X	X	X	X	X	✓	X
Active Power Loss Factor	✓	✓	✓	✓	✓	X	✓	X
DN under study	33-bus microgrid	IEEE 33 bus DN	33-bus microgrid	Microgrid	Residential DNs	Modified IEEE 33-bus microgrid	33 node test system	Kvarner archipelago DN
Goals	The techno-economic benefit of DN by incentive-based DR program	Information gap-based coordinated DR scheme for economic benefit and load shaving of DN	Economic and efficient operation of microgrid with incentive-based DR program	DR scheme for accelerated payback of the investment cost of a microgrid	Interval-based DR approach considering uncertainty for economic operation	Maximization of economic benefits of microgrid implementing interruptible DR program	Incentive based DR for maximizing economic and environmental benefits	Day-ahead market price-differential-based DR program for a smart island archipelago

Table 1.0.2. A concise literature review of the major works done on the sustainability of DNs (Contd.)

Goals	DN under study	Active Power Loss Factor	Environmental Factor	Economic Factor	Voltage Profile Factor	Algorithm	Source/Load Uncertainty	DR	Cogeneration sources	EV	FACTs devices	BESS/HESS/Capacitor	WIND	PV	Reference
Novel hybrid real-time incentive and RTP-based DR program for maximizing economic benefits	Chinese DN	X	X	✓	X	Three-level Stackelberg game-based distributed model	X	✓	X	X	X	X	✓	✓	Xu et al, 2021 **[57]**
RTP-based DR scheme for reducing DN energy losses and cost	Modified IEEE 33 bus system	✓	X	✓	X	k-Means algorithm for voltage sensitivity factor (VSF)-based peer	X	X	X	X	X	✓	X	✓	Tiwari, Jha, & Pindoriya, 2024 **[58]**
Integrated DR program for minimizing cost and environmental pollution of DNs	IEEE 13 bus, IEEE 33 bus, and IEEE 123	X	✓	✓	X	Multi-agent deep reinforcement learning method (MADRL)	X	X	✓	✓	X	✓	✓	✓	Khodadadi et. al., 2024 **[59]**
DR scheme for improving the cost effectiveness of a microgrid	Microgrid	X	X	✓	X	Mixed-integer linear programming (MILP)	X	X	X	X	X	✓	✓	✓	Seyednouri et al, 2024 **[60]**
Risk-constrained stochastic scheduling for maximizing economic and environmental benefits	Energy hub	X	✓	✓	X	Slime Mold Algorithm (SMA)	✓	✓	✓	✓	X	X	✓	✓	Yang, Wu, Li, & Fars, 2024 **[61]**
Hierarchical optimal planning in DR-driven DNs for minimizing operating cost and improvement of environmental benefits	IEEE 33 bus DN	✓	X	✓	X	Improved beluga whale optimization algorithm (IBWO)	✓	✓	X	X	X	X	✓	✓	Li et al, 2024 **[62]**
Application of a novel DR scheme for optimal operation of islanded and grid-connected microgrids	Microgrids	X	X	✓	X	Mixed-logic dynamic (MLD) framework	✓	✓	X	X	X	✓	✓	X	Abdelghany, Mariani, Liuzza, & Glielmo, 2024 **[63]**
Energy Management scheme for Internet of Things and Machine Learning driven DR program for smart grid	Smart Grid	✓	X	X	X	Energy Management Model using Machine Learning (EMM-ML)	✓	✓	X	X	X	✓	✓	✓	Ahmad et al, 2024 **[64]**

Table 1.0.2. A concise literature review of the major works done on the sustainability of DNs (Contd.)

Reference	Ashok Babu et al, 2024 **[65]**	Meng et al, 2024 **[66]**	Saxena, Kumar, & Nangia, 2024 **[67]**	Elshahed et al., 2024 **[68]**	Noori et al., 2021 **[69]**	Hardi et al., 2022 **[70]**	Amirrezai, Rezaie, & Goetz, 2023 **[71]**	Rakočević, Ćalasan, &. Abdel Aleem, 2021 **[72]**
PV	✓	✓	✓	✓	X	X	✓	✓
WIND	✓	✓	✓	X	X	X	X	X
BESS/HESS/Capacitor	✓	✓	✓	X	X	X	X	X
FACTs devices	X	X	X	✓	✓	✓	✓	✓
EV	X	✓	X	X	X	X	X	X
Cogeneration sources	X	X	X	X	X	X	X	X
DR	✓	✓	✓	X	X	X	X	X
Source/Load Uncertainty	✓	✓	✓	X	X	X	X	X
Algorithm	Deep Learning approach	Bi-level optimization strategy	Multilevel particle swarm optimization (MPSO)	Artificial rabbits' optimization algorithm (AROA)	Whale Optimization Algorithm (WOA)	Alternative transient program (ATP) software	Whale Optimization Algorithm (WOA)	Mixed-integer non-linear programming (MILP) and BONMIN embedded General Algebraic Modeling System
Voltage Profile Factor	✓	X	X	✓	✓	✓	✓	✓
Economic Factor	X	✓	X	X	X	X	✓	X
Environmental Factor	X	X	✓	X	X	X	X	X
Active Power Loss Factor	X	X	X	✓	✓	X	X	✓
DN under study	Microgrid	IEEE 33 bus DN	IEEE 33 bus DN	IEEE 33 bus DN	IEEE 33 and 59 bus DNs	IEEE 13 node DN	IEEE 13, 22, 33, and 69 bus DNs	IEEE 33 bus DN
Goals	Deep Learning approach for optimal operation of DR-driven DNs	Hybrid DR scheme for profit maximization of EV retailers and DR participants	DR scheme for optimal utilization of RES and reduction of CO_2 emission	Minimization of active power loss and voltage deviation	Minimization of active power loss and improvement of voltage profile	Mitigation of voltage sag of DNs	Enhancement of voltage profile and economic factor due to lower penalty costs by power factor improvement	Minimization of active power loss and improvement of voltage profile

Table 1.0.2. A concise literature review of the major works done on the sustainability of DNs (Contd.)

Reference	Galvani et al., 2021 **[73]**	Delghavi & Pashaei Choboghloo, 2021	Okelola et al. 2021 **[75]**	Yuvaraj et al. 2021 **[76]**	Moufid et al. 2022 **[77]**	Roy, Chatterjee, and Bhattacharya, 2023 **[78]**	Khan et al. 2022 **[79]**	Venkatesan et. al., 2021 **[80]**
PV	✓	✓	✓	✓	✓	✓	✓	✓
WIND	X	✓	X	✓	X	X	X	✓
BESS/HESS/Capacitor	X	X	X	X	X	X	X	✓
FACTs devices	X	X	X	✓	X	X	X	X
EV	✓	✓	✓	✓	✓	✓	✓	✓
Cogeneration sources	X	X	X	X	X	X	X	X
DR	X	X	X	X	X	X	X	X
Source/Load Uncertainty	X	X	X	X	X	X	X	X
Algorithm	Multi-objective biogeography-based optimization (MOBBO)	PSCAD/EMTDC software	Bat Algorithm (BA)	Blockchain technology and Bat Algorithm (BA)	MATLAB/Simulink Modelling	PSCAD/EMTDC platform	Improved bacterial search algorithm (IBFA)	Loss sensitivity factor (LSF) based particle swarm optimization (PSO)
Voltage Profile Factor	✓	✓	✓	✓	✓	✓	✓	✓
Economic Factor	X	X	X	X	X	X	X	X
Environmental Factor	X	X	X	X	X	X	X	X
Active Power Loss Factor	✓	X	✓	✓	X	X	✓	✓
DN under study	IEEE 57 bus DN	two-unit test DN	IEEE 33 bus and a Nigerian Ayepe 34-bus DN	IEEE 33 bus DN	Model test DN	Model HV DN	IEEE 33 bus DN	An e Indian Utility Power System (IUPS) at Chennai, India
Goals	Minimization of active power loss and voltage deviation	Mitigation of voltage sag of DNs	Maximization of voltage stability index and minimization of active power loss	Mitigation of voltage regulation and active power loss	Improvement of power quality by voltage sag mitigation	Improvement of power quality by voltage profile improvement	Minimization of active power losses and improvement of voltage stability	Voltage control and active power loss minimization

Table 1.0.2. A concise literature review of the major works done on the sustainability of DNs (Contd.)

Reference	Eid et al., 2022 **[81]**	Vimlesh, Mukherjee, & Singh **[82]**	Shalchi, Mozafari, & Firouz, 2021 **[83]**
PV	✓	✓	✓
WIND	✓	✓	✓
BESS/HESS/Capacitor	✓	✓	X
FACTs devices	X	X	X
EV	✓	✓	✓
Cogeneration sources	X	X	X
DR	X	X	X
Source/Load Uncertainty	X	X	✓
Algorithm	Bald Eagle Search algorithm (BESA)	Hybrid genetic algorithm (GA) and Monte Carlo simulation (MCS)	GA
Voltage Profile Factor	✓	✓	✓
Economic Factor	X	X	✓
Environmental Factor	X	X	X
Active Power Loss Factor	✓	✓	✓
DN under study	IEEE 33 and 118 bus DN	75 bus DN	IEEE 33 and 69 bus DN
Goals	Minimization of active power losses and mitigation of voltage fluctuation	Enhancement of voltage profile and network power factor improvement	Enhancement of voltage profile, economic factor, and active power loss reduction

1.3. Motivation and contribution of the work done

Most of the research works cited in **Table 1.0.2** propose a single-objective or bi-objective function with any two of the four components of objective as shown. The references **[11]**, **[18]**, **[20]**, **[22]**, **[23]**, **[35]**, **[47]**, and **[49]** have considered voltage profile improvement, economic benefits, and active power losses as the components of the objective function. Likewise, the references **[25]**, **[37], [38]**, **[44]**, and **[55]** have considered the economic benefit, environmental benefit, and active power loss reduction as the components of the objective function. The references **[27]**, **[30]**, and **[32]** have considered the technical benefit, environmental benefit, and active power loss reduction as the components of the objective function. But none of the above works considers the simultaneous voltage profile and economic and environmental benefits of radial networks, which are the three key determinants of sustainability.

This work considers DGs based on renewable energy sources, viz. PV and wind, and their role in enhancing the sustainability of DNs. The uncertain nature of PV and wind is modelled using Beta and Weibull probability distribution functions in some of the case studies. The hourly variation of solar irradiance by geographical modelling for the location, Jammu and Kashmir, India, is explored, and an estimation of the maximum number of PV modules required for DG installation is provided for different seasons in some of the case studies to make the system more realistic and practical.

This work explores the effectiveness of integrating BESS and SVCs with DNs in enhancing the technical, economic, and environmental benefits of DNs. The BESS reduces the intermittency of renewable energy sources, while SVC improves the voltage stability of DNs.

This work explores the potentiality of EVs in enhancing the technical, economic, and environmental benefits of DNs. The traffic at the parking lot with increasing EV penetration level and the charging/discharging modes and prices of EVs based on incentives provided by aggregators are analyzed.

This work considers incentive-based DR based on price elasticity, where a day-averaged (average of 24 hours) objective function is formulated that considers the simultaneous enhancement of day-averaged technical, economic, and environmental benefits of DNs while considering exponential load modeling with uncertainty and network load curtailment/shifting due to DR.

The effectiveness of DN's sustainability is tested on both IEEE test networks and real-time networks. The test networks considered are IEEE 33, 69, 85, and 141 bus systems. A real-time

13-bus substation DN situated in Maharashtra, India, is considered to validate some of the case studies practically.

The entire work has been simulated in MATLAB 2014b using the MATPOWER v7.1 power flow tool extension, which is an open-source tool for performing power system optimizations and simulations. The power flow study is undertaken using the power summation method.

The problem-specific algorithms in comparison, viz., PSO, PSO based on linearly decreasing inertia weight (LPSO), randomized inertia weight PSO (RPSO), PSO based on success rate (PSO-SR), the Cuckoo Search algorithm (CSA), Arithmetic Optimizer algorithm (AOA) algorithm, Aquila Optimizer algorithm (AQO), Coati Optimizer algorithm (COA), and Jaya algorithm (JAYA), are applied in the present work. The effectiveness of the comparing algorithms has been tested through statistical analysis conducted using the box-plot, normality, ANOVA, and post-hoc tests.

1.4. An overview of the evolutionary-computing algorithms under study

Table 1.0.3. provides an overview of the different evolutionary-computing algorithms applied in this work.

Table 1.0.3. An overview of the evolutionary-computing algorithms under study

Algorithm	Authored by	Salient Features / Phases	References
PSO	Kennedy, J. and Eberhart, R., 1995	It performs problem-solving by utilizing a population of candidate solutions, referred to as particles, and controlling their position and velocity within the search space.	[84]
LPSO	Bouhouras et al. 2016 and Kumar et al., 2014	This strategy enhances the efficiency and performance of the PSO technique by introducing a variable weight factor that changes with every iteration between its upper and lower limits. The upper and lower limits of the weight factor are kept at 1 and 0.1, respectively.	[85], [86]
RPSO	Kumar, Raja, and Jerome, 2016	It makes use of each particle's best position found so far in order to update its velocity and assigns a weight factor randomly varied between 0.5 and 1.	[87]
PSO-SR	Immanuel Selvakumar and Thanushkodi, 2007	In this method, the weight factor in the PSO algorithm is divided into two different parts: the cognitive coefficient, which accelerates the particle toward the finest position, and the cognitive component, which accelerates the particle away from the worst position. The two factors are varied in steps of 0.05, such as, the sum total of them is 2.	[88]

CSA	Yang and Deb, 2010 Basu and Chowdhury, 2013	The CSA is a metaheuristic optimization technique that solves numerical optimization problems by utilizing cuckoo breeding behavior. The method is based on the fact that certain species of cuckoos are brood parasites, meaning they lay their eggs in other birds' nests. The search pattern of the host nests by the cuckoos occurs in the Lévy flight pattern, which is a random walk punctuated by a sudden ninety-degree turn. The Lévy flight step size is taken as 1. If the host bird discovers that the eggs are not of its own, then it will either throw away the eggs or abandon the nest and build it elsewhere. The probability of alien egg discovery by the host bird is varied between 0 and 1.	[89], [90]
AQO	Abualigah, Y, Yousri D, et al, 2021	The natural activities of Aquila throughout the prey-catching process serves as the model for this algorithm. Four methods are thus used to represent the optimization process of the algorithm: swooping by walk and grab prey; contour flight with short glide attack for exploring within a diverge search space; low flight with slow descent attack for exploiting within a converge search space; and high soar with vertical stoop for selecting the search space.	[91]
AOA	Abualigah, Y, Diabat A, et al, 2021	It is a meta-heuristic method that utilizes the distribution behavior of the main arithmetic operators in mathematics, including addition, subtraction, multiplication, and division. AOA is mathematically modeled and implemented to perform the optimization processes in a wide range of search spaces. It has two phases, the exploration phase (multiplication and division operation) and the exploitation phase (addition and subtraction operation).	[92]
COA	Dehghani, M. et al., 2023	Its purpose is to replicate coatis' natural habits. The primary sources of inspiration for COA are coati attacks and hunting, as well as the way coatis flee from predators. The exploration and exploitation phases are its two stages, just like those of AOA.	[93]
JAYA	Rao, R., 2016	The concept behind this algorithm is that the solution to a problem should move away from the worst solution and instead progress toward the best one. This method does not require any control parameters unique to it; it simply needs the standard control parameters.	[94]

1.5. An overview of the network bus systems under study

Table 1.0.4. provides an overview of the different electrical power bus systems applied in this work.

Table 1.0.4. An overview of the network bus systems under study

Bus System	Authors	Salient Features	References
13 bus substation DN, Maharashtra, India	Markad, P., and D. A. Thosar, 2020	The substation, situated at Maharashtra, India, comprises two 50 MVA transformers that step down to 33 kV when supplied with 132 kV voltage. One of the thirteen 33 kV buses in the distribution system used for this investigation is a slack bus that supplies energy to different distribution substations. Through twelve different 33/11 kV substations, which are referred to as 33 kV buses, electrical energy is provided to a variety of users, including agriculture, commercial, residential, and industrial ones. The outgoing substation bus receives direct feeds of the electrical energy generated by the wind farm that has been erected close to this substation. The base active power loss is 3010.16 kW.	[95]
IEEE 33	Dolatabadi, S.H., et al, 2020 Baran, M.E. & Wu, F.F., 1989	There are 33 buses, 32 fixed and 5 switchable lines, and no reactive power balancing devices in the design of the IEEE 33 bus distribution system. The base active power loss is 201.89 kW.	[96], [97]
IEEE 69	Das D., 2008	The nominal voltage of the 69-bus distribution system is 12.66 kV, and its base apparent power is 10 MVA. This system consists of 69 nodes and 73 branches, including tie-lines 69–73. Under typical operating conditions, all five of these tie-lines remain open. The base power loss of the system is 224.59 KW.	[98]
IEEE 85	Das D., Kothari, D.P. & Kalam, A., 1995	The nominal base apparent power and voltages are 100 MVA and 11 kV, respectively. The network has only one generator connected at bus 1. The total base real power loss is 316.14 kW.	[99]
IEEE 141	Khodr, H.M., et al, 2008	The nominal voltage is 12.47 kV, and the reactive and active loads are 7.375 MVAr and 11.9029 MW. The loads have an average lagged power factor of 0.85. To provide active power to the load in this instance, the network incorporated PV, wind, and conventional generators. There are five PV generators connected at the buses 50, 60, 70, 80, and 90. Two wind turbines are located at the buses 106 and 118. The conventional generator unit is located at bus 136. All generators are considered to have a 1 MW capacity for simplicity. The total base real power loss is 629.06 kW.	[100]

1.6. Statistical methods applied for result analysis

The following statistical methods are applied for analyzing the results obtained from different case-studies using various evolutionary computational algorithms.

Box Plot - A box plot (also known as a box and whisker plot) employs boxes and lines to represent the distributions of one or more groups of numerical data. The box limits show the range of the central 50% of the data, with a central line representing the median value.

Normality Tests - A normality test is a statistical process that examines whether a dataset has a normal distribution. A normal distribution is a bell-shaped curve that is symmetric about the mean. In this work, the Kolmogorov-Smirnov and Shapiro-Wilk tests for normality are performed to ensure that the sample-data obtained from different algorithms for a given number of trials do not follow normal distribution curve (Normality reject).

ANOVA Tests - The Analysis of Variance (ANOVA) test is a statistical tool for comparing the means of two or more groups. It determines whether the means are statistically different. The Kruskal-Wallis H test (also known as the "one-way ANOVA on ranks") is a rank-based nonparametric test has been used in this work for different case-studies to evaluate whether there are statistically significant differences between two or more groups of an independent variable. When a group's mean rank exceeds the general average rank, its observation values tend to be higher than those of the other groups. The post-hoc Dunn test is done for pairwise comparison of the algorithms under study, when the Kruskal-Wallis test is positive.

1.7.Organization of the work

This work is divided into six chapters. **Chapter 1** describes the term sustainability of DNs, the extant literature of the work done in the recent years, motivation, contribution, overview of evolutionary computing techniques, bus systems under study, and organization of the work done. **Chapter 2** presents the impact of PV and wind-based DGs on the sustainability of DNs. **Chapter 3** explores the potential of BESS and SVCs in enhancing the sustainability of different types of DNs. The potentiality of EVs in enhancing the technical, economic, and environmental benefits of DNs is investigated in **Chapter 4**. The traffic at the parking lot with increasing EV penetration level and the charging/discharging modes and prices of EVs based on incentives provided by aggregators are analyzed. **Chapter 5** presents a demand-price elasticity-driven DR program to investigate the load curtailment and shifting patterns of different types of DNs. Further, the impact of the program in enhancing the technical, economic, and environmental indices of the DNs is analyzed. The crux of the work done and its scope in the future is concluded in **Chapter 6**.

CHAPTER 2: Impact of DGs on DN sustainability

This chapter presents the impact of DGs on the technical, economic, and environmental impacts of DNs. The DGs considered in the proposed work are PV and wind based DGs.

2.1. Introduction

Distributed generation (DG) is the term used to describe the electricity produced by numerous small, dispersed energy sources. Being located close to the end consumer is the main benefit of distributed generation versus conventional, centralized energy generation.

A schematic diagram of a DG is presented in **Fig. 2.0.1.**

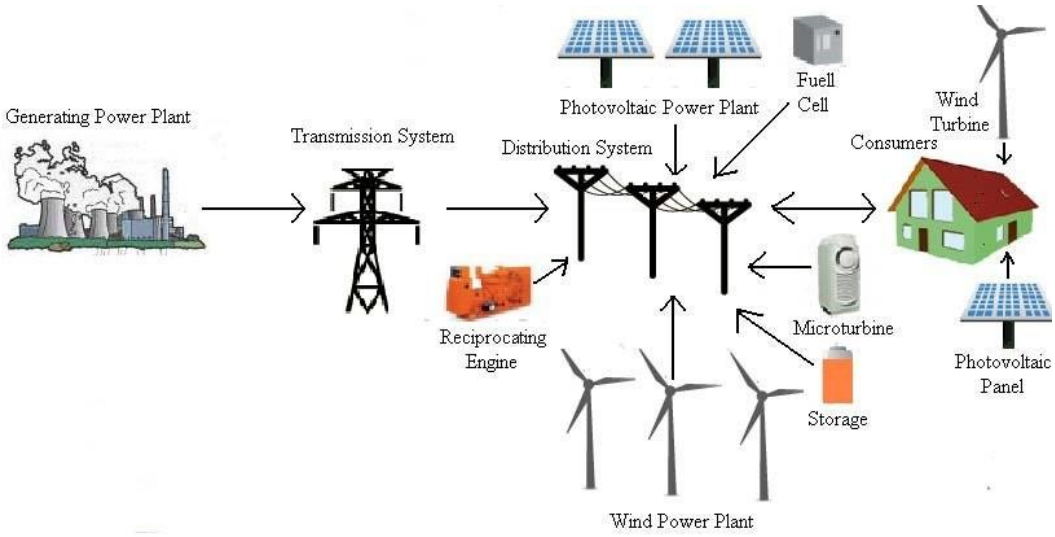

Fig. 2.0.1. A schematic diagram of distributed generation system

A summary of some common advantages and disadvantages of the DG is given below:

The following are a few **advantages** of DGs:

- *Decreased losses in transmission and distribution*

There are always losses involved when power is produced centrally and then sent over large distances to the final customer. Transmission and distribution losses are typically significantly reduced with distributed generation since electricity is produced near its intended applications.

- *Enhanced grid security and stability*

By offering backup power during a grid outage, distributed generation can contribute to the stability of the electrical system. Furthermore, distributed generation can offer energy security during emergencies or natural disasters.

- *Reduced impact on the environment*

Because DGs use renewable energy, it usually has a smaller environmental impact than traditional energy generation.

The following are a few **drawbacks** of DGs:

- *Requirement of increased power system protection*

One drawback of distributed generation is that it requires more protection than conventional distribution systems to handle power exchanges.

- *Complexity of signaling for resource deployment*

The process of signaling to deploy resources gets very complex.

- *Challenges in relationships & revenue contracts*

Establishing relationships with stake-holders and revenue contracts becomes challenging.

2.2. Types of DGs

PV based DG

One of the most popular kinds of DG systems is solar PV systems. Sunlight is converted into electricity using solar photovoltaic panels, which can power buildings and commercial establishments.

Wind based DG

Another kind of DG system that can be utilized to produce power is a wind turbine. In order to generate power, wind turbines use blades which rotate when wind flows.

Microturbines

These small turbines have the capacity to produce electricity. Microturbines can power buildings and commercial spaces and they are usually powered by biogas or natural gas.

Combined Heat and Power (CHP) systems are made to use a single fuel source to produce both heat and power. Because CHP systems run on waste heat, they are generally more efficient than conventional energy generation.

Fuel Cells Fired by Natural Gas

One type of DG system that uses natural gas to produce electricity is the natural-gas-fired fuel cell. In general, fuel cells are low-impact on the environment and highly efficient.

Generators for emergency backup

Usually, in the event of a power cut, residences and businesses are powered by emergency backup generators. Fuel options for backup generators include diesel, propane, and natural gas.

In this work, PV solar and wind-based DGs are considered for improvement of technical, economic, and environmental benefits of radial DNs.

2.3.Components and calculation of power output of PV based DG

In this sub-section, the components and power output of PV based DGs are discussed.

2.3.1. Components of PV based DG

The solar PV array, a charge controller, a battery bank, an inverter, and a utility meter are the five main parts of a solar photovoltaic system. The efficiency of the solar panels is dependent on the proper installation of each of these components.

A battery bank and charge controller are optional. Although these two elements aid in the storage and better use of the electricity generated, they can also increase the overall cost of the solar installation.

A schematic diagram of PV based DG system is presented in **Fig. 2.0.2.**

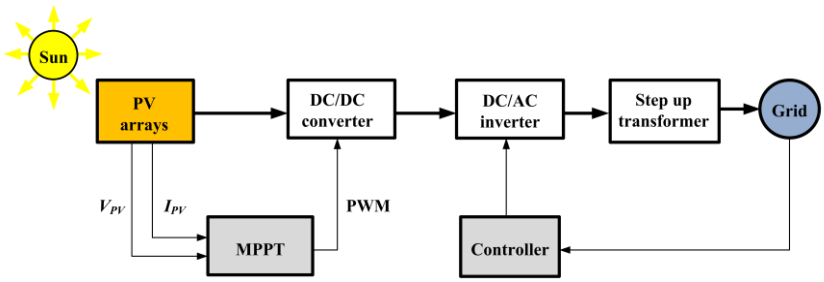

Fig. 2.0.2. A schematic diagram of PV based distributed generation system

2.3.1.1.Solar PV cell, module, and array

The cells, module, and array are the three separate components that constitutes a solar panel. The main component of a panel that aids in the photovoltaic system's processing of solar energy absorption is the solar cell. The solar cells are required in order to obtain a significant quantity of energy.

The solar cells are housed within the PV module, or the actual solar panel. This is the positioning of the solar cells in order to get the desired voltage or energy output in kilowatts.

The PV array, on the other hand, is made up of solar PV modules or panels that are connected to one another in series and parallel combinations in order to generate the necessary voltage and transfer it to the panel.

All things considered, all of these components serve a purpose, and it can also be said that the three components are reliant on one another for their operation. They are all beneficial and essential to the processes of absorbing solar irradiation and producing electricity.

2.3.1.2.Charge controller

To prevent electrical overload, overcharging, and perhaps overvoltage, a charge controller, charge regulator, or battery regulator restricts the rate at which electric current is supplied to or taken out of electric batteries. This avoids situations that could endanger safety and lower battery performance or lifespan. In order to save battery life, it may also prevent a battery from being fully depleted (also known as "deep discharging") or carry out controlled discharges, depending on the battery technology. The phrases "charge controller" and "charge regulator" can be used to describe a device that is standalone or to describe control circuitry that is built into a battery pack, equipment that runs on batteries, or battery charger.

2.3.1.3.Battery bank

A battery bank is made up of multiple batteries connected in parallel and series to create an energy storage bank. This bank stores solar energy from solar panels and uses a DC-AC inverter to supply loads with electricity. A solar power system's main component for energy storage is

a battery bank. Naturally, a solar power system's battery is charged by the sun during the day and discharged at night or on cloudy days. The battery functions as a solar energy storage device, storing solar energy during the day and supplying power during the night or during rainy conditions. As a result, solar batteries are constantly fully charged and completely drained.

2.3.1.4. Inverter

The variable DC output of a photovoltaic solar panel is converted into a utility frequency AC by a solar inverter, also known as a photovoltaic (PV) inverter. This AC can then be fed into a commercial electrical grid or used by a local off-grid electrical network. It is a crucial balance of system (BOS) component that permits the use of standard AC-powered devices in photovoltaic systems. For usage with photovoltaic arrays, solar power inverters offer specific features including maximum power point tracking and anti-islanding prevention.

2.3.1.5. Utility meter

PV system meters are an essential tool used to monitor and track energy usage and production. In an off-grid system, battery monitors are used to measure the state of the battery, which is necessary for optimizing battery life and determining when the batteries need to be charged or when charging is completed.

For grid-tied systems, meters are used to record PV production and home energy consumption. In some cases, the utility will require a separate meter to track PV production.

2.3.2. Calculation of power output of a PV based DG

This section explains the procedure of calculating the deterministic and probabilistic techniques for calculating the output of PV based DG.

2.3.2.1. Deterministic power output of PV array

The power output of a PV array can be calculated as a function of solar irradiation using the formulae below **[101]**.

$$PV_{out} = N_S \times N_P \times FF \times V_{oc} \times I_{sc} \quad (2.1)$$

N_S and N_P are the numbers of PV modules connected in series or parallel. **Equations 2.2** and **2.3** denote the open-circuit voltage and short-circuit current, respectively, as V_{oc} and I_{sc}. FF is the fill factor given in **equation 2.4**.

The open-circuit voltage of a solar cell is given by

$$V_{oc} = \frac{V_{Noc}}{1+c_2 \ln\left(\frac{G_N}{G}\right)} \cdot \left(\frac{T_N}{T_a}\right)^{c_1} \quad (2.2)$$

V_{Noc} is the nominal module open-circuit voltage. $G_N$is the nominal solar irradiance. $T_a$and T_N are the actual and nominal temperature of the module.

The short-circuit current of the solar cell is given by

$$I_{sc} = I_{Nsc}.\left(\frac{G_N}{G}\right)^{c_3} \tag{2.3}$$

I_{Nsc} is the module short circuit current.

$$FF = \left(1 - \frac{G_N}{\left(\frac{V_{oc}}{I_{sc}}\right)}\right).\left(\frac{\frac{V_{oc}}{\left(\frac{nKT}{q}\right)} - \ln\left(\frac{V_{oc}}{\frac{nKT}{q}} + 0.72\right)}{1 + \frac{V_{oc}}{\frac{nKT}{q}}}\right) \tag{2.4}$$

n, K and q represent the density factor, Boltzmann constant and charge of an electron respectively. c_1, c_2 and c_3 are constants.

If the solar irradiance, considered for a particular place and time, is not made to vary considering uncertain factors like weather changes, dust accumulation on the solar panels, etc., then, the output power estimation of the PV array is said to be deterministic.

2.3.2.2. Probabilistic power output of PV array

The probabilistic beta distribution function is used to represent the availability of solar irradiance **[101]** due to the unpredictable factors such as weather, the collection of dust on the panels, and other factors. The following equation can be used to describe the probability distribution function of the solar irradiance:

$$F_{PV}(G) = \begin{cases} \frac{\Gamma(\alpha+\beta)}{\Gamma(\alpha)+\Gamma(\beta)} \times G^{\alpha-1} \times (1-G)^{\beta-1} & if\ 0 \le G \le 1,\ 0 \le \alpha, \beta \\ 0 & otherwise \end{cases} \tag{2.5}$$

The parameters of $F_{PV}(G)$ are denoted by α and β respectively. These parameters are computed by making use of the mean (μ_s) and standard deviation (σ_s) of the solar irradiance. These are expressed in the following equations.

$$\beta = (1 - \mu_s) \times \left(\frac{\mu_s \times (1-\mu_s)}{{\sigma_s}^2}\right) - 1 \tag{2.6}$$

$$\sigma_s = (1 - \mu_s) \times \left(\frac{\mu_s \times \beta}{(1-\mu_s)}\right) - 1 \tag{2.7}$$

2.4. Components and calculation of power output of wind-based DG

The sun's heating of the uneven earth's surface results in a differential pressure that drives air to flow from high pressure areas to low pressure areas, which causes wind. Thus, it is possible to classify wind energy as a type of solar energy. The basic idea behind how a wind turbine operates is that, unlike a fan, which creates wind by using energy, a wind turbine creates electricity by utilizing wind. Wind rotates a turbine's propeller-like blades around a rotor, which turns a generator, producing power.

In this sub-section, the components and power output of wind-based DGs are discussed.
A schematic diagram of wind-based DG system is presented in **Fig. 2.0.3**.

2.4.1. Components of wind-based DG

A wind turbine has numerous smaller pieces in addition to five larger ones. The foundation, tower, nacelle, generator, rotor and hub (with three blades), and other parts are the essential components.

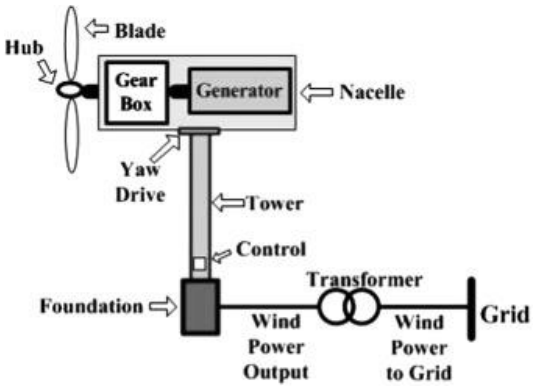

Fig. 2.0.3. A schematic diagram of wind based distributed generation system

2.4.1.1. Wind turbine foundation

The wind turbine's basement is where the entire weight of the machine will act upon. Normally, it is unseen and lies beneath the surface.
For onshore turbines, the base is buried and covered in dirt, making it inconspicuous. The entire turbine and the forces operating on it must be supported by this substantial, heavy concrete structural block.
The base of the offshore turbines is hidden underwater. Although the base of the offshore turbines located far from the sea floats, it has sufficient mass to support and sustain the weight of the turbine as well as any forces applied to it.

2.4.1.2. Wind energy tower

The majority of modern wind turbines have round steel tubes for their towers. As a general rule, the height of a turbine tower equals the diameter of the circle its spinning blades form. In general, turbines that are taller are more vulnerable to strong winds. It serves as the rotor and nacelle's supporting structure.

2.4.1.3. Wind turbine rotor and hub

The section of the turbine that rotates is called the rotor, and it has three blades with a hub in the middle that connects them.

A turbine does not always contain three blades, despite being the most frequent. However, there are benefits to the three-blade rotor, namely maximum efficiency. Because these are hollow and composed of a lightweight, durable composite material, the blades lack strength. The trend is to make them lighter, more robust, and larger (for more power). The blades are formed like an air foil, or an airplane's wings, for aerodynamic purposes. These possess a twist connecting their root and tip, and are not flat. The blade can rotate up to 90° around its axis. This movement is called pitch.

A wind turbine's nacelle is an intricate electromechanical system made up of numerous precise parts that work together as a unit. The generator and turbine shaft, which use a gearbox to transport wind energy to the generator, are important components of a turbine. The gearbox, which is located on the cable car, is a crucial component of the wind turbine.

The turbine's rotor must rotate in relation to the tower because it must follow the wind and change its direction based on its direction. The nacelle and rotor revolve around the tower axis in a motion known as yaw motion.

2.4.2. Calculation of power output of wind-based DG

The rotor blades of a wind turbine, which function similarly to an airplane wing or a helicopter rotor blade, use aerodynamic force to convert wind energy into electrical power. The air pressure on one side of the blade drops as the wind blows across it. Both lift and drag forces are produced by the difference in air pressure on the two sides of the blade. The rotor rotates because the lift force is greater than the drag force. If the generator is a direct-drive turbine, the rotor is connected to it directly. If not, the connection is made through a gearbox, comprising a shaft and set of gear, that accelerates spinning and makes the generator smaller in size. Electricity is produced by this conversion of aerodynamic force into a generator's rotation.

2.4.2.1. Modelling of probabilistic nature of wind velocity and power output of wind turbine

To determine the cost of wind-based DG, a probability density function must be employed to describe the intermittent nature of wind. The power output of the wind turbine can be approximated using this function. There is a possibility of an overestimation (excess) or underestimation (shortage) of the predicted capacity. The power output of a wind turbine must be estimated using a probability density function that describes the wind's unpredictability. The uncertain character of wind can be modelled as a Weibull distribution function **[102]**, which can be expressed as follows:

$$f_{WIND}(v) = \left(\frac{sh}{sc}\right)\left(\frac{v}{sc}\right)^{(v-1)}(e)^{-(v.sc)^{sh}} \quad (2.8)$$

sh, sc and v (m/s) are the Weibull shape parameter, scale parameter and wind speed respectively.

The cumulative distribution function $F_{WIND}(v)$ is given by

$$F_{WIND}(v) = \int_0^v f_{WIND}(\tau)d\tau \quad (2.9)$$

Substituting the value of $f_{WIND}(v)$ given by **equation 2.8** in **equation 2.9**:

$$F_{WIND}(v) = \left(1 - \exp\left(-\left(\frac{v}{sc}\right)^{sh}\right)\right) \quad (2.10)$$

Using a random variable, one can ascertain the unpredictability of the wind. Similarly, the power output (P_{WIND}) of a wind turbine for a given wind speed is given by **equations 2.11** to **2.13**, disregarding minor nonlinearities **[103]**.

$$P_{WIND} = 0, for\ \ v < v_{ci}\ and\ v > v_{co} \quad (2.11)$$

$$P_{WIND} = P_{WIND_r}\frac{v - v_{ci}}{v_r - v_{ci}} for\ \ v_{ci} < v < v_r \quad (2.12)$$

$$P_{WIND} = P_{WIND_r}\, for\ \ v_r < v < v_{co} \quad (2.13)$$

P_{WIND_r} is the wind turbine's rated power output, expressed in kW. v_{ci}, v_r, and v_{co} represent the cut-in, rated, and cut-out wind velocities, respectively. In the reference, the probability of wind power being zero, rated, or somewhere between zero and rated is provided.

When wind power is zero, the cumulative distribution is given by:

$$F_{WIND}\{P_{WIND} = 0\} = F_{WIND}(v_{ci}) + \left(1 - F_{WIND}(v_{co})\right) \quad (2.14)$$

Substituting the value of $F_{WIND}(v)$ from **equation 2.10** in equation **2.14**:

$$F_{WIND}\{P_{WIND} = 0\} = 1 - \exp\left(-\left(\frac{v_{ci}}{sc}\right)^{sh}\right) + \exp\left(-\left(\frac{v_{co}}{sc}\right)^{sh}\right) \quad (2.15)$$

The following expression provides the cumulative distribution of the wind power that is being rated:

$$F_{WIND}\{P_{WIND} = P_{WIND_r}\} = F_{WIND}(v_{co}) - F_{WIND}(v_r) \quad (2.16)$$

Applying the value of $F_{WIND}(v)$ derived from equation **2.10** to the equation **2.16**:

$$F_{WIND}\{P_{WIND} = P_{WIND_r}\} = \exp\left(-\left(\frac{v_{ci}}{sc}\right)^{sh}\right) - \exp\left(-\left(\frac{v_{co}}{sc}\right)^{sh}\right) \quad (2.17)$$

The following equation can be used to describe the cumulative distribution of wind power as being between zero and rated:

$$F_{WIND}\{0 \le P_{WIND} \le P_{WIND_r}\} = \frac{sh\ .l.v_{ci}}{P_r\ sc}\left(\frac{(1+\delta l)v_{ci}}{sc}\right)^{sh-1}\exp\left(-\left(\frac{(1+\delta l)v_{ci}}{sc}\right)^{sh}\right) \quad (2.18)$$

$\delta = \frac{P_{WIND}}{P_{WIND_r}}$ and $l = \frac{(v_r - v_{ci})}{v_{ci}}$ are the intermediate variables.

2.5. Cost modelling of PV based DG

The cost of PV includes the investment, hourly labor, and annual maintenance expenses, respectively. The investment cost consists of the price of the PV unit, the cost of installation, and the price of the protection system. The hourly working cost comprises of wages, fuel, and taxes.

The cost of PV based DG **[104]** over the entire planning horizon is given by:

$$Cost_{PV} = INVC_{PV} * PV_{out} + HWRC_{PV} * PV_{out} * PLTF * YR_{span} * 8760 * CCPR + AMC_{PV} * CCPR * YR_{span} \quad (2.19)$$

$INVC_{PV}$ is the investment cost of PV based DG. AMC_{PV} and $HWRC_{PV}$ are the annual maintenance and hourly working cost of the PV based DG. CPR and $CCPR$ are the cumulative price and cumulative current price. PV_{out} is the power output of the PV based DG.

2.6. Cost modelling of wind-based DG

The cost of wind-based DG over the entire planning horizon is given by

$$Cost_{WIND} = 8760 * YR_{span} * \sum_{i=1}^{N_{wt}} \left[C_{d,i}\left(P_{WIND_i}\right) + + C_{ue,i}\left(P_{WIND_{i,avl}} - P_{WIND_i}\right) + C_{oe,i}\left(P_{WIND_i} - P_{WIND_{i,avl}}\right) + \left\{\frac{1}{8760} * CRF * C_{om(esc)_i}\right\} + \left\{\frac{1}{8760 * YR_{span}} * CRF * C_{wt_i}\right\}\right] \quad (2.20)$$

$C_{d,i}\left(P_{WIND_i}\right)$ is the cost due to the direct power output from the i^{th} wind turbine of the wind farm **[105]**. $C_{ue,i}\left(P_{WIND_{i,avl}} - P_{WIND_i}\right)$ and $C_{oe,i}\left(P_{WIND_i} - P_{WIND_{i,avl}}\right)$ are the costs due to underestimation and overestimation of the i^{th} wind turbine respectively **[106]**. $C_{om(esc)_i}$ and C_{sp_i} are the annual O&M and specific costs respectively **[107]**. $P_{WIND_i}(0 \leq P_{WIND_i} \leq P_{WIND_r})$ is the forecasted power output from the wind turbine and $P_{WIND_{i,avl}}$ is its actual power output. The wind farm's total number of wind turbines is N_{wt}. CRF is the capital recovery factor.

The direct cost of the i^{th} wind turbine is given by:

$$C_{d,i}\left(P_{WIND_i}\right) = d_i P_{WIND_i} \quad (2.21)$$

When wind power generation falls short of the forecasted value due to overestimation, the shortfall must be made up with alternative energy sources. The cost of wind energy due to overestimation is given by:

$$C_{oe,i}\left(P_{WIND_i} - P_{WIND_{i,avl}}\right) = k_{res}\left(P_{WIND_i} - P_{WIND_{i,avl}}\right) = k_{res}\int_0^{P_{WIND_{i,avl}}}\left(P_{WIND_i} - P\right)F_{WIND}(P)dP \quad (2.22)$$

If excess wind power is produced as a result of underestimation, issues such as line congestion arise, impeding the network's ability to function normally. Due to underestimation, the cost of wind energy is provided by:

$$C_{ue,i}\left(P_{WIND_{i,avl}} - P_{WIND_i}\right) = k_{pen}\left(P_{WIND_{i,avl}} - P_{WIND_i}\right) = k_{pen}\int_{P_{WIND_i}}^{P_{WIND_{r_i}}}(P - P_{WIND_i})F_{WIND}(P)dP \quad (2.23)$$

k_{res} and k_{pen} are the reserve and penalty cost coefficients respectively.

The investment cost of the i^{th} wind turbine is given by:

$$C_{wt_i} = I_{wt_i}P_{WIND_{r_i}} \quad (2.24)$$

C_{wt_i} and I_{wt_i} are the cost and specific cost of the i^{th} wind turbine respectively.

The escalated cost of the i^{th} wind turbine due to operation and maintenance is given by:

$$C_{om(esc)_i} = \frac{C_{om_i}}{r-e_{om}}[1-(1+e_{om})^{YR_{span}}(1+r)^{-YR_{span}}] \quad (2.25)$$

C_{om_i} is the non-escalated operation and maintenance cost of the i^{th} wind turbine. e_{om} is the escalation ratio of maintenance and operation in percentage. r is the discount rate. YR_{span} is the lifetime of the system.

2.7. Formulation of the objective function (*OF*) due to DG integration

The Voltage Profile Enhancement Index (*VPEI*), Benefit Cost Ratio (*BCR*), and Environmental Cost Benefit Index (*ECBI*) have been developed to take the technical, financial, and environmental benefits of the objective function (*OF*) into consideration.

$$OF = \mu_1 * VPEI + \mu_2 * BCR + \mu_3 * ECBI \quad (2.26)$$

$$\mu_1 = \mu_2 = \mu_3 = 0.333 \quad (2.27)$$

Each of the network benefit indices are explained in the following subsections.

2.7.1. Voltage profile enhancement index (*VPEI*) due to DG integration

The following equation describes the $VPEI$ of a DN after DG allocation.

$$VPEI = \frac{(VPI)_{with\ DG}}{(VPI)_{without\ DG}} \quad (2.28)$$

The voltage profile index (VPI) is represented as follows:

$$VPI = \frac{1}{N_{BR}}\sum_{k=1}^{N_{BR}} VP_k \quad (2.29)$$

VP_k**[108]** represents the voltage profile of the k^{th} bus and is defined as:

$$VP_k = \frac{4(V_k - V_{lwr})(V_{upr} - V_k)}{(V_{upr} - V_{lwr})} \quad (2.30)$$

V_k is the voltage of the k^{th} bus.

N_{BR} is the number of branches of the network.

The nominal voltage (V_{nom}) is the average of the upper (V_{upr}) and lower (V_{lwr}) voltage limits.

$$V_{nom} = \frac{(V_{upr}+V_{lwr})}{2} \quad (2.31)$$

Calculating the voltage stability index (*VSI*) of a DN is one of the quickest and simplest methods to ascertain the voltage stability of a DN **[109], [110]**. When power flows from bus *j* to bus *k*, the *VSI* of bus *k* is denoted by

$$VSI(k) = V_j^4 - 4 * \{P(k) * X_L - Q(k) * R_L\}^2 - 4 * \{P(k) * R_L - Q(k) * X_L\} * V_j^2 \quad (2.32)$$

Before and after DG integration, the *VSI* characteristics of a network have been compared graphically in this work.

If *VPEI* is more than unity, the system is producing voltage profile improvement after DG allocation.

2.7.2. Benefit Cost Ratio (*BCR*) due to DG integration

After optimal DG allocation, the BCR of the DN is given by

$$BCR = \frac{Total\ Benefit_{DG}}{Total\ Cost_{DG}} \quad (2.33)$$

The variables $Total\ Benefit_{DG}$ and $Total\ Cost_{DG}$ are the total benefit derived and cost involved of the system in USD, respectively.

$$Total\ Cost_{DG} = Cost_{\ WIND} + Cost_{\ PV} \quad (2.34)$$

$Cost_{\ WIND}$ and $Cost_{\ PV}$ represent the costs of wind and PV power generation, respectively.

The total benefit of the DN ($Total\ Benefit_{DG}$) is given by

$$Total\ Benefit_{DG} = \{P_{out} * PLF + (PL_{W/O} - PL_W)\} * YR_{span} * 8760 * C_h * CCPR \quad (2.35)$$

P_{out} is the total power output from PV and wind based DGs. The cost for generating power is C_h. The plant factor is $PLTF$. The active power losses of the DN without and with DG allocation are denoted by $PL_{W/O}$ and PL_W, respectively. If *BCR* is more than unity, the system is producing financial gains after DG allocation.

2.7.3. Emission benefit index (ECBI) due to DG integration

The energy crisis presents a serious problem for modern society. Sustainable development is seen as one of the main corrective actions in this regard. As a result of the present energy crisis, the production of electricity is shifting away from fossil fuels and towards renewable energy sources. Furthermore, the harmful contaminants produced by fossil fuels, such as CO_x, NO_x,

and particulate matter, are detrimental to the environment. By incorporating DGs into a radial network, the consumption of fossil fuels will be decreased, thereby reducing the emission of the aforementioned pollutants.

The emission cost benefit index is given by:

$$ECBI = \frac{EC_{without\ DG} - EC_{with\ DG}}{EC_{without\ DG}} \quad (2.36)$$

$EC_{without\ DG}$ and $EC_{with\ DG}$ represent the emission costs with and without DG integration in the DNs, respectively. Using the following equation, their values are calculated.

$$EC = \sum_{tp=1}^{YR_{span}} EM * EM_{cost} * \frac{1}{(1+disc)^{tp}} \quad (2.37)$$

EM_{cost} represents the cost per tonne of CO_2 emitted by fossil fuels. $disc$ is the rate of discount. The following equation gives the quantity of CO_2 emitted (EM).

$$EM = EF_{grid} * G_{pow} \quad (2.38)$$

The main grid's emission factor and power output are denoted by the variables EF_{grid} and G_{pow}. A value of *ECBI* that is greater than zero indicates that there is an increase in emission benefit.

2.8. Operational Constraints

The objective function OF should be maximised as it consists of improvements that adhere to the following technical constraints.

i) Bus voltage limit constraint:

$$V_{upr} \leq V_k \leq V_{lwr} \quad (2.39)$$

ii) Line power flow limit constraint:

$$PFL_{line} \leq PFL_{line}^{max} \quad (2.40)$$

PFL_{line} is the line power flow. PFL_{line}^{max} is the maximum line power flow limit.

iii) Power generation limit constraint of the main generator:

$$P_{G,min} \leq P_G \leq P_{G,max} \quad (2.41)$$

P_G is the active power generated by the main generator. $P_{G,max}$ and $P_{G,min}$ are its limits.

$$Q_{G,min} \leq Q_G \leq Q_{G,max} \quad (2.42)$$

Q_G is the reactive power generated by the main generator. $Q_{G,max}$ and $Q_{G,min}$ are its limits.

iv) Power generation limit constraint of PV based DG:

$$P_{PV,min} \leq P_{PV} \leq P_{PV,max} \quad (2.43)$$

P_{PV} is the power output of PV based DG. $P_{PV,min}$ and $P_{PV,max}$ are the its limits.

v) Power generation limit of wind turbine:

$$P_{wind,min} \leq P_{wind} \leq P_{wind,max} \quad (2.44)$$

P_{wind} is the power output of PV based DG. $P_{wind,min}$ and $P_{wind,max}$ are the its limits.

2.9. Specifications of PV and wind-based DG

The specifications of PV and wind-based DG used to simulate the following test cases are given in **Table 2.0.1**. The values of different parameters in the table are taken from the reference **[111]**.

Table 2.0.1. Specifications of PV and wind-based DG

Parameter	Value	Parameter	Value	Parameter	Value	Parameter	Value
e_{om}	0-10	$INVC_{PV}$	1388USD/kW	I_{Nsc}	6.5A	q	1.6x10^{-19} C
$C_{om(esc)}$	15% of C_{wt}	EM_{cost}	10 USD/ton CO_2	G_N,G	1000 W/m^2, 192.917 W/m^2	c_1	1.21
INR	10%	EF_{grid}	910 kg CO_2/MWh	K	1.38×10^{-23} J/K	c_2	0.058
IFL	5%	C_h	120 USD/MWh	T_N	298K	c_3	1.15
$disc$, r	20%, 12%	PLF	0.25	AMC_{PV}	1% of $INVC_{PV}$	d_i	2 USD/kW
YR_{span}	10 years	v_{ci}, v_r, v_{co}	4 m/s, 14 m/s and 24 m/s	I_{wt}	1150 USD/kW	V_{upr}, V_{lwr}	0.9pu,1.1pu
$HWRC_{PV}$	0	k_{pen} and k_{res}	5 and 7	$P_{wind,min}$	0 kW	$P_{PV,min}$	0 kW
V_{Noc}	21V	T_a	288K	$P_{wind,max}$ from a single wind turbine	1100 kW	$P_{PV,max}$	30% of connected load

2.10. Case studies and their analysis

In order to study the effectiveness of PV and wind based DGs on the technical, economic, and environmental benefits of the DNs, two case studies are presented in this section which are as follows:

Case Study #2.1: *Optimal single, twin, and triple point allocation of deterministic PV-based DGs at the IEEE 33 and 69 bus DNs for the location of Jammu & Kashmir, India*
Case Study #2.2: *Optimal sizing and single, twin, and triple point allocation of probabilistic PV and wind-based DGs at the IEEE 85 and 141 bus DNs*
Each of the said case studies are elaborated in the following subsections.

2.10.1. **Case Study #2.1:** *Optimal single, twin, and triple point allocation of deterministic PV-based DGs at the IEEE 33 and 69 bus DNs for the location of Jammu & Kashmir, India*

Case Study Description: This case study aims at determining the optimal points of PV based DG injection using Jaya algorithm with an objective of increasing the technical, economic, and environmental benefits of DNs. The capacity of PV based DG has been calculated by deterministic approach for the location of Kashmir, India. PV-based distributed generators are injected at single, double, and triple points in conventional IEEE 33 bus and 69 bus test systems.

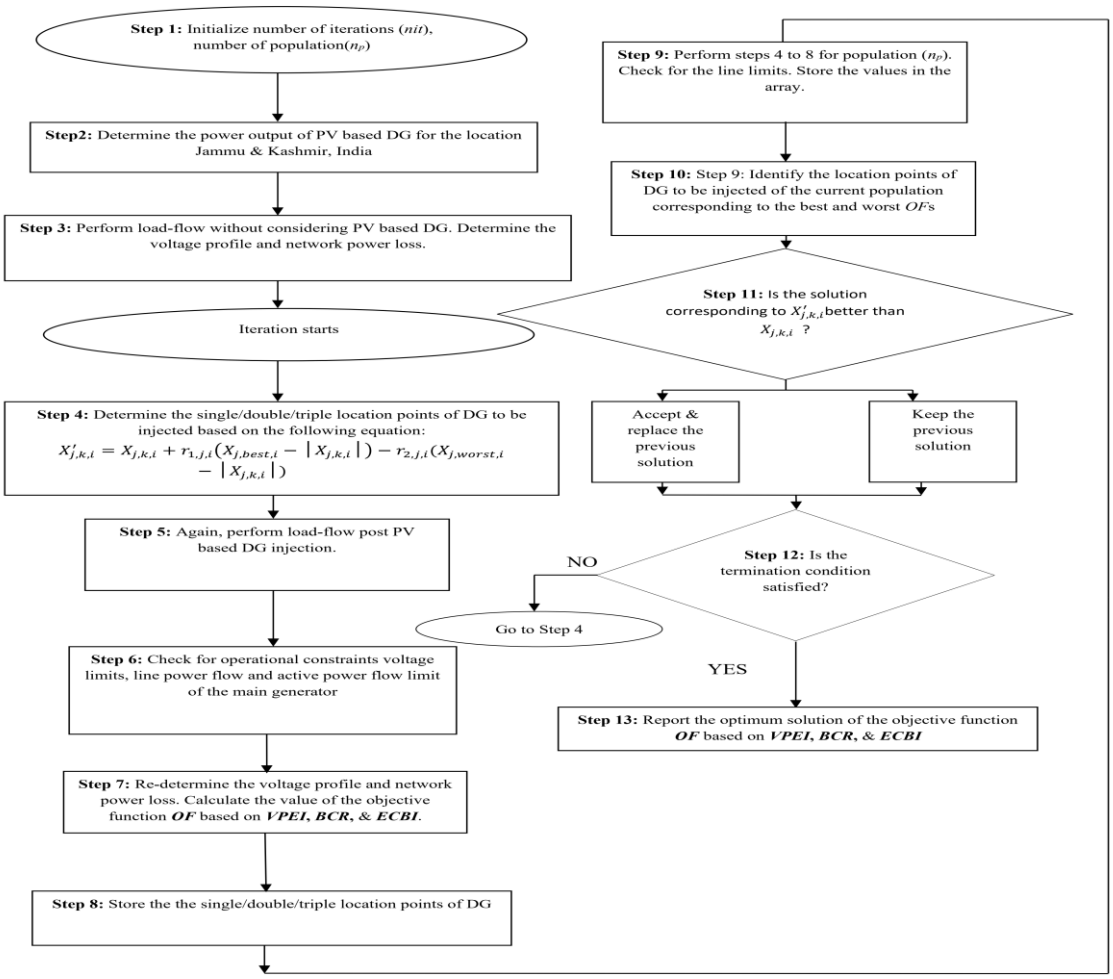

Fig. 2.1.1. Problem-specific flowchart showing Jaya algorithm applied to the problem defined under the Case-Study# 2.1

The simulation work is done in MATLAB v8.3. The configuration of the PC used is Intel(R) Core (TM) i3-7100 CPU @ 3.91 GHz, 4 GB DDR3 RAM. The calculated power output of the PV array is divided equally in three optimal points of standard IEEE 33 bus & 69 bus DNs for triple point DG injection. The same power is divided equally into two halves in case of twin point DG injection. Now, the optimal points will be calculated by means of Jaya algorithm with an objective of maximizing the technical, economic & environmental benefits subjected to the operating constraints as discussed in **Section 2.8**. The number of iterations & population are taken as 100 & 50 respectively.

The parameters given in **Table 2.0.1.** are used to determine the power output from the PV array. The site of the selection is in Srinagar, India. 348.34 kW is the estimated power output of the PV array that has been injected to the IEEE 33-bus test system. The computed power output for the IEEE 69-bus test system is 1006.7 kW.

2.10.1.1. ***Subcase #2.1.1:*** *Single point PV-based DG allocation*

The results of single point deterministic PV-based DG allocation for IEEE 33 and 69 bus DNs are given in **Table 2.1.1.** The overall objective functions for the said bus systems are 1.1172 and 2.4649, respectively. The reductions in the active power losses of the said bus DNs are 19.53% and 22.95%, respectively.

Table 2.1.1. Results of single point deterministic PV-based DG injection in case of standard IEEE 33 and 69 bus test DNs (Subcase #2.1.1) using the Jaya Algorithm under the Case-Study# 2.1

Test DN	**Points of DG injection**	***VPEI***	***BCR***	***ECBI***	***OF***	$PL_{W/O}$ **(kW)**	PL_W **(kW)**
IEEE 33 bus DN	17	1.1594	2.1067	0.0889	1.1172	201.89	162.46
IEEE 69 bus DN	64	1.0934	6.0603	0.2483	2.4649	224.59	173.04

2.10.1.2. ***Subcase #2.1.2:*** *Twin point PV-based DG allocation*

Table 2.1.2 shows the results of twin point deterministic PV-based DG allocation for IEEE 33 and 69 bus DNs. The overall objective functions for the said bus systems are 1.1220 and 2.4678, respectively. The reductions in the active power losses of the said bus DNs are 20.56% and 22.90%, respectively.

Table 2.1.2. Results of twin point deterministic PV-based DG injection in case of standard IEEE 33 and 69 bus test DNs (Subcase #2.1.2) using the Jaya Algorithm under the Case-Study# 2.1

Test DN	**Points of DG injection**	***VPEI***	***BCR***	***ECBI***	***OF***	$PL_{W/O}$ **(kW)**	PL_W **(kW)**
IEEE 33 bus DN	18, 33	1.1394	2.1412	0.0889	1.1220	201.89	160.39
IEEE 69 bus DN	61,64	1.0947	6.0677	0.2483	2.4678	224.59	173.15

2.10.1.3. ***Subcase #2.1.3:*** *Triple point PV-based DG allocation*

The results of triple point deterministic PV-based DG injection are given in **Table 2.1.3.** The overall objective functions for the said bus systems are 1.1245 and 2.4686 for the IEEE 33 and 69 bus DNs, respectively. The reductions in the active power losses of the DNs are 20.55% and 51%, respectively.

Table 2.1.3. Results of triple point deterministic PV-based DG injection in case of standard IEEE 33 and 69 bus test DNs using the Jaya Algorithm under the Case-Study# 2.1

Test DN	**Points of DG injection**	***VPEI***	***BCR***	***ECBI***	***OF***	$PL_{W/O}$ **(kW)**	PL_W **(kW)**
IEEE 33 bus DN	17, 18, 33	1.1467	2.1412	0.0889	1.1245	201.89	160.39
IEEE 69 bus DN	61,62,64	1.0944	6.0703	0.2483	2.4686	224.59	110.04

The improvements in the *VSI* characteristics are shown in **Fig. 2.1.2.** and **Fig. 2.1.3.,** respectively.

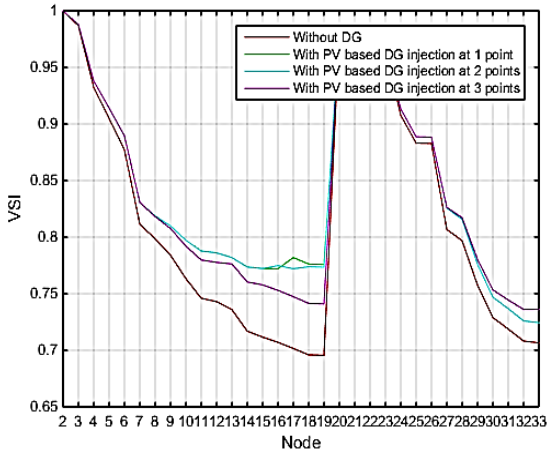

Fig. 2.1.2. Improvement in the *VSI* characteristics of the IEEE 33 bus DN for single, twin, and triple point PV-based DG allocation (deterministic approach) using the Jaya Algorithm under the Case-Study# 2.1

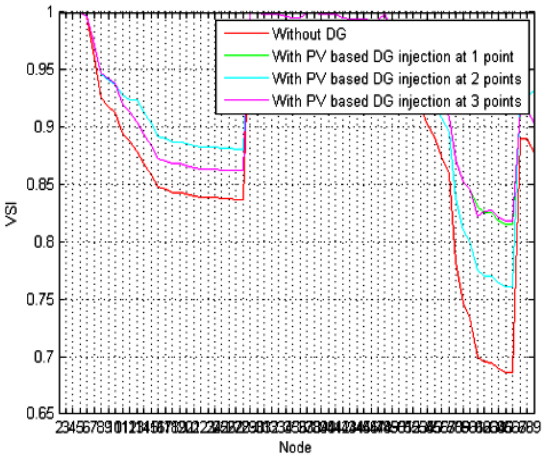

Fig. 2.1.3. *VSI* characteristics of the IEEE 69 bus DN for single, twin, and triple point wind-based DG allocation (deterministic approach) using the Jaya Algorithm under the Case-Study# 2.1

2.10.2. **Case Study #2.2:** *Optimal sizing and single, twin, and triple point allocation of probabilistic PV and wind-based DGs at the IEEE 85 and 141 bus DNs*

Case Study Description: This case study examines the benefits of radial DNs obtained by integrating PV and wind-based DGs. that are simultaneously sized and allocated optimally. In standard IEEE 85 and 141 bus test systems, DGs based on photovoltaic and wind energy are injected at single, double, and triple points. The intermittent natures of PV and wind are characterized using Beta and Weibull probability density functions.

In this case study, single-point, double-point, or triple-points of standard IEEE 85 and 141 bus radial DNs are optimally injected with PV, wind, or a combination of both types of DGs. MATLAB v7.0 with the MATPOWER v7.0 power flow tool extension is used for the simulation procedure, in an Intel Core i7 9750H, 2.60 GHz and 24 GB of RAM. PV and wind-based DGs have various installed capabilities for single, double, and triple point injections. The corresponding injected power for single-point injections is reduced to half for double-point injections and one-third for triple-point injections. This is done to make sure that the total power injected from the DGs is in proportion to the power coming from the grid.

As a result, the authors have considered the penetration capacities of PV and wind power for different DG injection points. The highest installed capacity of wind-based DG for single-point allocation is set to 1100 kW. Likewise, for each test bus system under consideration, the maximum installed capacity of PV for single point allocation is set to 30% of the total load demand. When double-point DG allocation ("PV+PV" or "WIND+WIND") is done, the maximum installed capacity for wind-based distributed generation is set at 550 kW, while the maximum installed capacity for photovoltaic systems is 15% of the total network load demand. The maximum installed capacities of wind and PV-based DGs for triple-point DG injection ("PV+PV+PV" or "WIND+WIND+WIND") are determined to be 366.67 kW and 10% of the total network load demand, respectively.

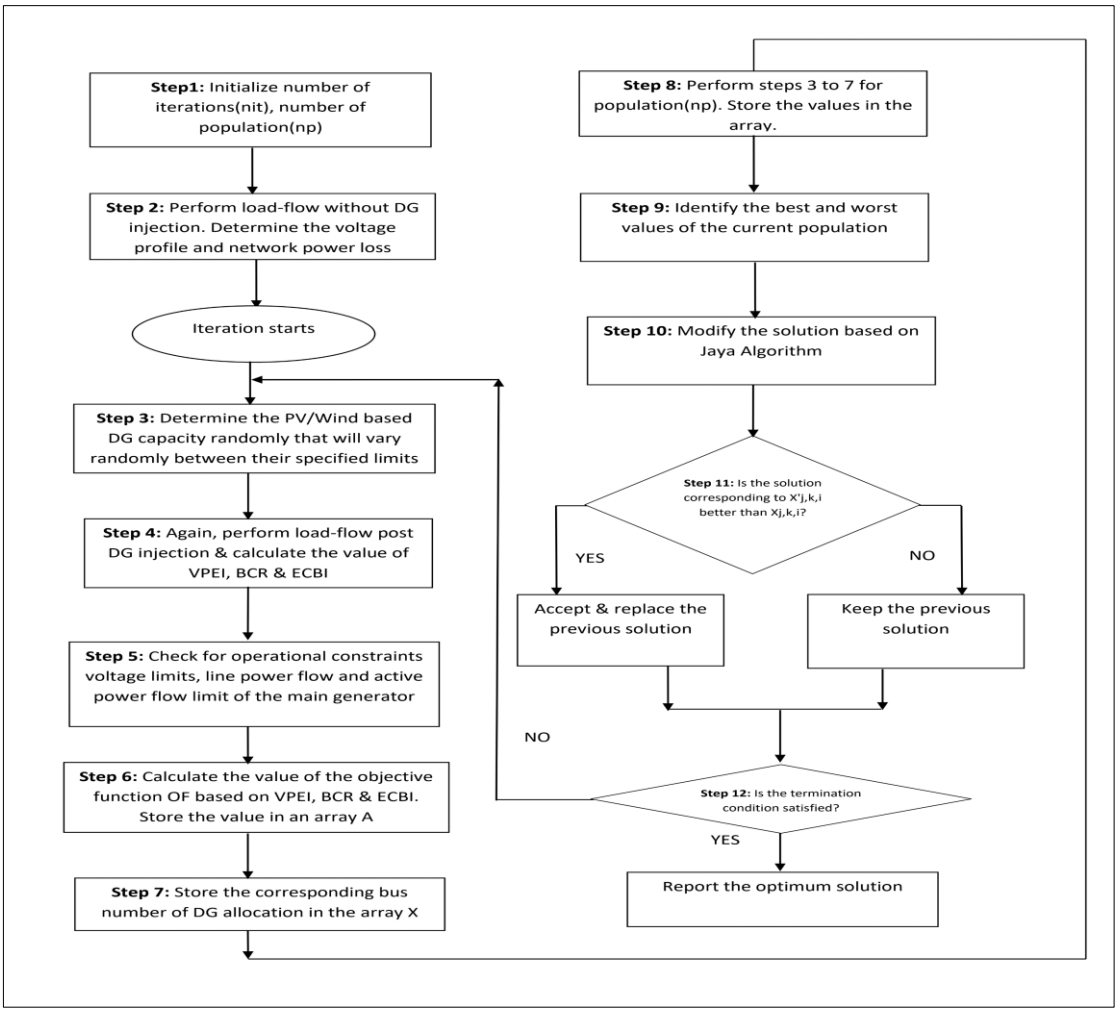

Fig. 2.2.1. Problem-specific flowchart showing Jaya algorithm applied to the problem defined in case-study# 2.2

The problem of determining the optimal DG penetration levels and allocation points by optimizing the benefits to the economy, environment, and technology is solved using the Jaya algorithm. The AQO, CSA, PSO, LPSO, RPSO, and PSO-SR algorithms are compared. The Jaya algorithm's effectiveness is evaluated in determining the ideal DG allocation points at IEEE 85 and 141 bus test systems. The problem-specific flowchart is given in **Fig. 2.2.1.** Nine test scenarios of different combinations of PV and wind based DGs are injected at the IEEE 85 and 141 bus test systems that are elaborated in the following sub-sections.

2.10.2.1. ***Subcase #2.2.1:*** *Single point PV injection*

Table 2.2.1. shows the values of the network indices, active power losses, optimal points of injection, and computation times for single point PV based DG injection using Jaya algorithm.

Table 2.2.1. Results of single point PV-based DG injection at the IEEE 85 and 141 bus DNs (Subcase #2.2.1) using Jaya Algorithm under Case Study #2.2										
Case	**Test DN**	***VPEI***	***BCR***	***ECBI***	***OF***	$PL_{W/O}$ **(kW)**	PL_W **(kW)**	**Injected value of DG (kW)**	**Optimal point of injection**	**Computation Time(secs)**
PV	**IEEE 85**	14.4880	4.4255	0.2756	6.3898	316.14	226.99	706.53	52	24.65
	IEEE 141	1.1572	17.8764	0.2809	6.4317	629.06	371.07	3262.30	44	36.88

2.10.2.2. ***Subcase #2.2.2:*** *Single point wind injection*

Table 2.2.2. shows the values of the network indices, active power losses, optimal points of injection, and computation times for single point wind-based DG injection using Jaya algorithm.

Table 2.2.2. Results of single point wind-based DG injection for at the IEEE 85 and 141 bus DNs (Subcase #2.2.2) using Jaya Algorithm under Case Study #2.2										
Case	**Test DN**	***VPEI***	***BCR***	***ECBI***	***OF***	$PL_{W/O}$ **(kW)**	PL_W **(kW)**	**Injected value of DG (kW)**	**Optimal point of injection**	**Computation Time(secs)**
WIND	**IEEE 85**	18.9698	30.0254	0.4096	16.4518	316.14	209.27	1075.70	48	80.22
	IEEE 141	1.0546	30.4115	0.0827	10.5058	629.06	532.08	939.46	86	137.12

2.10.2.3. ***Subcase #2.2.3:*** *Twin point PV injection*

Table 2.5.3. shows the values of the network indices, active power losses, optimal points of injection, and computation times for double point PV-based DG injection using Jaya algorithm.

Table 2.2.3. Results of double point PV based DG injection at the IEEE 85 and 141 bus DNs (Subcase #2.2.3) using Jaya Algorithm under Case Study #2.2										
Case	**Test DN**	***VPEI***	***BCR***	***ECBI***	***OF***	$PL_{W/O}$ **(kW)**	PL_W **(kW)**	**Injected value of DG (kW)**	**Optimal point of injection**	**Computation Time(secs)**
PV+PV	**IEEE 85**	14.9050	4.6281	0.2873	6.6002	316.14	222.02	361.80 373.51	50 53	28.91

	IEEE 141	1.1616	18.6367	0.2931	6.6904	629.06	360.96	1675.20 1729.40	46 63	37.55

2.10.2.4. ***Subcase #2.2.4:*** *Twin point WIND injection*

Table 2.2.4. shows the values of the network indices, active power losses, optimal points of injection, and computation times for double point wind-based DG injection using Jaya algorithm.

Table 2.2.4. Results of double point wind-based DG injection at the IEEE 85 and 141 bus DNs (Subcase #2.2.4) using Jaya Algorithm under Case Study #2.2

Case	**Test DN**	***VPEI***	***BCR***	***ECBI***	***OF***	$PL_{W/O}$ **(kW)**	PL_W **(kW)**	**Injected value of DG (kW)**	**Optimal point of injection**	**Computation Time(secs)**
WIND + WIND	**IEEE 85**	17.7866	31.5148	0.3916	16.5477	316.14	192.70	534.88 472.14	53 68	25.52
	IEEE 141	1.0353	30.7510	0.0525	10.6023	629.06	565.23	264.03 329.59	86 87	34.51

2.10.2.5. ***Subcase #2.2.5:*** *Twin point PV and WIND injection*

Table 2.2.5. shows the values of the network indices, active power losses, optimal points of injection, and computation times for double point PV and wind-based DG injection using Jaya algorithm.

Table 2.2.5. Results of double point PV and wind-based DG injection at the IEEE 85 and 141 bus DNs (Subcase #2.2.5) using Jaya Algorithm under Case Study #2.2

Case	**Test DN**	***VPEI***	***BCR***	***ECBI***	***OF***	$PL_{W/O}$ **(kW)**	PL_W **(kW)**	**Injected value of DG (kW)**	**Optimal point of injection**	**Computation Time(secs)**
PV+WIND	**IEEE 85**	15.0959	5.8481	0.2931	7.0719	316.14	220.41	349.59 400.82	52 49	72.04
	IEEE 141	1.1181	14.4898	0.1944	5.2622	629.06	429.24	1735 501.72	87 67	60.97

2.10.2.6. ***Subcase #2.2.6:*** *Triple point PV, PV, and PV injection*

Table 2.2.6. shows the values of the network indices, active power losses, optimal points of injection, and computation times for triple point PV-based DG injection using Jaya algorithm.

Table 2.2.6. Results of triple point PV-based DG injection at the IEEE 85 and 141 bus DNs (Subcase #2.2.6) using Jaya Algorithm under Case Study #2.2

Case	Test DN	*VPEI*	*BCR*	*ECBI*	*OF*	$PL_{W/O}$ (kW)	PL_W (kW)	Injected value of DG (kW)	Optimal point of injection	Computation Time(secs)
PV+PV+PV	**IEEE 85**	15.0030	4.9723	0.3025	6.7525	316.14	209.10	256.28 256.67 253.33	50 53 70	29.54
	IEEE 141	1.1713	19.2839	0.3047	6.9130	629.06	357.96	1186.60 1188.40 1173.00	80 29 50	36.05

2.10.2.7. ***Subcase #2.2.7:*** *Triple point WIND, WIND, and WIND injection*

Table 2.2.7. shows the values of the network indices, active power losses, optimal points of injection, and computation times for triple point wind-based DG injection using Jaya algorithm.

Table 2.2.7. Results of triple point wind-based DG injection at the IEEE 85 and 141 bus DNs (Subcase #2.2.7) using Jaya Algorithm under Case Study #2.2

Case	Test DN	*VPEI*	*BCR*	*ECBI*	*OF*	$PL_{W/O}$ (kW)	PL_W (kW)	Injected value of DG (kW)	Optimal point of injection	Computation Time(secs)
WIND + WIND + WIND	**IEEE 85**	16.5975	32.8396	0.3456	16.5776	316.14	200.35	317.65 278.14 286.10	53 70 48	29.58
	IEEE 141	1.0219	30.9320	0.0322	10.6514	629.06	588.96	101.92 128.36 132.85	52 87 85	35.94

2.10.2.8. ***Subcase #2.2.8:*** *Triple point PV, PV, and WIND injection*

Table 2.2.8. shows the values of the network indices, active power losses, optimal points of injection, and computation times for triple PV, PV, and wind-based DG injection using Jaya algorithm.

Table 2.2.8. Results of triple point PV, PV, and wind-based DG injection at the IEEE 85 and 141 bus DNs (Subcase #2.2.8) using Jaya Algorithm under Case Study #2.2

Case	Test DN	*VPEI*	*BCR*	*ECBI*	*OF*	$PL_{W/O}$ (kW)	PL_W (kW)	Injected value of DG (kW)	Optimal point of injection	Computation Time(secs)
PV + PV + WIND	**IEEE 85**	15.4390	6.1045	0.3033	7.2750	316.14	217.80	219.36 215.00 342.79	50 35 53	51.18
	IEEE 141	1.1361	17.7055	0.2312	6.3512	629.06	398.85	1187.1 1170.3 309.39	79 85 68	61.38

2.10.2.9. ***Subcase #2.2.9:*** *Triple point WIND, WIND, and PV injection*

Table 2.2.9. shows the values of the network indices, active power losses, optimal points of injection, and computation times for triple wind, wind, and PV-based DG injection using Jaya algorithm.

Table 2.2.9. Results of triple point wind, wind, and PV-based DG injection at the IEEE 85 and 141 bus DNs (Subcase #2.2.9) using Jaya Algorithm under Case Study #2.2

Case	Test DN	*VPEI*	*BCR*	*ECBI*	*OF*	$PL_{W/O}$ (kW)	PL_W (kW)	Injected value of DG (kW)	Optimal point of injection	Computation Time(secs)
WIND + WIND + PV	**IEEE 85**	16.3214	6.1604	0.3285	7.5958	316.14	212.63	326.20 333.78 184.91	45 52 51	49.01
	IEEE 141	1.1376	17.8081	0.2343	6.3869	629.06	396.50	1172.20 1186.30 345.58	80 86 64	75.03

2.10.2.10. Result analysis of ***Case Study #2.2***

Fig. 2.2.2. and **Fig. 2.2.3.** show the comparative chart of the network indices and network active power losses, respectively, for the IEEE 85 bus DN. The highest *VPEI*, *BCR*, *ECBI*, and *OF* are obtained for the test cases "WIND", "WIND+WIND+WIND", "WIND", and "WIND+WIND+WIND", respectively, of values 18.9698, 32.8396, 0.4096, and 16.5776,

respectively. The lowest *VPEI*, *BCR*, *ECBI*, and *OF* are obtained for the test case "PV" with values of 14.488, 4.4255, 0.2756, and 6.3898, respectively. The highest active power loss reduction of 39.05% is observed for the test case " WIND+WIND".

Fig. 2.5.4. and **Fig. 2.5.5.** show the comparative chart of the network indices and network active power losses, respectively, for the IEEE 141 bus DN. The highest *VPEI*, *BCR*, *ECBI*, and *OF* are obtained for the test cases "PV+PV+PV", "WIND+WIND+WIND", "PV+PV+PV", and "WIND+WIND+WIND", respectively, of values 1.1713, 30.9320, 0.3047, and 10.6514, respectively. The lowest *VPEI*, *BCR*, *ECBI*, and *OF* are obtained for the test cases "WIND+WIND+WIND", "PV+WIND", "WIND+WIND+WIND", and "PV+WIND", with values of 1.0219, 14.4898, 0.0322, and 5.2622, respectively. The highest active power loss reduction of 43.10% is observed for the test case " PV+PV+PV".

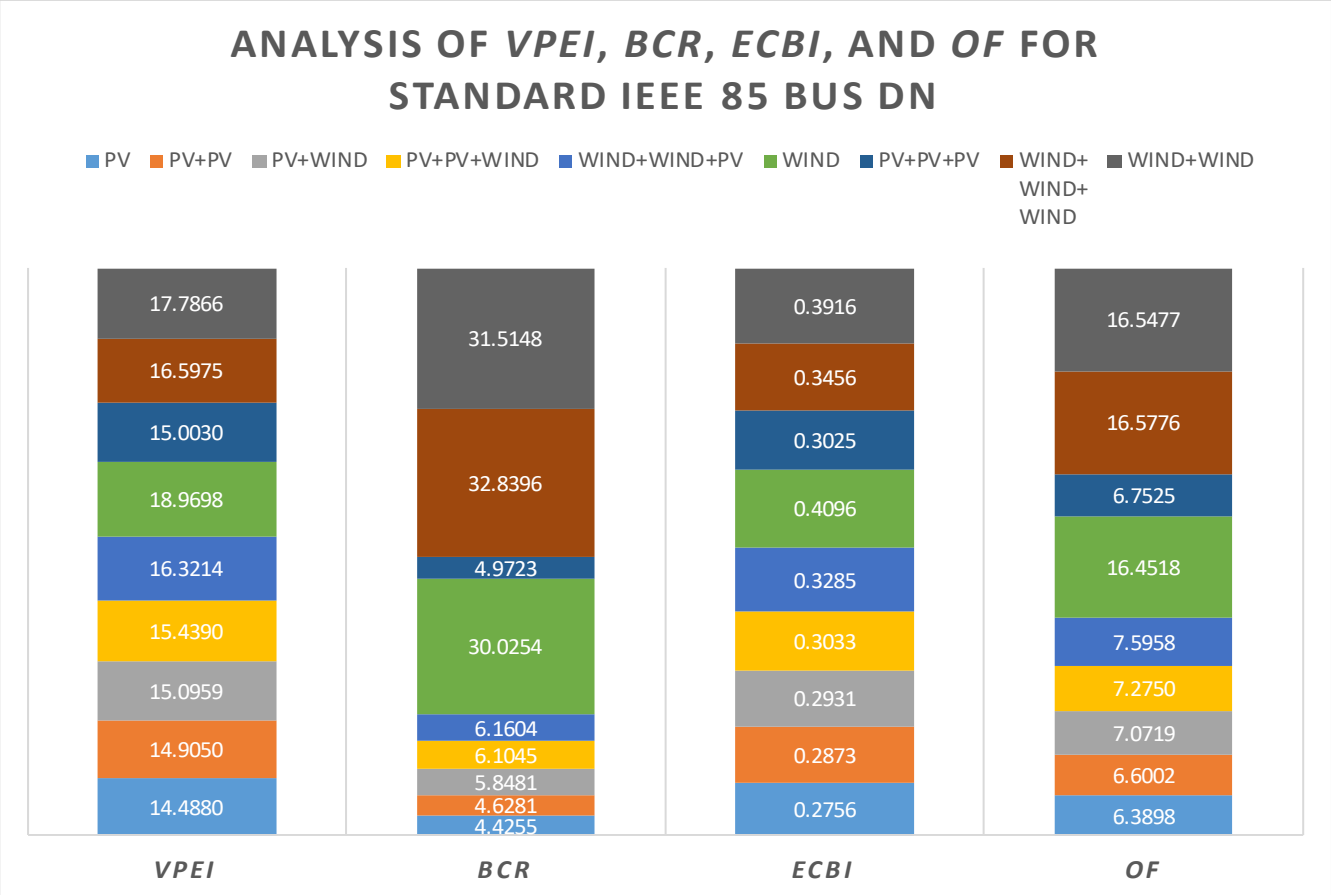

Fig. 2.2.2. Comparative chart of *VPEI*, *BCR*, *ECBI*, and *OF* obtained for IEEE 85 bus DN for all test scenarios under Case Study #2.2

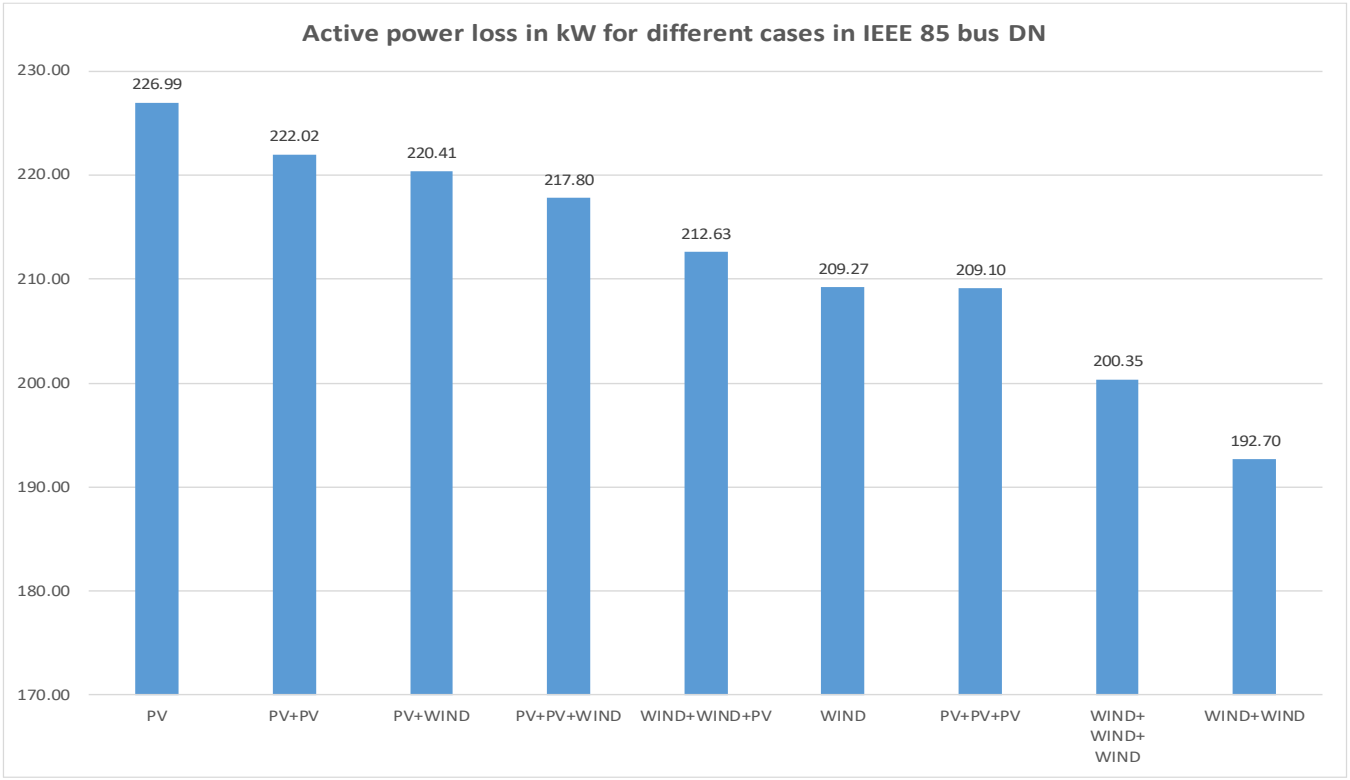

Fig. 2.2.3. Comparative chart of active power loss for IEEE 85 bus DN for all test scenarios under Case Study #2.2

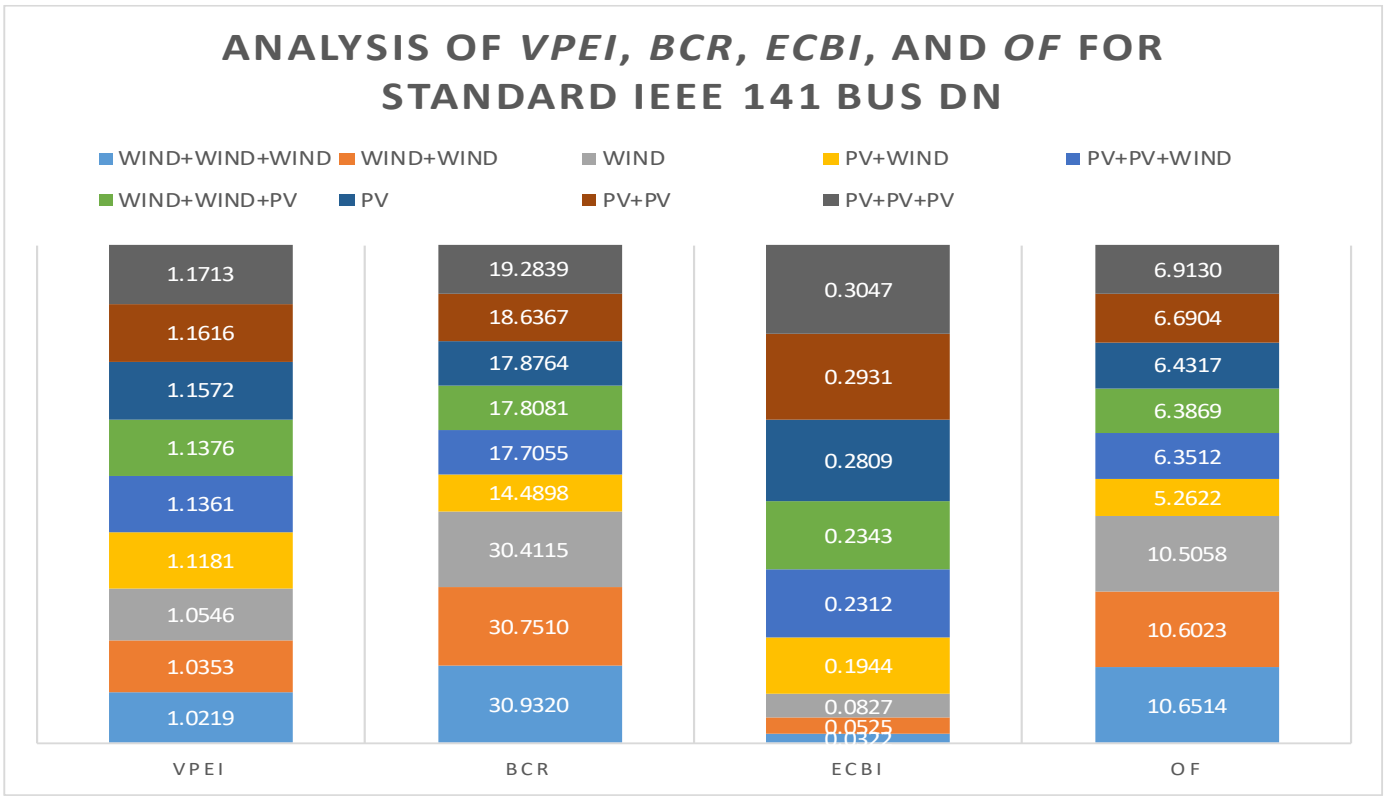

Fig. 2.2.4. Comparative chart of *VPEI*, *BCR*, *ECBI*, and *OF* obtained for IEEE 141 bus DN for all test scenarios under Case Study #2.2

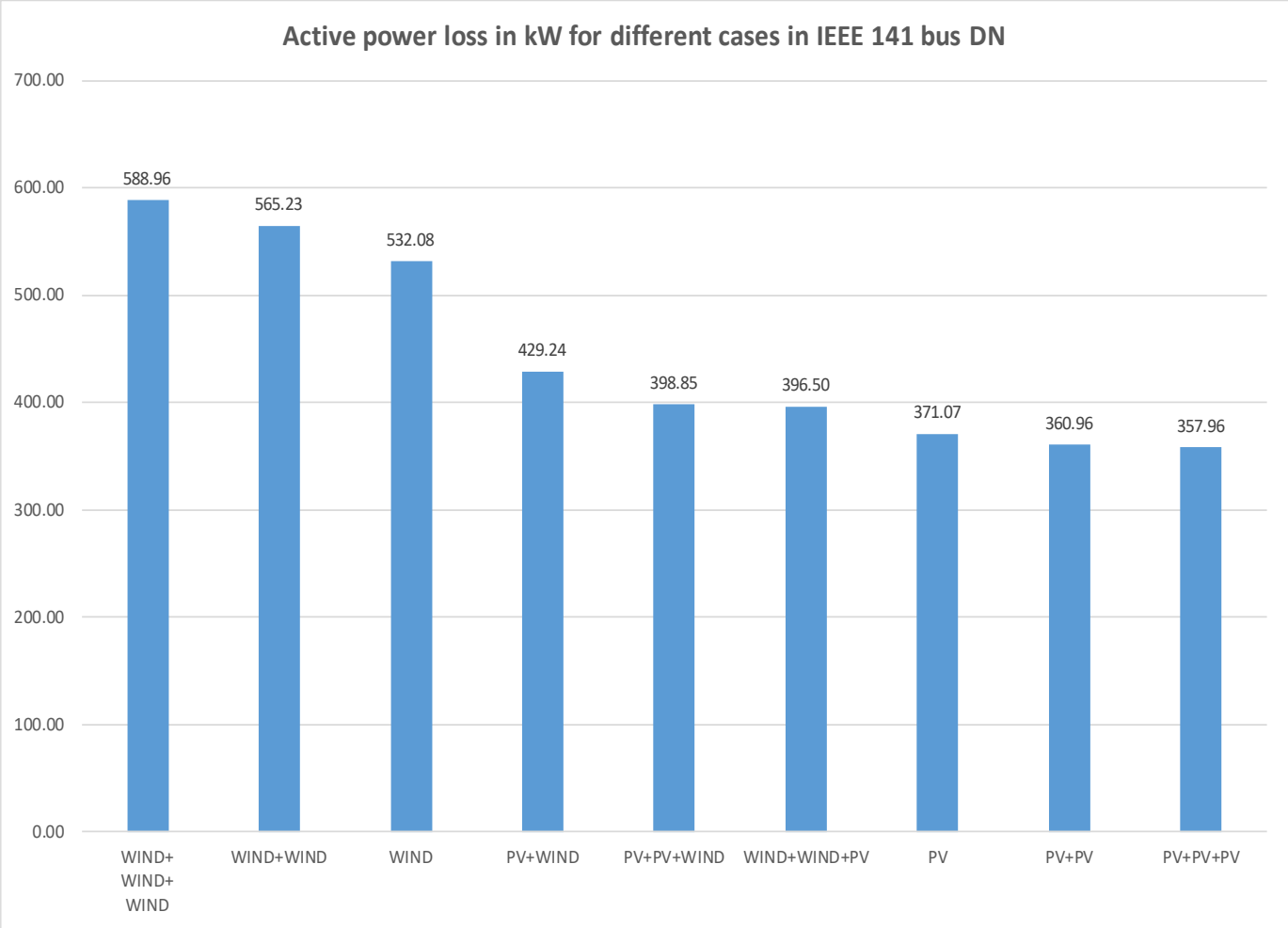

Fig. 2.2.5. Comparative chart of active power loss for IEEE 141 bus DN for all test scenarios under Case Study #2.2

The convergence characteristics of the *OF* obtained by using different algorithms for twin point PV-based DG allocation and twin point PV and wind-based DG allocation (PV+WIND) at the IEEE 85 and 141 bus DNs are shown in **Fig. 2.2.6**. and **Fig. 2.2.7**., respectively. The improvement in the *VSI* characteristics of the IEEE 141 bus DN for twin point PV and wind-based DG allocation (PV+WIND) are shown in **Fig. 2.2.8**.

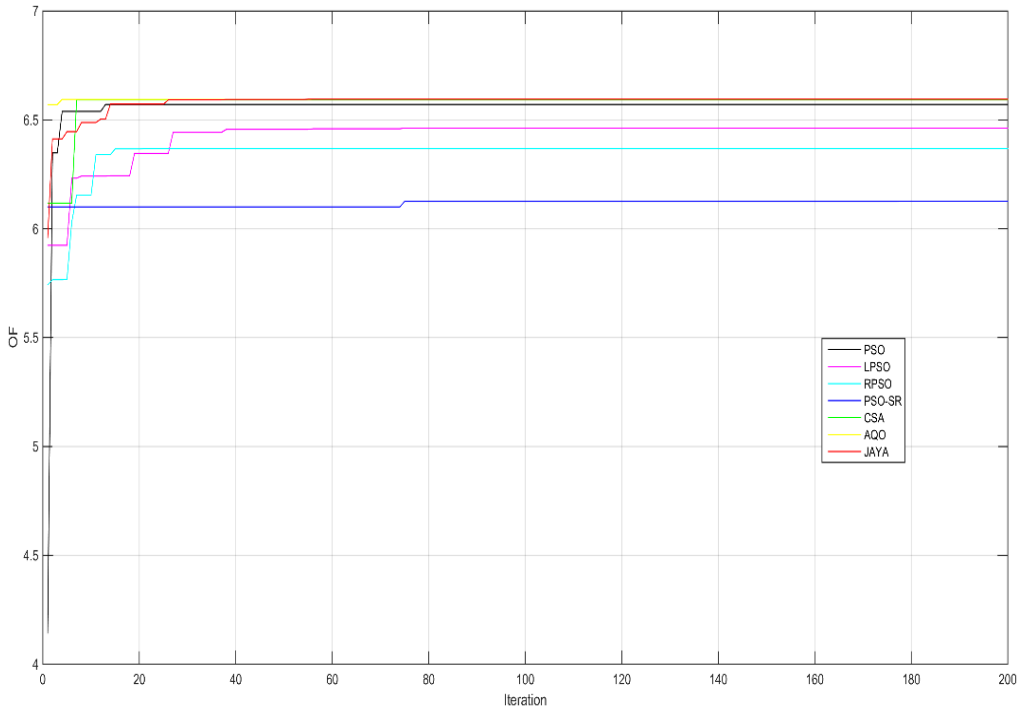

Fig. 2.2.6. Convergence characteristics of the *OF* obtained by using different algorithms for twin point PV-based DG allocation (PV+PV) at the IEEE 85 bus DN under the Case-Study# 2.2

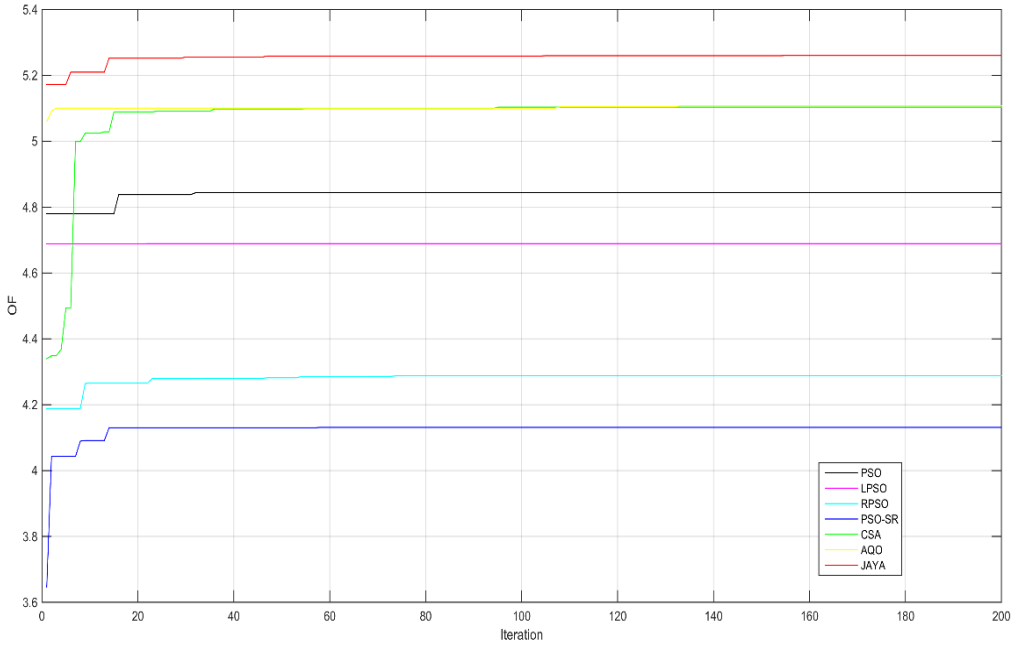

Fig. 2.2.7. Convergence characteristics of the *OF* obtained by using different algorithms for twin point PV and wind-based DG allocation (PV+WIND) at the IEEE 141 bus DN under the Case-Study# 2.2

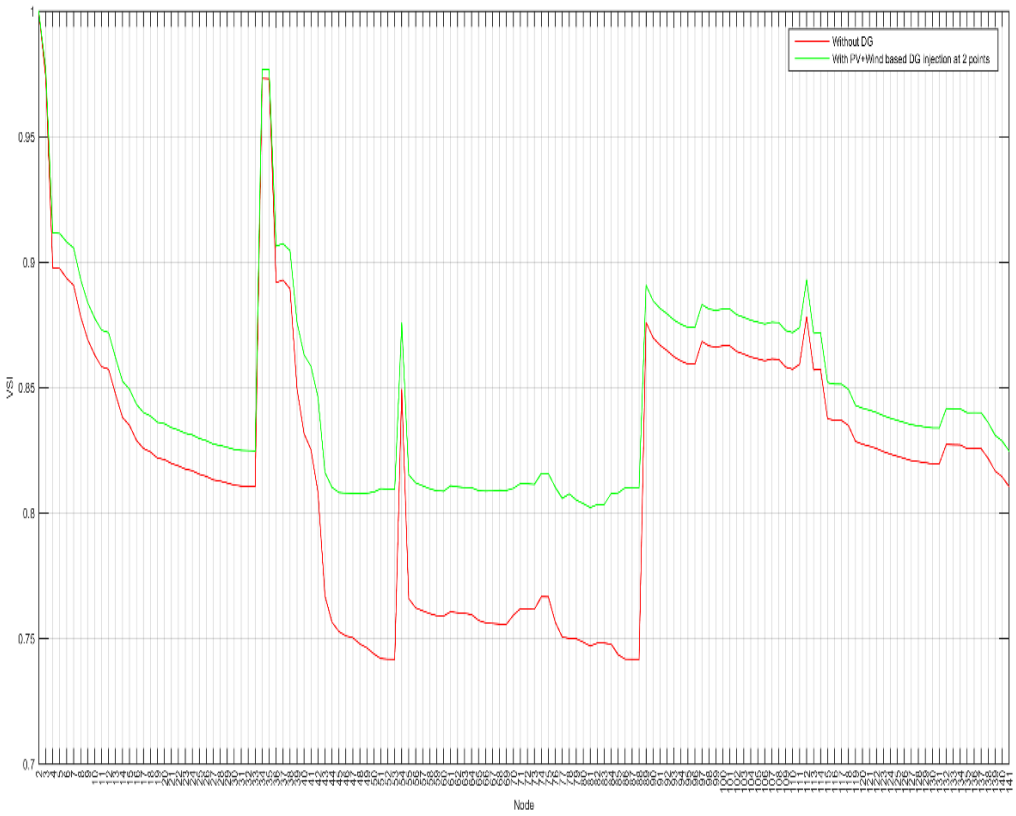

Fig. 2.2.8. Improvement in the *VSI* characteristics of the IEEE 141 bus DN for twin point PV and wind-based DG allocation (PV+WIND) under the Case-Study# 2.2

2.11. Performance of algorithms in comparison for *Subcase #2.2.6*

A comparative performance analysis of the algorithms is performed for one sub-case study presented in **Section 2.10** as an example. The sub-case study considered is ***Subcase #2.2.6***, which presents the effect of "PV+PV+PV" injection at the IEEE 141 bus DN.

The algorithms in comparison are PSO, LPSO, RPSO, PSO-SR, CSA, AQO, and Jaya. Each algorithm is run for 50 trials.

The maximum, minimum, mean, and standard deviations are recorded for each algorithm. **Fig. 2.2.9.** shows a box-whiskers plot, also known as a box-plot, which graphically displays differences in findings as boxes of different colors. A horizontal mark inside each box represents the mean value, and the horizontal marks on the top of vertical lines outside the box

represent the minimum and maximum values. The box range indicates the standard deviations, and the whiskers range is the minimum and maximum values. Therefore, the inter-quartile range is twice the standard deviation. From **Fig. 2.2.9.**, it is evident that the 1st and 3rd quartiles of the Jaya plot are significantly greater than PSO, LPSO, RPSO, PSOSR and CSA, but slightly greater than AQO. The relative maximum, minimum, mean, and standard deviation values of the *OF* using Jaya and other comparing algorithms are shown in **Fig. 2.2.10.** The mean difference plot (**Fig. 2.2.11**) reveals the Jaya algorithm's superiority over the comparing algorithms in terms of the *OF*.

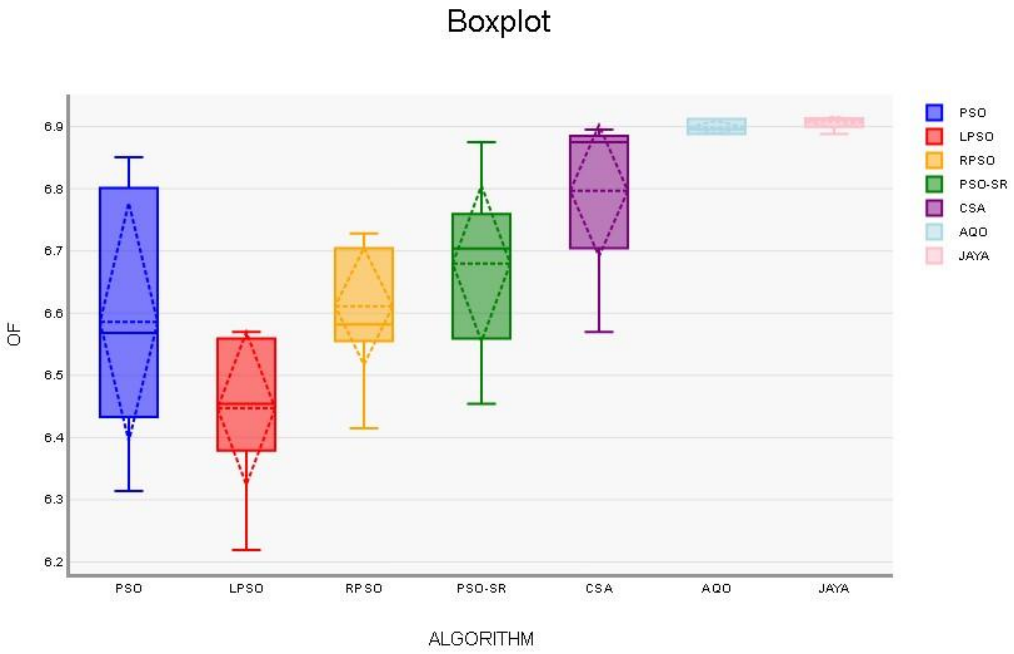

Fig. 2.2.9. Relative box plots of the *OF* obtained by the algorithms for the case "PV+PV+PV" of the IEEE 141 bus under Case Study #2.2

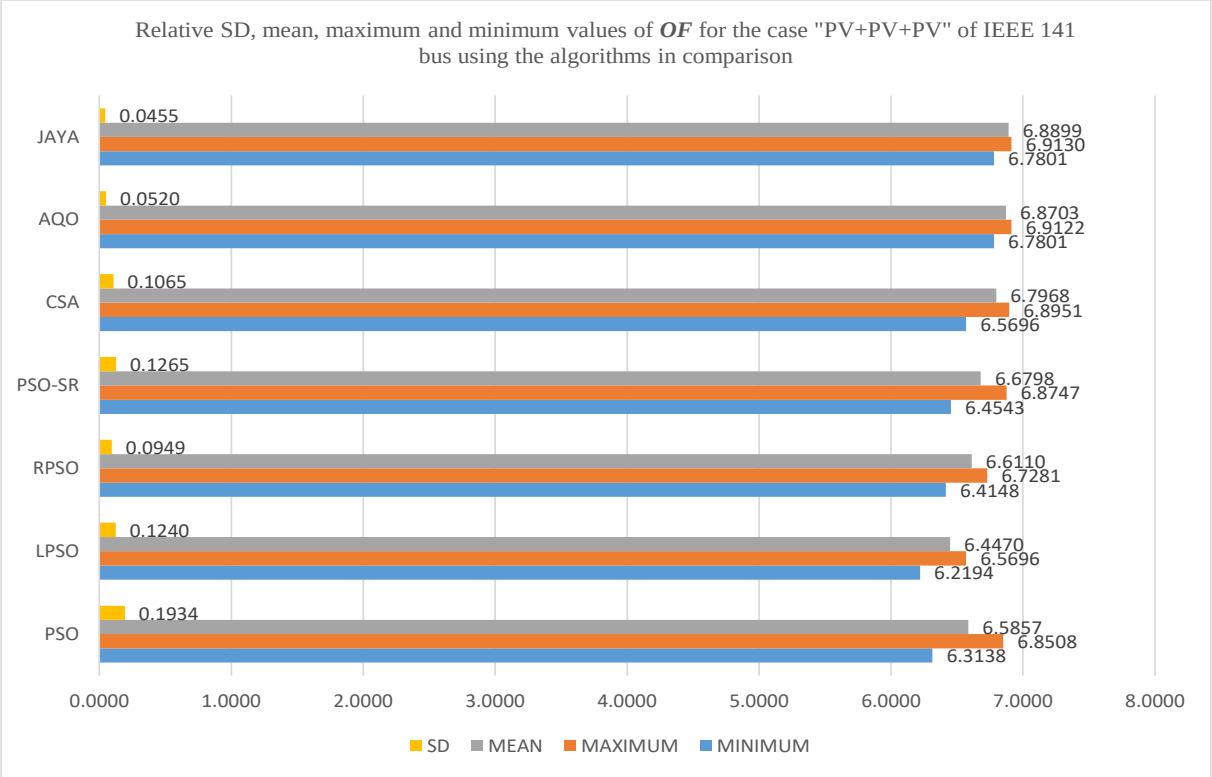

Fig. 2.2.10. Relative values of maximum, minimum, mean, and standard deviation of the *OF* obtained by the algorithms in comparison for the case "PV+PV+PV" of the IEEE 141 bus under Case Study #2.2

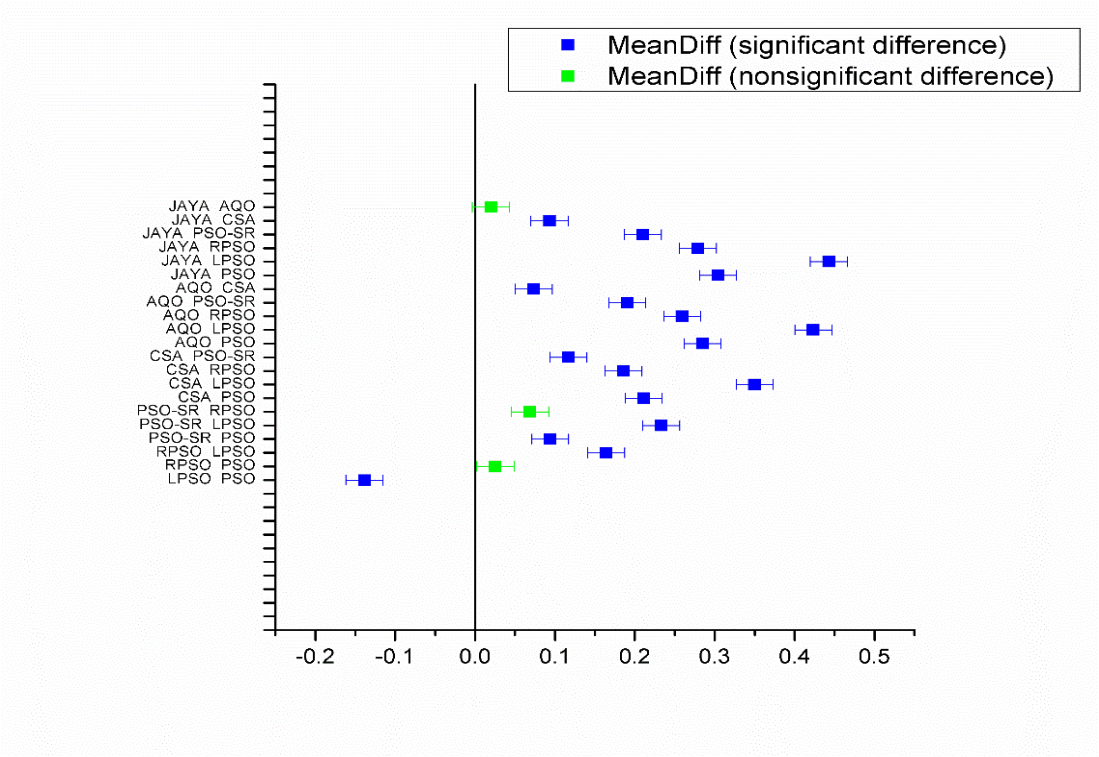

Fig. 2.2.11. Mean difference plot of the *OF* obtained by different algorithm pairs for the case "PV+PV+PV" of the IEEE 141 bus under Case Study #2.2

Table. 2.2.10. Statistical results for the test case of "PV+PV+PV" of IEEE 141 bus of Case Study #2.2							
Algorithms	**PSO**	**LPSO**	**RPSO**	**PSO-SR**	**CSA**	**AQO**	**JAYA**
Minimum *OF*	6.3138	6.2194	6.4148	6.4543	6.5696	6.7801	6.7801
Maximum *OF*	6.8508	6.5696	6.7281	6.8747	6.8951	6.9122	6.9130
Mean *OF*	6.5857	6.4470	6.6110	6.6798	6.7968	6.8703	6.8899
Standard Deviation of *OF*	0.1934	0.1240	0.0949	0.1265	0.1065	0.0520	0.0455
p-value* (Shapiro-Wilk test for normality) α=0.5	1.08e-05	3.17e-06	9.8e-05	0.000735	5.01e-07	1.32e-09	1.75e-11
p-value* (Kolmogorov–Smirnov test for normality) α=0.5	0.000134	2.58e-08	5.21e-05	0.000571	4.96e-13	0	1.11e-16
Mean Rank (Kruskal-Wallis non-parametric test) α=0.5^{++}	113.77	54.15	117.45	150.99	212.49	274.26	305.39

For each algorithm, the number of data samples has been set at 50.

Null hypothesis (H_0)- No statistical significance exists in a set of given observations.

* A probability that evaluates the evidence in contrast to the null hypothesis is referred to as the p-value. Evidence against the null hypothesis is strengthened when it is supported by lower probabilities.

**Normality is rejected at the 0.05 level.

$^{+}$ The average rank across all of the observations in a given sample is what is referred to as the mean rank. When a group's mean rank is higher than the overall average rank, the observation values in that group tend to be higher than those of the other groups.

$^{++}$The corrected α using Sidak correction method is 0.003414. Corrected $\alpha = 1-m\sqrt{(1 - \alpha)} = 1 - 15\sqrt{(1 - 0.05)} = 0.003414$.

m - the number of tests / pairs

The Shapiro-Wilk and Kolmogorov-Smirnov tests for normality have also been run to see if the data follows a normal distribution. **Table. 2.2.10.** displays the results of these normality tests, including the p-values for various scenarios. The threshold of 0.05 is used as the confidence level 'α' for these tests. As can be seen, the p values for all possible outcomes are less than the threshold value, indicating that the test rejects normality with a ninety-five percent level of confidence. As a result, it's safe to say that the data did not come from a normal distribution.

Kruskal-Wallis-H-ANOVA and post-hoc Dunn tests, have also been carried out in order to better understand the comparative performance studies. The results of these tests are shown in **Table 2.2.10.** and **Table 2.2.11.**, respectively. Using the Kruskal-Wallis-H analysis of variance (ANOVA) test, a comparative ranking of all the algorithms is produced. The test statistic H (to

be treated as) is 247.22, which is outside the 95% confidence interval. The Kruskal-Wallis-H test indicated that there is a significant difference in the dependent variable between the different groups ($\chi^2(6) = 247.22$, $p < 0.001$) with a mean rank score of 113.77 for PSO, 54.15 for LPSO, 117.45 for RPSO, 150.99 for PSO-SR, 212.49 for CSA, 274.26 for AQO, and 305.39 for Jaya.

Table. 2.2.11. Parametric comparison of algorithm pairs by post-hoc Dunn test for the test case of "PV+PV+PV" of IEEE 141 bus under Case Study #2.2

Pair	Mean Rank difference	Z	Standard Error difference	Critical value	p-value	p-value/2
PSO-LPSO	59.62	2.9497	20.2126	61.2579	0.003181	0.001591
PSO-RPSO	-3.68	0.1821			0.8555	0.4278
PSO-PSOSR	-37.22	1.8414			0.06556	0.03278
PSO-CSA	-98.72	4.8841			0.000001039	5.20e-07
PSO-AOA	-160.49	7.9401			2.00e-15	9.99e-16
PSO-JAYA	-191.62	9.4802			0	0
LPSO-RPSO	-63.3	3.1317			0.001738	0.0008689
LPSO-PSOSR	-96.84	4.7911			0.000001659	8.29e-07
LPSO-CSA	-158.34	7.8337			4.89e-15	2.44e-15
LPSO-AOA	-220.11	10.8898			0	0
LPSO-JAYA	-251.24	12.4299			0	0
RPSO-PSOSR	-33.54	1.6594			0.09704	0.04852
RPSO-CSA	-95.04	4.702			0.000002576	0.000001288
RPSO-AOA	-156.81	7.758			8.66e-15	4.33e-15
RPSO-JAYA	-187.94	9.2982			0	0
PSOSR-CSA	-61.5	3.0427			0.002345	0.001172
PSOSR-AOA	-123.27	6.0987			1.07e-09	5.35e-10

PSOSR-JAYA	-154.4	7.6388			2.18e-14	1.09e-14
CSA-AOA	-61.77	3.056			0.002243	0.001121
CSA-JAYA	-92.9	4.5962			0.000004304	0.000002152
AOA-JAYA	-31.13	1.5401			0.1235	0.06176

* The z-value gives an indication of how the average rank of each group stacks up against the overall average rank of all the observations.

- The greater the difference between a group's average rank and the general average rank, the higher the z value.
- A group's average rank being lower than the overall average rank is indicated by a negative z-value.
- A group's average rank being higher than the overall average rank is indicated by a positive z-value.

+ Stronger evidence is presented against the null hypothesis with lower p-values.

2.12. Summary

This section presents the salient observations regarding the effectiveness of PV and wind based DGs on the technical, economic, and environmental benefits of the DNs. These are presented under each case study as follows:

Case Study #2.1: *Optimal single, twin, and triple point allocation of deterministic PV-based DGs at the IEEE 33 and 69 bus DNs for the location of Jammu & Kashmir, India*

In this case study the optimal points of PV based DG injection are evaluated by deterministic approach using Jaya algorithm with an objective of increasing the technical, economic, and environmental benefits of DNs. PV-based distributed generators are injected at single, double, and triple points at the IEEE 33 bus and 69 bus DNs. The objective function increases with the increase in the number of injection points for the same amount of PV power being divided equally between the points of injection. Taking the objective function of single-point injection as the reference, the *OF* gets improved by 1.0043 and 1.0065 times for twin and triple point injections for the IEEE 33 bus DN, respectively. Similarly, the *OF* for the IEEE 69 bus DN gets improved by 1.0012 and 1.0015 for twin and triple point injections, respectively. It is observed that significant improvement in the *VSI* characteristics is observed when switched from single point injection to twin point injection but the same is less when switched from twin point to triple point injection.

Case Study #2.2: *Optimal sizing and single, twin, and triple point allocation of probabilistic PV and wind-based DGs at the IEEE 85 and 141 bus DNs*

The maximum reduction in active power losses of IEEE 85 and 141 bus DNs is observed by up to 39.05% and 43.10%, respectively. The maximum improvements in *OF* are up to 2.59 and

2.02 times for IEEE 85 and 141 bus DNs, respectively, considering the corresponding worst cases as references. Improvements in *VPEI* are observed by up to 1.31 and 1.15 times for IEEE 85 and 141 bus DNs, respectively, resulting in a better voltage profile and network stability. Improvement in *BCR* is observed by up to 7.42 and 2.13 times for IEEE 85 and 141 bus DNs, respectively, resulting in better cost effectiveness and economic operation of the DNs. Improvement in *ECBI* is seen by up to 1.49 and 9.46 times for IEEE 85 and 141 bus DNs, respectively, by lesser consumption of fossil fuel-based power, resulting in cleaner operation of the DNs. Improvements in the *VSI* characteristics are observed with probabilistic PV and wind-based DG injection for all the test cases and test systems under consideration. From **Section 2.11.**, it is clear that the Jaya algorithm is robust, consistent, and superior to all the algorithms in comparison.

CHAPTER 3: Impact of BESS and SVC on DN sustainability

This chapter presents the impact of BESS and SVC along with PV and wind-based DGs on the technical, economic, and environmental impacts of DNs.

3.1. Introduction

Energy can be stored in batteries for when it is needed. The BESS is an advanced technological solution that allows energy storage in multiple ways for later use. Given the possibility that an energy supply can experience fluctuations due to weather, blackouts, or for geopolitical reasons, battery systems are vital for utilities, businesses and homes to achieve a continual power flow. A BESS is no longer an afterthought or an add-on, but rather an important pillar of any energy strategy, especially any energy strategy that makes use of renewable solar power. Batteries can lessen the unpredictable nature of renewable energy by storing solar and wind-based electricity generated for usage by integrating battery energy storage with PV systems. This ensures an uninterrupted source of power at all times.

Reactive power compensation can lower power consumption, increase power quality, maximize the capabilities of equipment for power generation and supply, and lower electricity costs for consumers. It's an immediate solution that saves power and requires a lesser expenditure.

3.2. Components, working and advantages of BESS

This section illustrates and describes the working of BESS.

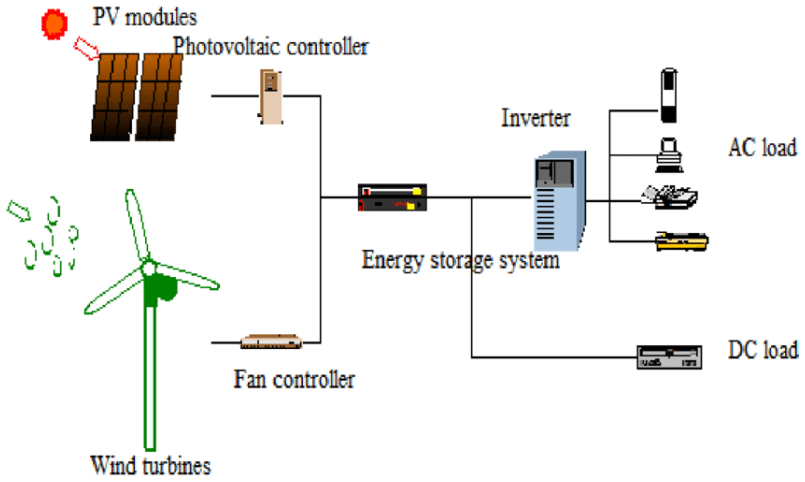

Fig. 3.0.1. Schematic diagram of BESS

A schematic diagram of BESS is shown in **Fig. 3.0.1**.

A BESS captures energy from both renewable and non-renewable sources and stores it in rechargeable batteries (storage devices) for future use. As a DC device, a BESS reduces any imbalance between energy supply and demand by discharging electrochemical energy as needed to fulfill electricity demand. BESS is a crucial technology for commercial and industrial organizations due to the rise in renewable energy sources and the push for net zero carbon emissions. Adopting BESS will help get closer to net zero emissions and offer an essential direction in making the transition to green energy.

A BESS uses battery storage technology to store energy that is obtained from the electrical grid, renewable energy sources like solar and/or wind power, and other sources. When necessary, such as during peak demand, power interruptions, or grid balancing, the batteries discharge to release energy. To enable the BESS to be connected to an electrical network, other parts are needed in addition to the batteries. The primary component that converts electricity between the DC battery terminals and the AC line voltage and permits power to flow both ways to charge and discharge the battery is a bidirectional inverter, also known as a power conversion system (PCS). Power in megawatt (MW) or kilowatt (kW) and energy in megawatt-hour (MWh) or kilowatt-hour (kWh) ratings must be given for a BESS to be effectively constructed. The advantages of BESS are as follows:

- *Improved use of renewable energy*

  The intermittent nature of renewable energy, especially PV and wind, gets reduced with increased penetration of BESS in the network. Thus, the intermittent unconventional power becomes usable

- *Backup power source*

  BESS serves as an emergency backup power supply when bad weather persists and, in certain regions of the world, prolonged blackouts occur. This increases DNs' power and reliability.

- *Reduced dependence on the main power grid*

  One of the key advantages of BESS is that it reduces reliance on the main electrical power grid by acting as a sole power source with increased penetration levels.

- *Reduced carbon footprint*

  Installing a BESS is a great approach to lessen carbon footprint as the globe works towards a net zero carbon target. By using BESS to harness renewable energy, greenhouse gas emissions are decreased and environmental pollution is mitigated, resulting in a lower carbon footprint.

- *Long-term cost savings*

  Even though these are expensive to install, BESS provides significant long-term energy savings that far exceed their costs over time.

The following are a few **drawbacks** of BESS:

- *High Initial Cost*

  The high initial cost of BESSs is one of the primary drawbacks that might have a substantial upfront cost, particularly when installation expenses are considered.

- *Limited Capacity*

  The limited storage capacity of solar batteries may pose a challenge for households that need to store large amounts of energy. Because these can be more costly, larger battery systems might not be affordable for certain houses.

- *Maintenance Requirements*

  To guarantee maximum performance and longevity, BESSs need to be maintained on a regular basis. This may entail keeping an eye on battery charge levels, doing routine maintenance, and swapping out batteries when necessary.

- *Safety Concerns*

  If BESSs are not installed or maintained correctly, there may be safety risks. If BESSs are broken or put in incorrectly which may overheat or catch fire.

3.3. Components, working and advantages of SVC

This section illustrates and describes the working of SVC. A static VAR compensator is a parallelly connected reactive power absorber or generator. The output is changed to replace the inductive or capacitive current, which controls or manages the corresponding current factors, primarily the bus voltage and power factor. The gate-switching capabilities in thyristors is necessary for a static VAR compensator operation. The thyristors' characteristics and capabilities allow them to control the reactive impedance of the SVC. The fixed capacitor (FC), thyristor switched capacitor (TSC), thyristor switched/controlled reactor (TSR/TCR), and switching resistor (SR) are the essential components of this device. A schematic diagram of SVC is shown in **Fig. 3.0.2**.

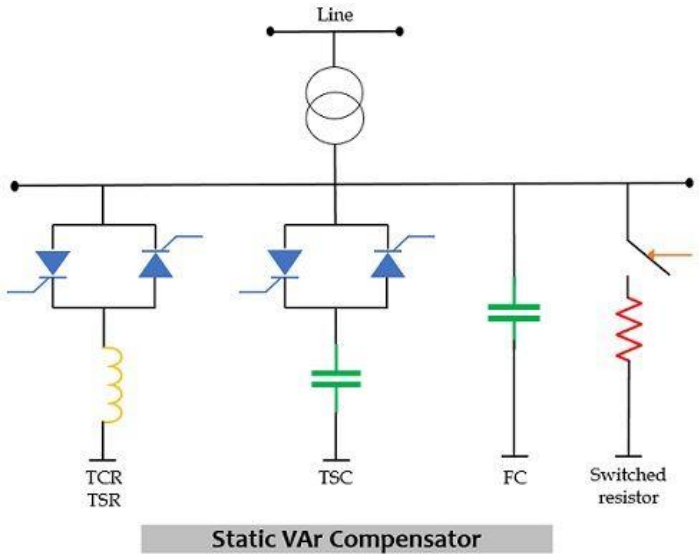

Fig. 3.0.2. Schematic diagram of SVC

The SVC has a control system comprising of:

- A distribution section that computes the firing angle and specifies when the TCR and TSC need to be switched internally and externally.
- A phase-locked loop that is synchronized with the pulse generator and the secondary voltage levels, which transmits the necessary number of pulses to the thyristors, is part of the synchronization section.
- The positive voltage that needs to be controlled is calculated in a separate section.
- A voltage control system that measures the difference in voltage levels between the reference and the calculated values.

The **advantages** of SVC are follows:

- *Improves the voltage stability of DNs*

  The SVC quickly supplies reactive power to control voltage levels. In doing so, the system's voltage is stabilized and the voltage fluctuations are reduced.
- *Power factor correction of DNs*

  SVC maintains the system's power factor at optimal levels by correcting the power factor using reactive power control. As a result, the energy efficiency of DNs get improved.
- *Reactive Power Control of DNs*

  Because of its fast-electronic switching components, the SVC can supply or absorb reactive power quickly. This offers quick response times along with improved power factor and voltage stability.

- *Fast Response Time*

  The benefits of SVC include improved energy system efficiency, decreased voltage fluctuations, and more reliable and efficient system operation of DNs. In doing so, DN performance gets improved and energy costs are reduced.

The following are a few **drawbacks** of SVCs:

- *Increased maintenance cost*

  SVC installation and commissioning may come with hefty upfront expenses. Adoption may be hampered by this, especially in areas with tight budgets or for smaller utilities.
- *Requirements for Maintenance*

  Similar to other intricate electrical apparatus, SVCs necessitate routine upkeep to guarantee peak efficiency. Maintenance tasks may result in downtime and related expenses.
- *Limited Capacity*

  Each SVC unit has a limited amount of capacity. Sometimes there might not be enough capacity to handle significant problems with voltage stability throughout the whole power supply.
- *Complex Control Systems*

  SVC control systems can be complicated, requiring specialized staff for maintenance, monitoring, and programming. The probability of errors or breakdowns in the control system may rise according to its complexity.

3.4. Cost modelling of BESS

The cost of BESS **[112]** is given by

$$Cost_{BESS} = INVC_{BESS} * BESS_{out} + AMC_{BESS} * CCPR * YR_{span} \quad (3.1)$$

$INVC_{BESS}$ and AMC_{BESS} are the investment and annual maintenance costs of BESS, respectively. The investment cost consists of the costs of the battery system, converter, and installation. The annual maintenance cost includes expenses due to maintenance, replacement, and energy.

3.5.Cost modelling of SVC

The cost of SVC **[104]** over the entire planning period is given by:

$$Cost_{SVC} = INVC_{SVC} * Q_{SVC} + (AMC_{SVC} * CCPR * YR_{span}) \quad (3.2)$$

$Q_{SVC}$is the reactive power output of the SVC in kVAR. $INVC_{SVC}$ and AMC_{SVC} are the investment and annual maintenance costs of the SVC, respectively.

3.6. Formulation of the objective function (*OF*) due to BESS/SVC integration

The components of the *OF* in equation 2.26 is redefined in this work due to integration of BESS and SVC along with PV and wind-based DGs. These are explained in the following subsections.

3.6.1. Voltage profile enhancement index (*VPEI*) due to BESS/SVC integration

The following equation describes the $VPEI$ of a DN after optimal DG, BESS, and SVC allocation.

$$VPEI = \frac{(VPI)_{with\ DG/BESS/SVC}}{(VPI)_{without\ DG/BESS/SVC}} \tag{3.3}$$

3.6.2. Benefit cost ratio (*BCR*) due to BESS/SVC integration

After optimal DG, BESS, and SVC allocation, the BCR of the DN is given by

$$BCR = \frac{Total\ Benefit_{DG/BESS/SVC}}{Total\ Cost_{DG/BESS/SVC}} \tag{3.4}$$

The variables $Total\ Benefit_{DG}$ and $Total\ Cost_{DG/BESS/SVC}$ are the total benefit derived and cost involved of the DN in USD in presence of DG, BESS, and SVC, respectively.

$$Total\ Cost_{DG/BESS/SVC} = Cost_{\ WIND} + Cost_{\ PV} + Cost_{\ SVC} \tag{3.5}$$

The total benefit of the network ($Total\ Benefit_{DG/BESS}$) in USD is given by

$$Total\ Benefit_{DG/BESS/SVC} = \left\{P_{out}{}' * PLTF + \left(PL_{W/O} - PL_W{}'\right)\right\} * YR_{span} * 8760 * C_{PGEN} * CCPR \tag{3.6}$$

$P_{out}{}'$ is the total active power output in kW from DG and BESS. $PL_W{}'$ is the active power loss of the network in kW in presence of DG, BESS, and SVC.

3.6.3. Emission cost benefit index (*ECBI*) due to BESS/SVC integration

The emission cost benefit index is given by:

$$ECBI = \frac{EC_{without\ DG/BESS/SVC} - EC_{with\ DG/BESS/SVC}}{EC_{without\ DG/BESS/SVC}} \tag{3.7}$$

$EC_{without\ DG/BESS/SVC}$ and $EC_{with\ DG/BESS/SVC}$ represent the emission costs with and without DG, BESS, and SVC integration in the DNs, respectively.

3.7.Operational Constraints

The objective function OF must adhere to the following additional constraints along with the constraints defined in equations 2.39 to 2.44.

i) Active power generation limits of BESS

$$P_{BESS,min} \leq P_{BESS} \leq P_{BESS,max} \quad (3.8)$$

P_{BESS} is the power output of BESS. $P_{BESS,min}$ and $P_{BESS,max}$ are the minimum and maximum limits.

ii) Reactive power generation limits of SVC

$$Q_{SVC,min} \leq Q_{SVC} \leq Q_{SVC,max} \quad (3.9)$$

Q_{SVC} is the reactive power generated by the main generator. $Q_{SVC,max}$ and$Q_{SVC,min}$ are the maximum and minimum limits.

3.8. Case studies under consideration

The following case studies of BESS and SVC integration with DG integrated DNs are presented and their detailed analyses are discussed in the following subsections.

Case study#3.1: *Optimal sizing and sitting of single, twin, and triple point allocation of probabilistic PV, wind, and BESS at the IEEE 85 and 141 bus DNs*

Case study #3.2: *Optimal sizing and single, twin, and triple point allocation of PV, wind, and SVC at the IEEE 141 bus and real-time 13 bus substation DNs considering renewables and load uncertainties*

Table 3.0.1. Data used for SVC/BESS Allocation

Parameter	Value	Parameter	Value
$INVC_{BESS}$	100USD/kW	AMC_{BESS}	15% of $INVC_{BESS}$
AMC_{SVC}	3% of IC_{SVC}	$INVC_{SVC}$	70 USD/kVAR
$P_{BESS,max}$, $P_{BESS,min}$	1000 kW, 0 kW	$Q_{SVC,max}$, $Q_{SVC,min}$	100 kVAR, 0 kVAR

Table 3.0.1. presents the data used for BESS/SVC allocation **[104]**. The data of PV and wind-based DGs are taken from **Table 2.0.1.**

3.8.1. **Case study#3.1:** Optimal sizing and sitting of single, twin, and triple point allocation of probabilistic PV, wind, and BESS at the IEEE 85 and 141 bus DNs.

Case Study Description: This case study explores the impact of optimal sizing and single, twin, and triple point allocation of PV, wind, and BESS at the IEEE 85 and 141 bus DNs. The algorithms in comparison are PSO, LPSO, RPSO, PSO-SR, CSA, and Jaya. The probabilistic natures of PV and wind are modelled using Beta and Weibull probability distribution functions, respectively.

The simulation process is done in MATPOWER v7.0, Intel Core i7 9750H, 2.60 GHz and 8 GB RAM. Six different case studies, namely, "BESS", "PV+BESS", "WIND+BESS", "PV+PV+BESS", "WIND+WIND+BESS", and "PV+WIND+BESS", are analyzed for each of the two DNs. The said case studies are detailed in the sub-cases **3.1.1** to **3.1.6**. The problem-specific flowchart is shown in **Fig. 3.1.1.**

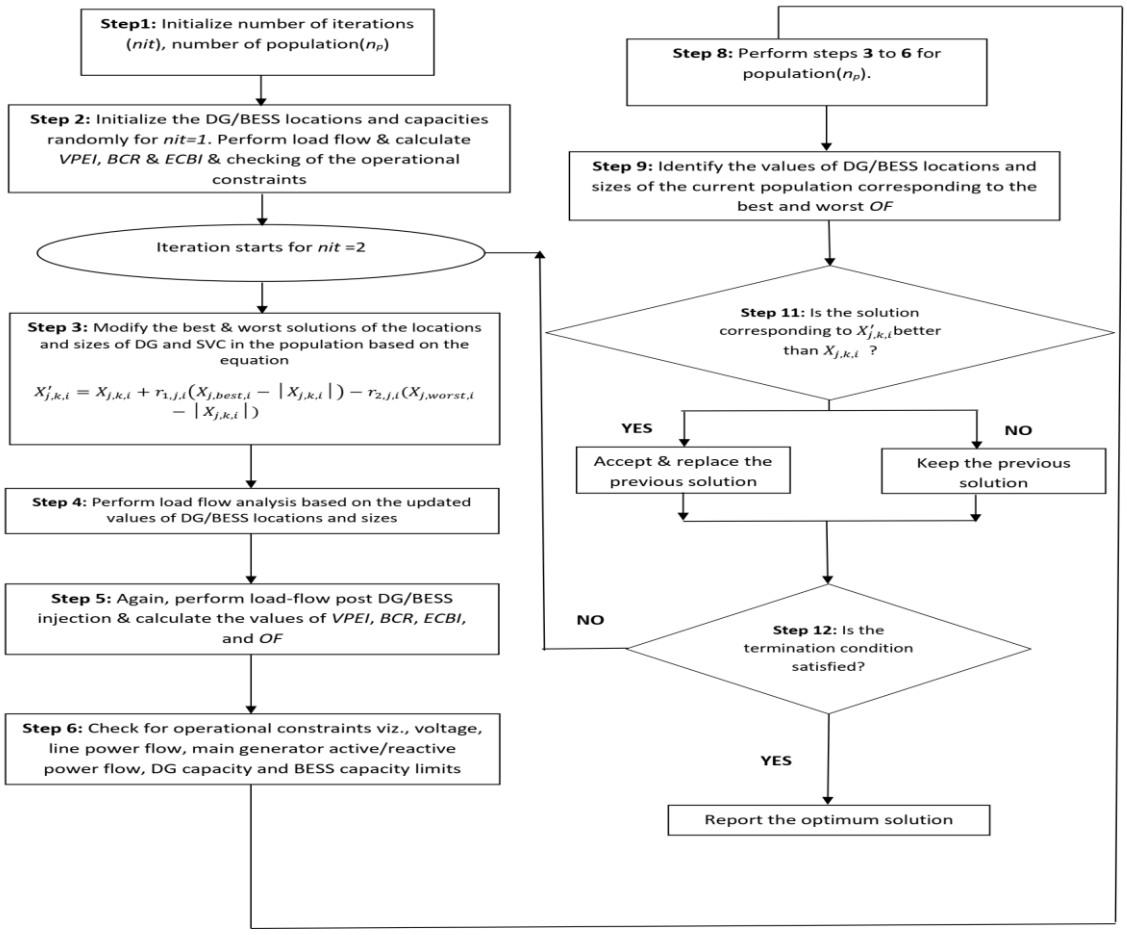

Fig. 3.1.1. Problem-specific flowchart showing Jaya Algorithm applied to the problem defined under the Case-Study# 3.1

3.8.1.1. ***Subcase #3.1.1:*** Single point BESS injection

Table 3.1.1. shows the values of the network indices, active power losses, optimal points of injection, and computation times for single point BESS injection using Jaya algorithm.

Table 3.1.1. Results of single point BESS injection at the IEEE 85 and 141 bus DNs (Subcase #3.1.1) using Jaya Algorithm under Case Study #3.1

Sub-Case	DN	*VPEI*	*BCR*	*ECBI*	*OF*	$PL_{W/O}$ (kW)	$PL_W{}'$ (kW)	Injected value of DG/BESS (kW)	Optimal point of injection	Computation Time (secs)
BESS	IEEE 85	16.4814	24.1122	0.3336	13.6288	316.14	214.50	861.37	48	26.08
	IEEE 141	1.0191	23.6487	0.0279	8.2237	629.06	594.11	315.11	51	38.83

3.8.1.2. ***Subcase #3.1.2:*** Twin point PV and BESS injection

Table 3.1.2. shows the values of the network indices, active power losses, optimal points of injection, and computation times for twin point PV and BESS injection using Jaya algorithm.

Table 3.1.2. Results of twin point PV+BESS injection at the IEEE 85 and 141 bus DNs (Subcase #3.1.2) using Jaya Algorithm under Case Study #3.1

Sub-Case	DN	*VPEI*	*BCR*	*ECBI*	*OF*	$PL_{W/O}$ (kW)	$PL_W{}'$ (kW)	Injected value of DG/BESS (kW)	Optimal point of injection	Computation Time (secs)
PV+BESS	IEEE 85	16.3893	6.1257	0.3281	7.6068	316.14	216.11	377.02 470.08	53 49	26.91
	IEEE 141	1.1121	13.9516	0.1831	5.0771	629.06	438.30	1777.00 326.28	49 80	40.03

3.8.1.3. ***Subcase #3.1.3:*** Twin point wind and BESS injection

Table 3.1.3. shows the values of the network indices, active power losses, optimal points of injection, and computation times for twin point wind and BESS injection using Jaya algorithm.

Table 3.1.3. Results of twin point WIND+BESS injection at the IEEE 85 and 141 bus DNs (Subcase #3.1.3) using Jaya Algorithm under Case Study #3.1

Sub-Case	DN	*VPEI*	*BCR*	*ECBI*	*OF*	$PL_{W/O}$ (kW)	$PL_W{}'$ (kW)	Injected value of DG/BESS (kW)	Optimal point of injection	Computation Time (secs)
WIND+ BESS	IEEE 85	13.6375	44.5237	0.2650	19.4559	316.14	221.65	612.67 57.80	35 76	25.75
	IEEE 141	1.0653	35.9192	0.1016	12.3497	629.06	513.04	872.18 285.57	50 43	35.59

3.8.1.4. ***Subcase #3.1.4:*** Triple point PV, PV, and BESS injection

Table 3.1.4. shows the values of the network indices, active power losses, optimal points of injection, and computation times for triple PV, PV, and BESS injection using Jaya algorithm.

Table 3.1.4. Results of triple point PV+PV+BESS injection at the IEEE 85 and 141 bus DNs (Subcase #3.1.4) using Jaya Algorithm under Case Study #3.1

Sub-Case	DN	*VPEI*	*BCR*	*ECBI*	*OF*	$PL_{W/O}$ (kW)	$PL_W{}'$ (kW)	Injected value of DG/BESS (kW)	Optimal point of injection	Computation Time (secs)
PV+PV+ BESS	IEEE 85	13.8634	5.5339	0.2625	6.5467	316.14	224.00	246.69 201.91 217.03	53 50 46	25.73
	IEEE 141	1.1222	15.6233	0.2036	5.6441	629.06	419.81	1179.40 886.90 276.05	87 79 67	34.64

3.8.1.5. ***Subcase #3.1.5:*** Triple point wind, wind, and BESS injection

Table 3.1.5. shows the values of the network indices, active power losses, optimal points of injection, and computation times for triple wind, wind, and BESS injection using Jaya algorithm.

Table 3.1.5. Results of triple point WIND+WIND+BESS injection at the IEEE 85 and 141 bus DNs (Subcase #3.1.5) using Jaya Algorithm under Case Study #3.1

Sub-Case	DN	*VPEI*	*BCR*	*ECBI*	*OF*	$PL_{W/O}$ (kW)	$PL_W{}'$ (kW)	Injected value of DG/BESS (kW)	Optimal point of injection	Computation Time (secs)
WIND + WIND + BESS	IEEE 85	15.5926	42.1591	0.3320	19.3419	316.14	201.48	343.77 331.61 168.50	68 52 32	26.04
	IEEE 141	1.0414	39.1233	0.0623	13.3956	629.06	554.84	327.07 355.25 23.81	86 87 123	36.7

3.8.1.6. ***Subcase #3.1.6:*** Triple point PV, wind, and BESS injection

Table 3.1.6. shows the values of the network indices, active power losses, optimal points of injection, and computation times for triple PV, wind, and BESS injection using Jaya algorithm.

Table 3.1.6. Results of triple point PV+WIND+BESS injection at the IEEE 85 and 141 bus DNs (Subcase #3.1.6) using Jaya Algorithm under Case Study #3.1

Sub-Case	DN	*VPEI*	*BCR*	*ECBI*	*OF*	$PL_{W/O}$ (kW)	$PL_W{}'$ (kW)	Injected value of DG/BESS (kW)	Optimal point of injection	Computation Time (secs)
PV+WIND+ BESS	IEEE 85	16.0568	8.0301	0.3448	8.1357	316.14	206.21	245.63 338.26 301.48	14 52 49	26.8
	IEEE 141	1.0922	13.3800	0.1470	4.8682	629.06	468.71	1132.50 299.46 249.98	50 46 80	38.25

3.8.1.7. Result analysis of ***Case Study #3.1***

The result analysis of the **Case Study #3.1** is presented in this sub-section for all the sub-cases of the IEEE 85 and 141 bus systems under consideration.

IEEE 85 bus DN

Fig. 3.1.2. and **Fig. 3.1.3.** show the comparative chart of the network indices and network active power losses, respectively, for the IEEE 85 bus DN. The highest *VPEI*, *BCR*, *ECBI*, and *OF* are obtained for the test cases "BESS", "WIND+BESS", "PV+WIND+BESS", and "WIND+BESS", respectively, of values 16.4814, 44.5237, 0.3448, and 19.4559, respectively.

The lowest *VPEI*, *BCR*, *ECBI*, and *OF* are obtained for the test case "WIND+BESS", "PV+PV+BESS", "PV+PV+BESS", and "PV+PV+BESS" with values of 13.6375, 5.5339, 0.2625, and 6.5467, respectively. The highest active power loss reduction of 36.27% is observed for the test case " WIND+WIND+BESS".

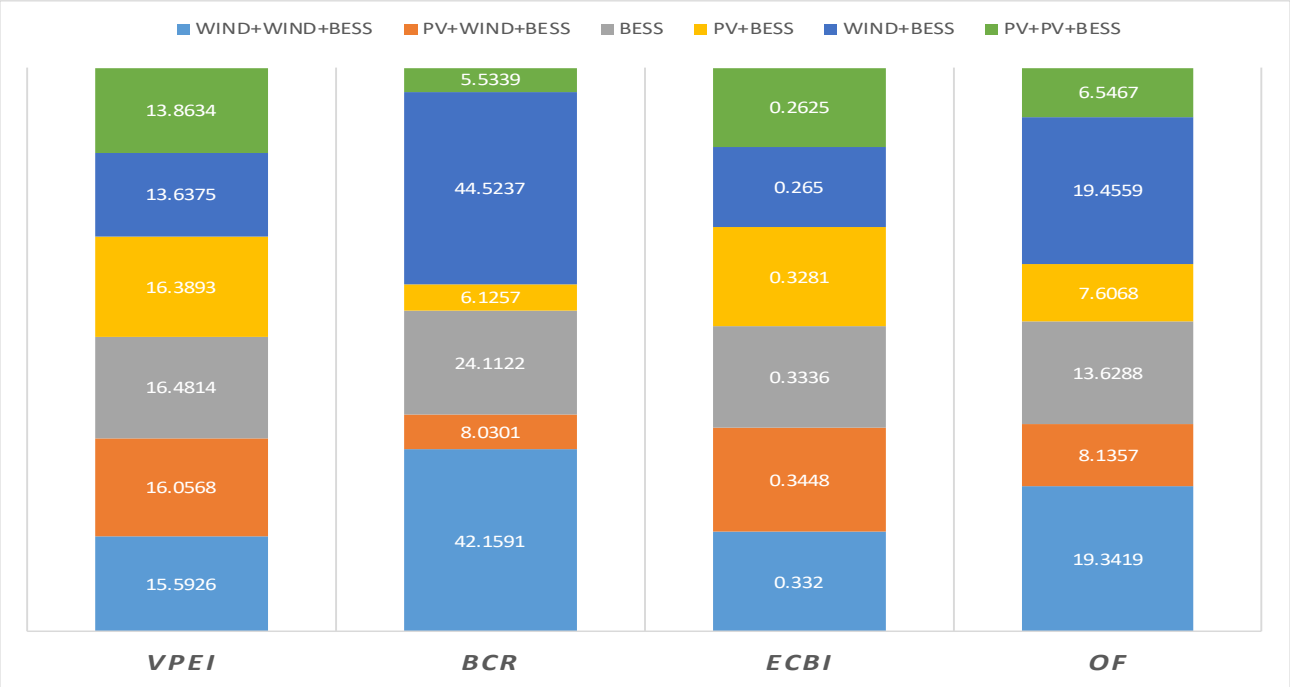

Fig. 3.1.2. Comparative chart showing *VPEI*, *BCR*, *ECBI*, and *OF* obtained for IEEE 85 bus DN for all test scenarios under Case Study #3.1

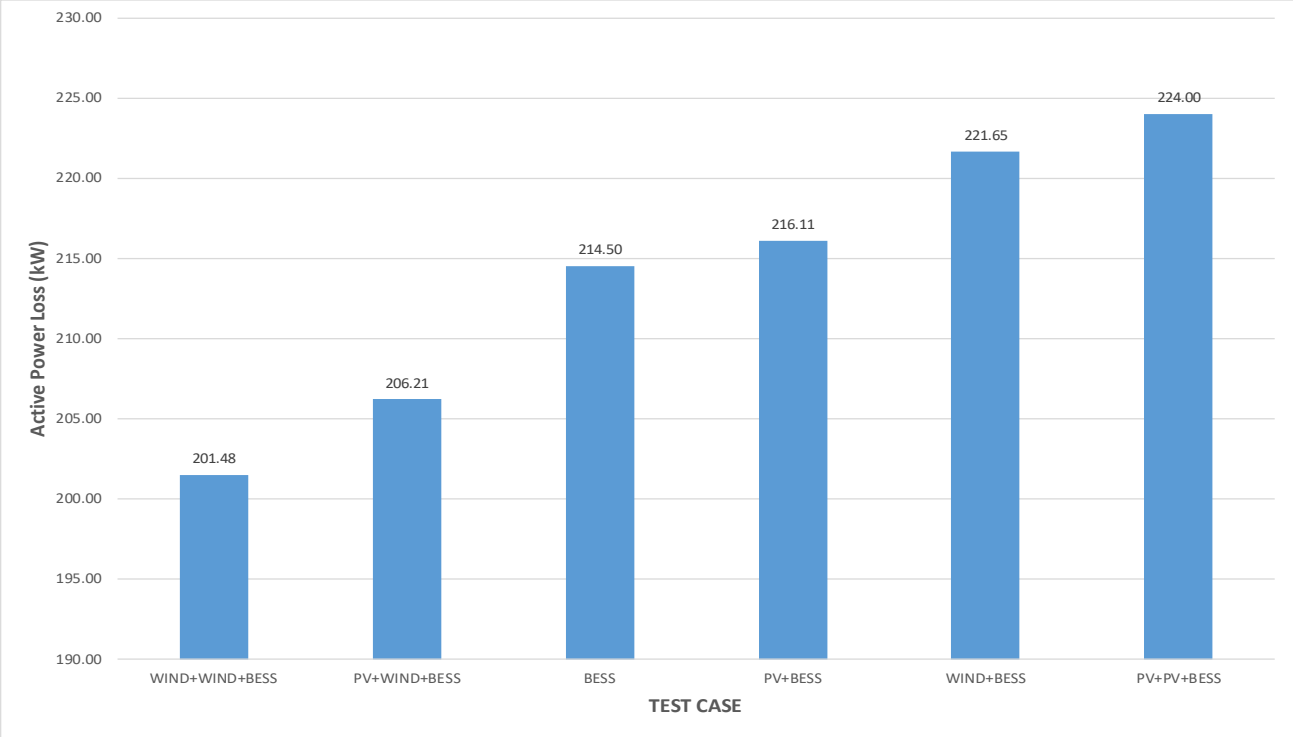

Fig. 3.1.3. Comparative chart showing active power loss for IEEE 85 bus DN for all test scenarios under Case Study #3.1

IEEE 141 bus DN

Fig. 3.1.4. and **Fig. 3.1.5.** show the comparative chart of the network indices and network active power losses, respectively, for the IEEE 141 bus DN. The highest *VPEI*, *BCR*, *ECBI*, and *OF* are obtained for the test cases "PV+PV+BESS", "WIND+WIND+BESS", "PV+PV+BESS", and "WIND+WIND+BESS", respectively, of values 1.1222, 39.1233, 0.2036, and 13.3956, respectively. The lowest *VPEI*, *BCR*, *ECBI*, and *OF* are obtained for the test cases "BESS", "PV+WIND+BESS", "BESS", and "PV+WIND+BESS", with values of 1.0191, 13.3800, 0.0279, and 4.8682, respectively. The highest active power loss reduction of 33.26% is observed for the test case "PV+PV+BESS".

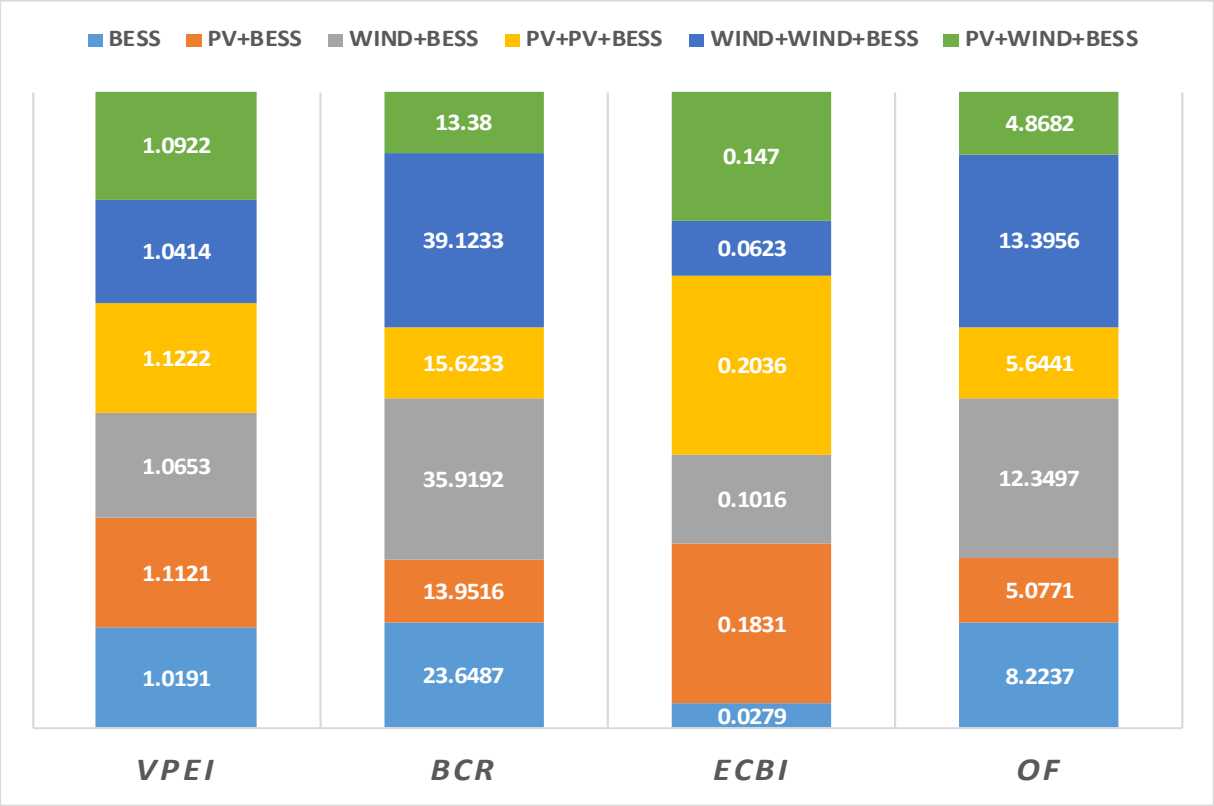

Fig. 3.1.4. Comparative chart showing *VPEI*, *BCR*, *ECBI*, and *OF* obtained for IEEE 141 bus DN for all test scenarios under Case Study #3.1

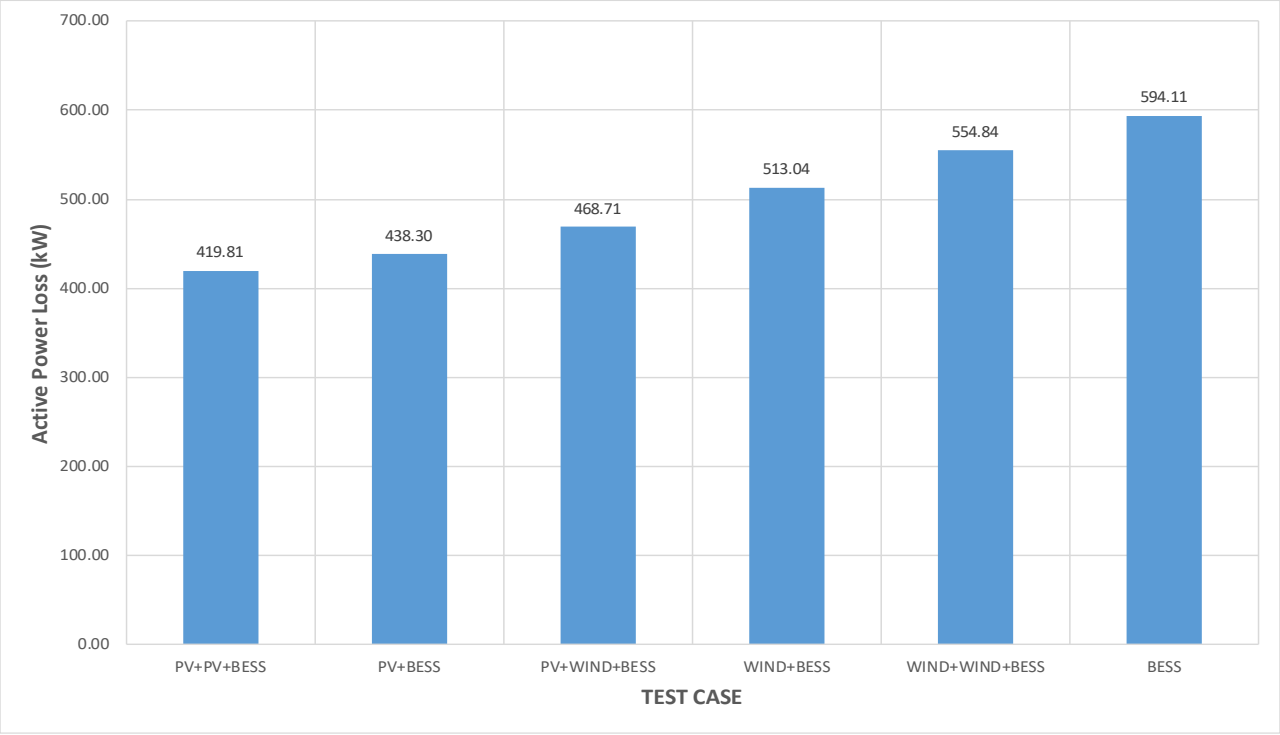

Fig. 3.1.5. Comparative chart showing active power loss for IEEE 141 bus DN for all test scenarios under Case Study #3.1

Fig. 3.1.6. *VSI* characteristics before and after PV+WIND+BESS allocation at IEEE 85 bus under the Case-Study# 3.1

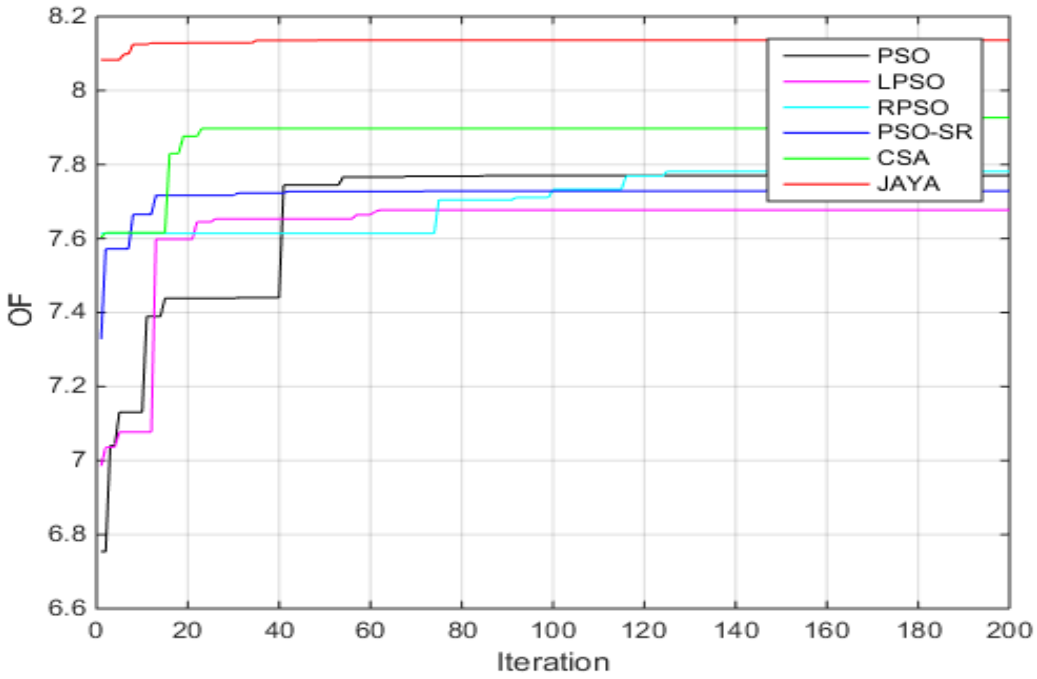

Fig. 3.1.7. Relative convergence characteristics of the objective function after PV+WIND+BESS allocation at IEEE 85 bus under the Case-Study# 3.1

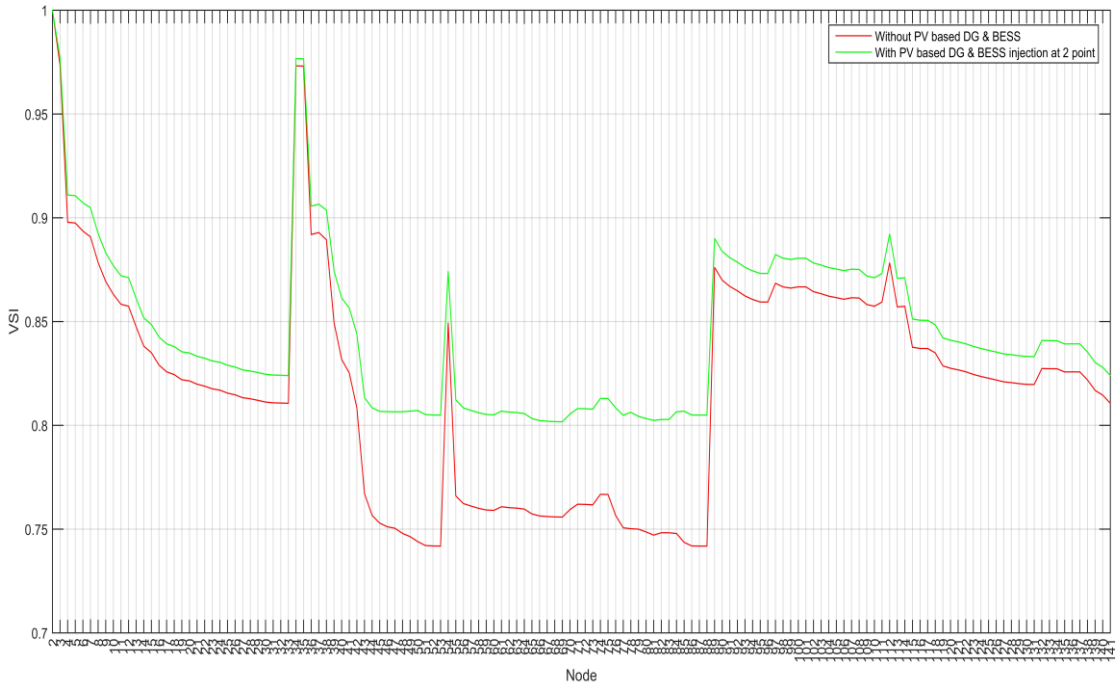

Fig. 3.1.8. *VSI* characteristics before and after PV+BESS allocation at IEEE 141 bus under the Case-Study# 3.1

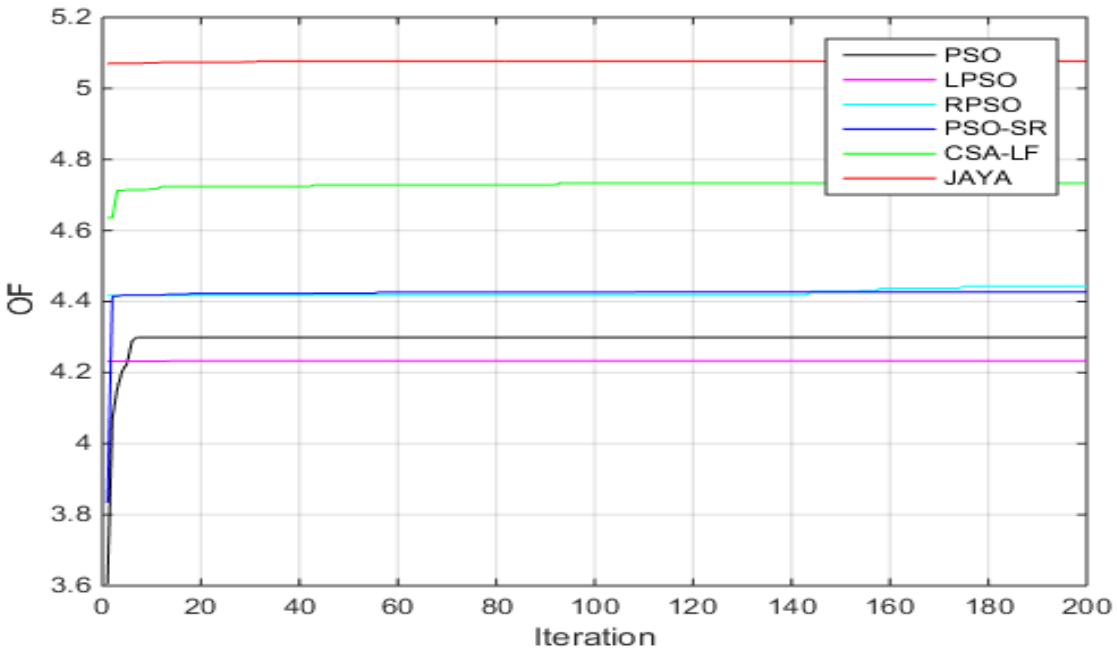

Fig. 3.1.9. Relative convergence characteristics of the objective function after PV+BESS allocation at IEEE 141 bus under the Case-Study# 3.1

The convergence characteristics of the *OF* obtained by using different algorithms for triple point PV, wind, and BESS allocation (PV+WIND+BESS) and twin point PV and BESS allocation (PV+BESS) at the IEEE 85 and 141 bus DNs are shown in **Fig. 3.1.7.** and **Fig. 3.1.9**., respectively as examples. Likewise, the improvement in the *VSI* characteristics of the IEEE 85 bus DN triple point PV, wind, and BESS (PV+WIND+BESS) allocation and the IEEE 141 bus DN for twin point PV and BESS allocation (PV+BESS) are shown in **Fig. 3.1.6**. and **Fig. 3.1.8**., respectively.

3.8.2. **Case study #3.2:** Optimal sizing and single, twin, and triple point allocation of PV, wind, and SVC at the IEEE 141 bus and real-time 13 bus substation DNs considering renewables and load uncertainties

Case Study Description: This case study explores the impact of optimal sizing and single, twin, and triple point allocation of PV, wind, and SVC at the IEEE 141 bus and real-time 13 bus substation DNs. The algorithms in comparison are PSO, LPSO, RPSO, PSO-SR, CSA, COA, and Jaya. The probabilistic natures of PV and wind are modelled using Beta and Weibull probability distribution functions, respectively. The uncertain nature of load is modelled using normal probability distribution function. The simulation process is done in MATPOWER v7.0, Intel Core i7 9750H, 2.60 GHz and 24 GB RAM. Eight different case studies, namely, “PV”, “WIND”, “PV+SVC”, “WIND+SVC”, “PV+PV+SVC”, “PV+SVC+SVC”, “WIND+WIND+SVC”, and “WIND+SVC+SVC”, are analyzed for each of the two DNs. The said case studies are detailed in the sub-cases **3.2.1** to **3.2.8**.

The problem-specific flowchart is shown in **Fig. 3.2.1.**

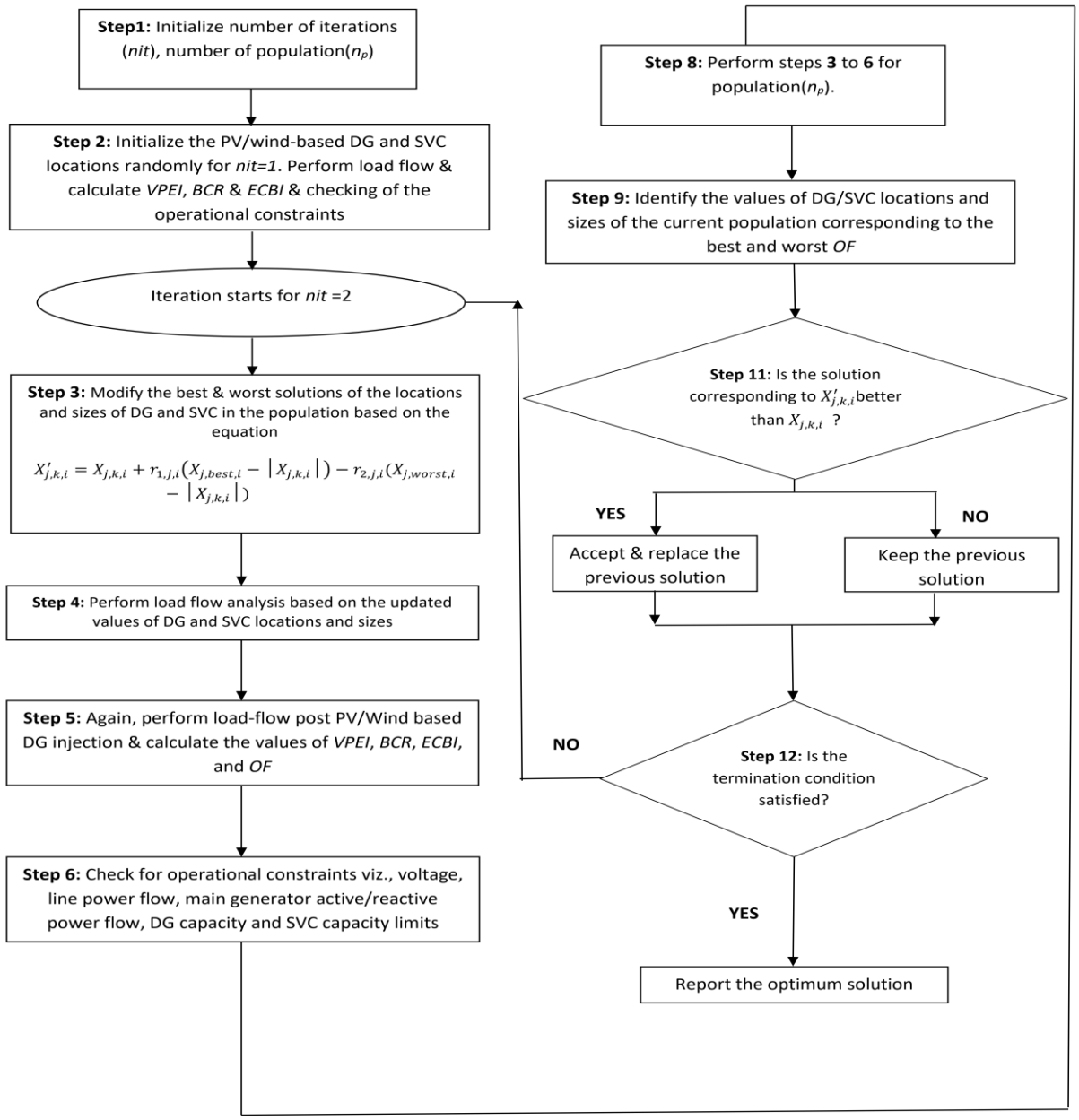

Fig. 3.2.1. Problem-specific flowchart showing Jaya algorithm applied to the problem defined under the Case-Study# 3.2

3.8.2.1. ***Subcase #3.2.1:*** *Single point PV injection*

Table 3.2.1 shows the values of the network indices, active power losses, optimal points of injection, and computation times for single point PV injection using Jaya algorithm.

Table 3.2.1. Results of single point PV based DG injection at the IEEE 141 bus and 13 bus Maharashtra substation DNs (Subcase #3.2.1) using Jaya Algorithm under Case Study #3.2

Sub-Case	DN	*VPEI*	*BCR*	*ECBI*	*OF*	$PL_{W/o}$ (kW)	$PL_W{}'$ (kW)	Values of DG (kW) /SVC (kVAR)	Optimal point of injection	Computation Time (secs)
PV	IEEE 141	1.1393	11.6194	0.2421	4.3293	629.06	396.56	2801.00	76	18.93
	13 bus	1.9898	14.4266	0.2592	5.553	3010.16	1818.90	8272.40	9	16.82

3.8.2.2. ***Subcase #3.2.2:*** *Single point wind injection*

Table 3.2.2 shows the values of the network indices, active power losses, optimal points of injection, and computation times for single point wind-based DG injection using Jaya algorithm.

Table 3.2.2. Results of single point wind-based DG injection at the IEEE 141 bus and 13 bus Maharashtra substation DNs (Subcase #3.2.2) using Jaya Algorithm under Case Study #3.2

Sub-Case	DN	*VPEI*	*BCR*	*ECBI*	*OF*	$PL_{W/o}$ (kW)	$PL_W{}'$ (kW)	Values of DG (kW) /SVC (kVAR)	Optimal point of injection	Computation Time (secs)
WIND	IEEE 141	1.0185	31.0076	0.0270	10.6737	629.06	595.21	304.30	51	55.65
	13 bus	1.3579	52.8113	0.0486	18.0546	3010.16	2517.50	1283.20	8	20.44

3.8.2.3. ***Subcase #3.2.3:*** *Twin point PV and SVC injection*

Table 3.2.3 shows the values of the network indices, active power losses, optimal points of injection, and computation times for twin point PV based DG and SVC injection using Jaya algorithm.

Table 3.2.3. Results of twin point PV based DG and SVC injection at the IEEE 141 bus and 13 bus Maharashtra substation DNs (Subcase #3.2.3) using Jaya Algorithm under Case Study #3.2

Sub-Case	DN	*VPEI*	*BCR*	*ECBI*	*OF*	$PL_{W/O}$ (kW)	$PL_W{}'$ (kW)	Values of DG (kW) /SVC (kVAR)	Optimal point of injection	Computation Time (secs)
PV + SVC	IEEE 141	1.1459	14.9269	0.2398	5.4321	629.06	388.68	2882.10 8.09	79 45	55.28
	13 bus	1.9499	20.0157	0.2246	7.3893	3010.16	1782.50	8157.50 22.35	12 2	16.75

3.8.2.4. ***Subcase #3.2.4:*** *Twin point wind and SVC injection*

Table 3.2.4 shows the values of the network indices, active power losses, optimal points of injection, and computation times for twin point wind-based DG and SVC injection using Jaya algorithm.

Table 3.2.4. Results of twin point wind-based DG and SVC injection at the IEEE 141 bus and 13 bus Maharashtra substation DNs (Subcase #3.2.4) using Jaya Algorithm under Case Study #3.2

Sub-Case	DN	*VPEI*	*BCR*	*ECBI*	*OF*	$PL_{W/O}$ (kW)	$PL_W{}'$ (kW)	Values of DG (kW) /SVC (kVAR)	Optimal point of injection	Computation Time (secs)
WIND + SVC	IEEE 141	1.2117	36.4004	0.1358	12.5701	629.06	146.78	476.22 63.72	15 32	29.10
	13 bus	1.5305	79.6754	0.0759	27.0668	3010.16	2295.40	2055.10 72.20	8 9	17.61

*3.8.2.5.****Subcase #3.2.5:*** *Triple point PV, PV, and SVC injection*

Table 3.2.5 shows the values of the network indices, active power losses, optimal points of injection, and computation times for triple point PV, PV, and SVC injection using Jaya algorithm.

Table 3.2.5. Results of triple point PV, PV, and SVC injection at the IEEE 141 bus and 13 bus Maharashtra substation DNs (Subcase #3.2.5) using Jaya Algorithm under Case Study #3.2

Sub-Case	DN	*VPEI*	***BC**R*	***EC**BI*	***OF***	$PL_{W/O}$ (kW)	$PL_W{}'$ (kW)	Values of DG (kW) /SVC (kVAR)	Optimal point of injection	Computation Time (secs)
PV+PV+ SVC	IEEE 141	1.1582	28.0641	0.2730	9.8219	629.06	366.57	1720.30 1549.90 12.86	49 60 46	58.43
	13 bus	2.6598	52.1328	0.2456	18.3277	3010.16	994.60	4135.00 3958.50 40.16	8 13 6	17.92

3.8.2.6. ***Subcase #3.2.6:*** *Triple point PV, SVC, and SVC injection*

Table 3.2.6 shows the values of the network indices, active power losses, optimal points of injection, and computation times for triple point PV, SVC, and SVC injection using Jaya algorithm.

Table 3.2.6. Results of triple point PV, SVC, and SVC injection at the IEEE 141 bus and 13 bus Maharashtra substation DNs (Subcase #3.2.6) using Jaya Algorithm under Case Study #3.2

Sub-Case	DN	*VPEI*	***BC**R*	***EC**BI*	***OF***	$PL_{W/O}$ (kW)	$PL_W{}'$ (kW)	Values of DG (kW) /SVC (kVAR)	Optimal point of injection	Computation Time (secs)
PV+ SVC+ SVC	IEEE 141	1.2782	17.8499	0.2871	6.4653	629.06	208.47	3482.70 45.29 6.35	76 11 43	57.06
	13 bus	2.5568	22.4073	0.2842	8.4077	3010.16	1546.90	9207.60 48.55 36.04	12 2 6	17.05

3.8.2.7. ***Subcase #3.2.7:*** Triple point wind, wind, and SVC injection

Table 3.2.7 shows the values of the network indices, active power losses, optimal points of injection, and computation times for triple point wind, wind, and SVC injection using Jaya algorithm.

Table 3.2.7. Results of triple point wind, wind, and SVC injection at the IEEE 141 bus and 13 bus Maharashtra substation DNs (Subcase #3.2.7) using Jaya Algorithm under Case Study #3.2

Sub-Case	DN	*VPEI*	*BCR*	*ECBI*	*OF*	$PL_{W/O}$ (kW)	PL_W' (kW)	Values of DG (kW) /SVC (kVAR)	Optimal point of injection	Computation Time (secs)
WIND+ WIND+ SVC	IEEE 141	1.0142	41.3083	0.0202	14.1001	629.06	602.60	147.24 85.10 40.75	86 80 51	54.67
	13 bus	1.4354	89.5539	0.0442	30.3142	3010.16	2510.00	649.01 624.56 7.58	8 13 2	18.06

*3.8.2.8.****Subcase #3.2.8:*** *Triple point wind, SVC, and SVC injection*

Table 3.2.8 shows the values of the network indices, active power losses, optimal points of injection, and computation times for triple point wind, SVC, and SVC injection using Jaya algorithm.

Table 3.2.8. Results of triple point wind, SVC, and SVC injection at the IEEE 141 bus and 13 bus Maharashtra substation DNs (Subcase #3.2.8) using Jaya Algorithm under Case Study #3.2

Sub-Case	DN	*VPEI*	*BCR*	*ECBI*	*OF*	$PL_{W/O}$ (kW)	PL_W' (kW)	Values of DG (kW) /SVC (kVAR)	Optimal point of injection	Computation Time (secs)
WIND + SVC + SVC	IEEE 141	1.0262	40.2581	0.0384	13.7604	629.06	581.32	433.62 41.89 37.46	86 141 103	54.52
	13 bus substation DN, Maharashtra	1.9539	81.9139	0.1063	27.9634	3010.16	1917.80	2787.80 141.75 146.73	8 12 13	17.44

3.8.2.9. Result analysis of ***Case Study #3.2***

The result analysis of the ***Case Study #3.2*** is presented in this sub-section for all the sub-cases of the IEEE 141 bus and 13 bus substation DNs.

IEEE 141 bus DN

Fig. 3.2.2. and Fig. 3.2.3. show the comparative chart of the network indices (*VPEI*, *BCR*, *ECBI*, and *OF*) and network active power losses, respectively, for the IEEE 141 bus DN. The highest *VPEI*, *BCR*, *ECBI*, and *OF* are obtained for the test cases "PV+SVC+SVC", "WIND+WIND+SVC", "PV+SVC+SVC", and "WIND+WIND+SVC", respectively, of values 1.2782, 41.3083, 0.2871, and 14.1001, respectively. The lowest *VPEI*, *BCR*, *ECBI*, and *OF* are obtained for the test cases "WIND+WIND+SVC", "PV", "WIND+WIND+SVC", and "PV" with values of 1.0142, 11.6194, 0.0202, and 4.3293, respectively. The highest active power loss reduction of 76.67% is observed for the test case " WIND+SVC".

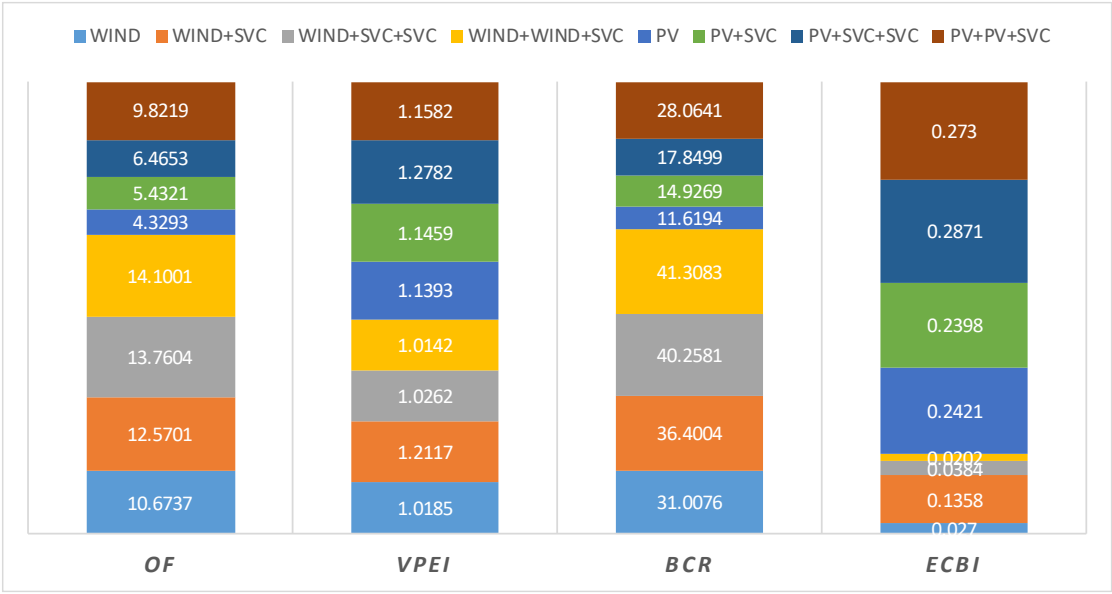

Fig. 3.2.2. Comparative chart showing *VPEI*, *BCR*, *ECBI*, and *OF* obtained for IEEE 141 bus DN for all test scenarios under Case Study #3.2

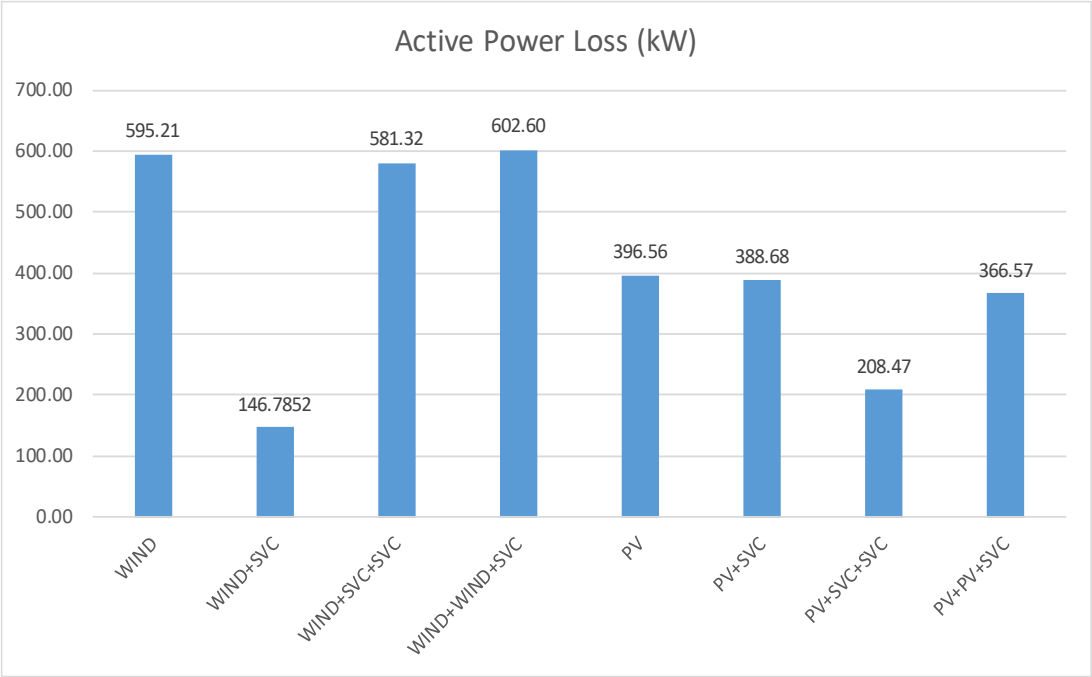

Fig. 3.2.3. Comparative chart showing active power loss for IEEE 141 bus DN for all test scenarios under Case Study #3.2

13 bus substation DN, Maharashtra, India

Fig. 3.2.4. **and Fig. 3.2.5**. show the comparative chart of the network indices (*VPEI*, *BCR*, *ECBI*, and *OF*) and network active power losses, respectively, for the 13-bus substation DN, Maharashtra. The highest *VPEI*, *BCR*, *ECBI*, and *OF* are obtained for the test cases "PV+PV+SVC", "WIND+WIND+SVC", "PV+SVC+SVC", and "WIND+WIND+SVC", respectively, of values 2.6598, 89.5539, 0.2842, and 30.3142, respectively. The lowest *VPEI*, *BCR*, *ECBI*, and *OF* are obtained for the test cases "WIND", "PV", "WIND+WIND+SVC", and "PV" with values of 1.3579, 14.4266, 0.0442, and 5.553, respectively. The highest active power loss reduction of 66.96% is observed for the test case " PV+PV+SVC".

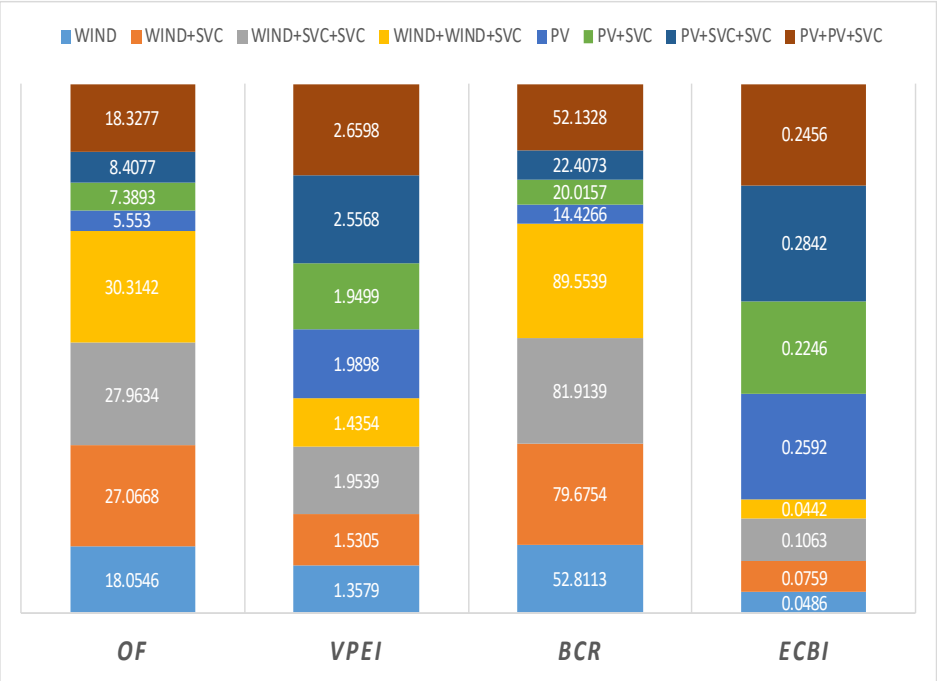

Fig. 3.2.4. Comparative chart showing *VPEI*, *BCR*, *ECBI*, and *OF* obtained for 13 bus substation DN, Maharashtra for all test scenarios under Case Study #3.2

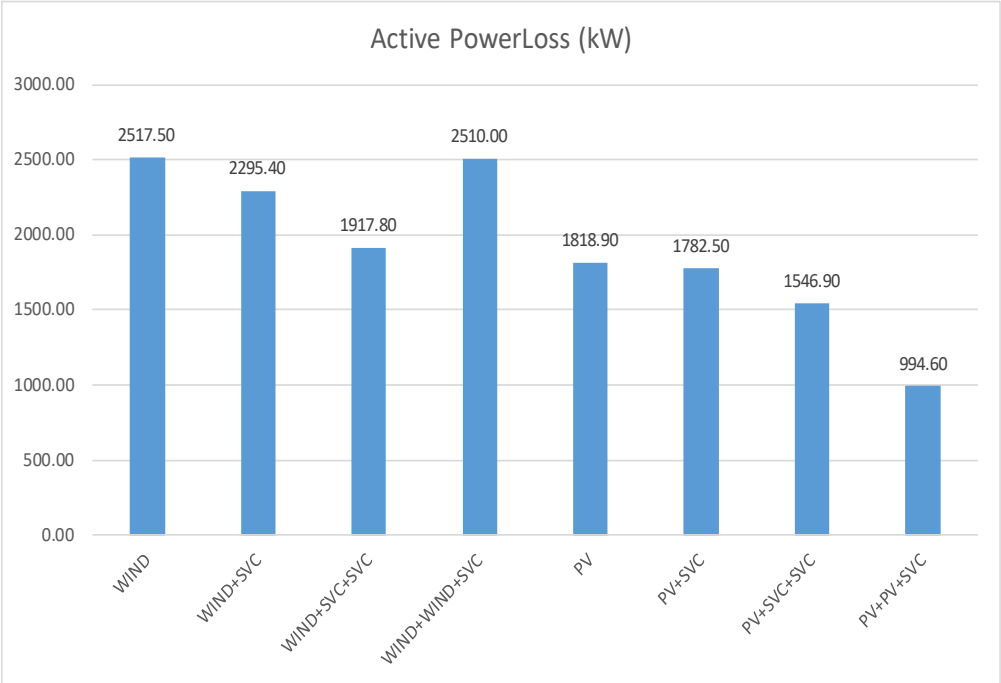

Fig. 3.2.5. Comparative chart showing active power loss for 13 bus substation DN, Maharashtra for all test scenarios under Case Study #3.2

3.9. Statistical analysis of the performance of algorithms in comparison for Subcase #3.2.7

In this section, the consistency, robustness, and superiority of Jaya algorithm are analysed with reference to the comparing algorithms, viz., PSO, LPSO, RPSO, PSO-SR, CSA, and COA. Test case " WIND+WIND+SVC" of 13 bus substation DN (***Subcase #3.2.7***), Maharashtra has been considered for analysis. Each algorithm had been executed for 50 independent trials. Their maximum, minimum, mean, and standard deviations had been recorded. The box-whiskers plot is shown in **Fig. 3.2.6.** The relative mean values of the *OF* using the Jaya algorithm and other comparing algorithms are shown in **Fig. 3.2.7.** It means that there is a significant difference in the *OF* obtained by the Jaya and other comparing algorithms.

Table 3.2.9. presents the p-values that resulted from doing these tests of normality and can be concluded that none of the sample results acquired by each method follow a normal distribution because of this reason.

The results of Kruskal-Wallis-H-ANOVA and post-hoc Dunn tests are reported in **Table 3.2.9.** and **Table 3.2.10**. The test statistic H is 245.7901, which is outside the 95% confidence interval. According to the results of the Kruskal-Wallis H test, there is a statistically significant difference in the dependent variable between all of the distinct groups ($\chi^2(6) = 245.79$, $p < .001$) with a mean rank score of 77.2 for PSO, 110.41 for LPSO, 118.46 for RPSO, 135.9 for PSO-SR, 194.24 for CSA, 266.79 for COA, and 325.5 for Jaya algorithm. The results of the post-hoc Dunn's test, which used a Sidak-corrected alpha of 0.0034, suggested that there is a significant difference between the mean ranks of the following pairs: PSO-CSA, PSO-COA, PSO-JAYA, LPSO-CSA, LPSO-COA, LPSO-JAYA, RPSO-CSA, RPSO-COA, RPSO-JAYA, PSOSR-COA, PSOSR-JAYA, CSA-COA, and CSA-JAYA.

Table 3.2.9. Statistical data recorded for the test case "WIND+WIND+SVC" of 13 bus substation DN using the Jaya Algorithm, Maharashtra under Case Study #3.2 (Subcase #3.2.7)

Parameters	PSO	LPSO	RPSO	PSO-SR	CSA	COA	JAYA
Mean *OF*	27.5631	28.0124	28.3494	28.4447	29.3402	30.1792	30.3072
Standard Deviation (σ)	0.8220	1.1636	1.0245	1.1706	1.0986	0.0295	0.0207
Max *OF*	28.5743	29.3367	29.9386	30.1341	30.1765	30.2051	30.3142
Min *OF*	26.2289	26.2289	27.3387	26.2289	26.2289	30.1341	30.2098

p-value* (Shapiro-Wilk test for normality) α=0.5	0.000006099	0.000007475	2.929e-7	0.0004029	9.184e-8	2.591e-8	1.613e-13
p-value* (Kolmogorov–Smirnov test for normality) α=0.5	0.00007735	0.0001108	3.609e-12	0.0008607	3.786e-14	1.755e-11	0
Mean Rank^{+} (Kruskal-Wallis non-parametric test) α=0.5^{++}	77.2	110.41	118.46	135.9	194.24	266.79	325.5

For each algorithm, the number of data samples has been set at 50.

Null hypothesis (H_0)- No statistical significance exists in a set of given observations.

* A probability that evaluates the evidence in contrast to the null hypothesis is referred to as the p-value. Evidence against the null hypothesis is strengthened when it is supported by lower probabilities.

**Normality is rejected at the 0.05 level.

$^{+}$ The average rank across all of the observations in a given sample is what is referred to as the mean rank. When a group's mean rank is higher than the overall average rank, the observation values in that group tend to be higher than those of the other groups.

$^{++}$The corrected α using Sidak correction method is 0.00244. Corrected $\alpha = 1-\sqrt[m]{(1-\alpha)} = 1-\sqrt[21]{(1-0.05)} = 0.00244$.

m - the number of tests / pairs

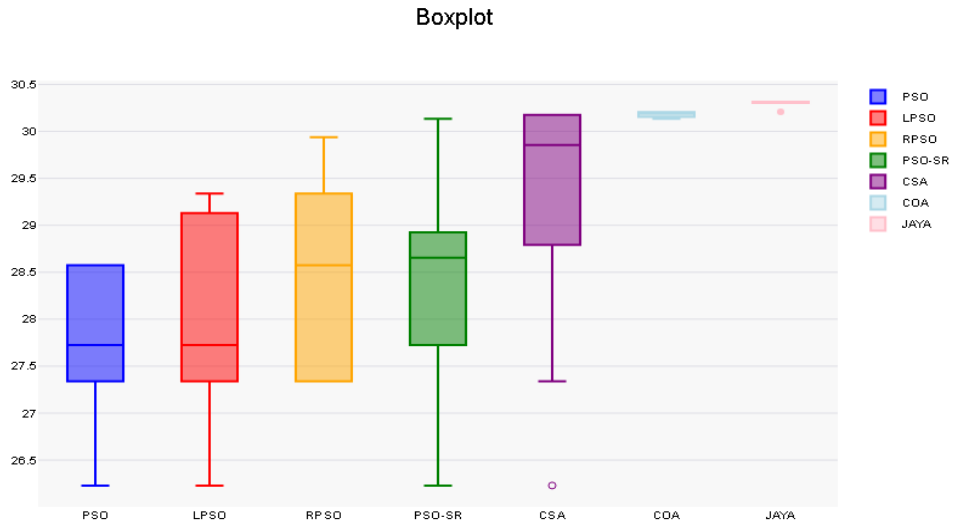

Fig. 3.2.6. Box-whiskers plot of *OF* using different algorithms for the test case "WIND+WIND+SVC" of 13 bus substation DN, Maharashtra (Subcase #3.2.7) under Case Study #3.2

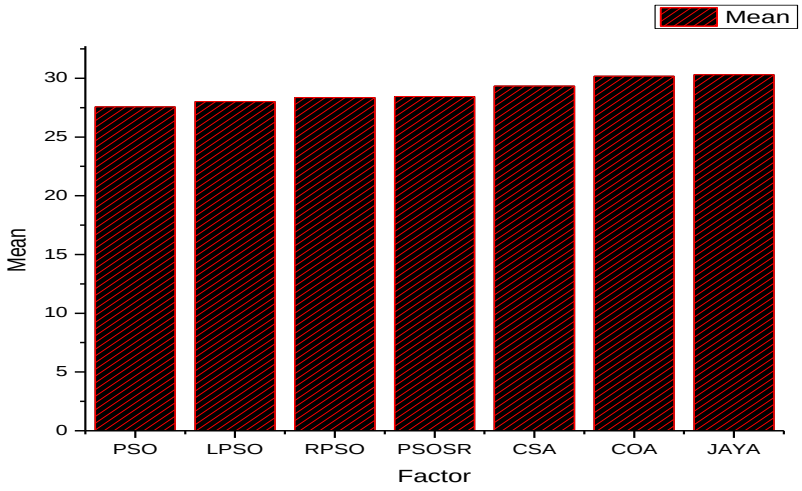

Fig. 3.2.7. Mean values of *OF* using different algorithms for the test case "WIND+WIND+SVC" of 13 bus substation DN, Maharashtra (Subcase #3.2.7) under Case Study #3.2

Table 3.2.10. Parametric comparison of algorithm pairs by post-hoc Dunn test for the test case "WIND+WIND+SVC" of 13 bus substation DN, Maharashtra (Subcase #3.2.7) under Case Study #3.2

Pair	Mean Rank difference	Z	SE	Critical value	p-value	p-value/2
PSO-LPSO	-33.21	1.648	20.1517	61.0733	0.09935	0.04968
PSO-RPSO	-41.26	2.0475	20.1517	61.0733	0.04061	0.02031
PSO-PSOSR	-58.7	2.9129	20.1517	61.0733	0.003581	0.00179
PSO-CSA	-117.04	5.808	20.1517	61.0733	6.32e-09	3.16e-09
PSO-COA	-189.59	9.4082	20.1517	61.0733	0	0
PSO-JAYA	-248.3	12.3216	20.1517	61.0733	0	0
LPSO-RPSO	-8.05	0.3995	20.1517	61.0733	0.6895	0.3448
LPSO-PSOSR	-25.49	1.2649	20.1517	61.0733	0.2059	0.103
LPSO-CSA	-83.83	4.16	20.1517	61.0733	0.00003183	0.00001592
LPSO-COA	-156.38	7.7602	20.1517	61.0733	8.44e-15	4.22e-15
LPSO-JAYA	-215.09	10.6736	20.1517	61.0733	0	0
RPSO-PSOSR	-17.44	0.8654	20.1517	61.0733	0.3868	0.1934
RPSO-CSA	-75.78	3.7605	20.1517	61.0733	0.0001696	0.00008479
RPSO-COA	-148.33	7.3607	20.1517	61.0733	1.83e-13	9.15e-14
RPSO-JAYA	-207.04	10.2741	20.1517	61.0733	0	0

PSOSR-CSA	-58.34	2.895	20.1517	61.0733	0.003791	0.001896
PSOSR-COA	-130.89	6.4952	20.1517	61.0733	8.29e-11	4.15e-11
PSOSR-JAYA	-189.6	9.4087	20.1517	61.0733	0	0
CSA-COA	-72.55	3.6002	20.1517	61.0733	0.000318	0.000159
CSA-JAYA	-131.26	6.5136	20.1517	61.0733	7.34e-11	3.67e-11
COA-JAYA	-58.71	2.9134	20.1517	61.0733	0.003575	0.001788

* The z-value gives an indication of how the average rank of each group stacks up against the overall average rank of all the observations.

▪ The greater the difference between a group's average rank and the general average rank, the higher the z value.

▪ A group's average rank being lower than the overall average rank is indicated by a negative z-value.

▪ A group's average rank being higher than the overall average rank is indicated by a positive z-value.

+ Stronger evidence is presented against the null hypothesis with lower p-values.

3.10. Summary

This section presents the salient observations regarding the effectiveness of BESS and SVC in presence of PV/wind-based DG on enhancing the technical, economic, and environmental benefits of the DNs. These are presented under each case study as follows:

Case study#3.1: *Optimal sizing and sitting of single, twin, and triple point allocation of probabilistic PV, wind, and BESS at the IEEE 85 and 141 bus DNs*

In this case study, different optimal capacities and combinations of PV, wind, and BESS are injected at optimal single, twin, and triple points of the IEEE 85 and 141 bus DNs, respectively. For all the test cases under study, the Jaya algorithm is found to be superior in terms of the overall objective function among all the algorithms in comparison. Now, the test cases corresponding to the highest objective function are “WIND+BESS” and “WIND+WIND+BESS” for the IEEE 85 and 141 bus DNs, respectively. The improvements in the objective functions of the aforementioned test cases for the specified bus system are 2.97 and 2.75 times, respectively, based on the corresponding worst cases. All the said test cases showed individual improvements in terms of the technical, economic, and environmental benefits of the IEEE 85 bus DN by 1.21, 8.05, and 1.31 times, respectively, considering the corresponding worst cases as references. Likewise, the technical, economic, and environmental improvements of the IEEE 141

bus DN are 1.1, 2.92, and 7.3 times, respectively. The Jaya algorithm yielded the highest overall objective among all the algorithms in comparison.

Case Study #3.2: *Optimal sizing and single, twin, and triple point allocation of PV, wind, and SVC at the IEEE 141 bus and real-time 13 bus substation DNs considering renewables and load uncertainties*

The maximum reduction in active power losses of IEEE 141bus and 13bus substation DNs is observed by up to 76.67% and 66.96%, respectively. The maximum improvements in *OF* are up to 3.26 and 5.46 for IEEE 141 bus and 13 bus substation DNs, respectively, considering the corresponding worst cases as references after optimal sizing and placement of DG and SVC. Improvements in *VPEI* are observed by up to 1.26 and 1.96 times for IEEE 141 bus and 13 bus substation DNs, respectively, resulting in a better voltage profile and network stability. Improvement in *BCR* is observed by up to 3.55 and 6.21 times for IEEE 141 bus and 13 bus substation DNs, respectively, resulting in better cost effectiveness and economic operation of the DNs. Improvement in *ECBI* is observed up to 14.21 and 6.43 times for the IEEE 141 bus and 13 bus substation DNs, respectively, by lesser consumption of fossil fuel-based power, resulting in cleaner operation of the DNs. Improvements in the *VSI* characteristics are observed with probabilistic PV and wind-based DG injection for all the test cases and test systems under consideration. From **Section 3.9**, it is clear that the Jaya algorithm is robust, consistent, and superior to all the algorithms in comparison.

CHAPTER 4: Impact of EVs on DN sustainability

This chapter presents the impact of EVs on the technical, economic, and environmental impacts of DNs. The penetration levels of the EVs at the DN charging station are varied and the optimal distribution of the number of EVs, charge-discharge connectivity, and charge-discharge prices for maximization of the said benefits are elaborately studied and graphically presented in this chapter.

4.1. Introduction

An EV **[113]** is a car that can be powered by an electric motor that is externally charged and runs on battery power. A plug-in hybrid EV (PEV) is a vehicle that can be powered by both an internal combustion engine and an electric motor that runs on batteries. Alternatively, an EV can be a vehicle that is powered only by an electric motor that runs on batteries.

An electric motor replaces the internal combustion engine in an all-electric car, is a battery EV (BEVs). The car's electric motor is powered by a sizable traction battery pack, which means it needs to be hooked into a wall outlet or EV supply equipment (EVSE) for charging. The car does not have a tailpipe or conventional liquid fuel components like a fuel pump, fuel line, or fuel tank as it is an EV.

Hybrid EVs (HEVs) are powered by an internal combustion engine in combination with one or more electric motors that use energy stored in batteries. HEVs combine the benefits of high fuel economy and low tailpipe emissions with the power and range of conventional vehicles.

4.2. EV global and Indian scenario

As the world shifts towards a sustainable future, EVs have become the go-to clean technology for transportation **[114]**. Global demand for EV services has surged because to the surge in e-commerce activities. To adjust to the new normal, EV services have embraced EVs and other cutting-edge technologies. The adoption of EVs in India and the rest of the world is examined in this article.

Since EVs' economics have greatly improved, these are now a competitive option to both CNG and conventional gasoline or diesel-powered cars. The demand for EV logistics services has increased due to the acceleration of the transition towards e-commerce caused by the COVID-

19 pandemic. The adoption of EVs has been accelerated by this increased demand, with an emphasis on efficiency and sustainability.

China holds the largest market share for EVs, with Norway having the highest percentage of electric cars sold overall. In 2020, growth in several European EV markets was triple digits. The United States has the third-largest EV market, but growth was only 4% in the previous year. With the support of international government campaigns to encourage the use of zero-emission vehicles, European nations such as the Netherlands are implementing zero-emission zones for commercial vehicles.

There is pressure on a worldwide scale to give environmental initiatives top priority. As organizations and vendors emphasize sustainable practices through green supply chain efforts, the shift to electric cars for is to gain worldwide popularity, including in India. Adopted in 2015, the legally binding Paris Agreement is regarded by many as a major step in the right direction toward resolving the world's climate issue. Its objective is to keep global warming well below 2 degrees Celsius over pre-industrial levels. It will be supported by a transparent framework for tracking and reporting progress as well as enhancing nations' capacity to adapt to the effects of climate change.

Businesses may significantly contribute to environmental preservation by using electric freight vehicles. BEVs have zero tailpipe emissions, which means they don't release hazardous gasses like carbon dioxide and nitrogen oxide that worsen air pollution and contribute to climate change. This is in contrast to conventional vehicles that generate harmful pollutants. BEVs can drastically lower carbon emissions and enhance urban air quality. Additionally, lowering reliance on fossil fuels can lessen greenhouse gas emissions, which will lessen the effects of climate change. All things considered, the switch to BEVs is essential to foster a more environmentally friendly and hygienic atmosphere.

Global enterprises must embrace the use of electric goods vehicles for environmental welfare. Businesses may improve air quality, cut fuel costs, and lessen their carbon footprint by implementing EVs. Adopting these eco-friendly procedures also helps companies maintain their competitiveness in a market where customers are becoming more and more concerned with sustainability. Businesses will support to benefit greatly in the long run from accepting this change.

It is anticipated that developments in battery and charging technology would result in additional cost savings, increasing the appeal of commercial EVs in India. The current state of EV adoption in India and around the world is highlighted below.

Current trends in India's deployment of EVs

Government Incentives:

A number of government programs are driving the fast evolution of India's EV adoption situation. Buyers and manufacturers of EVs can get financial incentives under the Faster Adoption and Manufacturing of Hybrid & Electric Vehicles (FAME) program. By 2030, the Indian government wants thirty percent of all cars sold there to be electric. Approximately 25–30% of India's EV fleets may use EVs by 2025.

Enterprises to prosper with EV fleets:

Owing to the long-term economic viability and ecological advantages of electric goods vehicles, a number of logistics firms in India have already embraced them. For example, “Big Basket” targets for 70% electrification by 2024, “Zomato” has promised 100% fleet electrification by 2030, and “Amazon India” expects to have one million EVs in its delivery fleet by 2030. The EV ecosystem has a large market opportunity because of this.

Global trends in the deployment of EVs:

Around the world, governments are moving to increase the demand in the next ten years for EVs. Fuel efficiency standards have been set globally, and developing nations have implemented legislation pertaining to EVs. Governments also provide purchasers and makers of electric goods vehicles with subsidies and incentives. Globally, initiatives are in motion to enhance infrastructure strategies and programs for rapid charging.

4.3. EV charging stations

A charging station **[115]** is a power supply device that provides electrical power for recharging PEVs, including BEVs, electric trucks, electric buses, neighbourhood electric vehicles, and plug-in hybrid vehicles. It is also referred to as a charge point or EVSE.

DC and AC charging stations are the two primary kinds of EV chargers. While most mains electricity is supplied as AC from the power grid, electric car batteries can only be charged by DC electricity. This is the reason why the majority of electric cars are equipped with an

integrated AC-to-DC converter called an "onboard charger" (OBC). This onboard charger receives grid electricity from an AC charging station, transforms it into DC power, and then recharges the battery. DC chargers bypass size and weight limits by integrating the converter into the charging station rather than the car, enabling higher power charging (which calls for considerably larger AC-to-DC converters).

Connectors that meet multiple international standards are offered by charging stations. Multiple connectors are a typical feature of DC charging stations, allowing them to charge a wide range of vehicles that use conflicting standards.

Street side, shopping malls, government buildings, and other parking lots are common locations for public charging stations. One can usually find private charging stations at hotels, offices, and homes.

Fig. 4.0.1. shows a schematic diagram of an EV charging station having different types of EVs connected to the main grid.

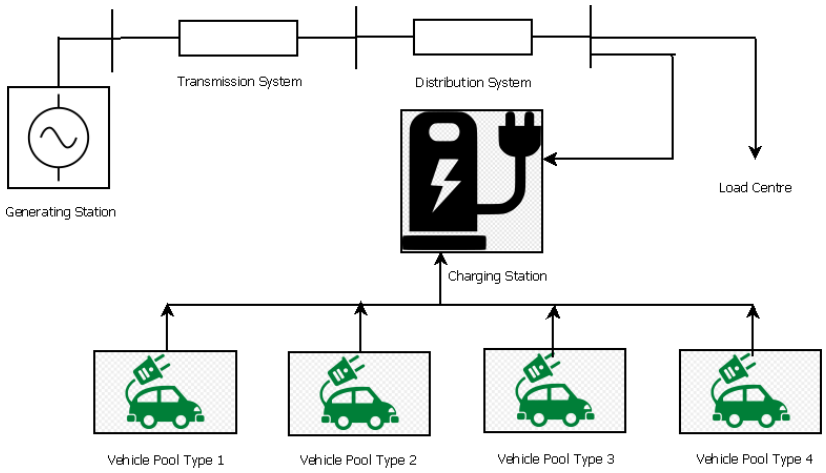

Fig. 4.0.1. Schematic diagram of an EV charging station having different types of EVs connected to the main grid

4.4. Components of EVs

The different components of EVs are discussed in this subsection.

4.4.1. EV batteries

All EVs, viz., BEV, HEV, and PHEV, require energy storage systems, which are typically batteries.

4.4.1.1. Types of EV batteries

The different types of EV batteries are discussed in this sub-section.

Lithium-ion batteries - As lithium-ion batteries have a higher energy density per unit mass and volume than conventional electrical energy storage devices, these are currently found in the majority of portable consumer gadgets, including laptops and cell phones. In addition, they feature a long lifespan, minimal self-discharge, strong performance at high temperatures, a high power-to-weight ratio, and high energy efficiency. Although the majority of lithium-ion battery components may be recycled, the industry still faces difficulties with material recovery costs. Lithium-ion batteries are used in the majority of modern PHEVs and all-electric cars, albeit their precise chemistry is frequently different from that of batteries used in consumer devices. In order to lower their relatively high cost, increase their usable life, utilize less cobalt, and solve safety issues regarding different fault circumstances, research and development are still ongoing.

Nickel-Metal Hydride Batteries - Commonly found in computer and medical equipment, nickel-metal hydride batteries provide satisfactory specific energy and specific power capacities. Compared to lead-acid batteries, nickel-metal hydride batteries are safe and resistant to misuse, and have a far longer life cycle. HEVs have made extensive use of these batteries. The primary drawbacks of nickel-metal hydride batteries are their high price, rapid rate of self-discharge, tendency to produce heat at high temperatures, and requirement to regulate hydrogen loss.

Lead-Acid Batteries - Lead-acid batteries are affordable, safe, reusable, and reliable. These can be made to have a high-power capacity. However, their short calendar and lifetime, low specific energy, and poor performance in frigid temperatures make them unusable. Although more sophisticated high-power lead-acid batteries are being developed, supplementary loads in commercially available electric-drive vehicles are the only applications for these batteries. In order to cut down on idling at stops and save gasoline, these are also utilized in internal combustion engine cars for stop-start capability.

Ultracapacitors - When voltage is applied, the contact between an electrode and an electrolyte in ultracapacitors stores energy. The electrolyte-electrode surface area grows with an increase in energy storage capacity. Ultracapacitors can deliver large amounts of power quickly because of their extremely high-power density, which makes up for their poor energy density. In addition to helping cars recover braking energy, ultracapacitors can give them more power during acceleration and hill climbing. Because these assist electrochemical batteries in

levelling load power, these may potentially prove valuable as supplementary energy-storage devices in electric-drive cars.

4.4.2. **EV charging cables**

The EV and the charging station are connected by the charging cable. It transmits the electric current to the EV's battery from the charging station. The effectiveness and speed of the charging process might be impacted by the kind and quality of charging cable utilized. The ease of use and security of the charging process might be impacted by the length and flexibility of the charging wire. While a longer cable might be required for charging in an open space or at a remote location, a shorter cable might be more practical for charging in a congested or small environment. While a more flexible cable could be simpler to handle and store, it might also be less strong and more prone to breaking. It's important to choose a charging cable that works with the EV model and particular charging requirements. There are several safety risks and potential harm to the EV's charging port when using an incompatible or broken charging cable.

Fig. 4.0.2. shows a schematic diagram of components of an EV charging cable.

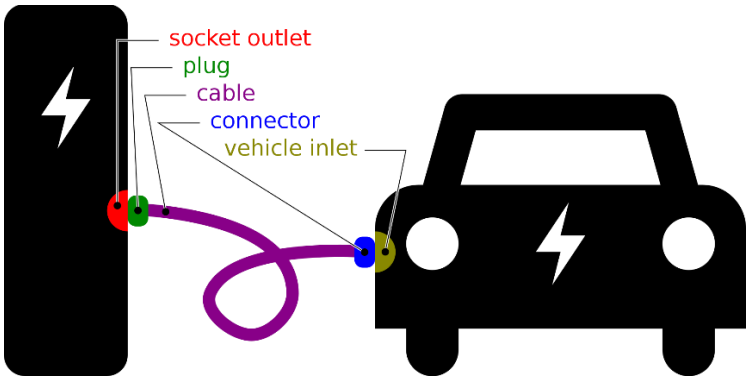

Fig. 4.0.2. Schematic diagram of components of an EV charging cable

4.4.3. **EV converter system**

The numerous kinds of vehicles that are always in motion cause air pollution, global warming, and resource depletion. Replacing conventional cars with EVs, hybrid cars, and fuel-cell electric cars is one way to address these problems. There are two kinds of energy storage devices used in hybrid and electric cars. The first is a rechargeable energy storage system (RESS), which offers high power capability and reversibility, and the second is a multi-function energy storage system (MESS), which is utilized to store high energy. RESS has a sophisticated

regenerative braking and accelerating technology, while MESS offers a long driving range. When configuring energy storage components with traction drive, vehicle engineers encounter difficulties due to the high voltage of the DC link. The energy storage device modifies its output voltage in response to load. Electrical powertrain components can be interfaced with the usage of DC-DC converters.

Vehicle converters need to be compact, lightweight, dependable, efficient, and emit minimal electromagnetic interference. The types of converters used in EVs are shown in **Fig. 4.0.3.** It illustrates how a minimum of one DC-DC converter connects the fuel cell battery or supercapacitors module to the DC link. Different energy sources, such as battery supercapacitors and fuel cells, are used in EVs. EVs employ one or more energy storage systems. This results in lower overall costs and volume while maintaining good performance. Batteries and supercapacitors are two frequently utilized energy storage devices. Different fuel cell stack configurations are used in these devices. Direct connections between two modules in parallel—fuel cell and battery, fuel cell and supercapacitors, or battery and supercapacitors—are the typical setup.

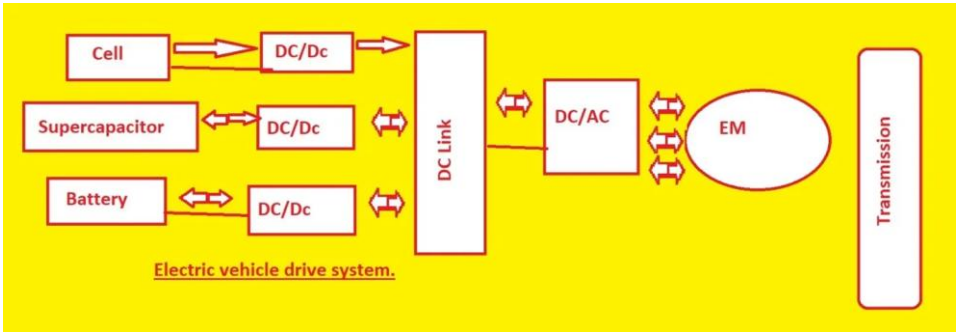

Fig. 4.0.3. Schematic diagram of components of an EV drive system

4.4.4. EV battery charge controller

The charge controller that is utilized has a major impact on how intelligent an AC charging station or infrastructure is. The main responsibility of a smart charge controller is to regulate and keep an eye on an electrical vehicle's charging process.

The schematic diagram of the EV charge controller is given in **Fig. 4.0.4.**

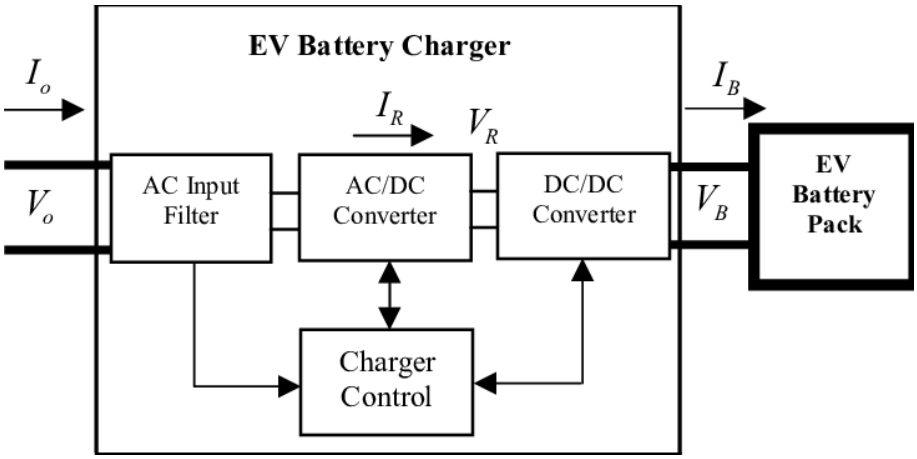

Fig. 4.0.4. Schematic diagram of components of an EV charge controller

4.5. Role of EVs in enhancing the sustainability of DNs

EVs have a lower environmental impact than conventional internal combustion engine vehicles (ICEVs). The fact that it produces little to no tailpipe emissions is an advantage, even though some components of their production may have comparable, decreased, or different environmental implications. Additionally, they assist in lowering greenhouse gas emissions, reducing reliance on petroleum, and lessening the negative health consequences of air and environmental pollution. Because these provide a way to lower urban carbon dioxide (CO_2) emissions, there has been a discernible research focus in recent years on EV integration into smart cities. Likewise, EVs can also act as power source like DGs when connected to DN charging stations. When used with appropriate charge/discharge control management, EVs can be used as sources of distributed energy storage and utilized to increase network performance in terms of technical, economic, and environmental benefits.

4.6. EV charging-discharging cost

The EV can act both as a power source or load when connected to a DN. In an EV charging station, a pool of different types of EVs are scheduled to charge and discharge at different intervals.

4.6.1. EV charging cost (C_{cost}) and rate (C_{rate})

The EV owners have to pay charging cost to the utility when they charge their EVs. The rate at which electricity is transferred from the grid to the EV is called EV charging rate.

4.6.2. EV discharging (grid-charging) cost (D_{cost}) and rate (D_{rate})

Likewise, an EV owner may wish to discharge to the network if provided with an incentive or discharge cost. The rate at which electricity is transferred from the EV to the grid is called EV discharging/grid charging rate.

4.7.Formulation of the objective function (*OF*) due to EV integration

The components of the *OF* in equation 2.26 is redefined in this work due to integration of EV. These are detailed in the following subsections.

4.7.1. Voltage profile enhancement index ($VPEI$) due to EV integration

The $VPEI$ of the EV-integrated DN is given by the following equation:

$$VPEI = \frac{VPI_{with\ EV\ charging}}{VPI_{without\ EV\ charging}} \tag{4.1}$$

If the $VPEI$ value is more than unity, the DN is getting technically improved in terms of voltage after EV allocation. If $VPEI$ is less than or equal to unity, then there is no technical improvement due to EV integration with DN.

The steps of calculating $VPEI$ and the *VSI* of the DN is same as equations 2.29 to 2.32 as provided in Chapter 2.

4.7.2. Benefit cost ratio (BCR) due to EV integration

The benefit cost ratio of the EV-integrated DN is defined as follows.

$$BCR = \frac{Network\ cost\ benefit\ due\ to\ net\ grid\ power\ transfer}{Cost\ of\ power\ transferred\ to\ EVs}$$

$$= \left(\frac{CP_{EV2G} - CP_{G2EV}}{CP_{G2EV}}\right) \tag{4.2}$$

CP_{EV2G} is the cost of power transferred to the grid from the EVs during EV discharging in USD over the entire planning horizon and is given by the following equation.

$$CP_{EV2G} = (D_{rate} * D_{cost} * \sum_{i=1}^{N_T} N_{d_i} * kWh_i)) * CCPR * YR_{span} * 8760 \tag{4.3}$$

N_T is the number of types of EVs considered.

CP_{G2EV} is the cost of power transferred to the EVs from the grid during EV charging in USD over the entire planning horizon and is given by the following equation.

$$CP_{G2EV} = (C_{rate} * C_{cost} * \sum_{i=1}^{N_T} N_{c_i} * kWh_i) * CCPR * YR_{span} * 8760 \tag{4.4}$$

In this work, the discharge cost is assumed to be more than the charging cost to make the network more financially beneficial.

If the BCR value is greater than unity, the system is creating financial gains after EV allocation; otherwise, no economic benefit occurs.

4.7.3. Emission cost benefit index ($ECBI$) due to EV integration

The $ECBI$ of the EV-integrated DN is given by the following equation:

$$ECBI = \frac{EC_{without\ EV} - EC_{with\ EV}}{EC_{without\ EV}} \tag{4.5}$$

If the $ECBI$ value is more than zero, the DN is deriving environmental benefits due to EV integration. If $ECBI$ is less than or equal to zero, then there is no environmental improvement due to EV integration with DN.

The steps of calculating $ECBI$ are same as equations 2.37 and 2.38 as provided in Chapter 2.

4.8. Operational Constraints

The objective function OF must adhere to the following additional constraints along with the constraints defined by **equations 2.39** to **2.42** given in **Chapter 2**.

vi) EV discharging rate constraint:

$$D_{ratemin} \leq D_{rate} \leq D_{ratemax} \tag{4.6}$$

$D_{ratemin}$ and $D_{ratemax}$ are the minimum and maximum rates of EV discharging.

vii) EV charging rate constraint:

$$C_{ratemin} \leq C_{rate} \leq C_{ratemax} \tag{4.7}$$

$C_{ratemin}$ and $C_{ratemax}$ are the minimum and maximum rates of EV charging.

viii) EV charging cost constraint:

$$C_{costmin} \leq C_{cost} \leq C_{costmax} \tag{4.8}$$

$C_{costmin}$ and $C_{costmax}$ are the minimum and maximum costs of EV charging.

ix) EV discharging cost constraint:

$$D_{costmin} \leq D_{cost} \leq D_{costmax} \tag{4.9}$$

$D_{costmin}$ and $D_{costmax}$ are the minimum and maximum costs of EV discharging.

x) EV parking lot capacity constraint

$$N_{type-1} + N_{type-2} + N_{type-3} + N_{type-4} \leq N_{capacity} \quad (4.10)$$

N_{type-1}, N_{type-2}, N_{type-3}, and N_{type-4} are the optimal number of vehicles of each type considered under study. $N_{capacity}$ is the total capacity of the EV charging station parking lot.

4.9. Case studies under consideration

In order to study the effectiveness of EVs on enhancing the technical, economic, and environmental benefits of the DN, a case study presented in this section which is as follows:

Case Study #4.1: *Technical, economic, and environmental benefits by optimal location of EV charging station, vehicle distribution, charge/discharge rates, and prices at the IEEE 85 and 141 bus DN*

The data provided in **Table 4.0.1** and **Table 4.0.2** are taken from references **[116]** and **[117],** respectively. The charge and discharge prices have been converted from RMB to USD as per exchange values as of 3rd March 2021 (1RMB=0.15484 USD).

Table 4.0.1. EVs used in the vehicle pool

Type	Manufacturer	EV Type	Rated Battery Capacity(kWh)
1	BYD	E6 (Type 1)	57
2	BAIC BJEV	EV 160 (Type 2)	25.6
3	GREELY NEW ENERGY	EV 300 (Type 3)	45.3
4	ZOTYE AUTO	CLOUD 100S (Type 4)	18

Table 4.0.2. Data used for finding the optimal location of EV charging station and distribution of vehicle charging discharging

Variable	Value	Variable	Value
$D_{ratemin}$	2 kWhr	$C_{costmin}$	0.28 USD/kWhr
$D_{ratemax}$	3 kWhr	$C_{costmax}$	0.51 USD/kWhr
$C_{ratemin}$	2 kWhr	$D_{costmin}$	0.28 USD/kWhr
$C_{ratemax}$	6 kWhr	$D_{costmax}$	0.51 USD/kWhr

4.9.1. **Case study#4.1:** *Technical, economic, and environmental benefits by optimal location of EV charging station, vehicle distribution, charge/discharge rates, and prices at the IEEE 85 and 141 bus DN*

Case study description: This case study examines how strategically placing a vehicle charging station can enhance the technical, financial, and environmental advantages of DNs. The benefits are obtained by optimal location of EV charging station, vehicle distribution, charge/discharge rates, and prices at the IEEE 85 and 141 bus DNs.

The simulation work is performed using MATLAB R2014b v8.4 software. The hardware specifications of the PC used are an Intel (R) Core (TM) i7-9750H hexacore CPU (2.60 GHz) and 24 GB of 2666 MHz DDR4 RAM. Two IEEE radial bus systems, viz., 85 and 141, are considered. The details of the vehicles and their parameters are provided in **Table 4.0.1** and **Table 4.0.2**, respectively. For each bus system, four EV penetration levels are considered: 40%, 60%, 80%, and 100%. For each penetration level, the parameters recorded are the net active power injected, the total number of vehicles of each type (TV), the number of charging vehicles of each type (CV), the number of discharging vehicles (DV) of each type, the optimal location of the charging station, the optimal charging price, the optimal discharging price, active power losses before and after EV penetration, *OF*, *VPEI*, *BCR*, *ECBI*, the computation time, and the total capacity of the charging station. The algorithm that yielded the highest value is considered the best of all the algorithms in comparison. The location corresponding to the best objective is taken as the optimal location of the EV charging station. Each algorithm is executed for 100 iterations and 10 trials. The total number of candidates is taken as 50.

The problem-specific flowchart is presented in **Fig. 4.1.1.**

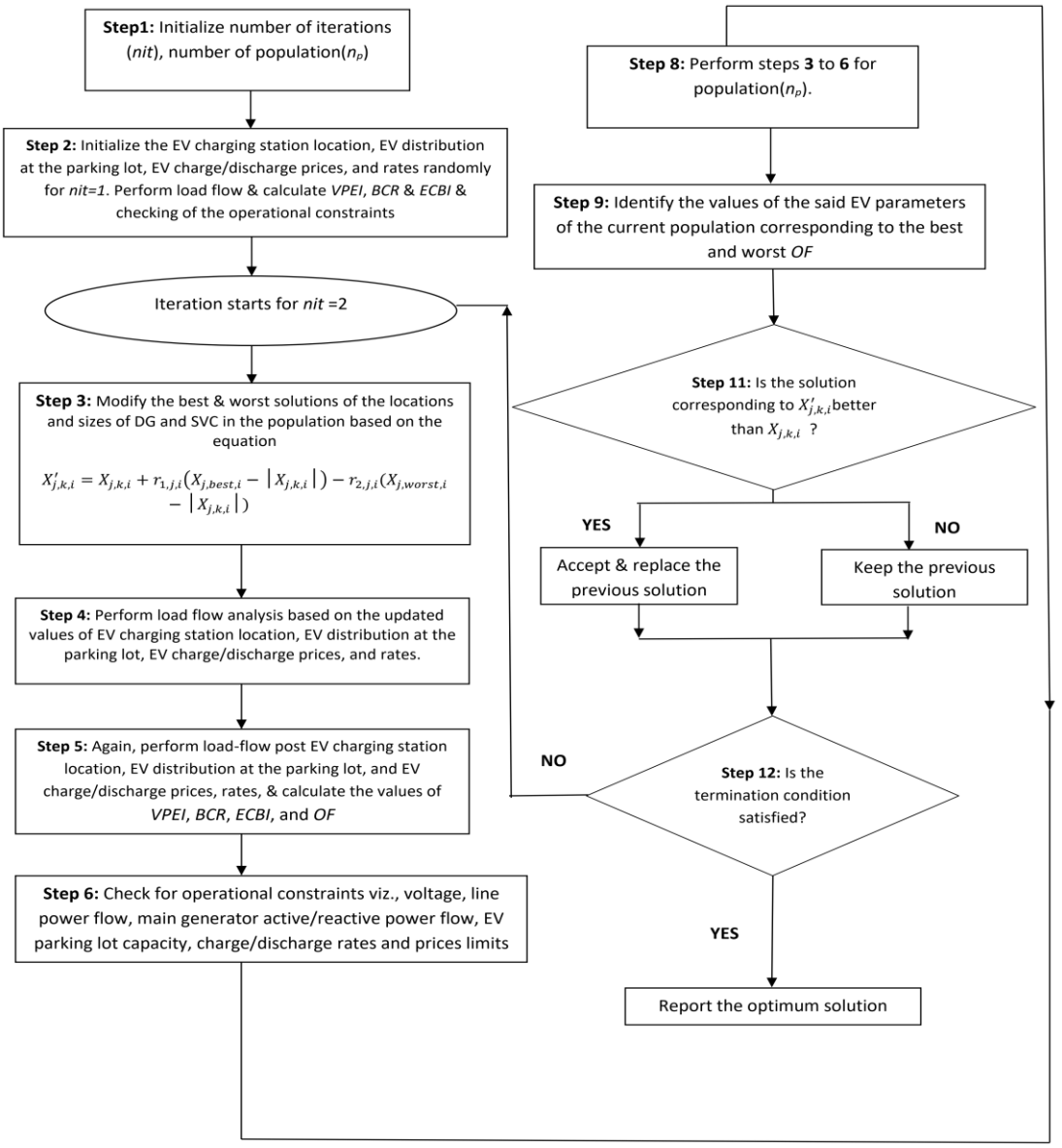

Fig. 4.1.1. Problem-specific flowchart depicting the Jaya algorithm applied to the problem of EV charging station allocation defined under the Case-Study# 4.1

*4.9.1.1.**Subcase #4.1.1:*** 40% EV penetration level

Table 4.1.1 shows the values of the network indices, active power losses, optimal point of EV charging station allocation, EV charge discharge pricing, and EV charge-discharge distribution with a penetration level of 40% for the IEEE 85 and 141 bus DN using Jaya algorithm.

Table 4.1.1. Results of optimal charging station allocation at the test DNs with 40% EV penetration level (Subcase #4.1.1) using Jaya Algorithm under the Case-Study# 4.1

Parameters	IEEE 85	IEEE 141	Parameters	IEEE 85	IEEE 141
Net Active Power transferred (kW)	1200	1505	**DV Type 4**	161	111
TV Type 1	103	191	**CV Type 4**	18	12
DV Type 1	93	172	**Optimal Location Point**	46	95
CV Type 1	10	19	**Optimal Charging Price (C_{cost})**	0.2853	0.2805
TV Type 2	177	214	**Optimal Discharging Price (D_{cost})**	0.5075	0.5097
DV Type 2	159	193	***OF***	14.4618	8.3520
CV Type 2	18	21	**Active Power Losses with EV (kW)**	232.29	556.98
TV Type 3	21	72	***VPEI***	19.7462	1.0393
DV Type 3	19	65	***BCR***	23.2379	23.9159
CV Type 3	2	7	***ECBI***	0.4447	0.1258
TV Type 4	179	123	**Computation Time (secs)**	193.85	260.2

4.9.1.2. ***Subcase #4.1.2****:* 60% EV penetration level

Table 4.1.2 shows the values of the network indices, active power losses, optimal point of EV charging station allocation, EV charge discharge pricing, and EV charge-discharge distribution with a penetration level of 60% for the IEEE 85 and 141 bus DN using Jaya algorithm.

Table 4.1.2. Results of optimal charging station allocation at the test DNs with 60% EV penetration level (Subcase #4.1.2) using Jaya Algorithm under the Case-Study# 4.1

Parameters	IEEE 85	IEEE 141	Parameters	IEEE 85	IEEE 141
Net Active Power transferred (kW)	1800	2255	**DV Type 4**	83	56
TV Type 1	482	194	**CV Type 4**	9	6
DV Type 1	434	175	**Optimal Location Point**	48	107

CV Type 1	48	19	**Optimal Charging Price (C_{cost})**	0.2801	0.2819
TV Type 2	40	33	**Optimal Discharging Price (D_{cost})**	0.5081	0.5068
DV Type 2	36	30	***OF***	16.1554	8.2509
CV Type 2	4	3	**Active Power Losses with EV (kW)**	237.08	529.05
TV Type 3	106	611	***VPEI***	24.4003	1.0574
DV Type 3	95	550	***BCR***	23.4635	23.5320
CV Type 3	11	61	***ECBI***	0.6509	0.1879
TV Type 4	92	62	**Computation Time (secs)**	198.16	290.27

*4.9.1.3.**Subcase #4.1.3**:* 80% EV penetration level

Table 4.1.3 shows the values of the network indices, active power losses, optimal point of EV charging station allocation, EV charge discharge pricing, and EV charge-discharge distribution with a penetration level of 80% for the IEEE 85 and 141 bus DN using Jaya algorithm.

Table 4.1.3. Results of optimal charging station allocation at the test DNs with 80% EV penetration level (Subcase #4.1.3) using Jaya Algorithm under the Case-Study# 4.1

Parameters	IEEE 85	IEEE 141	Parameters	IEEE 85	IEEE 141
Net Active Power transferred (kW)	2400	3000	**DV Type 4**	67	442
TV Type 1	379	252	**CV Type 4**	7	49
DV Type 1	341	227	**Optimal Location Point**	32	84
CV Type 1	38	25	**Optimal Charging Price (C_{cost})**	0.2821	0.2802
TV Type 2	238	86	**Optimal Discharging Price (D_{cost})**	0.5093	0.5078
DV Type 2	214	77	***OF***	16.9672	8.3003
CV Type 2	24	9	**Active Power Losses with EV (kW)**	233.15	391.56
TV Type 3	269	371	***VPEI***	26.7767	1.151

DV Type 3	242	334	***BCR***	23.3159	23.5167
CV Type 3	27	37	***ECBI***	0.8601	0.2583
TV Type 4	74	491	**Computation Time (secs)**	196.71	263.43

*4.9.1.4.**Subcase #4.1.4**:* 100% EV penetration level

Table 4.1.4 shows the values of the network indices, active power losses, optimal point of EV charging station allocation, EV charge discharge pricing, and EV charge-discharge distribution with a penetration level of 100% for the IEEE 85 and 141 bus DN using Jaya algorithm.

Table 4.1.4. Results of optimal charging station allocation at the test DNs with 100% EV penetration level (Subcase #4.1.4) using Jaya Algorithm under the Case-Study# 4.1

Parameters	**IEEE 85**	**IEEE 141**	**Parameters**	**IEEE 85**	**IEEE 141**
Net Active Power transferred (kW)	3000	3755	**DV Type 4**	594	210
TV Type 1	184	614	**CV Type 4**	66	23
DV Type 1	166	553	**Optimal Location Point**	28	48
CV Type 1	18	61	**Optimal Charging Price (C_{cost})**	0.2803	0.2806
TV Type 2	190	630	**Optimal Discharging Price (D_{cost})**	0.4984	0.5074
DV Type 2	171	567	***OF***	17.3969	8.3637
CV Type 2	19	63	**Active Power Losses with EV (kW)**	234.72	353.88
TV Type 3	166	23	***VPEI***	28.1385	1.1789
DV Type 3	149	21	***BCR***	23.0372	23.6157
CV Type 3	17	2	***ECBI***	1.0674	0.3216
TV Type 4	660	233	**Computation Time (secs)**	194.78	254.06

4.9.1.5. **Result analysis of *Case Study #4.1***

The results of the *sub-cases* **4.1.1.** to **4.1.4.** presented in **Table 4.1.1** – **Table 4.1.4** are analyzed for every bus system under consideration.

IEEE 85 bus DN

It is found that the highest value of the *OF* is obtained in the case of 100% EV penetration (17.3969) and a minimum at 40% EV penetration (14.4618) from **Fig. 4.1.3.** The highest value of *VPEI* is obtained in the case of 100% EV penetration (28.1385) and a minimum at 40% penetration (19.7462). The highest value of *BCR* obtained in the case of 60% EV penetration is 23.4635, and the minimum is 23.0372 in the case of 100% penetration. The highest value of *ECBI* obtained in the case of 100% EV penetration is 1.0674 and a minimum of 0.4447 in the case of 40% penetration. From **Fig. 4.1.2**, the maximum active power losses of 237.08 kW occurred at 60% penetration and a minimum of 232.28 kW at 40% penetration. The relative distribution of charging and discharging vehicles of each type is shown in **Fig. 4.1.4**. The maximum capacity of the vehicle pool for this case is taken as 1200. As per **Fig. 4.1.5**, the minimum value of the optimal discharging price is obtained in the case of 100% EV penetration, while the maximum value is obtained in the case of 80% EV penetration. Similarly, from **Fig. 4.1.6**, the minimum value of the optimal charging price is obtained in the case of 60% EV penetration, while the maximum value is obtained in the case of 40% EV penetration.

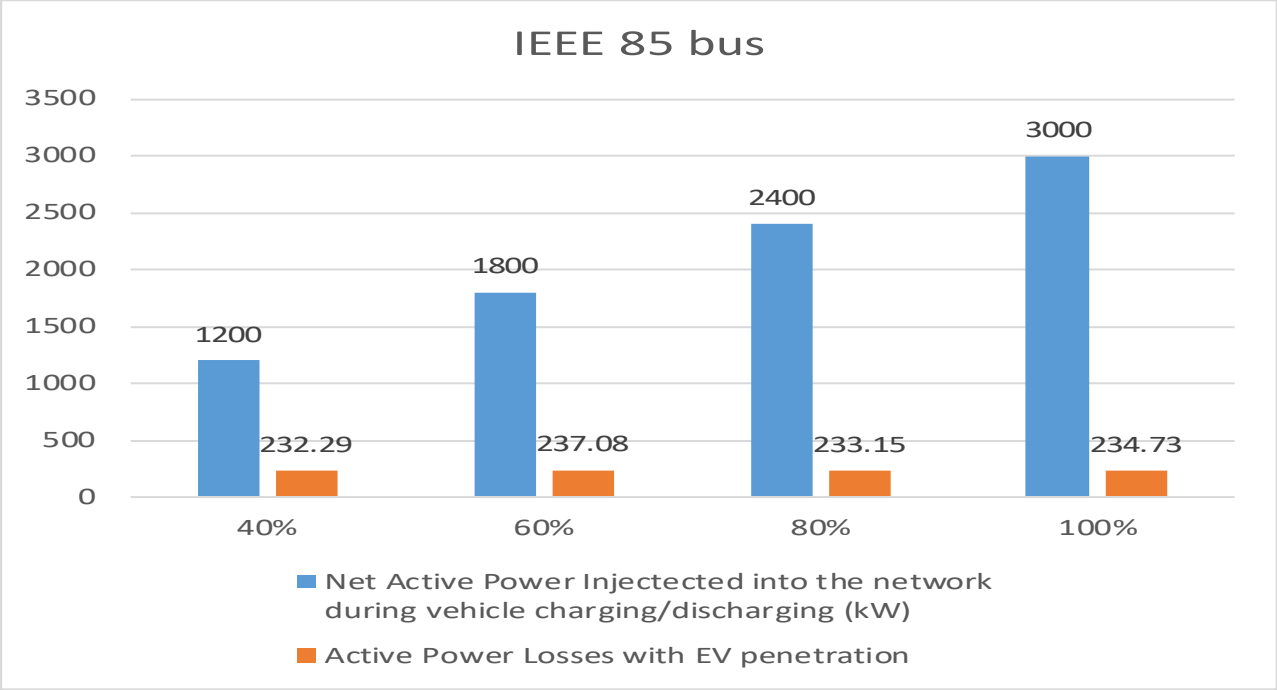

Fig. 4.1.2. Comparison of active power transferred to the IEEE 85 bus DN due to EV discharge and losses for different penetration levels under the Case-Study# 4.1

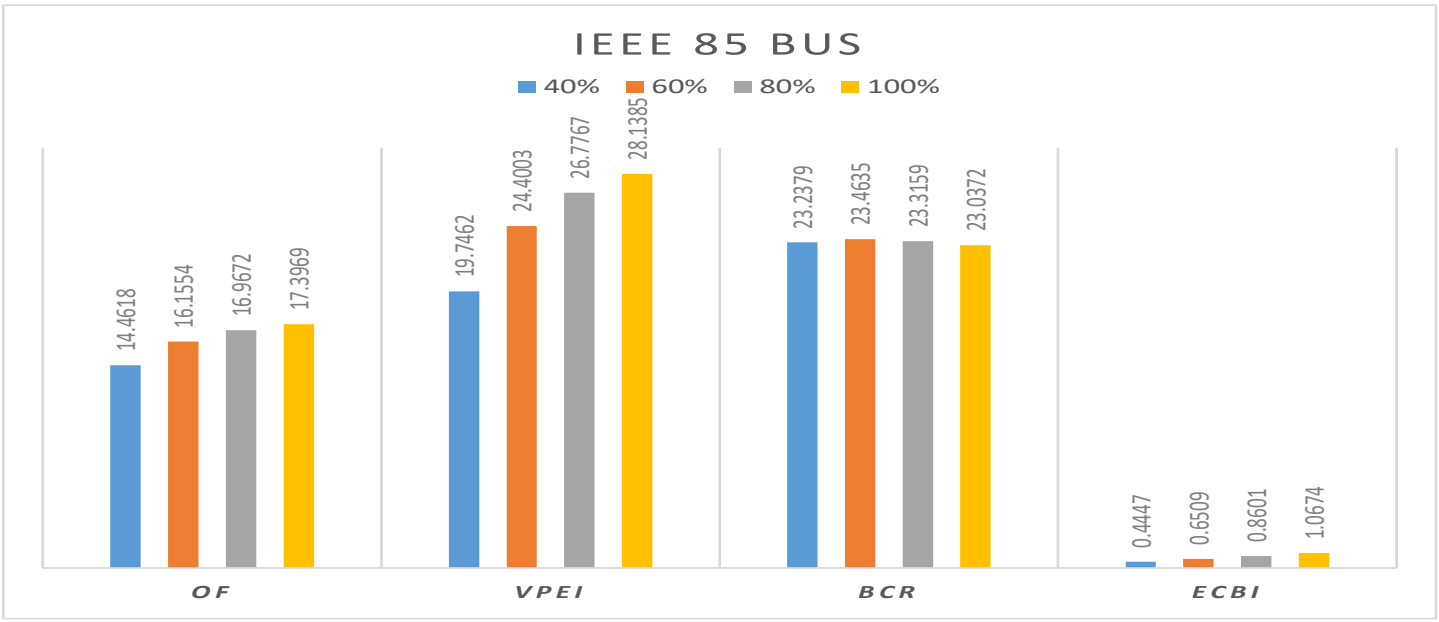

Fig. 4.1.3. Comparison of *OF*, *VPEI*, *BCR*, and *ECBI* for different penetration levels at the IEEE 85 bus DN under the Case-Study# 4.1

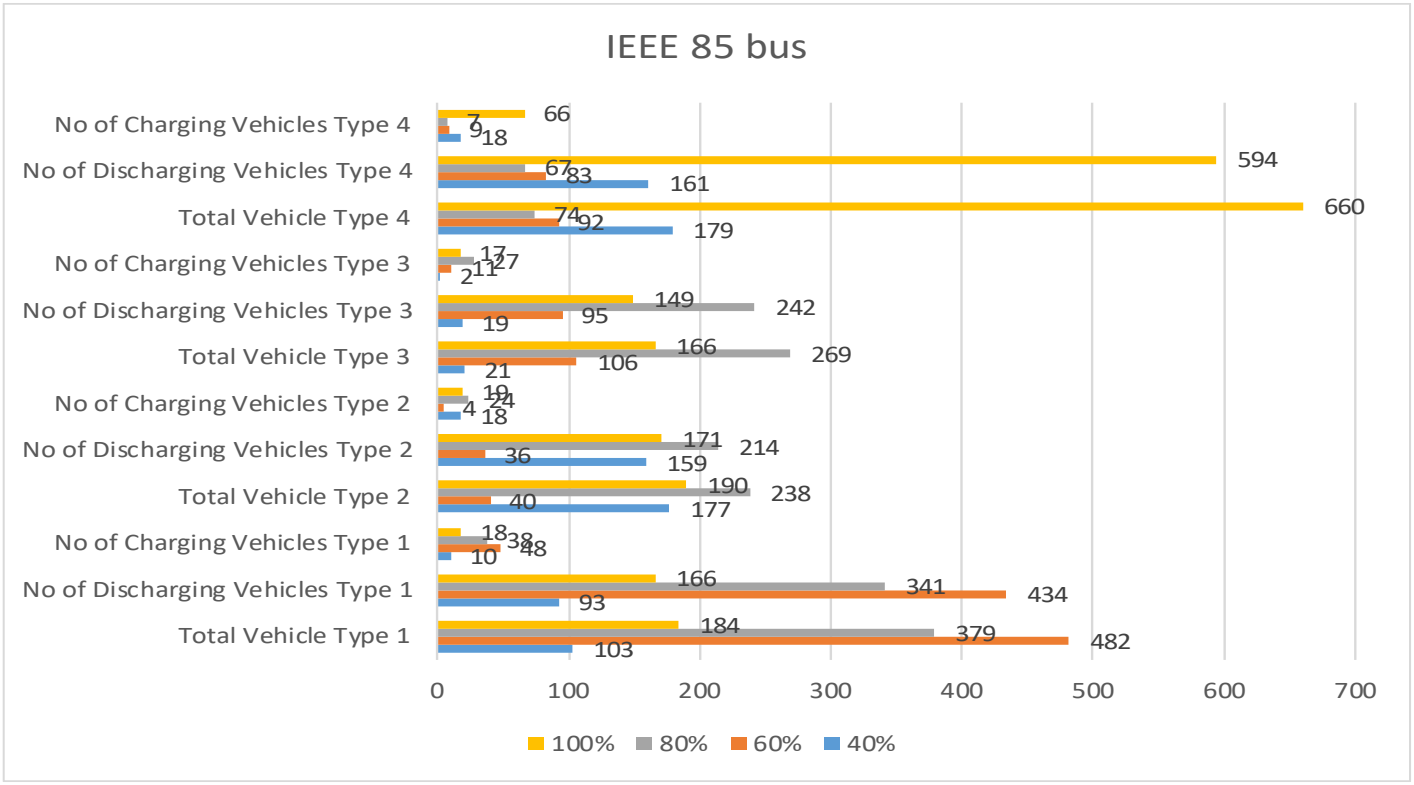

Fig 4.1.4. Distribution of the number of EVs of each type for different penetration levels at the IEEE 85 bus DN under the Case-Study# 4.1

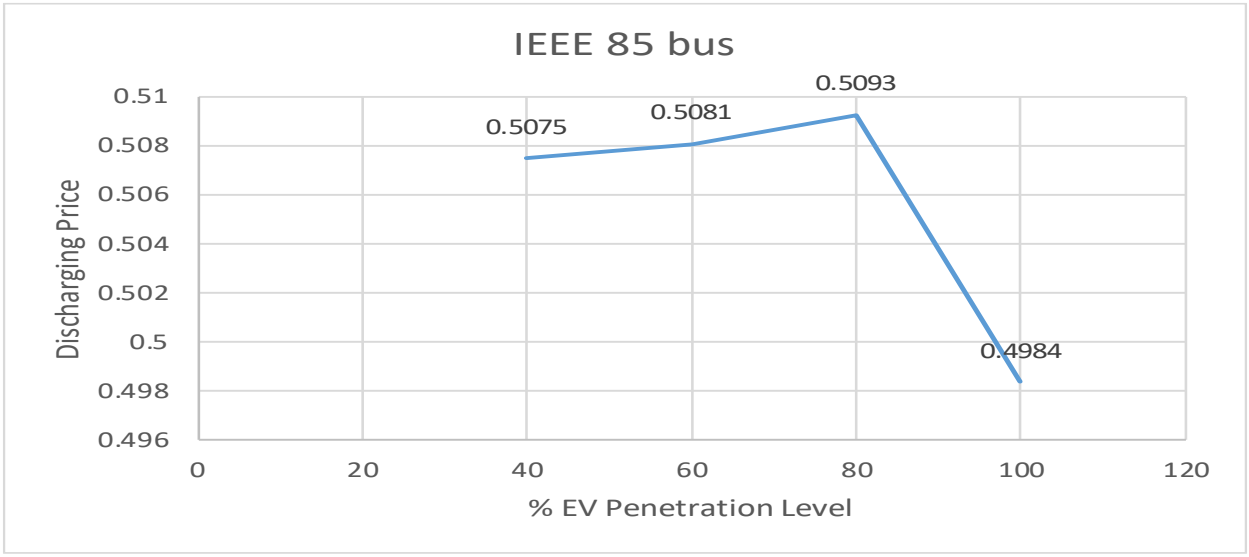

Fig. 4.1.5. Variation of optimal discharging price with increase in EV penetration level at the IEEE 85 bus network under the Case-Study# 4.1

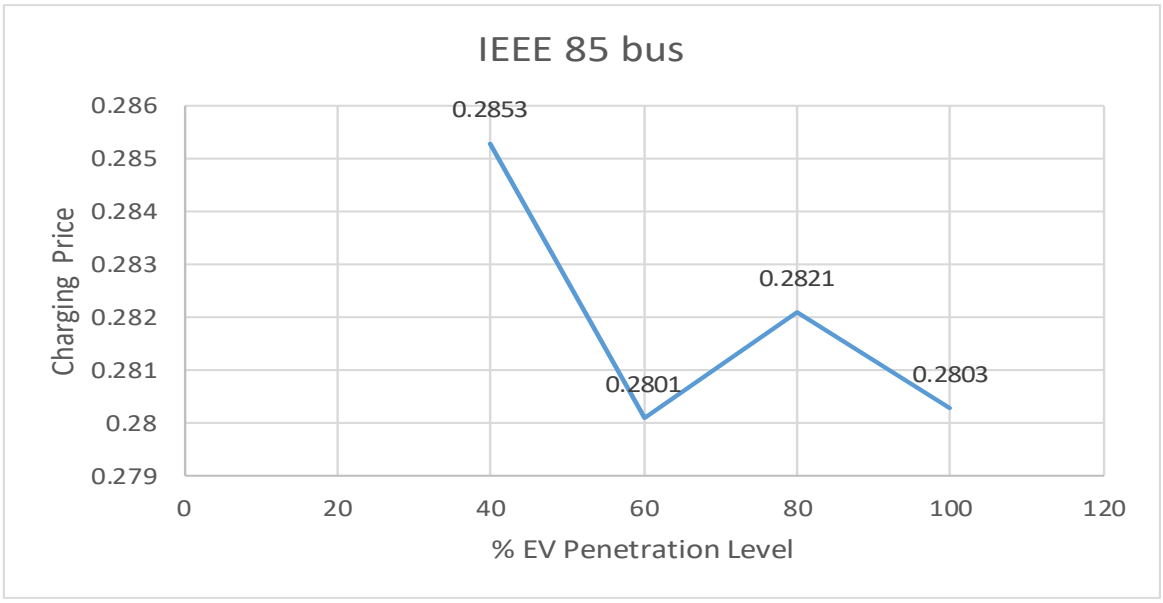

Fig. 4.1.6. Variation of optimal charging price with increase in EV penetration level at the IEEE 85 bus network under the Case-Study# 4.1

IEEE 141 bus DN

From **Fig. 4.1.8**, the highest value of the *OF* is obtained in the case of 100% EV penetration (8.3637) and a minimum of 8.2509 in the case of 60% penetration. The highest value of *VPEI* is obtained in the case of 100% EV penetration (1.1789) and a minimum of 1.0393 in the case of 40% penetration. The highest value of *BCR* is obtained in the case of 40% EV penetration (23.9159) and a minimum of 23.5167 in the case of 80% penetration. The highest value of *ECBI* is obtained at 100% EV penetration (0.3216) and a minimum of 0.1258 at 40% penetration. From **Fig. 4.1.7**, the maximum active power losses of 556.98 kW occurred at 40% penetration and a minimum of 353.88 kW at 100% penetration. The relative distribution of charging and discharging vehicles of each type is shown in **Fig. 4.1.9**. The maximum capacity of the vehicle pool for this case is taken as 1500. As per **Fig. 4.2.10**, the minimum value of the optimal discharging price is obtained in the case of 60% EV penetration, while the maximum value is obtained in the case of 40% EV penetration. Similarly, from **Fig. 4.2.11**, the minimum value of the optimal charging price is obtained in the case of 80% EV penetration, while the maximum value is obtained in the case of 60% EV penetration.

Figures **4.1.12** and **4.1.13** show the relative convergence characteristics of the PSO, LPSO, RPSO, PSO-SR, CSA, and Jaya algorithms. In every case, the objective function yielded the highest value in the Jaya algorithm. The corresponding *VSI* improvement characteristics are shown in the figures **4.1.14** and **4.1.15** of the IEEE 85 and 141 bus DNs for 80% and 100% EV penetrations, respectively. The buses 9-16 and 26-85 showed marked improvement in the *VSI* for the IEEE 85 bus network. Likewise, the *VSI* got markedly improved at buses 4-33, 43-53, and 55-141 of the IEEE 141bus network. The maximum percentage improvements in the *VSI* observed are 47.60% and 3.68% for the IEEE 85 and 141 bus networks, respectively.

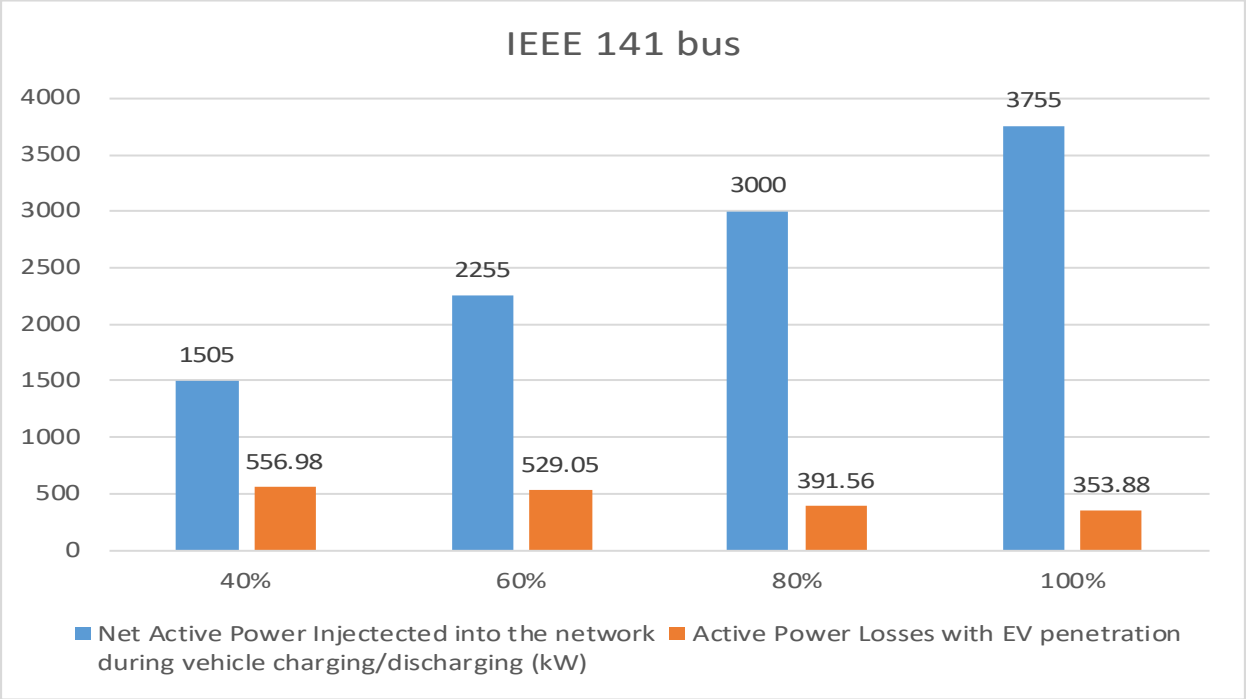

Fig. 4.1.7. Comparison of active power transferred due to EV discharge to the IEEE 141 bus DN and losses for different penetration levels under the Case-Study# 4.1

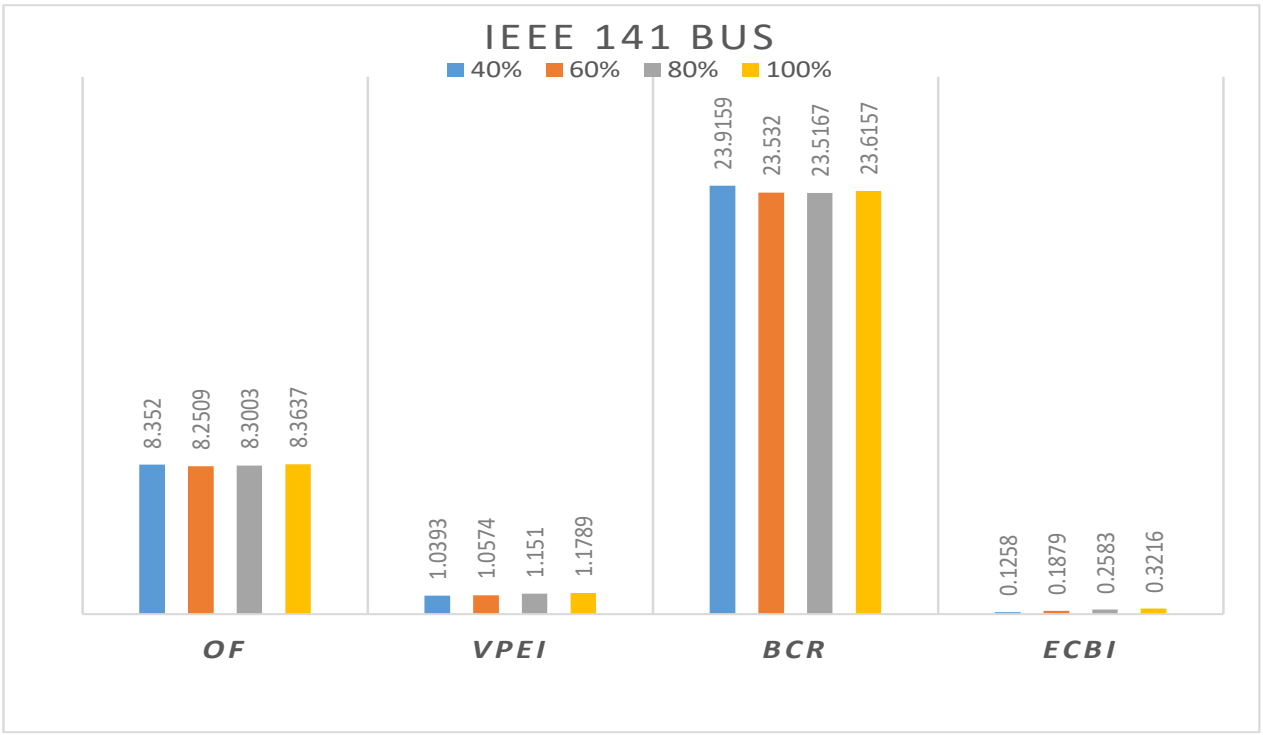

Fig. 4.1.8. Comparison of *OF*, *VPEI*, *BCR* and *ECBI* for different penetration levels at the IEEE 141 bus DN under the Case-Study# 4.1

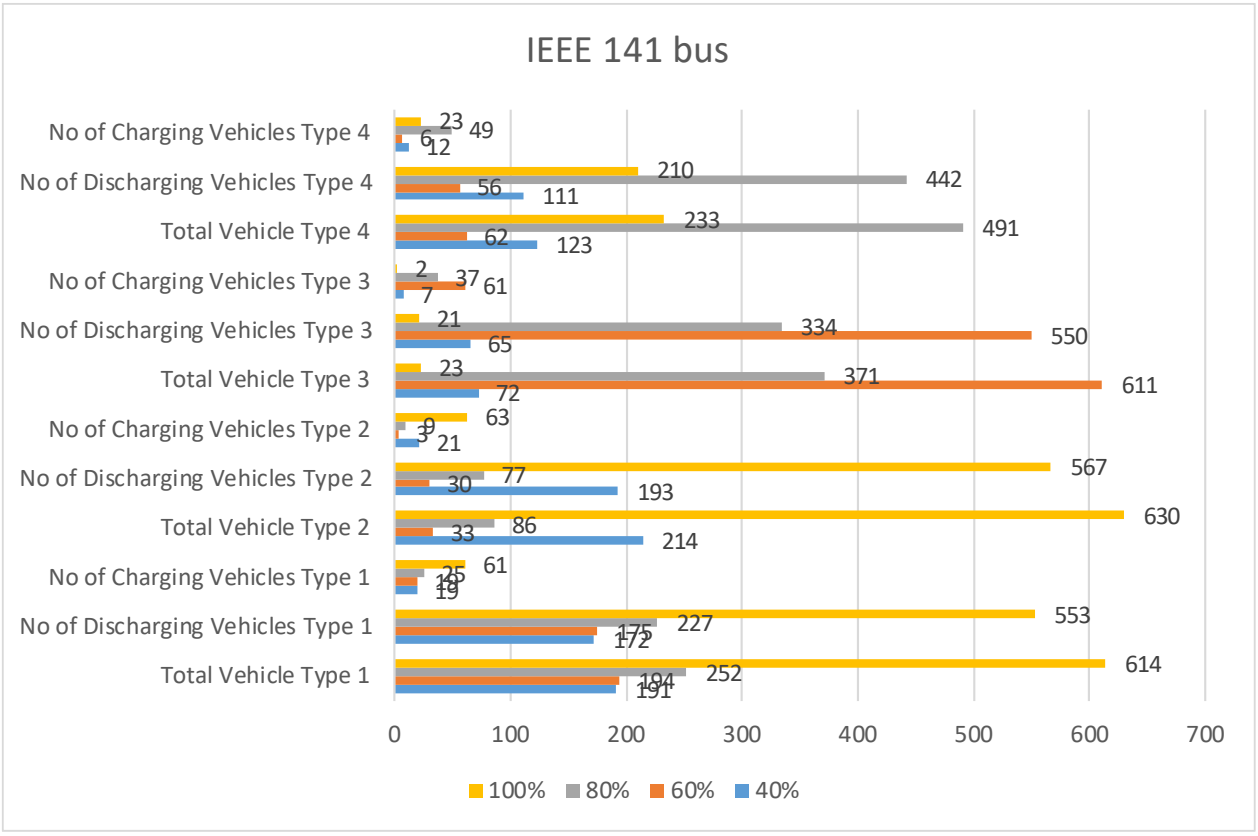

Fig. 4.1.9. Distribution of the number of EVs of each type for different penetration levels at the IEEE 141 bus DN under the Case-Study# 4.1

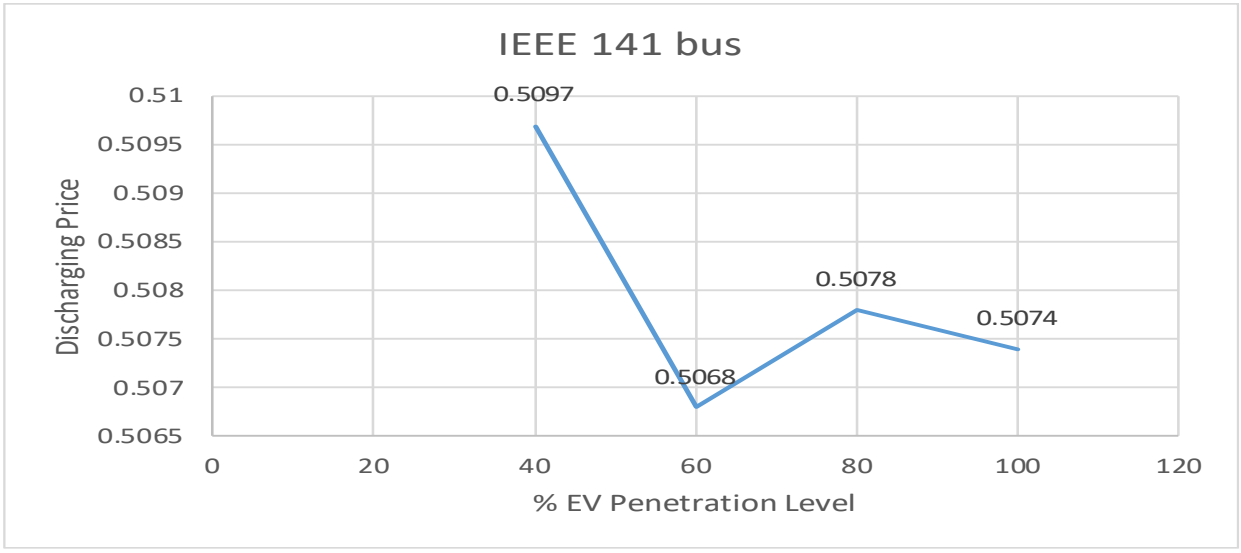

Fig. 4.1.10. Variation of optimal discharging price with increase in EV penetration level at IEEE 141 bus network under the Case-Study# 4.1

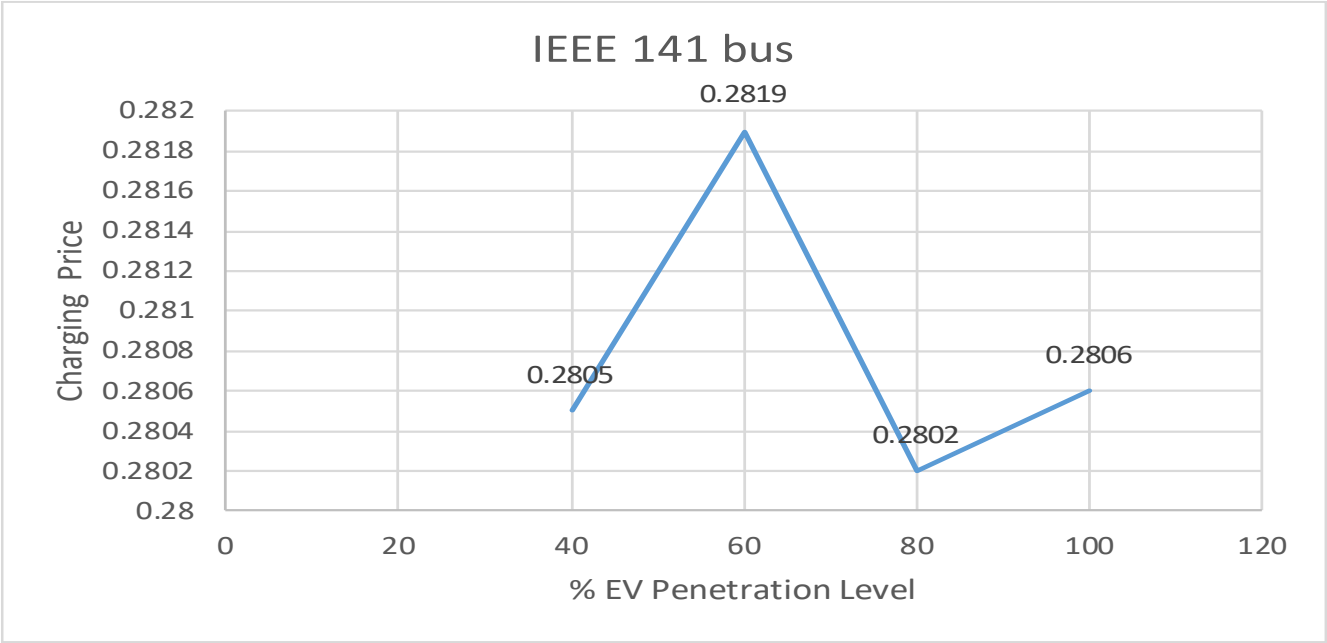

Fig. 4.1.11. Variation of optimal charging price with increase in EV penetration level at IEEE 141 bus network under the Case-Study# 4.1

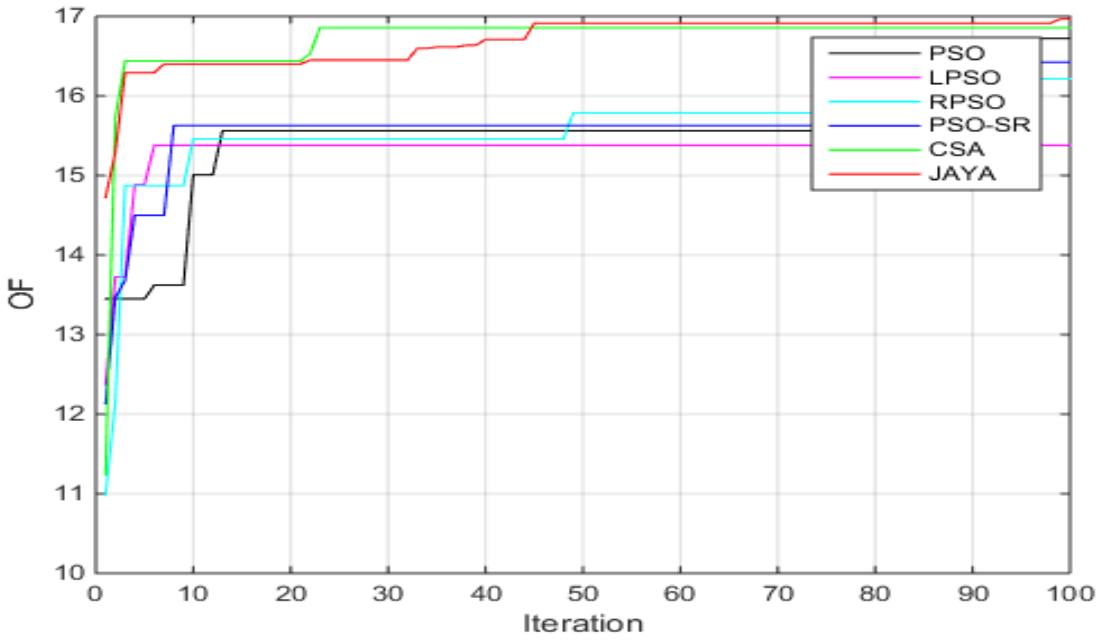

Fig. 4.1.12. Relative convergence characteristics of algorithms under comparison (Case: 80% EV penetration at IEEE 85 bus) under the Case-Study# 4.1

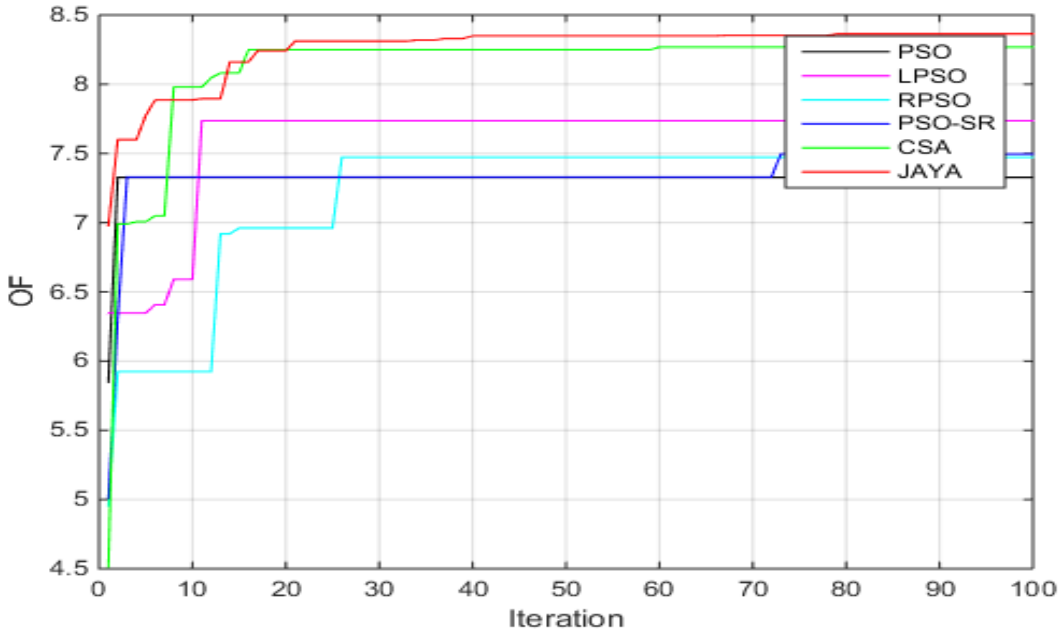

Fig. 4.1.13. Relative convergence characteristics of algorithms under comparison (Case: 100% EV penetration at IEEE 141 bus) under the Case-Study# 4.1

Fig. 4.1.14. *VSI* improvement characteristics (Case: Without EV & 80% EV penetration at IEEE 85 bus) under the Case-Study# 4.1

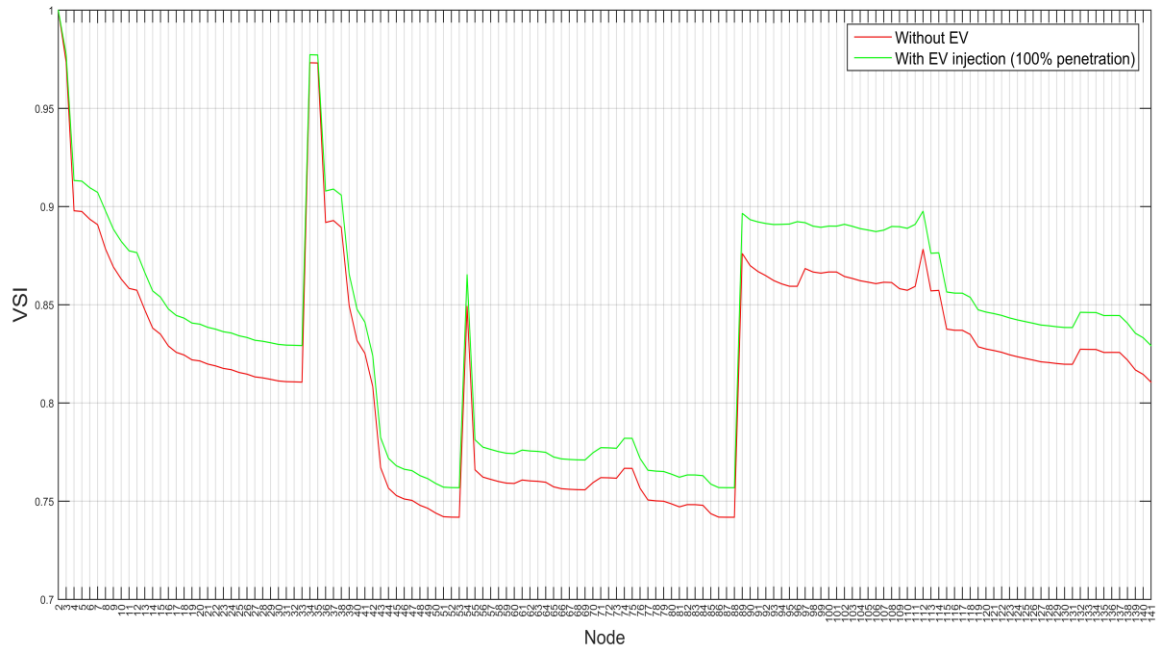

Fig. 4.1.15. *VSI* improvement characteristics (Case: Without EV & 100% EV penetration at IEEE 141 bus) under the Case-Study# 4.1

4.10. Statistical analysis of the performance of algorithms under comparison for *Subcase #4.1.4*

A comparative performance analysis of the algorithms is performed for one sub-case study presented in **Section 4.10** as an example. The sub-case study considered is **Subcase #4.1.4**, which presents the effect of EV at 100% penetration level at the IEEE 141 bus DN.

The algorithms in comparison are PSO, LPSO, RPSO, PSO-SR, CSA, and Jaya. Each algorithm is run for 50 trials.

From the box-whiskers plot, as shown in **Fig. 4.1.16**, it is evident that all the quartiles of the Jaya box-plot are significantly greater than PSO, LPSO, RPSO, PSOSR and CSA. The relative maximum, minimum, mean, and standard deviation values of the *OF* using Jaya and other comparing algorithms are shown in **Fig. 4.1.17.** The mean difference plot (**Fig. 4.1.18**) reveals the Jaya algorithm's superiority over the comparing algorithms in terms of the *OF*.

Table 4.1.5 displays the results of Shapiro-Wilk and Kolmogorov-Smirnov normality tests, including the p-values for various scenarios. It can be concluded that the data did not come from a normal distribution.

The results of the Kruskal-Wallis-H-ANOVA and post-hoc Dunn tests are shown in **Table 4.1.5** and **Table 4.1.6**, respectively. The test statistic H (to be treated as) is 293.16, which is outside the 95% confidence interval. The Kruskal-Wallis-H test indicated that there is a significant difference in the dependent variable between the different groups ($\chi^2(5) = 293.16$, $p < 0.001$) with a mean rank score of 25.50 for PSO, 175.50 for LPSO, 75.50 for RPSO, 125.50 for PSO-SR, 225.50 for CSA, and 275.50 for Jaya.

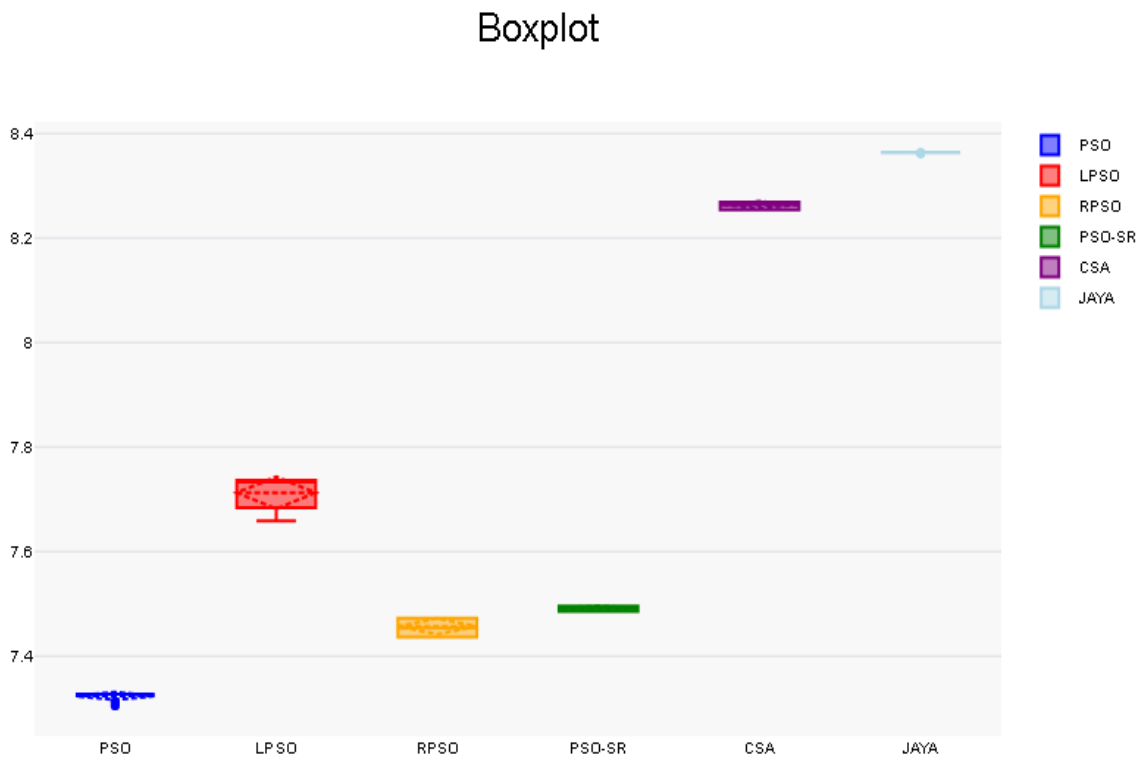

Fig. 4.1.16. Relative box plots of the *OF* obtained by the algorithms for the case EV at 100% penetration level at the IEEE 141 bus DN under Case Study #4.1 (Subcase #4.1.4)

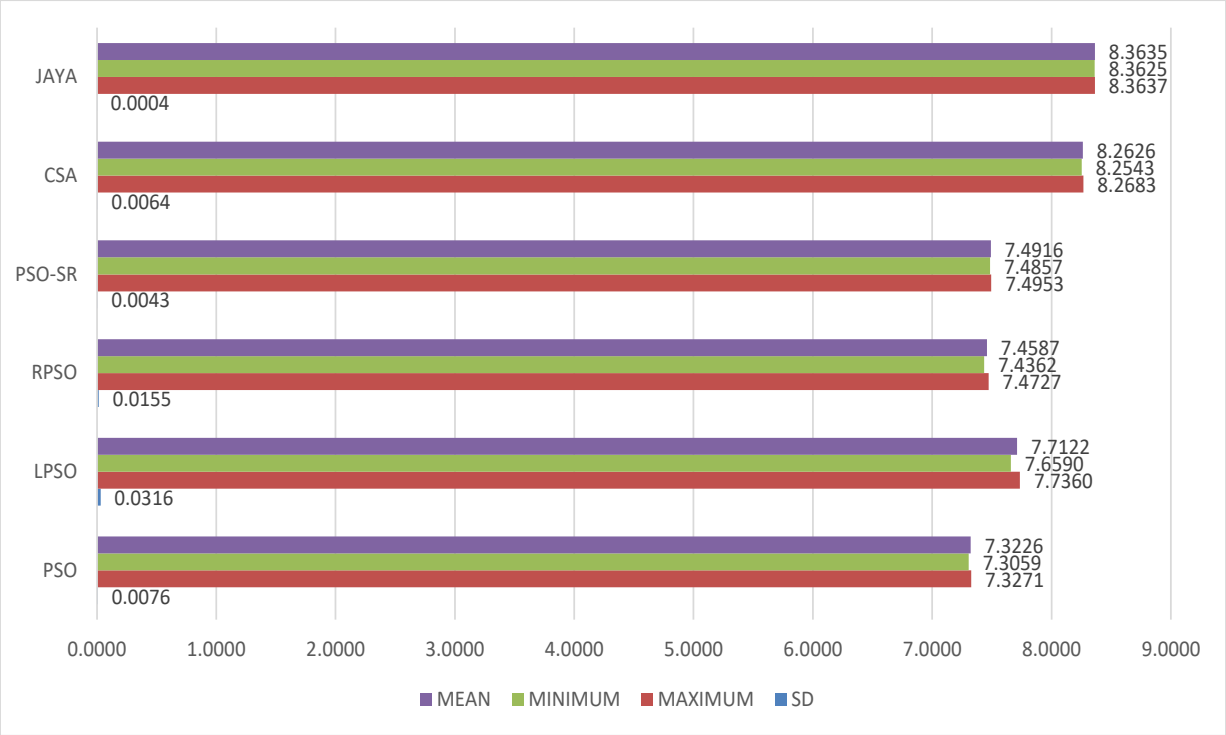

Fig. 4.1.17. Relative values of maximum, minimum, mean, and standard deviation of the *OF* obtained by the algorithms in comparison for the case EV at 100% penetration level at the IEEE 141 bus DN under Case Study #4.1 (Subcase #4.1.4)

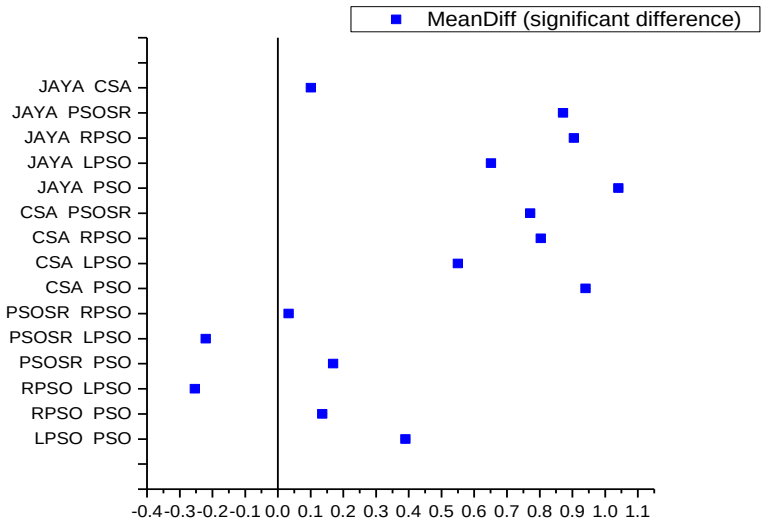

Fig. 4.1.18. Mean difference plot of the *OF* obtained by different algorithm pairs for the case EV at 100% penetration level at the IEEE 141 bus DN under Case Study #4.1 (Subcase #4.1.4)

Table. 4.1.5. Statistical results for the case EV at 100% penetration level at the IEEE 141 bus DN under Case Study #4.1 (Subcase #4.1.4)

Algorithms	**PSO**	**LPSO**	**RPSO**	**PSO-SR**	**CSA**	**JAYA**
Minimum *OF*	7.3059	7.6590	7.4362	7.4857	8.2543	8.3625
Maximum *OF*	7.3271	7.7360	7.4727	7.4953	8.2683	8.3637
Mean *OF*	7.3226	7.7122	7.4587	7.4916	8.2626	8.3635
Standard Deviation of *OF*	0.0076	0.0316	0.0155	0.0043	0.0064	0.0004
p-value* (Shapiro-Wilk test for normality) α=0.5	2.477e-10	0.00002323	3.01e-8	4.622e-9	4.624e-9	6.837e-13
p-value* (Kolmogorov–Smirnov test for normality) α=0.5	0	0	7.361e-14	0	0	0
Mean Rank (Kruskal-Wallis non-parametric test) α=0.5^{++}	25.50	175.50	75.50	125.50	225.50	275.50

Table 4.1.6. Parametric comparison of algorithm pairs by post-hoc Dunn test for the test case EV at 100% penetration level at the IEEE 141 bus DN under Case Study #4.1 (Subcase #4.1.4)

Pair	**Mean Rank difference**	**Z**	**Standard Error difference**	**Critical value**	**p-value**	**p-value/2**
PSO-LPSO	-150	8.6824	17.2763	50.5809	0	0
PSO-RPSO	-50	2.8941			0.003802	0.001901
PSO-PSOSR	-100	5.7883			7.111e-9	3.555e-9
PSO-CSA	-200	11.5766			0	0
PSO-JAYA	-250	14.4707			0	0
LPSO-RPSO	100	5.7883			7.111e-9	3.555e-9
LPSO - PSOSR	50	2.8941			0.003802	0.001901
LPSO - CSA	-50	2.8941			0.003802	0.001901
LPSO - JAYA	-100	5.7883			7.111e-9	3.555e-9
RPSO - PSOSR	-50	2.8941			0.003802	0.001901
RPSO - CSA	-150	8.6824			0	0
RPSO - JAYA	-200	11.5766			0	0
PSOSR - CSA	-100	5.7883			7.111e-9	3.555e-9
PSOSR - JAYA	-150	8.6824			0	0
CSA - JAYA	-50	2.8941			0.003802	0.001901

4.11. Summary

This section presents the salient observations regarding the effectiveness of EV integration with varying penetration levels on the technical, economic, and environmental benefits of the IEEE 85 and 141 bus DNs.

An in-depth analysis has been performed in **Case-Study 4.1**, considering the IEEE 85 and 141 bus DNs. The relative technical, economic, and environmental impacts have been studied, considering different levels of EV penetration. The conclusion of the work presented is summarized as follows:

It is seen that the most beneficial test system configurations in terms of overall objective (technical, economic, and environmental benefit) are:

a) IEEE 85 bus DN with 100% EV penetration
b) IEEE 141 bus DN with 100% EV penetration

The results of EV integration with the DNs show that the networks are getting technically, economically, and environmentally benefitted consistently when the power is fed to the DNs from the EVs. The *VSI* of most of the buses in both the test systems under consideration improved after optimal EV charging station allocation and the adoption of a charge-discharge strategy. The active power losses of the networks get reduced when the net power transferred from the EVs is positive because the EV charging station is working as a power source.

CHAPTER 5: Impact of Demand Response on DN's sustainability

This chapter presents the impact of DR on the technical, economic, and environmental impacts of DNs. A demand-price elasticity-based DR is proposed for maximization of the said benefits are elaborately studied and graphically presented in this chapter.

5.1. Introduction

DR is the process of persuading consumers to change their choice of electricity use when there is more availability of electricity or when there is less overall demand **[118]**. This is usually done through price adjustments or other financial incentives. DR is a crucial source of flexibility for controlling the effects of variable renewable energy sources and rising power demand on the stability and dependability of electrical networks, together with smart grids and energy storage.

The "Net Zero Emissions" by 2050 scenario places increasing demands on the power grid due to the electrification of end uses such as transportation and home heating, as well as the widespread deployment of solar PV and wind power, the output of which varies with the weather and time of day. DR and other similar technologies can help to mitigate these effects and lessen the need for expensive new transmission and distribution infrastructure.

Utilizing connected devices, new digital technologies can assist in automating DR and maximizing the potential of distributed energy resources like home energy storage systems, rooftop solar panels, and EV batteries. However, policy implementation and technology deployment must pick up speed in order to keep up with the Net Zero Scenario.

5.2. Objective of DR

DR gives users the chance to actively participate in the functioning of the electrical grid by adjusting or lowering their peak-time electricity use in response to time-based pricing or other types of monetary incentives. Some planners and operators of electric systems are using DR programs as a resource to balance supply and demand. These initiatives have the potential to reduce wholesale electricity prices, which would therefore result in reduced retail rates. Offering time-based rates, such as time-of-use pricing, critical peak pricing, variable peak pricing, real-time pricing, and critical peak rebates, is one way to get customers involved in DR initiatives. It also consists of direct load control schemes, which allow electricity providers

to switch on and off air-conditioners and water heaters during times of high demand in exchange for a monetary reward and cheaper electricity costs.

DR programs are seen by the electric power sector as a resource choice that is becoming more and more useful. Grid modernization initiatives have the potential to increase the capabilities and impacts of these programs. For instance, sensors are able to identify issues with peak load and use automatic switching to shift or cut electricity in key locations, eliminating the possibility of overload and the subsequent power outage. The breadth of time-based pricing plans that can be made available to customers is increased by advanced metering technology. By providing information on their power consumption and expenses, smart customer systems like home area networks and in-home displays can help consumers modify their behaviour and cut down on peak time consumption. By reducing peak demand and postponing the development of new power plants and power distribution systems, particularly those set aside for usage during peak hours, these plans may also enable electricity providers to make financial savings.

5.3. Types of DR

Inevitable facts like ever-increasing consumers and rapid growth of industries are leading to uncontrolled increases in the electrical load. The grid operators must adopt DSM strategies to maintain this precarious energy-load balance while complying with numerous operational constraints. The generation capacity needs to be increased, but due to limited fossil fuel reserves, it can be done with RES. PV, wind, etc. Besides, emissions from fossil fuels, viz., oxides of carbon, nitrogen, particulate matter, etc. have adverse effects on the environment and need to be checked. One of the most essential and fruitful means to perform DSM is DR. It allows consumers to reduce or shift their energy usage during peak load hours. There are two main types of DR programs depicted in **Fig. 5.0.1**, namely time-based rate (TBR) and incentive-based program (IBP). There are three types of TBR programs: time of use (TOU), real-time pricing (RTP), and critical peak pricing (CPP). The IBP is classified into three types: voluntary (Direct Load Control and Emergency DR Program), mandatory (Capacity Market Program and Interruptible/Curtailable service), and market clearing (Demand Bidding/Buyback and Ancillary Service Markets).

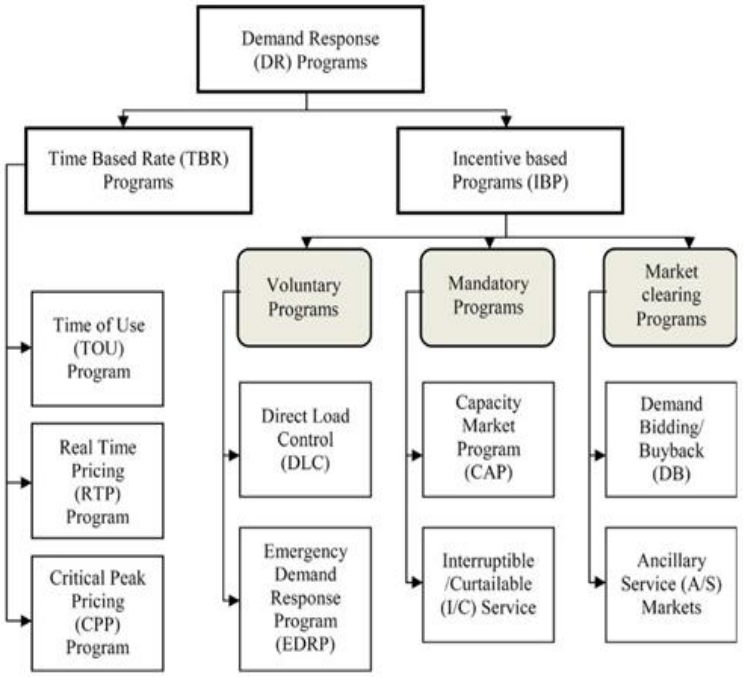

Fig. 5.0.1. Chart depicting different DR schemes

5.4. Load modelling and hourly load data

There are two main categories of load models for DN analysis. These are static and dynamic load models. Generally, power flow analysis is performed for static states and hence static load model has been taken under consideration in this work. The static load has been expressed in exponential form.

$$PL = PL_0(\frac{V}{V_0})^{np} \tag{5.1}$$

$$QL = QL_0(\frac{V}{V_0})^{nq} \tag{5.2}$$

np and nq stands for load components, PL_0 and $QL_0$are nominal active and reactive powers at nominal load bus voltage V_0. PL and QL are exponentially modelled active and reactive powers at load bus voltage V_0. The values of np and nq of different load components considered in this study are taken from **Table 5.0.1.**

The types of loads connected to IEEE 33 and 69 networks are shown in **Table 5.0.2,** and **Table 5.0.3**, respectively **[119].**

Table 5.0.1. Values of load components np and nq for different loads

Type of load	Symbol	np	nq
Constant impedance	L1	2.00	2.00
Constant current	L2	1.00	1.00
Constant power	L3	0.00	0.00
Battery charge	L4	2.59	4.06
Fluorescent lighting	L5	1.00	3.00
Fluorescent lamps	L6	2.07	3.21
Air Conditioner	L7	0.50	2.50
Incandescent lamp	L8	1.54	0.00
Compact fluorescent lamps	L9	1.00	0.35
Resistance space heater	L10	2.00	0.00
Fans, pumps and other motors	L11	0.08	1.60
Small industrial motors	L12	0.10	0.60
Large industrial motors	L13	0.05	0.50

Table 5.0.2. Types of loads connected at each node of the IEEE 33 bus DN

Node no.	Type of load connected	Node no.	Type of load connected
1	Source Node	18	L5
2	L4	19	L7
3	L6	20	L2
4	L1	21	L10
5	L5	22	L11
6	L7	23	L8
7	L2	24	L9
8	L10	25	L12
9	L11	26	L13
10	L8	27	L3
11	L9	28	L4
12	L12	29	L6
13	L13	30	L1

14	L3	31	L5
15	L4	32	L7
16	L6	33	L2
17	L1		

Table 5.0.3. Types of loads connected at each node of the IEEE 69 bus DN

Node no.	Type of load connected	Node no.	Type of load connected
1	Source Node	37	L9
2	L4	38	L12
3	L6	39	L13
4	L1	40	L3
5	L5	41	L4
6	L7	42	L6
7	L2	43	L1
8	L10	44	L5
9	L11	45	L7
10	L8	46	L2
11	L9	47	L10
12	L12	48	L11
13	L13	49	L8
14	L3	50	L9
15	L4	51	L12
16	L6	52	L13
17	L1	53	L3
18	L5	54	L4
19	L7	55	L6
20	L2	56	L1
21	L10	57	L5
22	L11	58	L7
23	L8	59	L2
24	L9	60	L10

25	L12	61	L11
26	L13	62	L8
27	L3	63	L9
28	L4	64	L12
29	L6	65	L13
30	L1	66	L3
31	L5	67	L4
32	L7	68	L6
33	L2	69	L1
34	L10		
35	L11		
36	L8		

5.5. Load equations after DR implementation

This study incorporates a DR program **[120]** with incentives based on the price elasticity of customer benefit and demand. Customer participation in the power markets was non-existent before the deregulation of the electrical sector. They lacked the knowledge and resources necessary to participate in the power market. A portion of the customers also prefers not to participate owing to the risk and price variations brought on by market volatility. Customers' non-participation drives up the cost of electricity and clogs the network. Price elasticity measures the impact of a 1% change in power prices on changes in electricity usage.

The point in **Fig. 5.0.2** where the supply curve and demand curve 1 cross each other has the coordinates (d1, P1), where d1 is the initial demand in MW and P1 is the price of electricity in USD. The new demand after DR in MW and the decreased electricity price in USD are, respectively, d2 and P2 for the demand curve 2. It demonstrates how a minor variation in load demand can have a significant impact on the price of electricity.

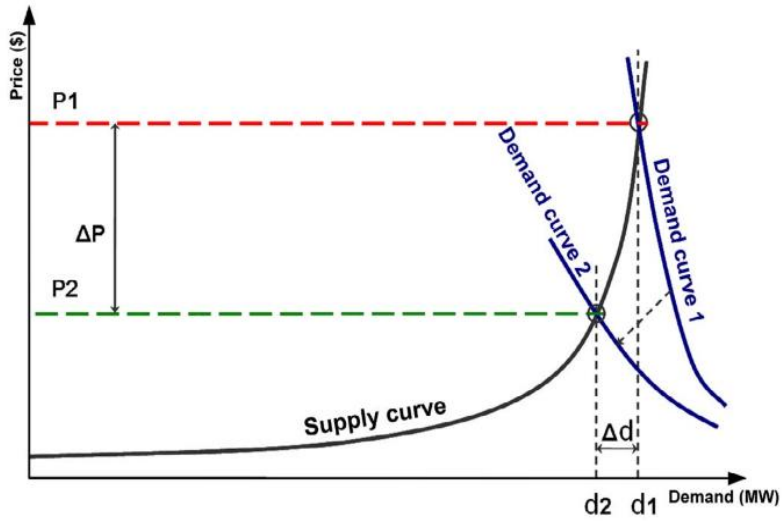

Fig. 5.0.2. Demand variation vs. electricity price

The change in load demand concerning the price of electricity is what is referred to as the price elasticity and is given by:

$$E = \frac{\rho_0}{dem_0} . \frac{\partial dem}{\partial \rho} \tag{5.3}$$

The price of electricity fluctuates during various periods, and customers respond in one of the following ways:

1) Certain loads, such as illumination loads, cannot be transferred from one interval to another and can only be turned "on" or "off." It is said that these types of loads are sensitive for a single period. This is referred to as "self-elasticity", and the price elasticity value is less than or equal to zero.

   From equation 5.3, it can be written as

$$E(k,m) = \frac{\Delta dem_k}{\Delta \rho_m} \leq 0 \tag{5.4}$$

2) The other categories of loads can be transferred from one interval (peak-load) to another (off-peak-load) and are sensitive to multiple periods. The term for this is cross-elasticity. In this instance, the price-elasticity value is greater than or equal to zero.

   Similarly, equation 5.3, for this case, can be modified as

$$E(k,m) = \frac{\Delta dem_k}{\Delta \rho_m} \geq 0 \quad (5.5)$$

The effects of the DR program are mathematically modelled in the following subsections as single and multi-period modelling.

5.5.1. Single period DR modelling

Let it be assumed that the customer shifts its load demand from $dem_0(i)$ to $dem(i)$ depending on the changes in electricity price and incentive offered.

$$\Delta dem(k) = dem_0(k) - dem(k) \quad (5.6)$$

$dem(k)$ and $\Delta dem(k)$ are demand and demand changes in the k^{th} hour. $dem_0(k)$ is the initial demand.

The amount of incentive *P* (USD) for demand change of $\Delta dem(k)$ is given by

$$P\big(\Delta dem(k)\big) = I(k).\Delta dem(k) \quad (5.7)$$

$I(k)$ is the incentive offered for the k^{th} hour.

Ben (USD) is the benefit of the customer in the k^{th} hour and is given by

$$Ben\big(\Delta dem(k)\big) = Rev\big(\Delta dem(k)\big) - dem(k).\rho(k) + P\big(\Delta dem(k)\big) \quad (5.8)$$

$\rho(k)$ is the spot electricity price of the k^{th} hour. $Rev\big(dem(k)\big)$ is the revenue function.

For obtaining the maximum customer benefit, the partial derivative of $S\big(\Delta dem(k)\big)$ with respect to $dem(k)$ should be equated to zero.

$$\frac{\partial Ben}{\partial dem(k)} = \frac{\partial Rev(dem(k))}{\partial dem(k)} - \rho(k) + \frac{\partial P\big(\Delta dem(k)\big)}{\partial dem(k)} = 0 \quad (5.9)$$

From equation 5.7 and 5.9, we get

$$\frac{\partial Rev(dem(k))}{\partial dem(k)} = \rho(k) + I(k) \quad (5.10)$$

$Rev(dem(k))$ can be expanded using Taylor's series and can be written as

$$Rev\big(dem(k)\big) = Rev\big(dem_0(k)\big) + \frac{\partial Rev(dem_0(k))}{\partial dem(k)} \Delta dem(k) + \frac{1}{2}.\frac{\partial Rev^2\big(dem_0(k)\big)}{\partial dem^2(k)} (\Delta dem(k))^2 \quad (5.11)$$

The benefit to customers before implementation of DR is given by

$$Ben_0\big(\Delta dem(k)\big) = Rev\big(\Delta dem_0(k)\big) - dem_0(k).\rho_0(k) \quad (5.12)$$

$\rho_0(k)$ is the nominal electricity price of the k^{th} hour.

Likewise, for getting the maximum customer benefit for DR,

$$\frac{\partial Ben_0}{\partial dem(k)} = \frac{\partial Rev(dem_0(k))}{\partial dem(k)} - \rho_0(k) = 0 \quad (5.13)$$

$$\frac{\partial Rev(d_0(k))}{\partial dem(k)} = \rho_0(k) \quad (5.14)$$

$$\frac{\partial Rev^2}{\partial dem^2} = \frac{\partial \rho}{\partial dem} = \frac{1}{E}\frac{\rho_0}{dem_0} \quad (5.15)$$

Substituting equations 5.13 and 5.14 in equation 5.11,

$$Rev\big(dem(k)\big) = Rev\big(dem_0(k)\big) + \rho_0(k).\Delta dem(k) + + \frac{1}{2}.\frac{\partial \rho_0(k)}{\partial dem(k)} (\Delta dem(k))^2 \quad (5.16)$$

The equation 5.16 can be re-written as

$$Rev\big(dem(k)\big) = Rev_0(k) + \rho_0(k).\big(dem(k) - dem_0(k)\big)\left\{1 + \frac{dem(k)-dem_0(k)}{2E(k).dem_0(k)}\right\} \quad (5.17)$$

Substituting equation 5.17 in 5.10,

$$\rho(k) + I(k) = \rho_0(k)\left\{1 + \frac{dem(k)-dem_0(k)}{E(k).dem_0(k)}\right\} \quad (5.18)$$

$$\rho(k) - \rho_0(k) + I(k) = \rho_0(k)\frac{dem(k)-dem_0(k)}{E(k).dem_0(k)} \quad (5.19)$$

So, the customers load consumption, post-DR, can be modelled as

$$dem(k) = dem_0(k)\left\{1 + \frac{E(k).[\rho(k)-\rho_0(k)+I(k)]}{\rho_0(k)}\right\} \quad (5.20)$$

If no incentive is awarded to the customer participating in DR, i.e., $I(k) = 0$, then $dem(k) = dem_0(k)$.

5.5.2. **Multiple period DR modelling**

For multi-period modelling, the cross-elasticity matrix is defined as

$$E(k,m) = \frac{\rho_0(m)}{dem_0(k)} . \frac{\partial dem(k)}{\partial \rho(m)} \begin{cases} E(k,m) \leq 0 \; if \; k = m \\ E(k,m) \geq 0 \; if \; k \neq m \end{cases} \quad (5.21)$$

The relationship between DR and electricity price is given by

$$dem(k) = dem_0(k) + \sum_{k=1}^{24} E(k,m) \frac{dem_0(k)}{\rho_0(m)} [\rho(m) - \rho_0(m) + I(m)] \quad k = 1,2, \ldots\ldots 24 \quad (5.22)$$

Combining equations 5.20 and 5.22,

$$dem(k) = dem_0(k) + E(k) \frac{dem_0(k)}{\rho_0(k)} [\rho(k) - \rho_0(k) + I(k)] +$$

$$\sum_{k=1}^{24} E(k,m) \frac{dem_0(k)}{\rho_0(m)} [\rho(m) - \rho_0(m) + I(m)] \quad where \; k = 1,2, \ldots\ldots 24 \quad (5.23)$$

A combined single & multi-period load demand model is presented by equation 5.23 considering demand-price elasticity.

5.6. Load-price elasticity

The measurement of how the load demand changes in response to electricity price changes is known as price elasticity of load demand. When there is a significant shift in demand due to a change in price, this is known as elastic demand. When there is little or no shift in load demand in response to price changes, this is known as inelastic demand. **Table 5.0.4** shows the values of demand-price elasticity for a period of 24 hours **[120]**.

Table 5.0.4 Price elasticity of load demand at the IEEE 33 and 69 bus DNs

Hour	1-5	6-9	10-14	15-19	20-24
1-5	-0.08	0.03	0.034	0.03	0.034
6-9	0.03	-0.11	0.05	0.03	0.04
10-14	0.034	0.04	-0.19	0.04	0.01
15-19	0.03	0.03	0.04	-0.11	0.04
20-24	0.034	0.4	0.01	0.03	-0.19

5.7. Hourly spot electricity price

In a competitive electricity market, the spot price is established by finding the intersection of the total supply and demand curves, which are generated from the combined supply and demand bids, for a specific hour in each region of the market as bid in a power/energy exchange. Spot electricity price curves frequently have jumps or spikes and typically show characteristics like multiple seasonality, mean reversion, and volatility.

Table 5.0.5 and **Fig. 5.0.3** show the hourly variation of spot electricity prices **[121]**.

Table 5.0.5 Hourly spot electricity price

Hour	1	2	3	4	5	6	7	8	9	10	11	12
Price (USD/MW)	22.15	22	23.1	22.65	23.25	22.95	22.5	22.15	22.8	29.35	30.15	31.65
Hour	13	14	15	16	17	18	19	20	21	22	23	24
Price (USD/MW)	24.6	24.5	22.5	22.3	22.25	22.05	22.2	22.65	23.1	22.95	22.75	22.55

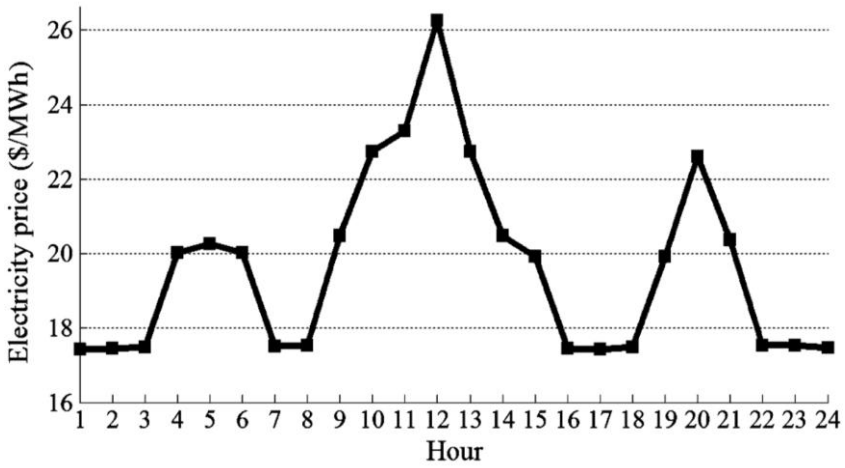

Fig. 5.0.3. Variation of spot electricity price over a period of 24 hours

5.8. Incentive provided to the DR participants

The shifting and curtailment of the load by the DR participants is subjected to the incentives provided to them in order to participate in the program. In this work, the incentive values and demand-price elasticities are provided in the **Table 5.0.6.**

Table 5.0.6. Test scenarios considered under Case Study# 5.1

Name of DR Program	Group	Subcase#	Incentive value (USD/MWh)	Price Elasticity
Base Case (Without DR)	NA	5.1.1	NA	NA
Price elasticity-based DR Program	I	5.1.2	I_1 =4	As Table 5.0.5 (A_1)
		5.1.3	I_2 =7	
		5.1.4	I_3 =10	
	II	5.1.5	I_1 =4	½*Table 5.0.5 (A_2)
		5.1.6	I_2 =7	
		5.1.7	I_3 =10	
	III	5.1.8	I_1 =4	2*Table 5.0.5 (A_3)
		5.1.9	I_2 =7	
		5.1.10	I_3 =10	

5.9. Hourly variation of solar irradiance based on geographical modelling

PV cells convert solar energy into electrical energy, which can then be stored in batteries and used to meet the network's increasing demands. As a renewable energy source, solar energy minimizes the use of fossil fuels that contribute to environmental pollution. Solar energy is divided into two categories: extra-terrestrial solar radiation and global solar radiation.

The component of extra-terrestrial solar irradiation G_{ex} on a horizontal surface **[101]** is given by

$$G_{exH} = G_0(1 + 0.0333cos\left(\frac{2\pi N}{365}\right))^2 (\sin L \sin\delta + \cos L \cos\delta \cos\omega) \quad (5.24)$$

This work uses the aforementioned model to determine, as an example, the hourly G_{exH} of the 180th day of a year for the location of Jammu and Kashmir, India. **Fig. 5.0.4** shows the plot of the hourly variation of solar irradiance.

5.10. Calculation of optimal number of PV modules required for DG installation considering seasonal variations

The maximum output of a PV module, taking uncertainties into account, is 148.86 W, and it happens in the 12th hour of the day, according to the hourly solar irradiance curve depicted in **Fig. 5.0.4**.

The Jaya algorithm is used to calculate the optimal value of the PV based DG power to be fed to the DN, which is assumed to vary between 20% and 30% of the load demand. Accordingly, the maximum installed capacity of the DG will be determined by taking 30% of the DN's load requirement. This assumption is supported by the information found in the literature on the integration of renewable energy sources into DNs. In practical power systems, the major portion of the connected load is supplied from conventional thermal power units. Due to the rapid integration of renewable energy sources, the proportionate share of the connected load supplied by them is almost 20% to 30%.

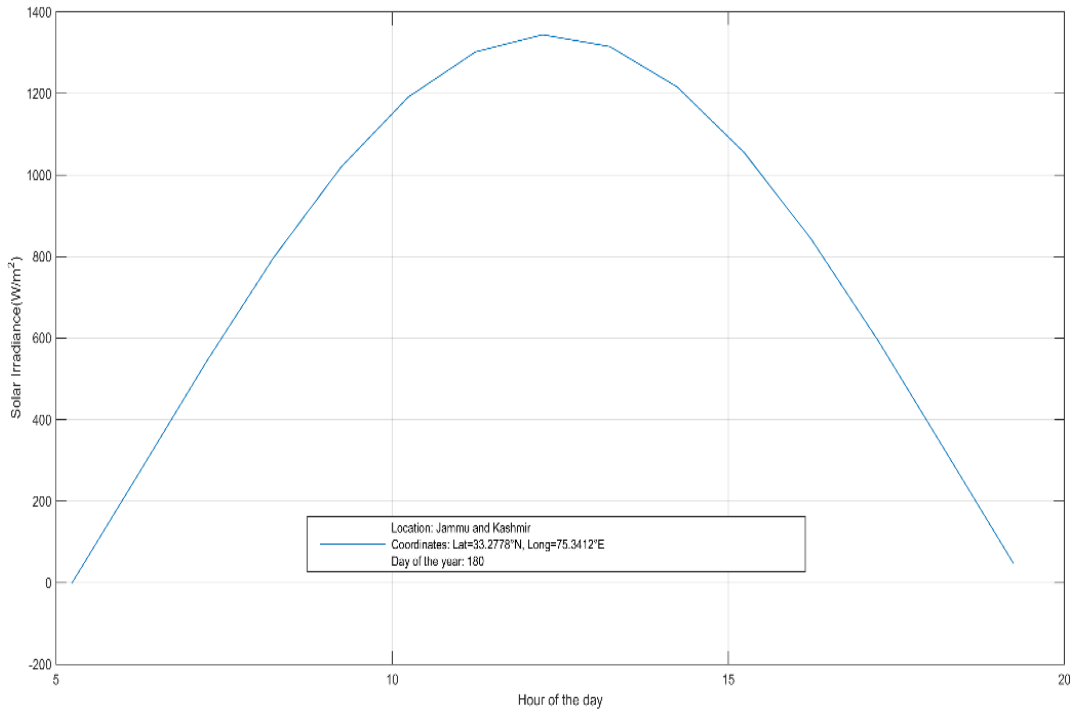

Fig. 5.0.4. Graphical plot showing solar irradiance vs hour of the 180th day of the year for the location Jammu & Kashmir, India

Table 5.0.7. Estimation of the effective number of working PV required for DG installation at the IEEE 69 bus DN for different Indian seasons

Seasons in India	Day no. of the year (N) corresponds to the tentative peak of the season	The horizontal component of extraterrestrial solar irradiance (G_{extH}) during Noon (W/m^2)	The solar power output of a PV module (PV_{out}) considering uncertainty (W)	The number of working PV modules required to cater 30% of the connected load (P_{LOAD})= P_{load}/PV_{out}
Vasanta (Spring)	90	1214	119.84	9513
Grishma (Summer)	180	1344	148.86	7658
Varsha (Monsoon)	240	1223	134.74	8461
Sharat (Autumn)	270	1079	114.83	9928
Hemanta (Pre-Winter)	330	799.70	95.61	11923
Shishira (Winter)	360	726.60	90.31	12624

There are six seasons in India, namely, Vasanta (Spring), Grishma (Summer), Varsha (Monsoon), Sharat (Autumn), Hemanta (Pre-Winter), and Shishira (Winter). **Table 5.0.7** presents a season-wise estimation of the effective number of working PV required to cater to 30% of the connected load. In the present case, the number of PV modules required and its optimal location are tested on IEEE 69 bus system as an example. The calculation of the requirement of the number of modules for DG installation should be based on the maximum output of each module because considering lower modular outputs will result in the requirement of more modules. In that case, the system will not be economic. The total connected load of the IEEE 69 bus is 3.80 MW and 30% of it is 1.14 MW. So, the installed capacity of the PV-based DG is 1.14 MW. The number of PV modules required for DG installation (considering the Grishma season for better economy) is (1.14× 106/148.85) = 7658.

5.11. Impact of DR on DN sustainability

A future where electricity use is as intelligent and dynamic as the devices it powers is promised by DR, which marks a fundamental change in the way energy is controlled. This idea goes beyond just saving energy; it also involves optimizing it and turning consumers from passive observers of the energy ecosystem into active players. In order to improve grid dependability, reduction in costs, and lessen the environmental effect of energy production, DR programs incentivize consumers to shift or reduce their electricity use during peak hours.

The knowledge that the price of power varies throughout the day and dependent on demand is the foundation of DR. Energy demand spikes during peak hours, which are often late afternoon to early evening. In order to keep up with the increased demand, utilities have to turn on more expensive and frequently less efficient power plants. DR seeks to level off these peaks by altering consumption patterns, which can save a lot of money and improve operations.

In terms of DR, the adoption of smart grid technologies has changed everything. Real-time data on electricity usage is made available to utilities and consumers through smart meters and residential energy management systems, allowing for more accurate control over consumption. This technology opens the door for a more flexible and resilient electricity grid in addition to enabling more effective DR. The United States alone had installed nearly 119 million smart meters as of 2022, demonstrating the nation's growing commitment to updating its energy infrastructure.

DR has equally compelling economic benefits. Utilities can postpone or completely avoid the need to build new power plants, which can be expensive and time-consuming, by lowering peak demand. Furthermore, by reducing the need for costly and environmentally harmful conventional power plants, DR can drastically lower operating costs. DR initiatives in the US residential sector saved about one terawatt-hour of energy in 2022.

Another essential component of DR is its environmental benefits. Greenhouse gas emissions can be greatly reduced by optimizing energy use and minimizing the need for additional power generation during peak hours. This is especially significant because one of the main global sources of carbon dioxide emissions is the production of energy. DR offers a more flexible demand structure that can adjust to the fluctuation of wind and solar power, which not only help to mitigate the effects of climate change but also encourages the integration of renewable energy sources into the grid.

DR has obstacles to its widespread adoption despite its many advantages. Although consumer participation is important, there is still a lack of understanding and engagement. It will take extensive education efforts, alluring rewards, and simple participation procedures to get beyond this obstacle. To enable the scalability of DR programs, legislative frameworks and market structures must also change. This will guarantee that all parties involved—from utilities to end users—are compensated for their contributions to a more sustainable energy future and their objectives are in line.

5.12. Formulation of the day-averaged objective function (*DAOF*) due to DR program implementation

The process for calculating *DAOF* is explained in this sub-section.

5.12.1. Day-averaged voltage profile enhancement index (*DAVPEI*) due to DR program implementation

The $DAVPEI$, over a period of 24 hours, is calculated by the following equation.

$$DAVPEI = 1/24 \sum_{i=1}^{24} VPEI_i \quad (5.25)$$

$VPEI_i$ is the voltage profile enhancement index of the i^{th} hour. It is desirable that $VPEI_i$ is greater than unity for every hour in order to have hourly technical improvements. However, since solar irradiation is not available uniformly throughout the day, it is not a necessary criterion for every hour of a day.

Installation of the DG is said to be technically beneficial over the day if $DAVPEI$ should be greater than unity.

5.12.2. Day-averaged benefit cost ratio (*DABCR*) due to DR program implementation

For 24 hours, the $DABCR$ is calculated as follows

$$DABCR = 1/24 \sum_{i=1}^{24} BCR_i \quad (5.26)$$

BCR_i is the benefit cost ratio of the i^{th} hour. Here also, it is desirable that BCR_i is greater than unity for every hour but it is not possible again due to the non-availability of solar energy throughout the day.

Installation of the DG is said to be economically beneficial over the day if $DABCR$ is greater than unity. It must be noted that since the formulation of BCR_i involves the cost of the DN active power loss, it will be minimized during the optimization process.

5.12.3. Day-averaged emission cost benefit index (*DAECBI*) due to DR program implementation

The $DAECBI$, for a period of 24 hours, is calculated using the following equation.

$$DAECBI = 1/24 \sum_{i=1}^{24} ECBI_i \quad (5.27)$$

$ECBI_i$ is the emission cost benefit index of the i^{th} hour. In this case also, it is not possible that $ECBI_i$ should be greater than zero for every hour due to non-uniformity of solar irradiation.

5.12.4. Day-averaged objective function (*DAOF*) due to DR program implementation

For 24 hours, the $DAOF$, which is to be maximized, is calculated as follows:

$$DAOF = 1/24 \sum_{i=1}^{24} OF_i \tag{5.28}$$

The processes of calculating $VPEI_i$, BCR_i, $ECBI_i$, and OF_i is done by using equations 2.28, 2.33, 2.36, and 2.26, respectively, as defined in Chapter 2.

5.13. Operational constraints

The maximization of $DAOF$ should satisfy the following technical constraints as well as those defined by the equations 2.39 to 2.43 in Chapter 2.

i) Incentive limit constraint of DR:

$$I(k)_{min} \leq I(k) \leq I(k)_{max} \tag{5.29}$$

ii) Electricity price limit:

$$\rho(k)_{min} \leq \rho(k) \leq \rho(k)_{max} \tag{5.30}$$

5.14. Case studies under consideration

In order to study the effectiveness of DR on the technical, economic, and environmental benefits of renewable energy integrated DNs, the following case-study is presented in this section:

Case Study #5.1: Implementation of price-elasticity based DR with fixed-incentive at PV integrated IEEE 33 and 69 bus DNs

5.14.1. **Case study#5.1:** Implementation of price-elasticity based DR with fixed-incentive at PV integrated IEEE 33 and 69 bus DNs

Case study description- The optimum hourly PV injected power to be integrated into the IEEE 33 and 69 bus DNs has been found using the Jaya algorithm. Under this case study, ten different

sub-cases (including the base case) of the DR program have been considered in this work for analysis as shown in **Table 5.0.6**.

The proposed work is simulated using MATPOWER v7.0. The PC in use features a 2.60 GHz Intel Core i7 9750H processor with 24GB of RAM. The hourly injected power of the PV-based DG is calculated using the Jaya algorithm.

The *nit* and n_p considered in this work are 50 and 20. respectively. The algorithm is executed for 10 trials. The results obtained by the Jaya algorithm are compared with those of PSO, LPSO, RPSO, PSO-SR, CSA, and AOA.

The different stages of the proposed work, viz., PV estimation, DG sizing, load flow, optimization, load modelling, and implementation of the DR program applied to the problem defined under the Case-Study# 5.1 is shown in **Fig. 5.1.1**.

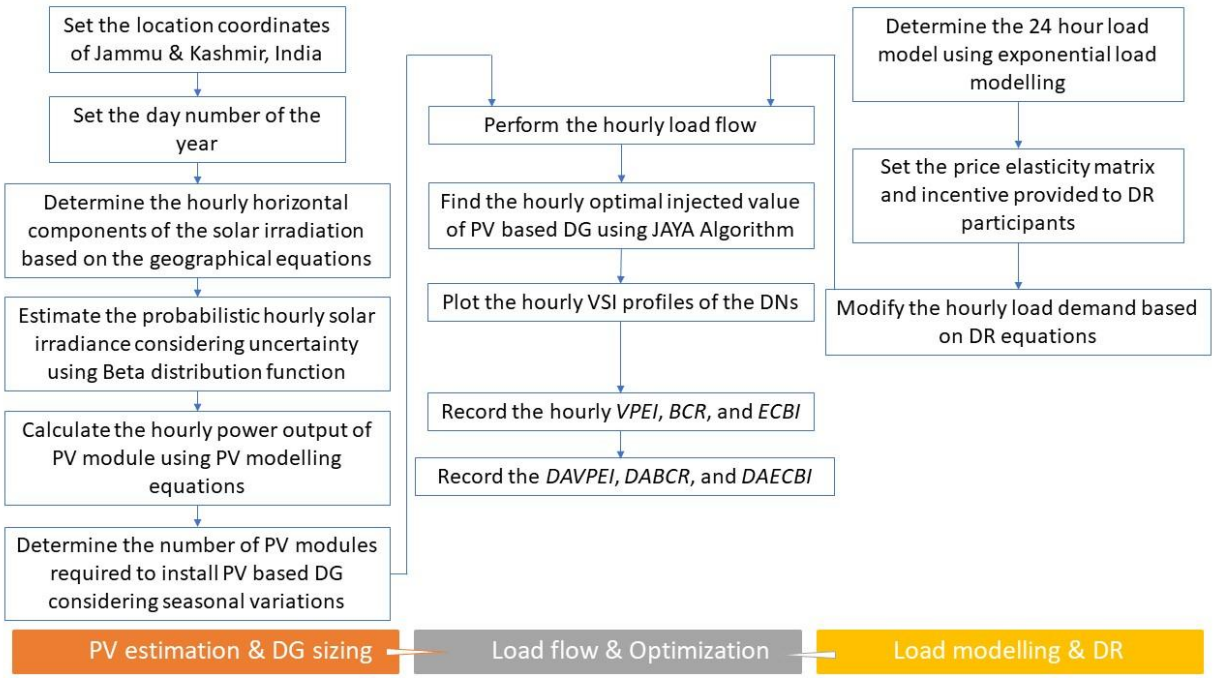

Fig. 5.1.1. The different stages viz., PV estimation, DG sizing, load flow, optimization, load modelling, and implementation of the DR program applied to the problem defined under the Case-Study# 5.1

5.14.1.1. ***Subcase #5.1.1:*** Base case (without DR)

Table 5.1.1. presents the average network parameters before DR implementation at the IEEE 33 and 69 bus DNs using the Jaya algorithm under **Subcase #5.1.1.**

Table 5.1.1. Average network parameters before DR implementation at the IEEE 33 and 69 bus DNs using Jaya Algorithm for subcase #5.1.1 (Base Case) under case study 5.1							
Test System	Average PV based DG power (kW)	*DAOF*	*DAVPEI*	*DABCR*	*DAECBI*	Avg. PL_W (kW)	Computation Time (secs)
IEEE 33 bus DN	673.40	1.1994	1.0040	2.4970	0.1007	190.06	150.01
IEEE 69 bus DN	657.54	1.3242	1.0192	2.8588	0.0985	211.69	200.86

5.14.1.2. ***Subcase #5.1.2:*** Incentive I_1, Elasticity A_1

Table 5.1.2. presents the average network parameters after DR implementation at the IEEE 33 and 69 bus DNs using the Jaya algorithm under **Subcase #5.1.2.**

Table 5.1.2. Average network parameters after DR implementation at the IEEE 33 and 69 bus DNs using Jaya Algorithm for subcase #5.1.2 (Incentive I_1, Elasticity A_1) under case study 5.1							
Test System	Average PV based DG power (kW)	*DAOF*	*DAVPEI*	*DABCR*	*DAECBI*	Avg. PL_W (kW)	Computation Time (secs)
IEEE 33 bus DN	674.31	1.2005	1.0040	2.5004	0.1008	190.06	153.36
IEEE 69 bus DN	663.74	1.3339	1.0194	2.8867	0.0995	211.54	200.90

5.14.1.3. ***Subcase #5.1.3:*** Incentive I_2, Elasticity A_1

Table 5.1.3. presents the average network parameters after DR implementation at the IEEE 33 and 69 bus DNs using the Jaya algorithm under **Subcase #5.1.3.**

Table 5.1.3. Average network parameters after DR implementation at the IEEE 33 and 69 bus DNs using Jaya Algorithm for subcase #5.1.3 (Incentive I_2, Elasticity A_1) under case study 5.1							
Test System	Average PV based DG power (kW)	*DAOF*	*DAVPEI*	*DABCR*	*DAECBI*	Avg. PL_W (kW)	Computation Time (secs)
IEEE 33 bus DN	674.33	1.2006	1.0040	2.5005	0.1008	190.06	160.82
IEEE 69 bus DN	664.35	1.3345	1.0194	2.8887	0.0996	211.55	207.60

5.14.1.4. ***Subcase #5.1.4:*** Incentive I_3, Elasticity A_1

Table 5.1.4. presents the average network parameters after DR implementation at the IEEE 33 and 69 bus DNs using the Jaya algorithm under **Subcase #5.1.4.**

Table 5.1.4. Average network parameters after DR implementation at the IEEE 33 and 69 bus DNs using Jaya Algorithm for subcase #5.1.4 (Incentive I_3, Elasticity A_1) under case study 5.1

Test System	Average PV based DG power (kW)	*DAOF*	*DAVPEI*	*DABCR*	*DAECBI*	Avg. PL_W (kW)	Computation Time (secs)
IEEE 33 bus DN	673.12	1.2018	1.0040	2.5043	0.1006	190.06	149.36
IEEE 69 bus DN	665.93	1.3369	1.0194	2.8953	0.0998	211.52	200.78

5.14.1.5. ***Subcase #5.1.5:*** Incentive I_1, Elasticity A_2

Table 5.1.5. presents the average network parameters after DR implementation at the IEEE 33 and 69 bus DNs using the Jaya algorithm under **Subcase #5.1.5.**

Table 5.1.5. Average network parameters after DR implementation at the IEEE 33 and 69 bus DNs using Jaya Algorithm for subcase #5.1.5 (Incentive I_1, Elasticity A_2) under case study 5.1

Test System	Average PV based DG power (kW)	*DAOF*	*DAVPEI*	*DABCR*	*DAECBI*	Avg. PL_W (kW)	Computation Time (secs)
IEEE 33 bus DN	673.82	1.1999	1.0040	2.4985	0.1007	190.06	153.41
IEEE 69 bus DN	657.93	1.3249	1.0192	2.8609	0.0986	211.67	201.13

5.14.1.6. ***Subcase #5.1.6:*** Incentive I_2, Elasticity A_2

Table 5.1.6. presents the average network parameters after DR implementation at the IEEE 33 and 69 bus DNs using the Jaya algorithm under **Subcase #5.1.6.**

Table 5.1.6. Average network parameters after DR implementation at the IEEE 33 and 69 bus DNs using Jaya Algorithm for subcase #5.1.6 (Incentive I_2, Elasticity A_2) under case study 5.1							
Test System	Average PV based DG power (kW)	*DAOF*	*DAVPEI*	*DABCR*	*DAECBI*	Avg. PL_W (kW)	Computation Time (secs)
IEEE 33 bus DN	673.96	1.2001	1.0040	2.4991	0.1008	190.06	148.34
IEEE 69 bus DN	663.27	1.3329	1.0194	2.8839	0.0994	211.57	200.40

5.14.1.7. ***Subcase #5.1.7:*** Incentive I_3, Elasticity A_2

Table 5.1.7. presents the average network parameters after DR implementation at the IEEE 33 and 69 bus DNs using the Jaya algorithm under **Subcase #5.1.7.**

Table 5.1.7. Average network parameters after DR implementation at the IEEE 33 and 69 bus DNs using Jaya Algorithm for subcase #5.1.7 (Incentive I_3, Elasticity A_2) under case study 5.1							
Test System	Average PV based DG power (kW)	*DAOF*	*DAVPEI*	*DABCR*	*DAECBI*	Avg. PL_W (kW)	Computation Time (secs)
IEEE 33 bus DN	673.62	1.2052	1.0040	2.5146	0.1007	190.06	152.37
IEEE 69 bus DN	665.17	1.3358	1.0194	2.8924	0.0997	211.53	201.13

5.14.1.8. ***Subcase #5.1.8:*** Incentive I_1, Elasticity A_3

Table 5.1.8. presents the average network parameters after DR implementation at the IEEE 33 and 69 bus DNs using the Jaya algorithm under **Subcase #5.1.8.**

Table 5.1.8. Average network parameters after DR implementation at the IEEE 33 and 69 bus DNs using Jaya Algorithm for subcase #5.1.8 (Incentive I_1, Elasticity A_3) under case study 5.1							
Test System	Average PV based DG power (kW)	*DAOF*	*DAVPEI*	*DABCR*	*DAECBI*	Avg. PL_W (kW)	Computation Time (secs)
IEEE 33 bus DN	673.95	1.2001	1.004	2.4991	0.1008	190.06	147.93
IEEE 69 bus DN	661.55	1.3303	1.0193	2.8764	0.0992	211.61	205.01

5.14.1.9. ***Subcase #5.1.9:*** Incentive I_2, Elasticity A_3

Table 5.1.9. presents the average network parameters after DR implementation at the IEEE 33 and 69 bus DNs using the Jaya algorithm under **Subcase #5.1.9.**

Table 5.1.9. Average network parameters after DR implementation at the IEEE 33 and 69 bus DNs using Jaya Algorithm for subcase #5.1.9 (Incentive I_2, Elasticity A_3) under case study 5.1

Test System	Average PV based DG power (kW)	*DAOF*	*DAVPEI*	*DABCR*	*DAECBI*	Avg. PL_W (kW)	Computation Time (secs)
IEEE 33 bus DN	674.23	1.2004	1.004	2.5001	0.1008	190.06	147.31
IEEE 69 bus DN	663.08	1.3325	1.0193	2.8827	0.0994	211.59	206.70

5.14.1.10. ***Subcase #5.1.10:*** Incentive I_3, Elasticity A_3

Table 5.1.10. presents the average network parameters after DR implementation at the IEEE 33 and 69 bus DNs using the Jaya algorithm under **Subcase #5.1.10.**

Table 5.1.10. Average network parameters after DR implementation at the IEEE 33 and 69 bus DNs using Jaya Algorithm for subcase #5.1.10 (Incentive I_3, Elasticity A_3) under case study 5.1

Test System	Average PV based DG power (kW)	*DAOF*	*DAVPEI*	*DABCR*	*DAECBI*	Avg. PL_W (kW)	Computation Time (secs)
IEEE 33 bus DN	673.07	1.2130	1.0040	2.5381	0.1006	190.06	146.61
IEEE 69 bus DN	663.85	1.3335	1.0194	2.8856	0.0995	211.58	229.11

5.14.1.11. Result analysis of Case study#5.1

This section presents a critical analysis of the average and hourly technical, economic, and environmental indices of the DR driven PV integrated IEEE 33 and 69 bus DNs.

Result analysis of IEEE 33 bus DN

Fig. 5.1.2 shows the relative values of *DAVPEI*, *DABCR*, *DAECBI*, and *DAOF* of the IEEE 33 bus DN after DR implementation for the all the subcases (5.1.1 to 5.1.10) under **case study#5.1**. It is derived from the data related to IEEE 33 bus DN presented in **Table 5.1.1** to **Table 5.1.10**.

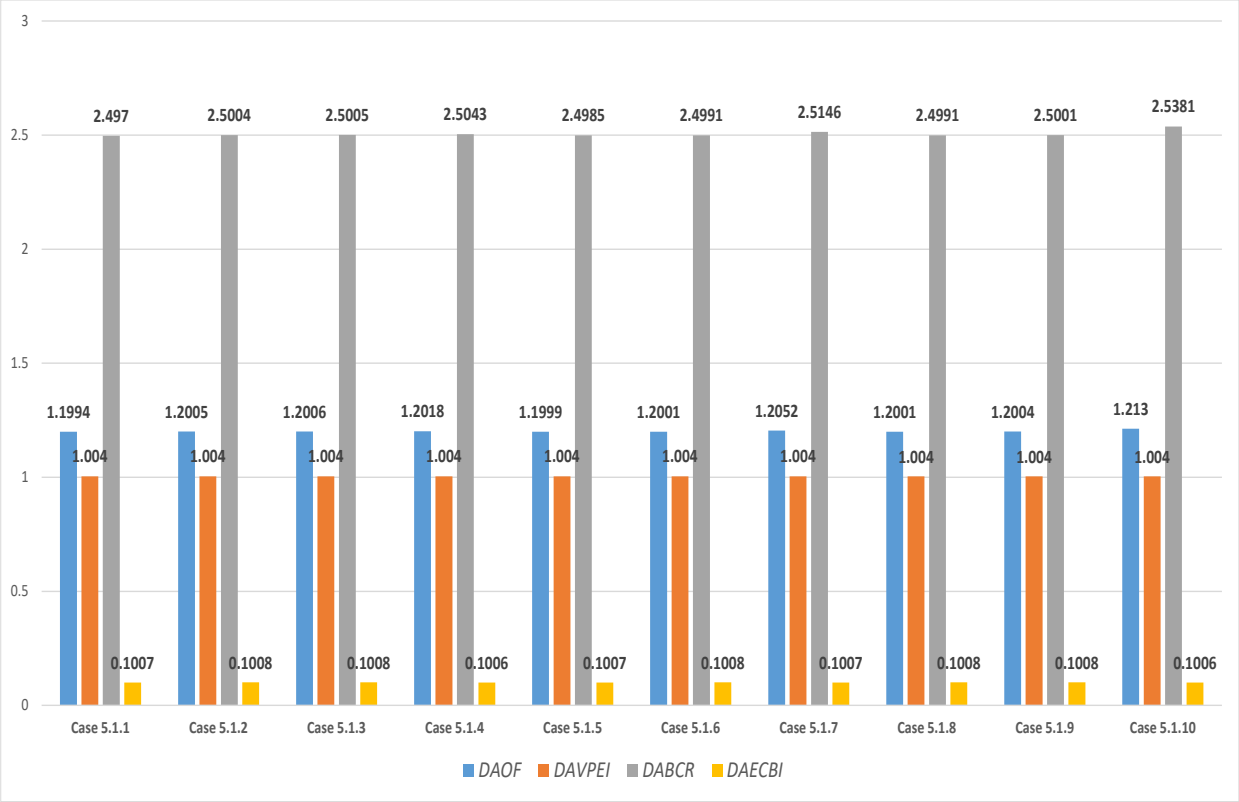

Fig. 5.1.2. *DAVPEI*, *DABCR*, *DAECBI*, and *DAOF* of the IEEE 33 bus DN after DR implementation for the all the subcases (5.1.1 to 5.1.10) under case study#5.1

Subcase #5.1.1 (Base Case of IEEE 33 bus)- This is the case study without implementation of the DR program but with PV-based DG integrated for 24 hours. The value of *DAOF* obtained is 1.1994 as per **Table 5.1.1**. The values of *DAVPEI*, *DABCR*, and *DAECBI* are 1.0040, 2.4970, and 0.1007 respectively. The fruitfulness of implementing DR for the rest of the nine cases will be achieved if the value of *DAOF* is greater than this case. It is evident from **Fig. 5.1.2** that the values of *DAOF* obtained for the nine cases using the Jaya Algorithm are higher than 1.1994. The average active power loss obtained in this case is 190.06 kW, which is 5.91% lower than when no PV-based DG and DR are there. The average value of DG injected, in this case, is 673.40 kW.

Subcase #5.1.10 (IEEE 33 bus)- This is the best test sub-case (out of all ten sub-cases) as maximum *DAOF* is achieved of value 1.2130. This is 1.011 times higher than the corresponding base case. The highest *DABCR* is obtained in this case of value 2.5381 which is 1.016 times higher than the base case. The value of *DAECBI* obtained is 0.1006 which is almost same with the base case (no improvement). The highest incentive of 10 USD/MWh is provided to the DR participants for the sub-cases **5.1.4**, **5.1.7**, and **5.1.10**, respectively. The average value of DG injected, in this case, is 673.07 kW.

Hourly analysis of VPEI, BCR, ECBI, and OF (IEEE 33 bus DN)

Fig. 5.1.3 presents the hourly variation of the parameters *VPEI*, *BCR*, *ECBI*, and *OF* of the IEEE 33 bus DN after DR implementation for the **subcase# 5.1.10** under **case study#5.1**. The hourly *OF* is on the higher side (>2) from 9AM to 3PM. The highest *OF* is obtained in the 12th hour of value 2.884 due to maximum availability of solar irradiance. The corresponding values of *VPEI*, *BCR*, and *ECBI* are 1.012, 7.357, and 0.292, respectively. The hourly *OF* is moderate (≤ 2) during 6AM to 8AM and 4PM to 6PM as the solar irradiance is moderate during these periods. The value of the *OF* is minimum (0.333) due to non-availability of solar irradiance.

Load curtailment and shifting of IEEE 33 bus DN

Fig. 5.1.4 shows the hour-wise total load demand of the IEEE 33 bus DN after all the test cases of DR implementation. It is seen that consumers are curtailing load demand during the peak load hours (10 AM–2 PM and 8 PM–12 AM). The load curtailment increases with the increase in incentives provided to various customers. The curtailed loads are shifted to the off-peak hours (1 AM–9 AM and 3 PM–7 PM). **Table 5.1.11** shows hour-wise load curtailment and load shifting at both DNs for the **sub-case 5.1.10**. The load curtailment and load shift increase with the increase in elasticity and incentive as seen in **Fig. 5.1.4**, and increase by up to 98.86% and 43.76%, respectively.

Table 5.1.11. Percentage load curtailment and shift at the DR driven IEEE 33 bus DN for subcase# 5.1.10 under case study#5.1

Hour	**1:00 AM**	**2:00 AM**	**3:00 AM**	**4:00 AM**	**5:00 AM**	**6:00 AM**	**7:00 AM**	**8:00 AM**	**9:00 AM**	**10:00 AM**	**11:00 AM**	**12:00 PM**
% Load change	+35.53	+35.55	+35.52	+35.52	+35.53	+43.76	+43.76	+43.77	+43.76	-98.85	-98.85	-98.85
Hour	**1:00 PM**	**2:00 PM**	**3:00 PM**	**4:00 PM**	**5:00 PM**	**6:00 PM**	**7:00 PM**	**8:00 PM**	**9:00 PM**	**10:00 PM**	**11:00 PM**	**12:00 AM**
% Load change	-98.86	-98.85	+28.51	+28.50	+28.50	+28.50	+28.52	-53.31	-53.30	-53.30	-53.29	-53.30

* "-" indicates load curtailment and "+" indicates load shift

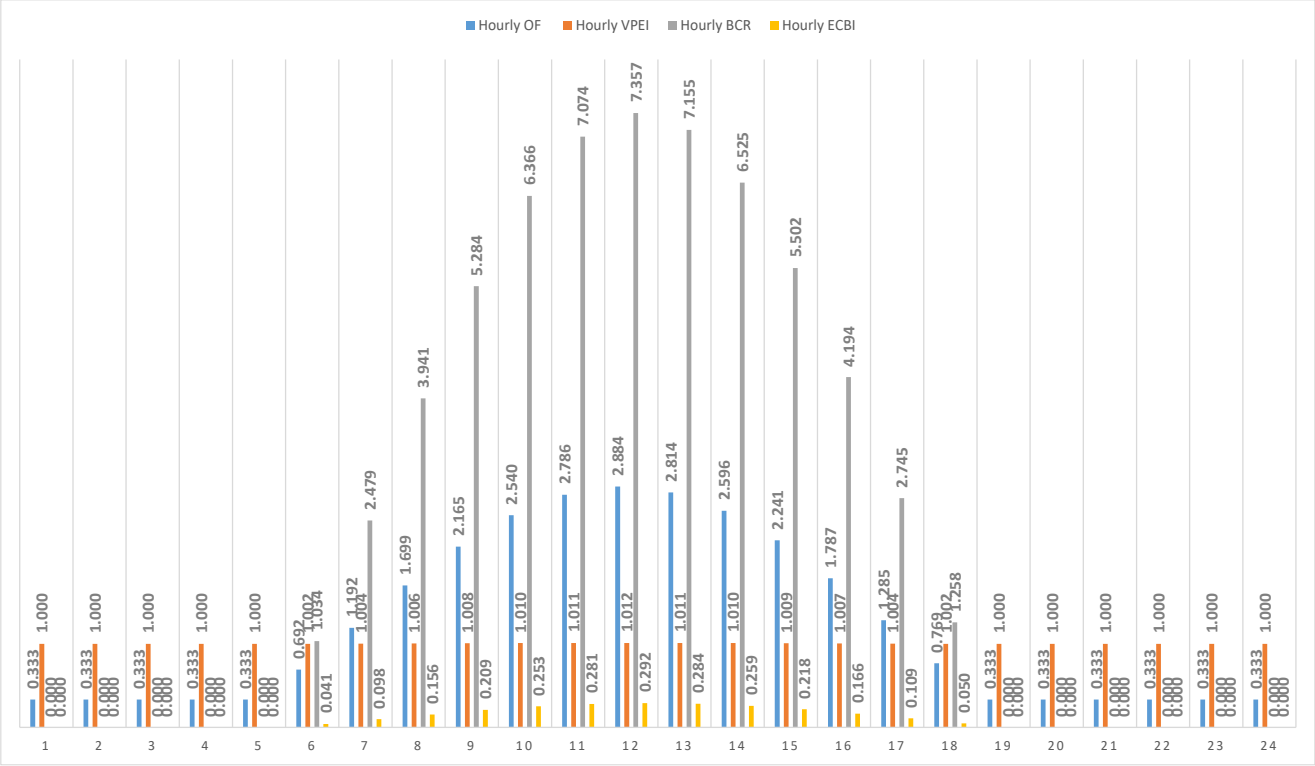

Fig. 5.1.3. Hourly *VPEI*, *BCR*, *ECBI*, and *OF* of the IEEE 33 bus DN after DR implementation for the subcase# 5.1.10 under case study#5.1

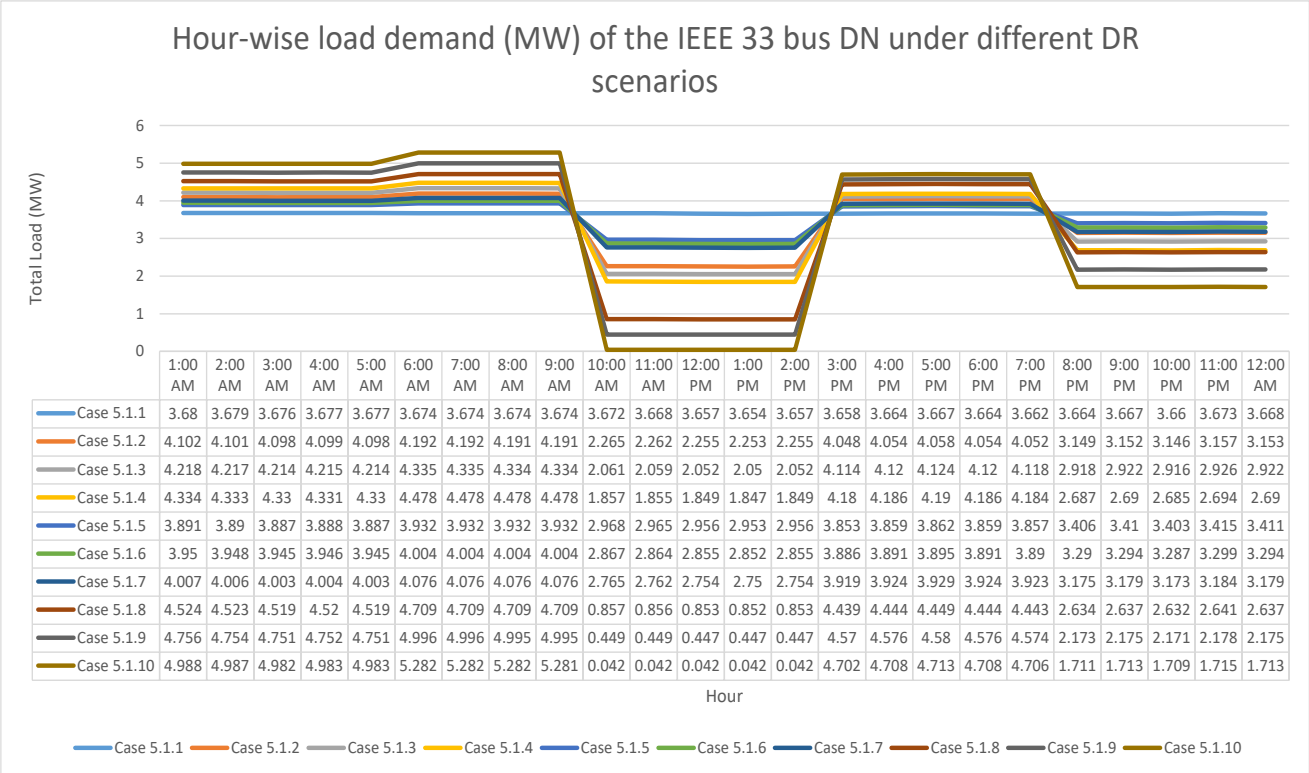

	1:00 AM	2:00 AM	3:00 AM	4:00 AM	5:00 AM	6:00 AM	7:00 AM	8:00 AM	9:00 AM	10:00 AM	11:00 AM	12:00 PM	1:00 PM	2:00 PM	3:00 PM	4:00 PM	5:00 PM	6:00 PM	7:00 PM	8:00 PM	9:00 PM	10:00 PM	11:00 PM	12:00 AM
Case 5.1.1	3.68	3.679	3.676	3.677	3.677	3.674	3.674	3.674	3.674	3.672	3.668	3.657	3.654	3.657	3.658	3.664	3.667	3.664	3.662	3.664	3.667	3.66	3.673	3.668
Case 5.1.2	4.102	4.101	4.098	4.099	4.098	4.192	4.192	4.191	4.191	2.265	2.262	2.255	2.253	2.255	4.048	4.054	4.058	4.054	4.052	3.149	3.152	3.146	3.157	3.153
Case 5.1.3	4.218	4.217	4.214	4.215	4.214	4.335	4.335	4.334	4.334	2.061	2.059	2.052	2.05	2.052	4.114	4.12	4.124	4.12	4.118	2.918	2.922	2.916	2.926	2.922
Case 5.1.4	4.334	4.333	4.33	4.331	4.33	4.478	4.478	4.478	4.478	1.857	1.855	1.849	1.847	1.849	4.18	4.186	4.19	4.186	4.184	2.687	2.69	2.685	2.694	2.69
Case 5.1.5	3.891	3.89	3.887	3.888	3.887	3.932	3.932	3.932	3.932	2.968	2.965	2.956	2.953	2.956	3.853	3.859	3.862	3.859	3.857	3.406	3.41	3.403	3.415	3.411
Case 5.1.6	3.95	3.948	3.945	3.946	3.945	4.004	4.004	4.004	4.004	2.867	2.864	2.855	2.852	2.855	3.886	3.891	3.895	3.891	3.89	3.29	3.294	3.287	3.299	3.294
Case 5.1.7	4.007	4.006	4.003	4.004	4.003	4.076	4.076	4.076	4.076	2.765	2.762	2.754	2.75	2.754	3.919	3.924	3.929	3.924	3.923	3.175	3.179	3.173	3.184	3.179
Case 5.1.8	4.524	4.523	4.519	4.52	4.519	4.709	4.709	4.709	4.709	0.857	0.856	0.853	0.852	0.853	4.439	4.444	4.449	4.444	4.443	2.634	2.637	2.632	2.641	2.637
Case 5.1.9	4.756	4.754	4.751	4.752	4.751	4.996	4.996	4.995	4.995	0.449	0.449	0.447	0.447	0.447	4.57	4.576	4.58	4.576	4.574	2.173	2.175	2.171	2.178	2.175
Case 5.1.10	4.988	4.987	4.982	4.983	4.983	5.282	5.282	5.282	5.281	0.042	0.042	0.042	0.042	0.042	4.702	4.708	4.713	4.708	4.706	1.711	1.713	1.709	1.715	1.713

Fig. 5.1.4. Hour-wise total load demand (MW) of the IEEE 33 bus DN under different DR sub-cases under case study#5.1

Result analysis of IEEE 69 bus DN

Fig. 5.1.5 shows the relative values of *DAVPEI*, *DABCR*, *DAECBI*, and *DAOF* of the IEEE 69 bus DN after DR implementation for the all the subcases (5.1.1 to 5.1.10) under **case study#5.1**. It is derived from the data related to IEEE 69 bus DN presented in **Table 5.1.1** to **Table 5.1.10**.

Subcase #5.1.1 (Base Case of IEEE 69 bus)- This is the case study without implementation of DR program but with PV-based DG integrated for 24 hours. The value of *DAOF* obtained is 1.3242 as per **Table 5.1.1**. The corresponding values of *DAVPEI*, *DABCR*, and *DAECBI* are 1.0192, 2.8588, and 0.0985, respectively. It is evident from **Fig. 5.1.5** that the values of *DAOF* obtained for the nine cases using the Jaya Algorithm are higher than 1.3242. The average active power loss obtained in this case is 211.69 kW, which is 5.49% lower than when no PV-based DG and DR are there. The average value of DG injected, in this case, is 657.54 kW.

Subcase #5.1.4 (IEEE 69 bus)- This is the best sub-case as maximum *DAOF* is achieved of value 1.3369. This is 1.01 times higher than the corresponding base case (Subcase #5.1.1). The values of *DAVPEI*, *DABCR*, and *DAECBI* are 1.0194, 2.8953, and 0.0998, respectively. Their respective improvements with reference to the base-case are 1.0002, 1.013, and 1.013 times. The average value of DG injected and average active power loss, in this case, are 665.93 kW and 211.52 kW, respectively.

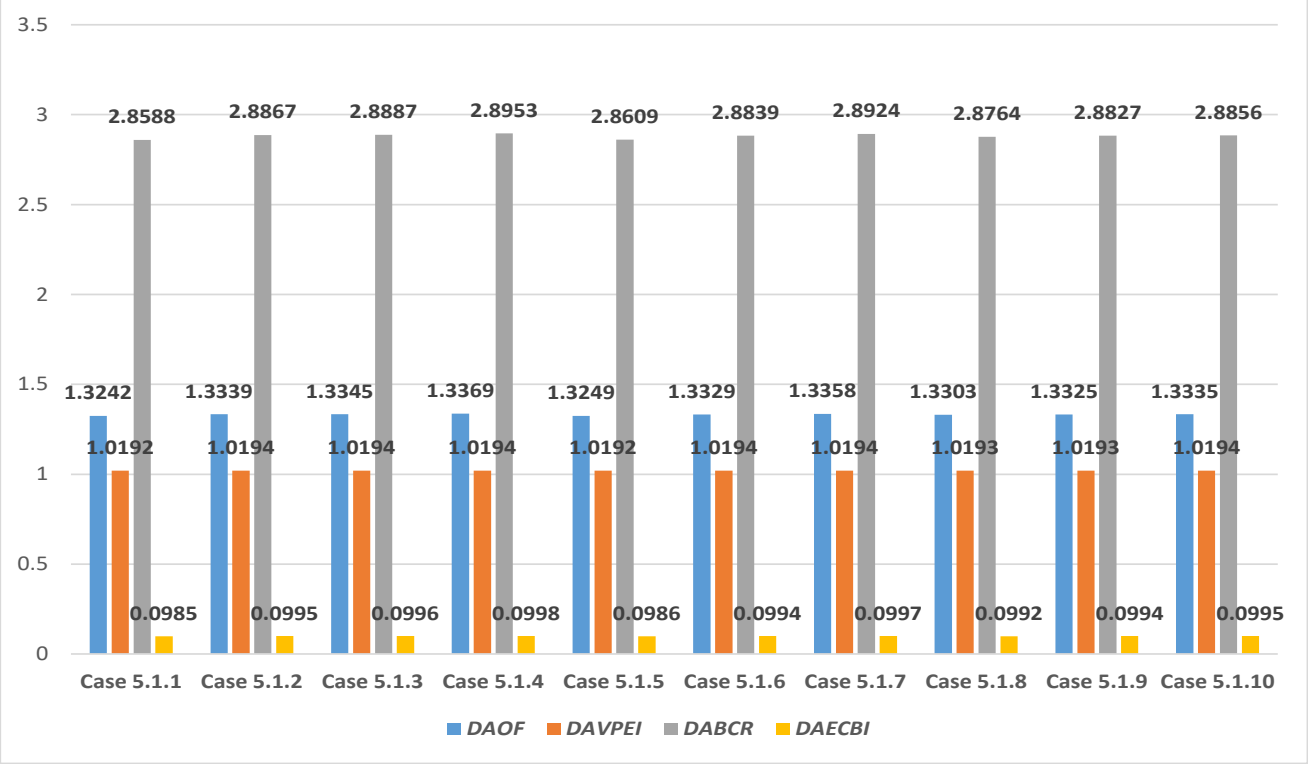

Fig. 5.1.5. *DAVPEI*, *DABCR*, *DAECBI*, and *DAOF* of the IEEE 69 bus DN after DR implementation for the all the subcases (5.1.1 to 5.1.10) under case study#5.1

Hourly analysis of VPEI, BCR, ECBI, and OF (IEEE 69 bus DN)

Fig. 5.1.6 presents the hourly variation of the parameters *VPEI*, *BCR*, *ECBI*, and *OF* of the IEEE 33 bus DN after DR implementation for the **subcase# 5.1.10** under **case study#5.1**. The hourly *OF* is on the higher side (>3) from 11AM to 1PM. The highest *OF* is obtained in the 12^{th} hour of value 3.229 due to maximum availability of solar irradiance. The corresponding hourly values of *VPEI*, *BCR*, and *ECBI* are 1.055, 8.351, and 0.292, respectively. The hourly *OF* is moderate (lies between 1 and 3) during 7AM to 10AM and 2PM to 5PM as the solar irradiance is moderate during these periods. For the rest of the hours, it is low due to low/non-availability of solar irradiance.

Load curtailment and shifting of IEEE 69 bus DN

Fig. 5.1.7 shows the hour-wise total load demand of the IEEE 69 bus DN after all the test cases of DR implementation. It is also observed that consumers are curtailing load demand during the peak load hours (10 AM–2 PM and 8 PM–12 AM). The load curtailment increases with the increase in incentives provided to various customers. The curtailed loads are shifted to the off-peak hours (1AM–9 AM and 3 PM–7 PM) after implementation of the DR program.

The load curtailment and load shift increase with the increase in elasticity and incentive as seen in **Fig. 5.1.7**.

Table 5.1.12 shows hour-wise load curtailment and load shifting at the IEEE 69 bus DN for the **subcase #5.1.4**. It is seen that load curtailment occurs by up to 49.44% during peak load hours. The load shift occurs by up to 21.87% during the light load hours.

Table 5.1.12. Percentage load curtailment and shift during DR at the IEEE 69 bus when provided with the highest incentive (Subcase# 5.1.4)

Hour	1:00 AM	2:00 AM	3:00 AM	4:00 AM	5:00 AM	6:00 AM	7:00 AM	8:00 AM	9:00 AM	10:00 AM	11:00 AM	12:00 PM
% Load change	+ 17.75	+ 17.75	+ 17.76	+ 17.77	+ 17.77	+ 21.87	+ 21.87	+ 21.87	+ 21.87	- 49.44	- 49.44	- 49.43
Hour	1:00 PM	2:00 PM	3:00 PM	4:00 PM	5:00 PM	6:00 PM	7:00 PM	8:00 PM	9:00 PM	10:00 PM	11:00 PM	12:00 AM
% Load change	- 49.44	- 49.44	+ 14.25	+ 14.26	+ 14.26	+ 14.26	+ 14.28	- 26.65	- 26.65	- 26.65	- 26.65	- 26.65

* "-" indicates load curtailment and "+" indicates load shift

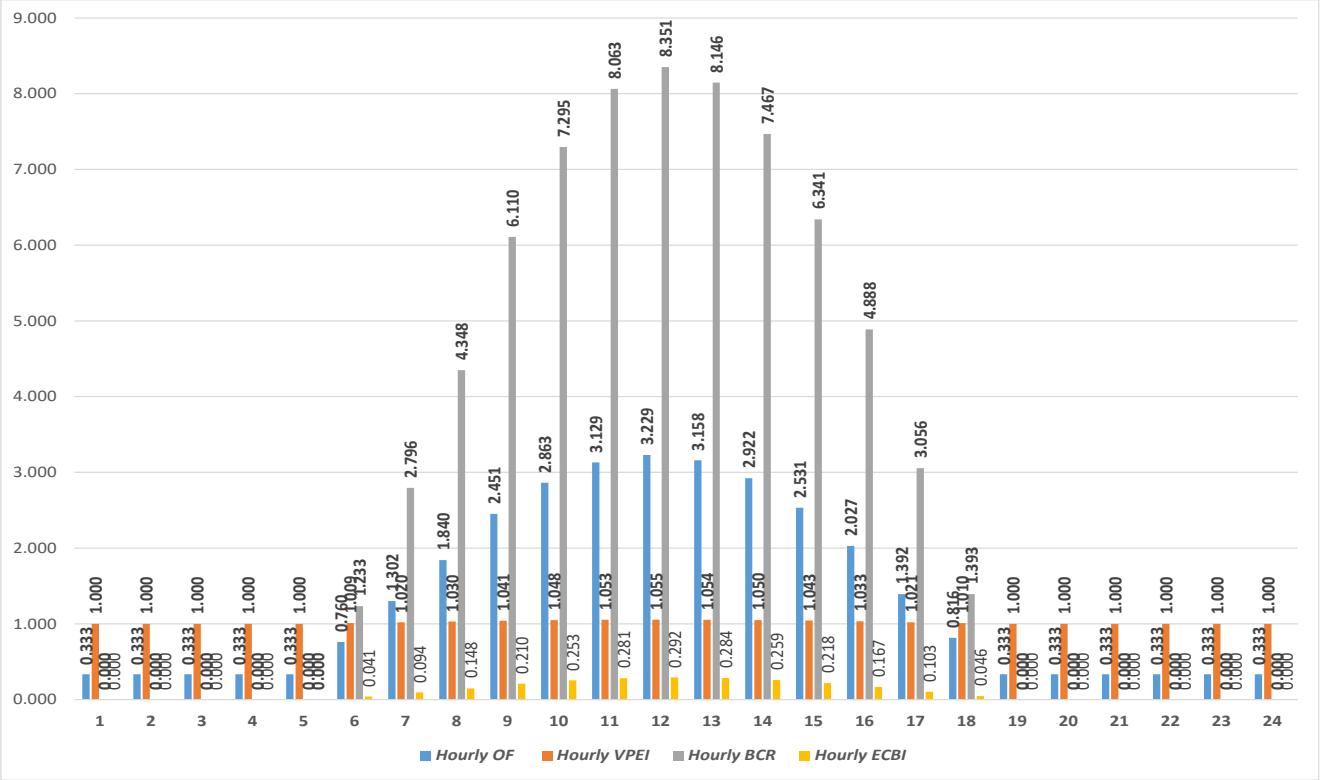

Fig. 5.1.6. Hourly *VPEI*, *BCR*, *ECBI*, and *OF* of the IEEE 69 bus DN after DR implementation for the subcase# 5.1.10 under case study#5.1

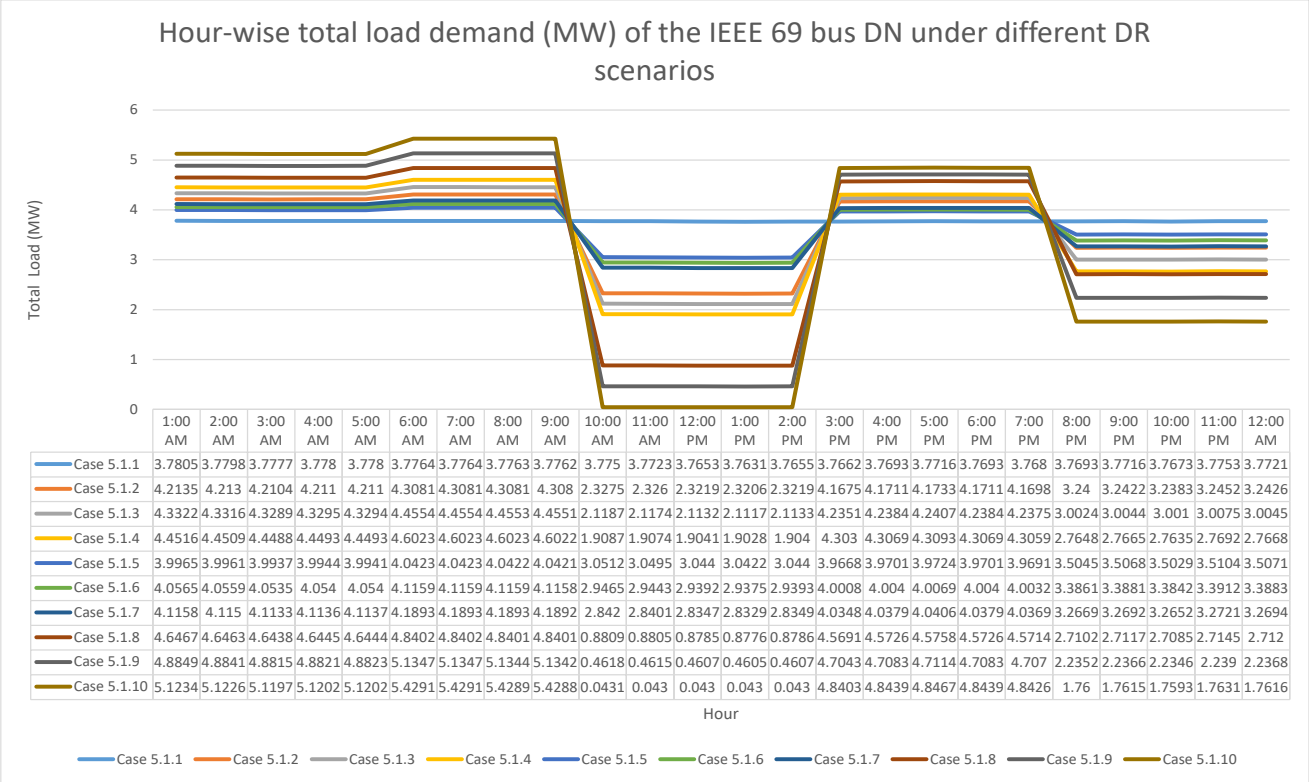

	1:00 AM	2:00 AM	3:00 AM	4:00 AM	5:00 AM	6:00 AM	7:00 AM	8:00 AM	9:00 AM	10:00 AM	11:00 AM	12:00 PM	1:00 PM	2:00 PM	3:00 PM	4:00 PM	5:00 PM	6:00 PM	7:00 PM	8:00 PM	9:00 PM	10:00 PM	11:00 PM	12:00 AM
Case 5.1.1	3.7805	3.7798	3.7777	3.778	3.778	3.7764	3.7764	3.7763	3.7762	3.775	3.7723	3.7653	3.7631	3.7655	3.7662	3.7693	3.7716	3.7693	3.768	3.7693	3.7716	3.7673	3.7753	3.7721
Case 5.1.2	4.2135	4.213	4.2104	4.211	4.211	4.3081	4.3081	4.3081	4.308	2.3275	2.326	2.3219	2.3206	2.3219	4.1675	4.1711	4.1733	4.1711	4.1698	3.24	3.2422	3.2383	3.2452	3.2426
Case 5.1.3	4.3322	4.3316	4.3289	4.3295	4.3294	4.4554	4.4554	4.4553	4.4551	2.1187	2.1174	2.1132	2.1117	2.1133	4.2351	4.2384	4.2407	4.2384	4.2375	3.0024	3.0044	3.001	3.0075	3.0045
Case 5.1.4	4.4516	4.4509	4.4488	4.4493	4.4493	4.6023	4.6023	4.6023	4.6022	1.9087	1.9074	1.9041	1.9028	1.904	4.303	4.3069	4.3093	4.3069	4.3059	2.7648	2.7665	2.7635	2.7692	2.7668
Case 5.1.5	3.9965	3.9961	3.9937	3.9944	3.9941	4.0423	4.0423	4.0422	4.0421	3.0512	3.0495	3.044	3.0422	3.044	3.9668	3.9701	3.9724	3.9701	3.9691	3.5045	3.5068	3.5029	3.5104	3.5071
Case 5.1.6	4.0565	4.0559	4.0535	4.054	4.054	4.1159	4.1159	4.1159	4.1158	2.9465	2.9443	2.9392	2.9375	2.9393	4.0008	4.004	4.0069	4.004	4.0032	3.3861	3.3881	3.3842	3.3912	3.3883
Case 5.1.7	4.1158	4.115	4.1133	4.1136	4.1137	4.1893	4.1893	4.1893	4.1892	2.842	2.8401	2.8347	2.8329	2.8349	4.0348	4.0379	4.0406	4.0379	4.0369	3.2669	3.2692	3.2652	3.2721	3.2694
Case 5.1.8	4.6467	4.6463	4.6438	4.6445	4.6444	4.8402	4.8402	4.8401	4.8401	0.8809	0.8805	0.8785	0.8776	0.8786	4.5691	4.5726	4.5758	4.5726	4.5714	2.7102	2.7117	2.7085	2.7145	2.712
Case 5.1.9	4.8849	4.8841	4.8815	4.8821	4.8823	5.1347	5.1347	5.1344	5.1342	0.4618	0.4615	0.4607	0.4605	0.4607	4.7043	4.7083	4.7114	4.7083	4.707	2.2352	2.2366	2.2346	2.239	2.2368
Case 5.1.10	5.1234	5.1226	5.1197	5.1202	5.1202	5.4291	5.4291	5.4289	5.4288	0.0431	0.043	0.043	0.043	0.043	4.8403	4.8439	4.8467	4.8439	4.8426	1.76	1.7615	1.7593	1.7631	1.7616

Fig. 5.1.7. Hour-wise total load demand (MW) of the IEEE 69 bus DN under different DR sub-cases under case study#5.1

5.15. Statistical analysis of the performance of algorithms in comparison for *Subcase #5.1.10*

A comparative performance analysis of the algorithms is performed for one sub-case study presented under sub-section **5.14.1.10** as an example. The **subcase #5.1.10** of the IEEE 33 bus DN is considered for the analysis.

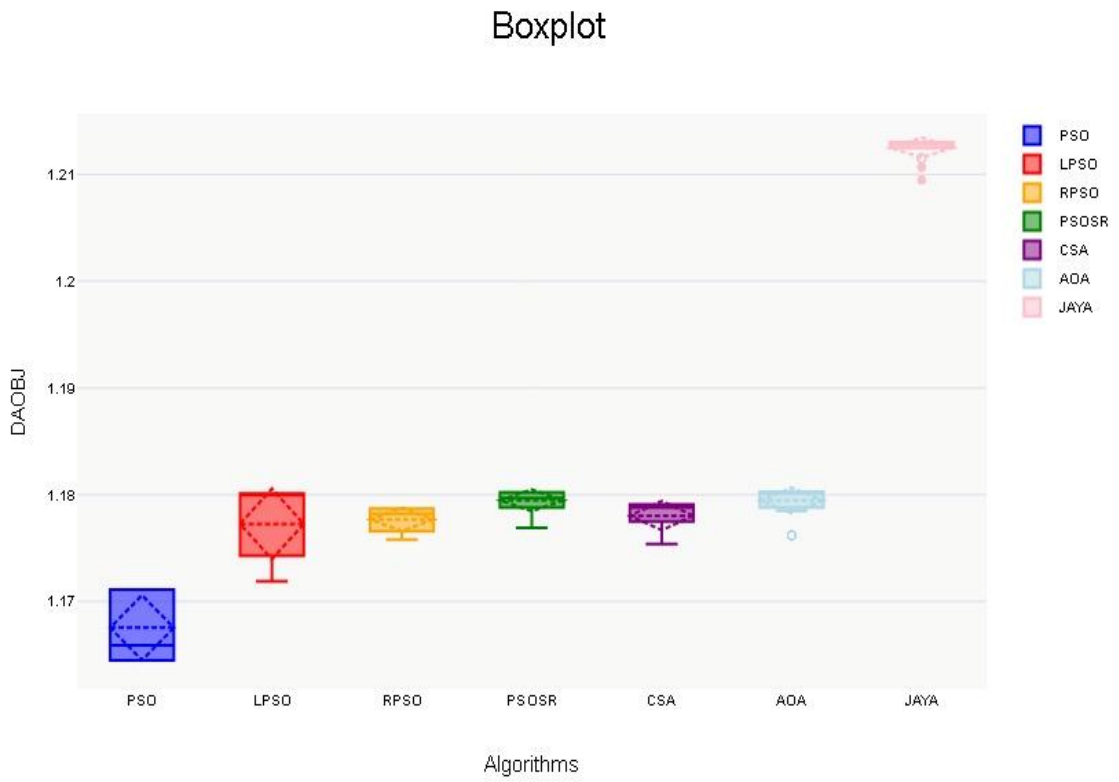

Fig. 5.1.8. Relative box plots of the *OF* obtained by the algorithms for the sub-test case # 5.1.10 of IEEE 33 bus under Case Study #5.1

The algorithms in comparison are PSO, LPSO, RPSO, PSO-SR, CSA, AOA, and Jaya. Each algorithm is run for 50 trials.

From the box-plot, as shown in **Fig. 5.1.8**, it is evident that the 1st and 3rd quartiles of the Jaya plot are significantly greater than those of PSO, LPSO, RPSO, PSOSR, CSA, and AOA. The relative maximum, minimum, mean, and standard deviation values of the *OF* using Jaya and other comparing algorithms are shown in **Table 5.1.13** and **Fig. 5.1.9.** The mean difference plot (**Fig. 5.1.10**) reveals the Jaya algorithm's superiority over the comparing algorithms in terms of the *OF*.

Table. 5.1.13 displays the results of the Shapiro-Wilk and Kolmogorov-Smirnov normality tests, including the p-values for various scenarios and it can be concluded that the data did not come from a normal distribution.

The results of Kruskal-Wallis-H-ANOVA and post-hoc Dunn tests are shown in **Table 5.1.13** and **Table 5.1.14**, respectively. Using the Kruskal-Wallis-H analysis of variance (ANOVA) test, a comparative ranking of all the algorithms is produced. The test statistic H is 260.14, which is outside the 95% confidence interval. The Kruskal-Wallis-H test indicated that there is a significant difference in the dependent variable between the different groups ($\chi^2(6) = 260.14$, $p < .001$) with a mean rank score of 25.5 for PSO, 158.38 for LPSO, 125.46 for RPSO, 216.08 for PSOSR, 148.22 for CSA, 229.36 for AOA, and 325.5 for JAYA.

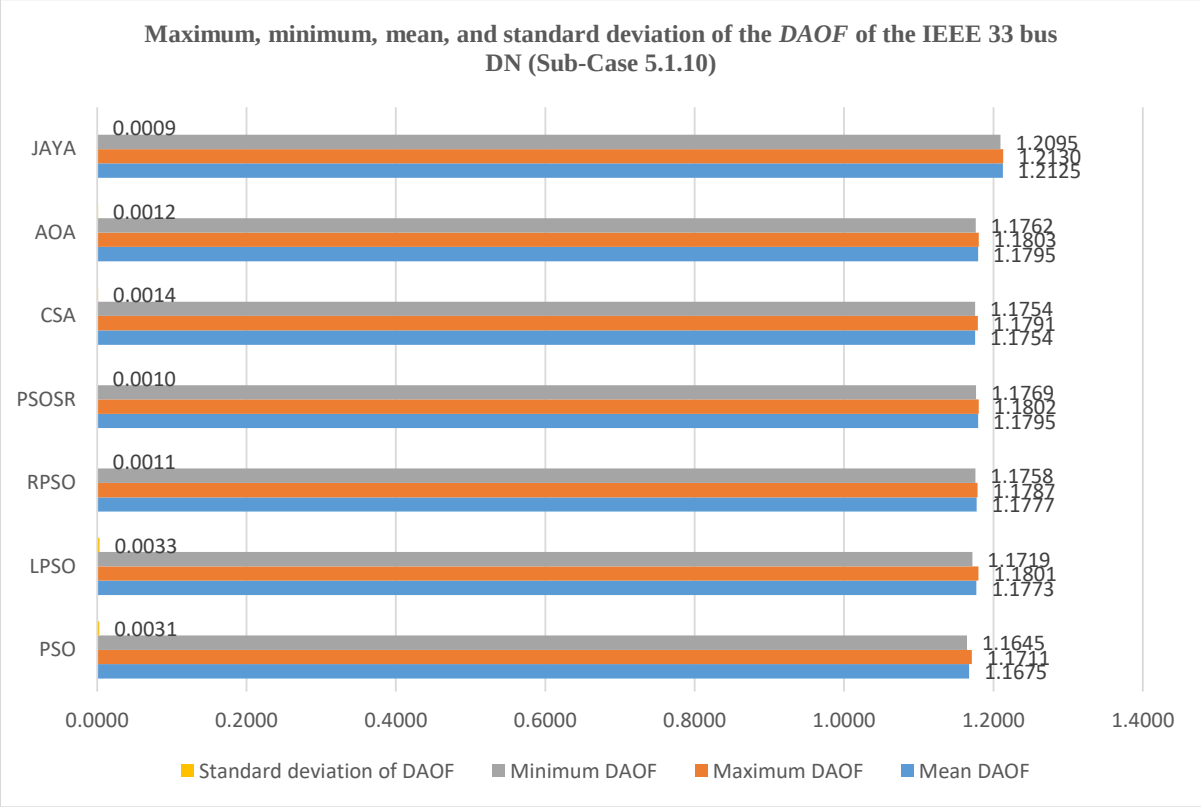

Fig. 5.1.9. Relative values of maximum, minimum, mean, and standard deviation of the *OF* obtained by the algorithms in comparison for the sub-test case # 5.1.10 of IEEE 33 bus under Case Study #5.1

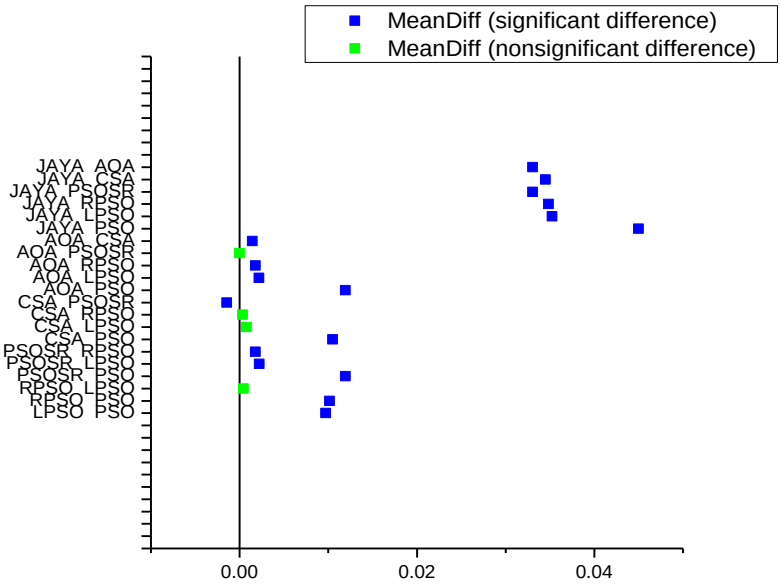

Fig. 5.1.10. Mean difference plot of the *OF* obtained by different algorithm pairs for the sub-test case # 5.1.10 of IEEE 33 bus under Case Study #5.1

Table 5.1.13 Statistical results for the sub-test case # 5.1.10 of IEEE 33 bus under Case Study #5.1

Algorithms	**PSO**	**LPSO**	**RPSO**	**PSO-SR**	**CSA**	**AOA**	**JAYA**
Minimum *DAOF*	1.1645	1.1719	1.1758	1.1769	1.1754	1.1762	1.2120
Maximum *DAOF*	1.1711	1.1801	1.1787	1.1802	1.1791	1.1803	1.2130
Mean *DAOF*	1.1675	1.1773	1.1777	1.1795	1.1754	1.1795	1.2095
Standard Deviation *DAOF*	0.0031	0.0033	0.0011	0.0010	0.0014	0.0012	0.0009
p-value* (Shapiro-Wilk test for normality) α=0.5	6.948e-9	1.498e-8	3.283e-7	1.212e-8	1.968e-8	8.074e-9	9.11e-11
p-value* (Kolmogorov–Smirnov test for normality) α=0.5	1.612e-9	0	5.859e-11	1.863e-8	4.117e-7	6.639e-14	0
Mean Rank (Kruskal-Wallis non-parametric test) α=0.5^{++}	25.50	158.38	125.46	216.08	148.22	229.36	325.50

Table 5.1.14 Parametric comparison of algorithm pairs by post-hoc Dunn test for the sub-test case # 5.1.10 of IEEE 33 bus under Case Study #5.1						
Pair	**Mean Rank difference**	**Z**	**Standard Error difference**	**Critical value**	**p-value**	**p-value/2**
PSO-LPSO	-132.88	6.5773			4.789e-11	2.395e-11
PSO -RPSO	-99.96	4.9479			7.504e-7	3.752e-7
PSO -PSOSR	-190.58	9.4334			0	0
PSO -CSA	-122.72	6.0744			1.244e-9	6.221e-10
PSO -AOA	-203.86	10.0907			0	0
PSO -JAYA	-300	14.8495			0	0
LPSO - RPSO	32.92	1.6295			0.1032	0.05161
LPSO - PSOSR	-57.7	2.8561			0.004289	0.002145
LPSO - CSA	10.16	0.5029			0.615	0.3075
LPSO - AOA	-70.98	3.5134			0.0004424	0.0002212
LPSO - JAYA	-167.12	8.2722	20.2027	61.228	0	0
RPSO - PSOSR	-90.62	4.4855			0.000007273	0.000003636
RPSO - CSA	-22.76	1.1266			0.2599	0.13
RPSO - AOA	-103.9	5.1429			2.706e-7	1.353e-7
RPSO - JAYA	-200.04	9.9016			0	0
PSOSR - CSA	67.86	3.359			0.0007824	0.0003912
PSOSR - AOA	-13.28	0.6573			0.511	0.2555
PSOSR - JAYA	-109.42	5.4161			6.091e-8	3.046e-8
CSA - AOA	-81.14	4.0163			0.00005912	0.00002956
CSA - JAYA	-177.28	8.7751			0	0
AOA - JAYA	-96.14	4.7588			0.000001948	9.739e-7

5.16. Summary

This section presents the salient observations regarding the effectiveness of PV and wind based DGs on the technical, economic, and environmental benefits of the DN. These are presented under each case study as follows:

Case Study #5.1: *Implementation of price-elasticity based DR with fixed-incentive at PV integrated IEEE 33 and 69 bus DNs*

For all the ten test sub-cases, improvements in the technical, economic, and environmental benefits are observed individually, resulting in an improvement in the overall hourly and daily average objectives. Considering each group of elasticity, there is an improvement in *DAOBJ* with an increase in incentive. The load curtailment and shift occur effectively during the peak and light load hours, respectively. With the increase in demand-load elasticity and incentives provided to the DR participants, the load-curtailment and shift occurs effectively. For all the test cases, the Jaya algorithm produced the highest *DAOBJ* concerning the algorithms under comparison. This is because the Jaya algorithm can explore and exploit the entire search space to yield better global-optimal results. It yielded the highest mean and minimum standard deviation values of the *DAOBJ* among all the algorithms under comparison, thus producing relatively more consistent results. This shows that the Jaya algorithm is the most consistent and robust among all the algorithms under study. The optimal number of PV modules required for DG installation is determined based on the availability of hourly solar irradiance based on geographical modelling and seasonal variations.

CHAPTER 6: Conclusion, Limitations & Future Scope

This chapter presents the salient observations made from the thesis regarding the effectiveness of PV, wind, BESS, EVs, and DR program in enhancing the technical, economic, and environmental benefits of the DNs. The crux of the work, it's limitations, and future scope are presented for each chapter in details.

6.1 Conclusion

DG integration with DNs

This chapter investigated the impact of PV and wind-based DG on radial DNs. Different test cases of single, twin, and triple points of DG injections are considered with deterministic and probabilistic approaches. The optimal capacities and sizes of DG are found out using different algorithms, namely, PSO, LPSO, RPSO, PSO-SR, CSA, and Jaya. It is seen that for all the test cases, the DNs under study showed improvements in technical, economic, and environmental indices. The active power losses of the DNs got reduced for all the test cases considered. All DNs under consideration showed improvements in *VSI* characteristics after DG injection depending upon its capacity and location.

DG, BESS, and SVC integration with DNs

This chapter investigated the technical, economic, and environmental impacts of BESS and SVC on DG integrated radial DNs. Different test cases of single, twin, and triple points of DG injections are considered with deterministic and probabilistic approaches. In a few test cases, the uncertain nature of load is considered.

All the test cases considering different combinations PV, wind, and BESS integration at the DNs under consideration showed overall improvements in *OF* along with individual improvements in the *VPEI*, *BCR*, and *ECBI*. The active power losses of the DNs got reduced for all the test cases considered. All DNs under study showed considerable improvements in the *VSI* characteristics after DG and BESS injection depending upon its capacity and location.

The real-time 13 bus DN substation situated at Maharashtra, India showed technical, economic, and environmental improvements when integrated with different combinations of wind, PV, SVC, and BESS powers along with improvement in its *VSI* characteristics. So, the proposed plan for improving the technical, economic, and environmental benefits of a DN can be

implemented in practice. But the level of improvement of the overall objective depends on the nearby facilities available, weather conditions, and geographical location of the DN.

EV integration with DNs

An in-depth analysis has been conducted, considering a variety of test cases from the IEEE 85 and 141 bus DNs. Various degrees of EV penetration have been taken into consideration while analyzing the relative technical, economic, and environmental effects.

The outcomes of EV integration demonstrate that when EV power is injected into the grid, networks continuously benefit technically, economically, and environmentally. Following the implementation of a charge-discharge method and the appropriate arrangement of EV charging stations, the *VSI* of the majority of the buses in both test systems under consideration improved. When the net power transferred from the EVs is positive, the EV charging station functions as a power source, reducing the active power losses of the networks.

Implementation of price-elasticity based DR program with DNs

Improvements in the technical, economic, and environmental benefits can be observed separately for each case study, which leads to an improvement in the overall hourly and daily average objectives following the implementation of the DR program. Effective load shift and curtailment take place during peak and light load hours, respectively. They increase with the DR participants' incentives and demand-load elasticity. In compared to the other algorithms, the Jaya algorithm produced the highest *DAOBJ* for every test instance. Out of all the algorithms evaluated, the Jaya algorithm yielded the highest mean and lowest standard deviation values of *DAOBJ*. The availability of hourly solar irradiance, which is based on seasonal changes and geographic modeling, determines the ideal amount of PV modules needed for DG installation.

Performance of Jaya Algorithm

The statistical analysis's findings demonstrate the Jaya algorithm's superiority, consistency, and robustness when compared to all other algorithms. In contrast to the other methods, the Jaya algorithm also requires fewer iterations to converge. It also showed a low computation complexity because it is very simple and doesn't require any control parameters to be changed.

To achieve better global optimality, the Jaya algorithm investigates and utilizes the entire search space.

It is clear from the box-whiskers and mean plots of many case studies that the Jaya algorithm consistently and reliably delivered the maximum mean solution with the lowest standard deviation. The Jaya algorithm is the most efficient of all, as indicated by the convergence characteristics, since it often required less iterations to converge. The Jaya algorithm is better and more reliable than the comparing algorithms, as shown by the post-hoc Dunn tests that follow the Kruskal-Wallis H test.

6.2 Limitations & Future Scope

This part of the work, however, has some limitations, such as the inability to account for BESS/EV battery charging discharging times, uncertain nature of BESS, uncertain EV traffic, load growth throughout the entire planning period. It has been assumed that the EV charging station is entirely occupied, yet this may not always be the case. An EV may be idle rather than connected in charging or discharging mode.

The integration of Machine Learning (ML) models for predicting solar irradiance, wind-speed, and load demands will lead to more accurate estimation of DG installed capacities. The intermittent nature of DGs can be further reduced by using higher capacity BESS which in turn will improve the technical, economic, and environmental benefits of the DNs. The DN benefits can be further improved by integrating multiple EV charging stations having larger parking capacities. Using faster charging power electronic converters, the network indices may be further enhanced by incorporating newer and effective DR models. The joint impacts of DG, BESS, EV, and DR programs on DN parameters are being explored in order to make the system more real-time and futuristic.

References

[1] Khasanov M, Kamel S, Halim Houssein E, Rahmann C, Hashim FA. Optimal allocation strategy of photovoltaic-and wind turbine-based distributed generation units in radial distribution networks considering uncertainty. Neural Computing and Applications. 2023 Jan;35(3):2883-908. https://doi.org/10.1007/s00521-022-07715-2

[2] javad Aliabadi M, Radmehr M. Optimization of hybrid renewable energy system in radial distribution networks considering uncertainty using meta-heuristic crow search algorithm. Applied Soft Computing. 2021 Aug 1;107:107384. https://doi.org/10.1016/j.asoc.2021.107384

[3] Home-Ortiz JM, Pourakbari-Kasmaei M, Lehtonen M, Mantovani JR. Optimal location-allocation of storage devices and renewable-based DG in distribution systems. Electric Power Systems Research. 2019 Jul 1;172:11-21. https://doi.org/10.1016/j.epsr.2019.02.013

[4] Fathi R, Tousi B, Galvani S. A new approach for optimal allocation of photovoltaic and wind clean energy resources in distribution networks with reconfiguration considering uncertainty based on info-gap decision theory with risk aversion strategy. Journal of Cleaner Production. 2021 May 1;295:125984. https://doi.org/10.1016/j.jclepro.2021.125984

[5] Ali ES, El-Sehiemy RA, Abou El-Ela AA, Mahmoud K, Lehtonen M, Darwish MM. An effective Bi-stage method for renewable energy sources integration into unbalanced distribution systems considering uncertainty. Processes. 2021 Mar 6;9(3):471. https://doi.org/10.3390/pr9030471

[6] Gangwar T, Padhy NP, Jena P. Storage allocation in active distribution networks considering life cycle and uncertainty. IEEE Transactions on Industrial Informatics. 2022 Apr 14;19(1):339-50. https://doi.org/10.1109/TII.2022.3167382

[7] Ramadan A, Ebeed M, Kamel S, Nasrat L. Optimal power flow for distribution systems with uncertainty. InUncertainties in modern power systems 2021 Jan 1 (pp. 145-162). Academic Press. https://doi.org/10.1016/B978-0-12-820491-7.00005-0

[8] Boroumandfar G, Khajehzadeh A, Eslami M, Syah RB. Information gap decision theory with risk aversion strategy for robust planning of hybrid photovoltaic/wind/battery storage system in distribution networks considering uncertainty. Energy. 2023 Sep 1;278:127778. https://doi.org/10.1016/j.energy.2023.127778

[9] Abdel-Mawgoud H, Kamel S, Khasanov M, Khurshaid T. A strategy for PV and BESS allocation considering uncertainty based on a modified Henry gas solubility optimizer. Electric Power Systems Research. 2021 Feb 1;191:106886. https://doi.org/10.1016/j.epsr.2020.106886

[10] Rawat MS, Vadhera S. Probabilistic approach to determine penetration of hybrid renewable DGs in distribution network based on voltage stability index. Arabian Journal for Science and Engineering. 2020 Mar;45(3):1473-98. https://doi.org/10.1007/s13369-019-04023-1

[11] Elkadeem MR, Abd Elaziz M, Ullah Z, Wang S, Sharshir SW. Optimal planning of renewable energy-integrated distribution system considering uncertainties. IEEE Access. 2019 Oct 14;7:164887-907. https://doi.org/10.1109/ACCESS.2019.2947308

[12] Rathore A, Patidar NP. Optimal sizing and allocation of renewable based distribution generation with gravity energy storage considering stochastic nature using particle swarm optimization in radial

distribution network. Journal of Energy Storage. 2021 Mar 1;35:102282. https://doi.org/10.1016/j.est.2021.102282

[13] Samala RK, Kotapuri MR. Optimal allocation of distributed generations using hybrid technique with fuzzy logic controller radial distribution system. SN Applied Sciences. 2020 Feb;2(2):191. https://doi.org/10.1007/s42452-020-1957-3

[14] Ahmadi SE, Kazemi-Razi SM, Marzband M, Ikpehai A, Abusorrah A. Multi-objective stochastic techno-economic-environmental optimization of distribution networks with G2V and V2G systems. Electric Power Systems Research. 2023 May 1;218:109195. https://doi.org/10.1016/j.epsr.2023.109195

[15] Naderipour A, Nowdeh SA, Saftjani PB, Abdul-Malek Z, Mustafa MW, Kamyab H, Davoudkhani IF. Deterministic and probabilistic multi-objective placement and sizing of wind renewable energy sources using improved spotted hyena optimizer. Journal of Cleaner Production. 2021 Mar 1;286:124941. https://doi.org/10.1016/j.jclepro.2020.124941

[16] Yamchi HB, Shahsavari H, Kalantari NT, Safari A, Farrokhifar M. A cost-efficient application of different battery energy storage technologies in microgrids considering load uncertainty. Journal of Energy Storage. 2019 Apr 1;22:17-26. https://doi.org/10.1016/j.est.2019.01.023

[17] Nematollahi AF, Shahinzadeh H, Nafisi H, Vahidi B, Amirat Y, Benbouzid M. Sizing and sitting of DERs in active distribution networks incorporating load prevailing uncertainties using probabilistic approaches. Applied Sciences. 2021 May 1;11(9):4156. https://doi.org/10.3390/app11094156

[18] Abid MS, Apon HJ, Morshed KA, Ahmed A. Optimal planning of multiple renewable energy-integrated distribution system with uncertainties using artificial hummingbird algorithm. IEEE Access. 2022 Apr 14;10:40716-30. https://doi.org/10.1109/ACCESS.2022.3167395

[19] Xu T, Ren Y, Guo L, Wang X, Liang L, Wu Y. Multi-objective robust optimization of active distribution networks considering uncertainties of photovoltaic. International Journal of Electrical Power & Energy Systems. 2021 Dec 1;133:107197. https://doi.org/10.1016/j.ijepes.2021.107197

[20] Ullah Z, Elkadeem MR, Wang S, Sharshir SW, Azam M. Planning optimization and stochastic analysis of RE-DGs for techno-economic benefit maximization in distribution networks. Internet of Things. 2020 Sep 1;11:100210. https://doi.org/10.1016/j.iot.2020.100210

[21] Wang W, Xu J, Zhang G, Yang M, Xu X, Armghan H. A novel chance constrained joint optimization method under uncertainties in distribution networks. International Journal of Electrical Power & Energy Systems. 2023 May 1;147:108849. https://doi.org/10.1016/j.ijepes.2022.108849

[22] Davoudkhani IF, Zishan F, Mansouri S, Abdollahpour F, Grisales-Noreña LF, Montoya OD. Allocation of renewable energy resources in distribution systems while considering the uncertainty of wind and solar resources via the multi-objective Salp Swarm algorithm. Energies. 2023 Jan 1;16(1):474. https://doi.org/10.3390/en16010474

[23] Pakdel D, Ramezani M. Enhancement of distribution network performance in the presence of uncertain parameters. IET Renewable Power Generation. 2020 Mar;14(4):515-25. https://doi.org/10.1049/iet-rpg.2019.0475

[24] Sharma S, Niazi KR, Verma K, Rawat T. Coordination of different DGs, BESS and demand response for multi-objective optimization of distribution network with special reference to Indian power sector.

International Journal of Electrical Power & Energy Systems. 2020 Oct 1;121:106074. https://doi.org/10.1016/j.ijepes.2020.106074

[25] Maity S, Paul S, Karbouj H, Rather ZH. Optimal sizing and placement of wind farm in a radial distribution network considering reliability, operational, economic and environmental factors. IEEE Transactions on Power Delivery. 2020 Oct 20;36(5):3043-54. https://doi.org/10.1109/TPWRD.2020.3032370

[26] Pandraju TK, Janamala V. An Enhanced Pathfinder Algorithm for Optimal Integration of Solar Photovoltaics and Rapid Charging Stations in Low-Voltage Radial Feeders. Journal of Solar Energy Research. 2023 Oct 1;8(4):1680-90. https://doi.org/10.22059/jser.2023.359041.1300

[27] Sreenivasulu Reddy D, Janamala V. Optimal allocation of renewable sources with battery and capacitors in radial feeders for reliable power supply using pathfinder algorithm. Journal of Solar Energy Research. 2023 Oct 1;8(4):1651-62. https://doi.org/10.22059/jser.2023.358718.1299

[28] Janamala V, Radha Rani K, Sobha Rani P, Venkateswarlu AN, Inkollu SR. Optimal switching operations of soft open points in active distribution network for handling variable penetration of photovoltaic and electric vehicles using artificial rabbits optimization. Process Integration and Optimization for Sustainability. 2023 Mar;7(1):419-37. https://doi.org/10.1007/s41660-022-00304-9

[29] Giridhar MS, Rani KR, Rani PS, Janamala V. Mayfly Algorithm for Optimal Integration of Hybrid Photovoltaic/Battery Energy Storage/D-STATCOM System for Islanding Operation. International Journal of Intelligent Engineering & Systems. 2022 May 1;15(3). https://inass.org/wp-content/uploads/2021/12/2022063019-2.pdf

[30] Janamala V, Radha Rani K. Optimal allocation of solar photovoltaic distributed generation in electrical distribution networks using Archimedes optimization algorithm. Clean Energy. 2022 Apr 1;6(2):271-87. https://doi.org/10.1093/ce/zkac010

[31] Janamala V, Reddy DS. Coyote optimization algorithm for optimal allocation of interline–Photovoltaic battery storage system in islanded electrical distribution network considering EV load penetration. Journal of Energy Storage. 2021 Sep 1;41:102981. https://doi.org/10.1016/j.est.2021.102981

[32] Janamala V, Kamal Kumar U, Pandraju TK. Future search algorithm for optimal integration of distributed generation and electric vehicle fleets in radial distribution networks considering techno-environmental aspects. SN Applied Sciences. 2021 Apr;3(4):464. https://doi.org/10.1007/s42452-021-04466-y

[33] Janamala V. A new meta-heuristic pathfinder algorithm for solving optimal allocation of solar photovoltaic system in multi-lateral distribution system for improving resilience. SN applied sciences. 2021 Jan;3(1):118. https://doi.org/10.1007/s42452-020-04044-8

[34] Gao H, Li Y, He S, Tang Z, Liu J. Distributionally robust planning for power distribution network considering multi-energy station enabled integrated demand response. Energy. 2024 Oct 15;306:132460. https://doi.org/10.1016/j.energy.2024.132460

[35] Dey B, Misra S, Marquez FP. Microgrid system energy management with demand response program for clean and economical operation. Applied Energy. 2023 Mar 15;334:120717. https://doi.org/10.1016/j.apenergy.2023.120717

[36] Yousri D, Farag HE, Zeineldin H, El-Saadany EF. Integrated model for optimal energy management and demand response of microgrids considering hybrid hydrogen-battery storage systems. Energy Conversion and Management. 2023 Mar 15;280:116809. https://doi.org/10.1016/j.apenergy.2023.120717

[37] Dixit S, Singh P, Ogale J, Bansal P, Sawle Y. Energy management in microgrids with renewable energy sources and demand response. Computers and Electrical Engineering. 2023 Sep 1;110:108848. https://doi.org/10.1016/j.compeleceng.2023.108848

[38] Zhang G, Ge Y, Ye Z, Al-Bahrani M. Multi-objective planning of energy hub on economic aspects and resources with heat and power sources, energizable, electric vehicle and hydrogen storage system due to uncertainties and demand response. Journal of Energy Storage. 2023 Jan 1;57:106160. https://doi.org/10.1016/j.est.2022.106160

[39] Liu D, Qin Z, Hua H, Ding Y, Cao J. Incremental incentive mechanism design for diversified consumers in demand response. Applied Energy. 2023 Jan 1;329:120240. https://doi.org/10.1016/j.apenergy.2022.120240

[40] Alikhani M, Moghaddam MP, Moazzen F, Azadi A. Optimal implementation of consumer demand response program with consideration of uncertain generation in a microgrid. Electric Power Systems Research. 2023 Dec 1;225:109859. https://doi.org/10.1016/j.epsr.2023.109859

[41] Li Y, Li K, Yang Z, Yu Y, Xu R, Yang M. Stochastic optimal scheduling of demand response-enabled microgrids with renewable generations: An analytical-heuristic approach. Journal of Cleaner Production. 2022 Jan 1;330:129840. https://doi.org/10.1016/j.jclepro.2021.129840

[42] Amin A, Kem O, Gallegos P, Chervet P, Ksontini F, Mourshed M. Demand response in buildings: Unlocking energy flexibility through district-level electro-thermal simulation. Applied Energy. 2022 Jan 1;305:117836. https://doi.org/10.1016/j.apenergy.2021.117836

[43] Tan H, Yan W, Ren Z, Wang Q, Mohamed MA. A robust dispatch model for integrated electricity and heat networks considering price-based integrated demand response. Energy. 2022 Jan 15;239:121875. https://doi.org/10.1016/j.energy.2021.121875

[44] Shen Y, Hu W, Liu M, Yang F, Kong X. Energy storage optimization method for microgrid considering multi-energy coupling demand response. Journal of Energy Storage. 2022 Jan 1;45:103521. https://doi.org/10.1016/j.est.2021.103521

[45] Eghbali N, Hakimi SM, Hasankhani A, Derakhshan G, Abdi B. Stochastic energy management for a renewable energy based microgrid considering battery, hydrogen storage, and demand response. Sustainable Energy, Grids and Networks. 2022 Jun 1;30:100652. https://doi.org/10.1016/j.segan.2022.100652

[46] Lu Q, Zhang Y. A multi-objective optimization model considering users' satisfaction and multi-type demand response in dynamic electricity price. Energy. 2022 Feb 1;240:122504. https://doi.org/10.1016/j.energy.2021.122504

[47] Prajapati VK, Mahajan V. Demand response based congestion management of power system with uncertain renewable resources. International Journal of Ambient Energy. 2022 Dec 31;43(1):103-16. https://doi.org/10.1080/01430750.2019.1630307

[48] Siahchehre Kholerdi S, Ghasemi-Marzbali A. Effect of Demand Response Programs on Industrial Specific Energy Consumption: Study at Three Cement Plants. International Transactions on Electrical Energy Systems. 2022;2022(1):8550927. https://doi.org/10.1155/2022/8550927

[49] Harsh P, Das D. Energy management in microgrid using incentive-based demand response and reconfigured network considering uncertainties in renewable energy sources. Sustainable Energy Technologies and Assessments. 2021 Aug 1;46:101225.https://doi.org/10.1016/j.seta.2021.101225

[50] Chen Q, Wang W, Wang H, Dong Y, He S. Information gap-based coordination scheme for active distribution network considering charging/discharging optimization for electric vehicles and demand response. International Journal of Electrical Power & Energy Systems. 2023 Feb 1;145:108652. https://doi.org/10.1016/j.ijepes.2022.108652

[51] Gupta S, Maulik A, Das D, Singh A. Coordinated stochastic optimal energy management of grid-connected microgrids considering demand response, plug-in hybrid electric vehicles, and smart transformers. Renewable and Sustainable Energy Reviews. 2022 Mar 1;155:111861. https://doi.org/10.1016/j.rser.2021.111861

[52] Astriani Y, Shafiullah GM, Shahnia F. Incentive determination of a demand response program for microgrids. Applied Energy. 2021 Jun 15; 292 :1 16624. https://doi.org/10.1016/j.apenergy.2021.116624

[53] Wang L, Hou C, Ye B, Wang X, Yin C, Cong H. Optimal operation analysis of integrated community energy system considering the uncertainty of demand response. IEEE Transactions on Power Systems. 2021 Jan 14;36(4):3681-91. https://doi.org/10.1109/TPWRS.2021.3051720

[54] Nourollahi, R., Salyani, P., Zare, K. and Mohammadi-Ivatloo, B., 2021. Resiliency-oriented optimal scheduling of microgrids in the presence of demand response programs using a hybrid stochastic-robust optimization approach. International Journal of Electrical Power & Energy Systems, 128, p.106723. https://doi.org/10.1016/j.ijepes.2020.106723

[55] Nayak A, Maulik A, Das D. An integrated optimal operating strategy for a grid-connected AC microgrid under load and renewable generation uncertainty considering demand response. Sustainable Energy Technologies and Assessments. 2021 Jun 1;45:101169. https://doi.org/10.1016/j.seta.2021.101169

[56] Mimica M, Dominković DF, Capuder T, Krajačić G. On the value and potential of demand response in the smart island archipelago. Renewable energy. 2021 Oct 1;176:153-68. https://doi.org/10.1016/j.renene.2021.05.043

[57] Xu, B., Wang, J., Guo, M., Lu, J., Li, G. and Han, L., 2021. A hybrid demand response mechanism based on real-time incentive and real-time pricing. Energy, 231, p.120940. https://doi.org/10.1016/j.energy.2021.120940

[58] Tiwari A, Jha BK, Pindoriya NM. Multi-objective optimization-based demand response program with network aware peer-to-peer energy sharing. International Journal of Electrical Power & Energy Systems. 2024 Jun 1;157:109887. https://doi.org/10.1016/j.ijepes.2024.109887

[59] Khodadadi A, Adinehpour S, Sepehrzad R, Al-Durra A, Anvari-Moghaddam A. Data-Driven hierarchical energy management in multi-integrated energy systems considering integrated demand response programs and energy storage system participation based on MADRL approach. Sustainable Cities and Society. 2024 Apr 1;103:105264. https://doi.org/10.1016/j.scs.2024.105264

[60] Seyednouri SR, Safari A, Quteishat A, Younis MA, Salehi J, Najafi S, Taghizadegan N. Stochastic energy management of a multi-microgrid system with battery/supercapacitor energy storages considering demand response and transactive energy. Renewable Energy Focus. 2024 Mar 1;48:100531.https://doi.org/10.1016/j.ref.2023.100531

[61] Yang C, Wu Z, Li X, Fars A. Risk-constrained stochastic scheduling for energy hub: Integrating renewables, demand response, and electric vehicles. Energy. 2024 Feb 1;288:129680. https://doi.org/10.1016/j.energy.2023.129680

[62] Li LL, Fan XD, Wu KJ, Sethanan K, Tseng ML. Multi-objective distributed generation hierarchical optimal planning in distribution network: Improved beluga whale optimization algorithm. Expert Systems with Applications. 2024 Mar 1;237:121406. https://doi.org/10.1016/j.eswa.2023.121406

[63] Abdelghany MB, Mariani V, Liuzza D, Glielmo L. Hierarchical model predictive control for islanded and grid-connected microgrids with wind generation and hydrogen energy storage systems. International Journal of Hydrogen Energy. 2024 Jan 2;51:595-610. https://doi.org/10.1016/j.ijhydene.2023.08.056

[64] Ahmad AY, William P, Uike D, Murgai A, Bajaj KK, Deepak A, Shrivastava A. Framework for sustainable energy management using smart grid panels integrated with machine learning and iot based approach. International Journal of Intelligent Systems and Applications in Engineering. 2024;12(2s):581-90. https://ijisae.org/index.php/IJISAE/article/view/3670

[65] Ashok Babu P, Mazher Iqbal JL, Siva Priyanka S, Jithender Reddy M, Sunil Kumar G, Ayyasamy R. Power control and optimization for power loss reduction using deep learning in microgrid systems. Electric Power Components and Systems. 2024 Jan 20;52(2):219-32. https://doi.org/10.1080/15325008.2023.2217175

[66] Meng W, Song D, Huang L, Chen X, Yang J, Dong M, Talaat M. A Bi-level optimization strategy for electric vehicle retailers based on robust pricing and hybrid demand response. Energy. 2024 Feb 15;289:129913. https://doi.org/10.1016/j.energy.2023.129913

[67] Saxena V, Kumar N, Nangia U. Coal power plant-enabled grid resilience through distributed energy resources and demand response integration. Electrical Engineering. 2024 Jan 29:1-23. https://doi.org/10.1007/s00202-024-02239-5

[68] Elshahed M, Tolba MA, El-Rifaie AM, Ginidi A, Shaheen A, Mohamed SA. An artificial rabbits' optimization to allocate PVSTATCOM for ancillary service provision in distribution systems. Mathematics. 2023 Jan 9;11(2):339. https://doi.org/10.3390/math11020339

[69] Noori A, Zhang Y, Nouri N, and Hajivand M, "Multi-objective optimal placement and sizing of distribution static compensator in radial distribution networks with variable residential, commercial and industrial demands considering reliability". IEEE Access, 9, pp.46911-46926, 2021. https://doi.org/10.1109/ACCESS.2021.3065883

[70] Hardi S, Marpaung V, Hariadi IN, Nisja I. Mitigation of voltage sags in distribution line system using static VAR compensator and static synchronous compensator. InJournal of Physics: Conference Series 2022 Feb 1 (Vol. 2193, No. 1, p. 012040). IOP Publishing. https://doi.org/10.1088/1742-6596/2193/1/012040

[71] Amirrezai M, Rezaie H, Goetz SM. Feasibility study of incorporating static compensators in distribution networks containing distributed generation considering system power factor. Electric Power Systems Research. 2023 Jun 1;219:109253. https://doi.org/10.1016/j.epsr.2023.109253

[72] Rakočević S, Ćalasan M, Abdel Aleem SH. Smart and coordinated allocation of static VAR compensators, shunt capacitors and distributed generators in power systems toward power loss minimization. Energy Sources, Part A: Recovery, Utilization, and Environmental Effects. 2024 Dec 31;46(1):9136-54. https://doi.org/10.1080/15567036.2021.1930289

[73] Galvani S, Mohammadi-Ivatloo B, Nazari-Heris M, Rezaeian-Marjani S. Optimal allocation of static synchronous series compensator (SSSC) in wind-integrated power system considering predictability. Electric Power Systems Research. 2021 Feb 1;191:106871. https://doi.org/10.1016/j.epsr.2020.106871

[74] Delghavi MB, Pashaei Choboghloo S. Voltage Sag Mitigation in DER-Connected Distribution Networks by STATCOM. Electric Power Components and Systems. 2021 Jun 15;48(19-20):2156-67. https://doi.org/10.1080/15325008.2021.1910380

[75] Okelola MO, Salimon SA, Adegbola OA, Ogunwole EI, Ayanlade SO, Aderemi BA. Optimal siting and sizing of D-STATCOM in distribution system using new voltage stability index and bat algorithm. In2021 International Congress of Advanced Technology and Engineering (ICOTEN) 2021 Jul 4 (pp. 1-5). IEEE. https://doi.org/10.1109/ICOTEN52080.2021.9493461

[76] Yuvaraj T, Devabalaji KR, Srinivasan S, Prabaharan N, Hariharan R, Alhelou HH, Ashokkumar B. Comparative analysis of various compensating devices in energy trading radial distribution system for voltage regulation and loss mitigation using blockchain technology and bat algorithm. Energy Reports. 2021 Nov 1;7:8312-21. https://doi.org/10.1016/j.egyr.2021.08.184

[77] Moufid I, En-Nay Z, Naciri S, El Moussaoui H, Lamhamdi T, El Markhi H. Impact of static synchronous compensator STATCOM installation in power quality improvement. International Journal of Power Electronics and Drive Systems. 2022 Dec 1;13(4):2296. https://doi.org/10.11591/ijpeds.v13.i4.pp2296-2304

[78] Roy C, Chatterjee D, Bhattacharya T. An Economic Hybrid Shunt Compensator for Power Factor Correction and Mitigation of Large Unbalance as in HV Traction Distribution System. IEEE Transactions on Industry Applications. 2023 May 10;59(5):5989-99. https://doi.org/10.1109/TIA.2023.3274612

[79] Khan B, Redae K, Gidey E, Mahela OP, Taha IB, Hussien MG. Optimal integration of DSTATCOM using improved bacterial search algorithm for distribution network optimization. Alexandria Engineering Journal. 2022 Jul 1;61(7):5539-55. https://doi.org/10.1016/j.aej.2021.11.012

[80] Venkatesan C, Kannadasan R, Alsharif MH, Kim MK, Nebhen J. Assessment and integration of renewable energy resources installations with reactive power compensator in Indian utility power system network. Electronics. 2021 Apr 11;10(8):912. https://doi.org/10.3390/electronics10080912

[81] Eid A, Kamel S, Zawbaa HM, Dardeer M. Improvement of active distribution systems with high penetration capacities of shunt reactive compensators and distributed generators using Bald Eagle Search. Ain Shams Engineering Journal. 2022 Nov 1;13(6):101792. https://doi.org/10.1016/j.asej.2022.101792

[82] Vimlesh, Mukherjee V, Singh B. Hybrid GA-MCS based optimization for integration of DG, DVR, and DSTATCOM planning in distribution networks. International Transactions on Electrical Energy Systems. 2021 Dec;31(12):e13223. https://doi.org/10.1002/2050-7038.13223

[83] Shalchi F, Mozafari B, Firouz MH. Simultaneous sitting and sizing photovoltaic unit and distribution static compensator in distribution grid considering the effect of geographical conditions. International Journal of Numerical Modelling: Electronic Networks, Devices and Fields. 2021 Jan;34(1): e2801. https://doi.org/10.1002/jnm.2801

[84] Kennedy, J. and Eberhart, R., 1995, November. Particle swarm optimization. In Proceedings of ICNN'95-international conference on neural networks (Vol. 4, pp. 1942-1948). IEEE. https://doi.org/10.1109/ICNN.1995.488968

[85] Bouhouras AS, Sgouras KI, Gkaidatzis PA, Labridis DP. Optimal active and reactive nodal power requirements towards loss minimization under reverse power flow constraint defining DG type. International Journal of Electrical Power & Energy Systems. 2016 Jun 1; 78:445-54. https://doi.org/10.1016/j.ijepes.2015.12.014

[86] Kumar T, Thakur T. Comparative analysis of particle swarm optimization variants on distributed generation allocation for network loss minimization. In2014 First International Conference on Networks & Soft Computing (ICNSC2014) 2014 Aug 19 (pp. 167-171). IEEE. https://doi.org/10.1109/CNSC.2014.6906682

[87] Kumar EV, Raaja GS, Jerome J. Adaptive PSO for optimal LQR tracking control of 2 DoF laboratory helicopter. Applied Soft Computing. 2016 Apr 1;41:77-90. https://doi.org/10.1016/j.asoc.2015.12.023

[88] Selvakumar AI, Thanushkodi K. A new particle swarm optimization solution to nonconvex economic dispatch problems. IEEE transactions on power systems. 2007 Jan 29;22(1):42-51. https://doi.org/10.1109/TPWRS.2006.889132

[89] Yang XS, Deb S. Engineering optimisation by cuckoo search. International Journal of Mathematical Modelling and Numerical Optimisation. 2010 Jan 1;1(4):330-43. https://doi.org/10.1504/IJMMNO.2010.03543

[90] Basu MA, Chowdhury A. Cuckoo search algorithm for economic dispatch. Energy. 2013 Oct 1;60:99-108. https://doi.org/10.1016/j.energy.2013.07.011

[91] Abualigah L, Yousri D, Abd Elaziz M, Ewees AA, Al-Qaness MA, Gandomi AH. Aquila optimizer: a novel meta-heuristic optimization algorithm. Computers & Industrial Engineering. 2021 Jul 1;157:107250. https://doi.org/10.1016/j.cie.2021.107250

[92] Abualigah L, Diabat A, Mirjalili S, Abd Elaziz M, Gandomi AH. The arithmetic optimization algorithm. Computer methods in applied mechanics and engineering. 2021 Apr 1;376:113609. https://doi.org/10.1016/j.cma.2020.113609

[93] Dehghani, M., Montazeri, Z., Trojovská, E. and Trojovský, P., 2023. Coati Optimization Algorithm: A new bio-inspired metaheuristic algorithm for solving optimization problems. Knowledge-Based Systems, 259, p.110011.https://doi.org/10.1016/j.knosys.2022.110011

[94] Rao, R., 2016. Jaya: A simple and new optimization algorithm for solving constrained and unconstrained optimization problems. International Journal of Industrial Engineering Computations, 7(1), pp.19-34. https://doi.org/10.5267/j.ijiec.2015.8.004

[95] Markad, P., and D. A. Thosar, 2020. "Optimum Location and Size of DG Using GA with Sensitivity Analysis for a Real Time Radial Distribution System." In 2nd International Conference on Communication & Information Processing (ICCIP). https://dx.doi.org/10.2139/ssrn.3645871.

[96] Dolatabadi, S.H., Ghorbanian, M., Siano, P. and Hatziargyriou, N.D., 2020. An enhanced IEEE 33 bus benchmark test system for distribution system studies. IEEE Transactions on Power Systems, 36(3), pp.2565-2572. https://doi.org/10.1109/TPWRS.2020.3038030

[97] Baran, M.E. and Wu, F.F., 1989. Network reconfiguration in distribution systems for loss reduction and load balancing. IEEE Transactions on Power delivery, 4(2), pp.1401-1407. https://doi.org/10.1109/61.25627

[98] Das, D., 2008. Optimal placement of capacitors in radial distribution system using a Fuzzy-GA method. International Journal of Electrical Power & Energy Systems, 30(6-7), pp.361-367. https://doi.org/10.1016/j.ijepes.2007.08.004

[99] Das, D., Kothari, D.P. and Kalam, A., 1995. Simple and efficient method for load flow solution of radial distribution networks. International Journal of Electrical Power & Energy Systems, 17(5), pp.335-346. https://doi.org/10.1016/0142-0615(95)00050-0

[100] Khodr, H.M., Olsina, F.G., De Oliveira-De Jesus, P.M. and Yusta, J.M., 2008. Maximum savings approach for location and sizing of capacitors in distribution systems. Electric power systems research, 78(7), pp.1192-1203. https://doi.org/10.1016/j.epsr.2007.10.002

[101] Zobaa, A.F. and Aleem, S.A., 2020. Uncertainties in modern power systems. Academic Press. https://doi.org/10.1016/C2019-0-01693-7

[102] Patel, M.R. and Beik, O., 2021. Wind and solar power systems: design, analysis, and operation. CRC press. https://doi.org/10.1201/9781003042952

[103] Yao, F., Dong, Z.Y., Meng, K., Xu, Z., Iu, H.H.C. and Wong, K.P., 2012. Quantum-inspired particle swarm optimization for power system operations considering wind power uncertainty and carbon tax in Australia. IEEE transactions on industrial informatics, 8(4), pp.880-888. https://doi.org/10.1109/TII.2012.2210431

[104] Ghatak, S.R., Sannigrahi, S. and Acharjee, P., 2017. Comparative performance analysis of DG and DSTATCOM using improved PSO based on success rate for deregulated environment. IEEE Systems Journal, 12(3), pp.2791-2802. https://doi.org/10.1109/JSYST.2017.2691759

[105] Hetzer, J., David, C.Y. and Bhattarai, K., 2008. An economic dispatch model incorporating wind power. IEEE Transactions on energy conversion, 23(2), pp.603-611. https://doi.org/10.1109/TEC.2007.914171

[106] Ackermann, T., Ancell, G., Borup, L.D., Eriksen, P.B., Ernst, B., Groome, F., Lange, M., Mohrlen, C., Orths, A.G., O'Sullivan, J. and de la Torre, M., 2009. Where the wind blows. IEEE Power and Energy Magazine, 7(6), pp.65-75. https://doi.org/10.1109/MPE.2009.934658

[107] Adaramola, M.S., Paul, S.S. and Oyewola, O.M., 2014. Assessment of decentralized hybrid PV solar-diesel power system for applications in Northern part of Nigeria. Energy for Sustainable Development, 19, pp.72-82. https://doi.org/10.1016/j.esd.2013.12.007

[108] Dahal, S. and Salehfar, H., 2016. Impact of distributed generators in the power loss and voltage profile of three phase unbalanced distribution network. International Journal of Electrical Power & Energy Systems, 77, pp.256-262. https://doi.org/10.1016/j.ijepes.2015.11.038

[109] Modarresi, J., Gholipour, E. and Khodabakhshian, A., 2016. A comprehensive review of the voltage stability indices. Renewable and Sustainable Energy Reviews, 63, pp.1-12. https://doi.org/10.1016/j.rser.2016.05.010

[110] Muthukumar, K. and Jayalalitha, S., 2016. Optimal placement and sizing of distributed generators and shunt capacitors for power loss minimization in radial distribution networks using hybrid heuristic search optimization technique. International Journal of Electrical Power & Energy Systems, 78, pp.299-319. https://doi.org/10.1016/j.ijepes.2015.11.019

[111] Chowdhury, A., Roy, R. and Mandal, K.K., 2024. Enhancement of Technical, Economic and Environmental Benefits of RDN Using Jaya Algorithm Considering Renewables Uncertainties. Electric Power Components and Systems, pp.1-15. https://doi.org/10.1080/15325008.2024.2303066

[112] Carpinelli, G., Khormali, S., Mottola, F. and Proto, D., 2014. Battery energy storage sizing when time of use pricing is applied. The Scientific World Journal, 2014(1), p.906284. https://doi.org/10.1155/2014/906284

[113] Types of Electric Vehicles: e-AMRIT-Accelerated e-Mobility Revolution for India's Transportation. https://e-amrit.niti.gov.in/types-of-electric-vehicles. (*Accessed on 22.01.2025.*)

[114] How Is The Last Mile EV Adoption Scenario In India And Globally Altigreen. https://www.altigreen.com/blog-3/how-is-the-last-mile-ev-adoption-scenario-in-india-and-globally (*Accessed on 22.01.2025.*)

[115] Electric Vehicles Charging Stations. US Department of Energy. https://afdc.energy.gov/fuels/electricity-stations. (*Accessed on 22.01.2025.*)

[116] Dong, X., Mu, Y., Xu, X., Jia, H., Wu, J., Yu, X. and Qi, Y., 2018. A charging pricing strategy of electric vehicle fast charging stations for the voltage control of electricity distribution networks. Applied energy, 225, pp.857-868. https://doi.org/10.1016/j.apenergy.2018.05.042

[117] Yin, W., Mavaluru, D., Ahmed, M., Abbas, M. and Darvishan, A., 2020. Application of new multi-objective optimization algorithm for EV scheduling in smart grid through the uncertainties. Journal of Ambient Intelligence and Humanized Computing, 11, pp.2071-2103. https://doi.org/10.1007/s12652-019-01233-1

[118] Silva, C., Faria, P., Vale, Z. and Corchado, J.M., 2022. Demand response performance and uncertainty: A systematic literature review. Energy Strategy Reviews, 41, p.100857. https://doi.org/10.1016/j.esr.2022.100857

[119] Prajapati, K. and Roy, R., 2011, November. A novel method for distribution system reconfiguration including static load models and daily load curve. In 2011 2nd International Conference on Electric Power and Energy Conversion Systems (EPECS) (pp. 1-5). IEEE. https://doi.org/10.1109/EPECS.2011.6126829

[120] Abdollahi, A., Moghaddam, M.P., Rashidinejad, M. and Sheikh-El-Eslami, M.K., 2011. Investigation of economic and environmental-driven demand response measures incorporating UC. IEEE transactions on smart grid, 3(1), pp.12-25. https://doi.org/10.1109/TSG.2011.2172996

[121] Govardhan, M. and Roy, R., 2015. Economic analysis of unit commitment with distributed energy resources. International Journal of Electrical Power & Energy Systems, 71, pp.1-14. https://doi.org/10.1016/j.ijepes.2015.01.028

Anirban Chowdhury
09/09/25.

9/9/25

Professor
Dept. of Power Engineering
Jadavpur University
Salt Lake, 2nd Campus
Kolkata-700 098

09.09.25

Dean (E & T)
SRM University Delhi-NCR
39, RGEC, Sonepat -131029, HR.